DEFORMATION AND RUPTURE OF STRUCTURES DUE TO COMBINED CYCLIC PLASTICITY AND CREEP

by

David A. Lavender

A thesis submitted to
the University of Leicester for
the degree of Doctor of Philosophy

1987

ProQuest LLC
789 East Eisenhower Parkway
P.O. Box 1346
Ann Arbor, MI 48106-1346

ACKNOWLEDGEMENTS

The author wishes to thank Professor D. R. Hayhurst for the guidance and encouragement provided throughout this work. The author is also grateful to the many people who have given help with the background theory and computer problems, especially Mr. P. R. Brown and Dr. M. Dowson.

The completion of this thesis may not have occurred without the moral and temporal support generously offered by Dr. M. R. Goldthorpe.

Thanks are also due to Miss S. Krajewski who typed the text of this thesis.

Finally, the financial support of the Science and Engineering Research Council is gratefully acknowledged.

CONTENTS

CHAPTER 1

INTRODUCTION

1.1 Background

Often, engineering components are required to operate safely, reliably and economically under severe conditions. An important example of such conditions is the combination of high temperatures and fluctuating loads. These conditions are to be found, for example, in the power generation industry, where plant is required to operate at high temperatures in order to increase efficiency, and where fluctuating loads occur due to periodic shutdowns for maintenance and inspection, as well as to variations in the operating conditions. These conditions also exist in turbines and aircraft engines. Components which are to be exposed to these service conditions must be designed and tested before they are put into service, since failure is both dangerous and costly - especially in the case of nuclear power or aviation.

Unfortunately, the methods available to the designer often leave a large margin of uncertainty. The search for better methods has resulted in much research and, although many have been proposed, there is still no general agreement as to which is the best. The combination of high temperatures and fluctuating loads produces a mixture of creep and fatigue types of behaviour and this has become known as creep-fatigue behaviour. The reason for the uncertainty is that these two phenomena interact and the nature of this is not completely understood.

Another problem in design is that the precise operating conditions of a component are often not known beforehand, and thus large safety margins are needed to take this into account. The increasing cheapness and availability of microprocessors could help to overcome this drawback: using such devices, it is possible to monitor continuously the actual operating conditions of a component and, given a sufficiently accurate model of the component and its constituent material, to assess the effect that these conditions have on the component's expected life. Thus, if the actual conditions prove to be less severe than those assumed in the original design, the component could be allowed to remain in service for longer than the design life. Safety would also be improved because any unusual conditions would be detected and if these lead to a significant shortening of the life of a component then this would be reported and the appropriate action taken before the component fails in service.

1.2 Approach

The previous section outlined the nature of the problems that this thesis aims to help to solve. The solution adopted here is to improve the material models and to incorporate them into a finite element solver. The finite element method is able to cope with most structural problems and, although currently expensive to use, the ever decreasing cost of computer hardware will enable it to be used for the cheap and routine solution of the nonlinear problems associated with creep

and fatigue in structures.

The material models used here will be based on continuum damage mechanics. This is used because it is easy to incorporate into a finite element formulation and it is general enough to be applied to many problems, including creep and fatigue. This generality will enable the solution of a wide range of problems using a single method. Another advantage of continuum methods is that the theory for creep-fatigue may be derived from those for pure creep and pure fatigue, and so it is only necessary to gather experimental data for creep and fatigue separately, thus avoiding the need for complex and expensive experiments over the whole range of creep-fatigue conditions.

The behaviour of metals under cyclic loading is very complex and all aspects will not be modelled here. In particular, although most metals display a certain amount of cyclic hardening (or softening) during the first 50 cycles or so, the constitutive models will not take this into account and the material will be assumed to take up the stable cyclic state from the first cycle. This assumption is made to simplify the calculations. It is assumed that omitting this initial hardening does not have a significant effect on the predicted total life of a component. On the other hand, the final stages of life of a material will be modelled as closely as possible. Thus, any weakening of a material that occurs before failure will be included in the constitutive model. Also, once failed, the material continues to play a part in compression and this too will be modelled. Nonlinear

work hardening will be assumed for cyclic plasticity, so that stress-strain hysteresis loops over a wide stress range may be accurately modelled. The mathematical laws which describe materials will be taken from the literature, although some modifications will be made to describe the weakening of the material.

An important part of the work presented here will be the application of the material models to the study of the behaviour and failure of structures. The extension from the behaviour of materials to that of structures is rarely straightforward, since the interaction between different parts of a structure or component can be relatively complex. In particular, it was found that, in structures involving multiaxial models, the effect of the underlying models can be obscured by the complexity of the structural response. Hence, most of the investigation was carried out for uniaxial structures, which also simplified the required calculations.

1.3 Summary of Remaining Chapters

Chapter 2 is a brief review of damage theories. The chapter contains a short review of the literature and a discussion as to how damage and failure will be employed in this thesis. An example of the use of damage in a simple structure is presented in Chapter 3. A different set of constitutive laws with better properties than those used in Chapter 3 is then introduced and studied in Chapter 4. These are used in Chapter 5 in a further study of the simple structure. Up to that point only fatigue phenomena will have been considered. Chapter

6 introduces creep and a study is made of the interaction between creep and fatigue and the results of this are compared with some published experimental results. Also in that chapter, there is a description of how the constitutive model was fitted to experimental data so that it could be used for comparison with actual experiments.

Finite elements are used in Chapter 7 to solve a simple plasticity problem and the results are compared with accurate solutions. The techniques for solving nonlinear multiaxial problems are reviewed in that chapter and some of these are chosen for the example solutions. Chapter 8 looks in more detail at multiaxial constitutive laws and at how fissuring and failure can be modelled for use in the finite element method. The final chapter discusses what conclusions may be drawn from the results of the investigations and looks at what future work will be necessary to improve the accuracy of the models and to include them in a full finite element solver.

CHAPTER 2

DAMAGE AND FAILURE: SOME BACKGROUND INFORMATION

2.1 Introduction

Materials which are subjected to load and harsh environments often degrade and become weaker. Damage theories attempt to quantify this degradation in terms of the conditions to which the material is subjected. In this thesis, the materials of interest are metals and the damaging processes to be studied are those of fluctuating loads and high temperatures.

When materials are subject to fluctuating loads, then fatigue occurs; the material becomes weaker, or less stiff, and finally fails. In metals, at temperatures greater than about one-third the melting point, creep is significant. It consists in non-recoverable strain that accumulates over time, even though the load remains constant during that time. The strain rate initially decreases, but eventually begins to increase, as the material becomes weaker, and finally, the material fails.

A degradation process can be said to increase a property of a material called damage or cumulative damage. A theory of cumulative damage is basically a description of the endurance of a material as a function of the conditions that the material is subjected to. Measurement of remaining lives of specimens is used to ascertain this function (see sub-section 2.3.1). Often, a relationship can be found between damage and some physical effect of the loading, such as cavitation or fissuring. If such a relationship exists or is assumed, then the damage

is often regarded as continuum damage, which means that the weakening of the material is assumed to be due to the physical damage, and that the local effect of individual defects in the material is neglected. Thus, an element of material is supposed to be uniform, with the effect of defects averaged over that element and only their global effect being considered. The theory of material behaviour which is based on these assumptions is called continuum damage mechanics.

This chapter presents a brief review of the way damage theories have been used in the past and some of the definitions of damage that have been used. The concept of failure is also examined and its use described. Finally, there is a discussion on the way damage and failure are to be used in the rest of this thesis.

2.2 Review of Damage Theories

2.2.1 Creep

The introduction of the concept of continuum damage in the case of creep is usually attributed to Kachanov (1958). He used an extra variable, which he called damage, to account for the increase in strain rate during tertiary creep. Kachanov originally assumed that the damage was directly related to the loss of effective area due to the growth of cavities and fissures. However, Kachanov's original creep laws have been developed as a purely phenomenological theory of creep behaviour, since it soon became apparent that loss of area was not a sufficient explanation for the increase in strain rate.

The original equations were uniaxial and have been

extended to multiaxial equations by others (see Leckie and Hayhurst, 1974). These multiaxial equations and the corresponding failure criteria have been developed (Hayhurst et al., 1984a) for the study of the progress of creep damage in components, such as notched bars, and from this it is possible to predict the failure of such components due to creep. These studies use the finite element method and provide, not only the lifetime, but also the complete stress and deformation history of a component subject to creep. These methods have become generally accepted due to their success and to the fact that creep damage is not localized, so that a continuum damage mechanics approach is appropriate.

Although the formulation and growth of intergranular cavities was recognised as being the cause of weakening due to creep, these developments assumed only a phenomenological damage theory. However, recently, through the examination of the macroscopic and microscopic behaviour of an alloy, Dyson and McLean (1977) proposed a constitutive relation based on continuum damage and showed the connexion between physical damage, in the form of voids, and the deformation and failure of the material.

It may be noted here that there are other constitutive laws for creep which also account for tertiary creep but do not include damage. One such law has been investigated by the author with others (Hayhurst et al., 1985). This law can be used to extrapolate short term creep rupture data to provide long term predictions of time to rupture.

2.2.2 Fatigue

There is no widely accepted foundation in physical processes for the application of cumulative damage theories to fatigue like there is for creep. This is because damage theories ignore the local processes at the tip of a fatigue crack, and assume that a bulk description is possible and adequate for life prediction. Initially, cumulative damage was used as a purely phenomenological method. The use of this theory is based on the assumption that each cycle of loading does a certain amount of damage to the material and that failure occurs when the amount of damage equals some failure level. The advantage of this approach is that failure can in principle be predicted for complicated loading sequences simply by summing the damage contributions from each cycle of the sequence.

Miner (1945), in a rule named after him, proposed that the damage accumulated at a particular loading level is proportional to n_i/N_i, where n_i is the number of cycles at the ith loading level and N_i is the number of cycles to failure at that level. Failure occurs when the sum of these life fractions becomes unity:

$$\Sigma(n_i/N_i) = 1 \qquad (2.1)$$

The rule is also known as the linear accumulation rule since it does not matter in what order the loads are applied. Experimental work has shown, however, that this linear rule is not obeyed and that departures from it may be considerable and non-conservative. This has lead

to attempts to improve upon it, one of which is the double linear cumulative damage rule proposed by Manson et al. (1965). Other damage rules were proposed, but in the main, fatigue failure is now studied using parametric failure criteria (see, for example, Brown and Miller, 1973) or derived from fatigue crack growth rates as studied in fracture mechanics (see Fuchs and Stephens, 1980).

However, the concept of cumulative damage is still being studied for use in prediction, especially in the area of creep-fatigue. Among those using damage are Chaboche (1978), who has proposed a nonlinear continuum damage growth law; Hashin and Rotem (1978), who derive damage accumulation laws from theoretical considerations; and Majumdar and Maiya (1980), who have derived empirical equations based on cavity sizes and crack lengths to link creep and fatigue damage and call their approach the damage rate method.

2.3 The Definition of Damage

Although damage is an intuitive concept, before it can be used it must be defined properly. Unfortunately, different authors use different definitions and there can be quite a lot of variation between them. In this section, some of these definitions will be quoted and discussed.

Generally, damage is normalized so that it is initially zero and so that failure occurs at some critical value D_c, which is often assumed to be equal to 1.

2.3.1 Remaining Life

This is perhaps the most important use for cumulative damage; i.e. to predict the remaining life of a component. In phenomenological theories, this remaining life is used to quantify the damage. It is not assumed by these theories that there is any connexion between the life of a specimen and its physical properties or condition. All that is required for a life prediction is a knowledge of the damage growth laws for the material and a knowledge of the loading sequence. The growth laws are obtained experimentally by studying the results of tests carried out with two or more levels of loading applied during the life of a specimen. For example, this is the basis of the theory of fatigue damage due to Hashin and Rotem (1978).

It is important to note there that the exact form of the damage growth law is not significant, but it is the difference between the curves for different loadings which matters. For example, Fig. 2.1 shows how a fatigue life prediction could be made, using the remaining life concept, for a test with two loading levels. The loading sequence consists initially of n_1 cycles at the first level, after which the loading is changed to the second level. The change from one curve to the other is accomplished by assuming that the damage is constant. The remaining life can then be read from the curve as shown. The lower graph demonstrates why the remaining life prediction is unaffected by a one to one transformation of the damage variable from D to D*: both graphs in the figure predict that the total number of cycles

to failure is $n_1 + n_2$.

2.3.2 Physical Measures

It has been observed experimentally that the physical properties of materials change as damage changes. The obvious examples of this are the initiation and growth of cracks in fatigue and the nucleation and growth of cavities in creep. Hence, crack length is sometimes used as the damage variable in fatigue studies (e.g. Miller and Zachariah, 1977) and cavity volume in creep studies (e.g. Dyson and McLean, 1977).

Other properties of a material are also affected by damage. These include the speed of sound and the electrical resistivity of the material (Lemaitre and Chaboche, 1985), and variations in these quantities can be used to measure changes in damage. In fatigue, the area of the fatigue crack can also be related to damage (Raynor and Skelton, 1983).

Damage also affects the relationship between stress and strain. For example, the Young's modulus of a material changes as damage accumulates. Note that this must be understood within the context of continuum damage mechanics since it implicitly assumes that any imperfections in the material are being averaged over a representative volume; it does not mean that the relationship between atoms in the material has changed in some way. Damage is observed to have an effect on most aspects of the stress-strain behaviour of the material and, in general, the exact effect of damage on the constitutive equations must be determined by

experiment. However, it is often sufficient to use the effective stress hypothesis used by Lemaitre and Chaboche (1985). This states that the deformation of a damaged material is given by replacing the stress, σ, in the constitutive equations by the effective stress, $\sigma/(1-D)$. This assumption seems to be accurate enough to be adopted as a general principle in damage mechanics, but it remains a hypothesis since it is not necessarily true that remaining life and deformation can be connected in this manner.

2.3.3 Relationship between Damage According to Remaining Life and to the Effective Stress Hypothesis

If it is assumed that a formula describing the growth of damage according to the remaining life definition has been found, then this may be transformed to satisfy the effective stress hypothesis. That such a transformation is possible was demonstrated in sub-section 2.3.1. At present the exact form of the link must be determined empirically, but it is possible that a more exact link could be determined through a theory connecting physical damage and both remaining life and deformation.

2.4 Failure

2.4.1 The Definition of Failure

When damage in a specimen reaches some critical value, D_c (usually $D_c=1$), then it is deemed to have failed, or come to the end of its life. What should this mean physically? The simplest answer is that the material has broken into two separate pieces. This definition

is not always regarded as convenient or meaningful and various other definitions have been adopted. Two examples are given here.

Hayhurst et al. (1984a), in finite element analyses of creep in notched bars, assumed that D=0.99 constituted failure and that material attaining this point took no further part in the analysis. This definition does not quite correspond to separation since the failed material remains as part of the structure, but with changed properties.

Chaboche (1981), in analysis of fatigue in components, assumes that D=1 corresponds to the initiation of a detectable crack. This corresponds to the appearance of a crack about 1mm long which dominates any other shorter cracks. Further analysis may then be carried out using standard fracture mechanics techniques. Using this definition, damage mechanics possibly provides an answer to the short crack problem as enunciated by Miller (1982).

2.4.2 Crack Propagation

The progress, in a structure, of areas of material which has failed can be thought of as representing the progress of a crack. In a recent review paper, Lemaitre (1986) lists many references to researchers who have used continuum damage mechanics to study the propagation of fissuring and cracking in components. This type of approach has been criticized, but Lemaitre lists many situations where other methods such as fracture mechanics do not succeed in providing satisfactory answers.

Hayhurst et al. (1984a and 1984b) use this approach to study the progress of creep cracking through a finite element mesh. Comparison of the computed crack directions and crack discernable in micrographs of experimental specimens shows excellent agreement and justifies the use of this approach for creep cracking.

2.5 The Usage of Damage and Failure in this Thesis

This section is a summary of the way in which damage is used and what is meant by failure in the rest of this thesis.

One of the aims of this thesis is to examine the possibility of obtaining complete stress and strain histories for components under creep-fatigue conditions and to predict the progress of cracking through the component and its consequent failure. Some connexion between continuum damage and deformation is therefore required. Here, it is provided by the effective stress hypothesis, and so, for any constitutive law that is used, the law for damage material is obtained from the original by replacing σ by $\sigma/(1-D)$. It is assumed that the growth of continuum damage is consistent with the remaining life defintion: i.e. that lifetimes can be predicted for any loading scheme using the damage growth laws.

An example of these assumptions in use is given by Fig. 2.2. The graphs in this figure represent the (idealized) stress-strain response of uniaxial specimens under cyclic loading. Figure 2.2.(a) is the response for a strain controlled test. The strain amplitude remains

constant but the stress amplitude decays. In this case it is assumed that σ_{max} , the maximum stress, becomes (1-D) σ_{max} . Hence, σ_{max} decays to zero at failure at N_f where D=1. In Fig. 2.2(b), which is for stress or load control, the strain grows according to σ_{max} /(1-D), Figure 2.2.(a) may be compared with an experimental envelope such as the one in Raynor and Skelton (1983). Notice that it is assumed in Fig. 2.2 that no cyclic hardening or softening occurs.

Failure will occur when damage equals 1. Here, failure means that the material becomes a 'no-tension' material and will be unable to support a tensile stress, but it is assumed that the material is still able to support compressive stresses and this will be important when a component is subject to cyclic loads. The behaviour of the failed material is based on that of cracked concrete given by Phillips and Zienkiewicz (1976), and will be supposed to be as follows. In compression the material will be assumed to behave as if it were undamaged, having the same relationship between stress and strain as the original undamaged material. If the stress reaches zero and the strain rate is positive, then the stress will remain zero but the material will be allowed to strain as dictated by the rest of the structure or surrounding material. When the strain returns to the same value at which the stress had first become zero, then any further negative strain will cause the material to go into compression and the properties will again be those of the original material. Notice that this is essentially a continuum damage mechanics

definition since the material is assumed to remain intact, but its properties are changed. This fact will be more important in the multiaxial case than in the uniaxial case.

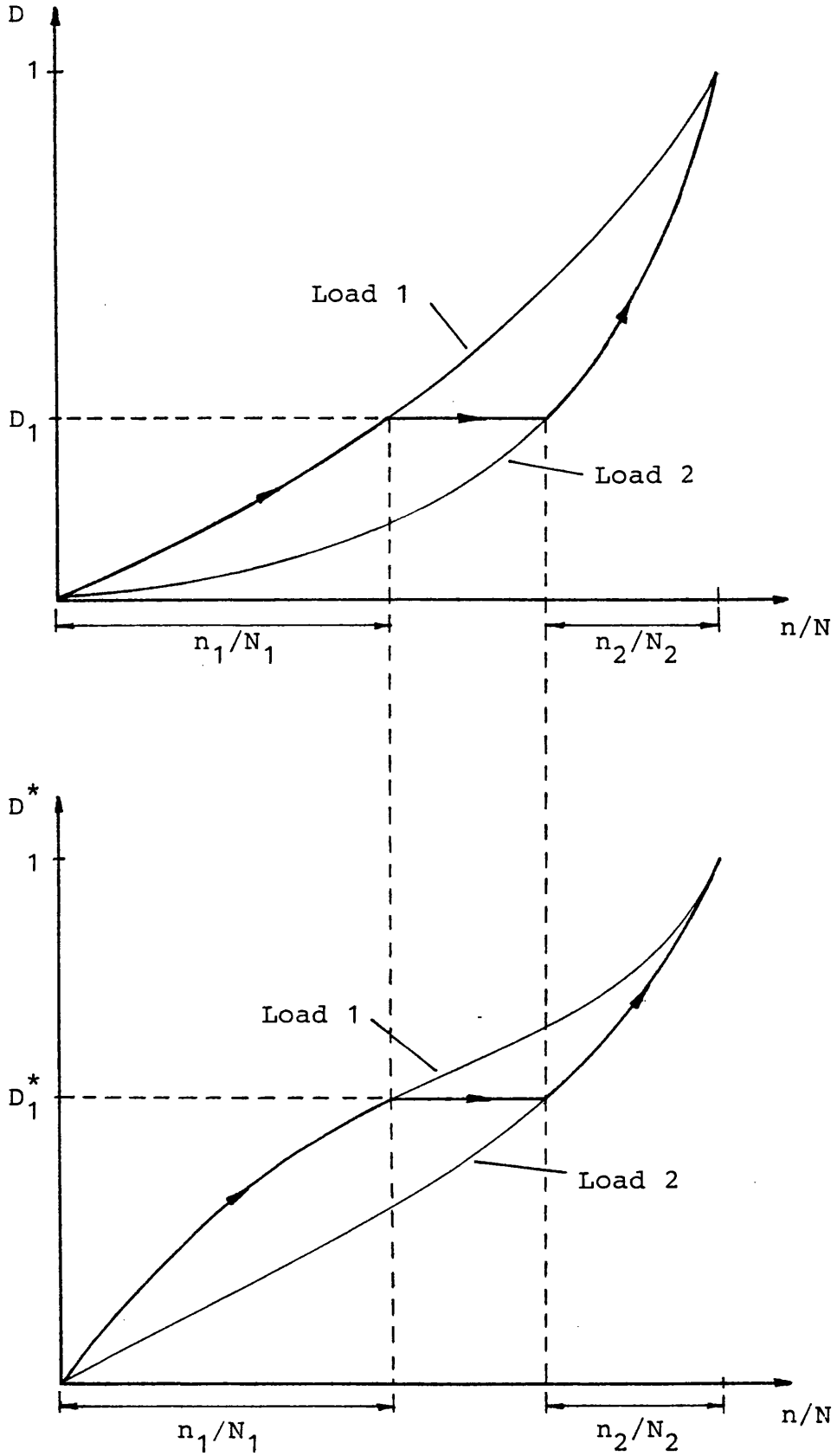

Figure 2.1: An illustration of the method of life prediction for a test with two load levels and the correspondence between D and D* obtained by a one to one transformation.

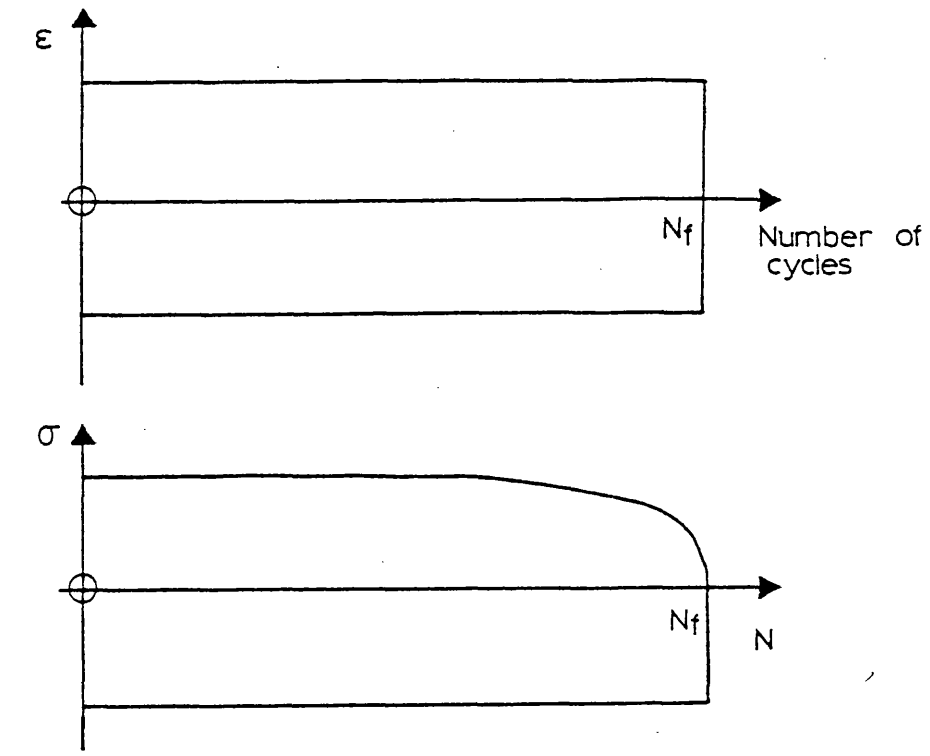

a) Strain control

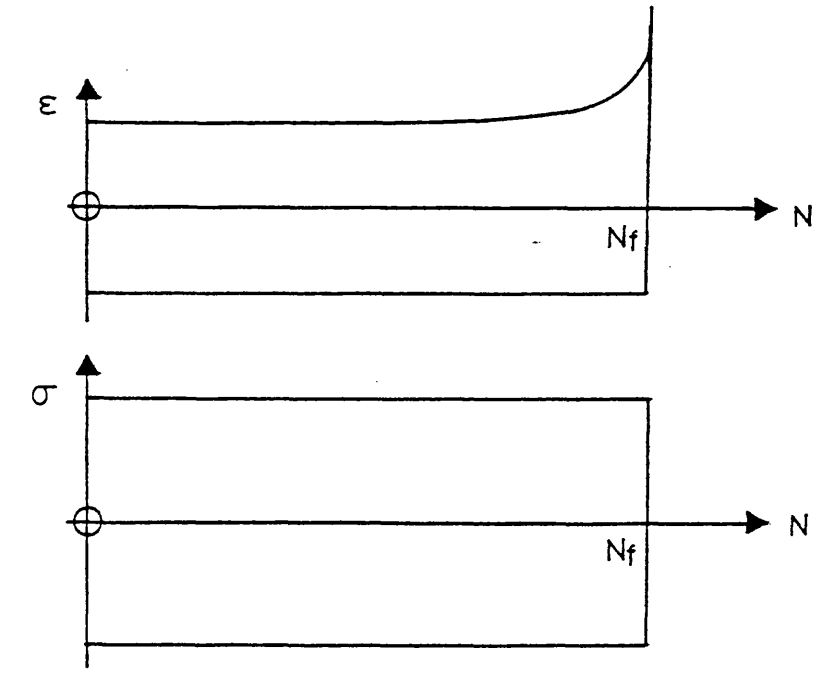

b) Stress control

Figure 2.2 : Envelopes of maximum and minimum stresses and strains for cyclic loading tests on uniaxial specimens.

CHAPTER 3

A PRELIMINARY INVESTIGATION INTO THE SIGNIFICANCE OF STRESS REDISTRIBUTION IN STRUCTURES DUE TO CUMULATIVE FATIGUE DAMAGE

3.1 Introduction

In this chapter a uniaxial model structure will be used to determine how stress redistribution due to fatigue damage growth affects lifetime. Hayhurst et al. (1984b) have shown that stress redistribution due to creep damage growth has a significant effect on the life of a structure at high temperature and that it is important to take this into account if accurate or economical predictions are to be made. Similarly in fatigue, if stress redistribution has a significant effect on the life of a component, then it will be important to take it into account when assessing its reliability under fluctuating loads. The investigation in this chapter sets out to establish whether stress redistribution is an important factor in fatigue life by using a simple structure and simplified constitutive and damage evolution laws.

3.2 Material Behaviour

3.2.1 Uniaxial Models for Damage Growth due to Cyclic Plasticity

In this chapter the rate of change of fatigue damage is postulated to be given by

$$\frac{\delta\psi}{\delta N} = \left\langle \frac{\sigma_A - \sigma_Y}{B(1-\psi)} \right\rangle^r \frac{1}{(1-\psi)^p} , \qquad (3.1)$$

where ψ is the fatigue damage, σ_A is the stress amplitude, σ_Y the yield stress and B, r and p are material constants. The angle brackets indicate

$$< x > = \begin{cases} x & \text{if } x > 0 \\ 0 & \text{if } x < 0 \end{cases} \qquad (3.2)$$

This equation is based on an equation used by Lemaitre and Plumtree (1979), but has been modified slightly so that it is consistent with the constitutive equations. The connection between plastic strain amplitude and the stress amplitude is assumed to be given by

$$\eta_A = \left\langle \frac{\sigma_A - \sigma_Y}{K(1-\psi)} \right\rangle^q \qquad (3.3)$$

where η_A is the plastic strain amplitude, and K and q are constants. Equation (3.1) can now be expressed in terms of plastic strain:

Substitution of (3.3)into (3.1) gives

$$\frac{\delta\psi}{\delta N} = \left[\frac{K}{B} \right]^r \eta_A^{r/q} \quad \frac{1}{(1-\psi)^p} \qquad (3.4)$$

This equation now allows the standard strain-controlled cycling tests to be used to evaluate the material constants B, r and p. Integration of (3.4) over the lifetime of a specimen from ψ = 0 to 1 and N = 0 to N_f gives the number of cycles to failure as

$$N_f = \frac{1}{(p+1) \left[\frac{K}{B} \right]^r \eta_A^{r/q}} \qquad (3.5)$$

Substitution of this back into (3.4) gives

$$\frac{\delta\psi}{\delta N} = \frac{1}{(p+1)(1-\psi)^{p}N_f} \qquad (3.6)$$

This can be integrated to give the damage after N cycles

$$1-\psi = [1-\frac{N}{N_f}]^{1/(p+1)} \qquad (3.7)$$

By the effective stress hypothesis, the term $(1-\psi)$ can be found from the decrease in stress observed during a strain controlled fatigue test. If log $(1-\psi)$ is plotted against log $(1-N/N_f)$ then the slope of the line gives p+1. Equation (3.5) is basically the Manson-Coffin relation between plastic strain amplitude and number of cycles to failure. Hence a series of fatigue tests is necessary to determine the remaining two constants B and r, if the Manson-Coffin equation is assumed. A similar procedure can also be carried out for stress controlled tests. This formulation of damage growth has been used in predicting lifetimes for specimens under mixed creep and fatigue conditions by Lemaitre and Plumtree (1979) and Blackmon et al. (1983).

3.3 A Numerical Study of a Multibar Model

3.3.1 Multibar Model Structures

The model structure that will be used in the studies in this and other chapters is the multibar structure. It will be used because its components can be described by uniaxial laws, and hence it is a relatively simple

structure to analyse and calculations for it are comparatively easy to perform. On the other hand, the interactions within a non-trivial multibar structure are relatively complex and reflect the type of behaviour that is exhibited by more complex structures and components. Thus, by using multibar models, structural behaviour may be studied without the necessity of using techniques such as the finite element method which would require complicated computer software and extended computations.

A multibar model consists of a number of parallel bars of uniform cross-sectional area. Each bar is fixed at one end while the other end is attached to a block to which all of the bars are fixed. This block is allowed to move in a single direction parallel to the axes of the bars. An example of such a structure is illustrated in Fig. 3.1. Details of how non-linear problems involving plasticity are solved for this structure are given in Appendix A.

3.3.2 Constitutive Equations and the Incorporation of Damage

The manner in which the constitutive laws are employed in the solution of the model structure will now be discussed. It is assumed that the loading history is regular and has constant maximum and minimum values, P_{max} and P_{min} respectively, as shown in Fig. 3.2.

The relationship between stress and strain in the uniaxial case is based on the equation,

$$\varepsilon = \begin{cases} \frac{\sigma}{E} & \text{if } \sigma \leq \sigma_Y \\ \frac{\sigma}{E} + \left\{ \frac{\sigma - \sigma_Y}{K} \right\}^q & \text{if } \sigma > \sigma_Y \end{cases} \qquad (3.8)$$

where ε and σ are respectively uniaxial values for strain and stress. K and q are material constants and E is Young's modulus. This equation is only used as it is shown here during the initial loading. Subsequently, in order to model the hysteresis loop in stress-strain co-ordinates which results from cyclic loading, the relationship becomes

$$\varepsilon = \begin{cases} \frac{\sigma}{E} + \eta_{min} & \text{if } \sigma \leq \sigma_{min} + 2\sigma_Y; \\ \frac{\sigma}{E} + 2 \left| \frac{\sigma - \sigma_{min} - 2\sigma_Y}{2K} \right|^q + \eta_{min} & \text{if } \sigma > \sigma_{min} + 2\sigma_Y, \end{cases} \qquad (3.9)$$

when going from P_{min} to P_{max}, and

$$\varepsilon = \begin{cases} \frac{\sigma}{E} + \eta_{max} & \text{if } \sigma \geq \sigma_{max} - 2\sigma_Y; \\ \frac{\sigma}{E} - 2 \left| \frac{-\sigma + \sigma_{max} - 2\sigma_Y}{2K} \right|^q + \eta_{max} & \text{if } \sigma < \sigma_{max} - 2\sigma_Y, \end{cases} \qquad (3.10)$$

when going from P_{max} to P_{min}. In these equations the subscript max indicates the value of a quantity when $P=P_{max}$ and the subscript min indicates its value at $P=P_{min}$. The factor of 2 in (3.9) and (3.10) is due

to the application of Masing's rule (Masing, 1926) which allows a closed hystersis loop to be constructed by doubling the monotonic curve given in (3.8). A typical hysteresis loop is illustrated in Fig. 3.3.

When damage is non-zero it is incorporated into the constitutive equations by assuming that it only affects the upward part of the stress-strain cycle. Thus, for the upward part of the cycle, (3.9) is replaced by:

$$\varepsilon = \begin{cases} \frac{\sigma}{E} + \eta_{min} & \text{if } \sigma < \sigma_{min} + 2\sigma_Y, \\ \eta_{min} + \frac{\sigma}{E} + 2 \left| \frac{\sigma - 2\sigma_Y - \sigma_{min}}{2K(1-\psi)} \right|^q & \text{if } \sigma > \sigma_{min} + 2\sigma_Y \end{cases} \qquad (3.11)$$

For the part of the cycle from P_{max} to P_{min}, (3.10) is used.

Damage is assumed to be constant during a cycle of load from P_{min} to P_{min}. The damage is changed when the load is P_{min}. The new value of damage is calculated by assuming that the plastic-strain range or stress range remains constant during the cycle, which allows (3.6) to be integrated over one cycle to give

$$\psi_{new} = 1 - [(1-\psi)^{p+1} - \frac{1}{N_f}]^{\frac{1}{p+1}} \qquad (3.12)$$

where N_f is calculated from (3.5) using the plastic strain amplitude of the previous load cycle. (The plastic-strain amplitude is calculated as half of the plastic strain range incurred by the bar on loading from P_{min} to P_{max}.)

A bar fails when damage reaches a value of 1. This is indicated, during the calculation for ψ_{new} in (3.12), when

$$(1-\psi)^{p+1} - \frac{1}{N_f} < 0 \qquad (3.13)$$

The fraction of the next cycle at which the bar falls, ΔN, can be calculated approximately by setting the l.h.s. of (3.13) to zero:

$$\Delta N = N_f \ (1-\psi)^{p+1} \qquad (3.14)$$

This is added to the number of cycles so far to give the point of failure of the bar. The value of ψ is set to one and the structure is loaded from P_{max} to P_{min} during which the failed bar follows (3.10). During loading from P_{min} to P_{max} a failed bar is assumed to be completely elastic: while the stress is less than zero, the bar has its initial elastic modulus, but when the stress reaches zero the modulus is changed to a very small fraction of the initial value. On loading from P_{max} to P_{min} the bar continues to obey (3.10) once in compression. A possible path of stress and strain is shown in Fig. 3.4.

3.3.3 Normalization

In what follows normalized quantities have been used; stress is normalized by dividing by the yield stress:

$$\sigma = \frac{\sigma'}{\sigma_Y} \qquad (3.15)$$

where a prime denotes the actual value. Normalized strain is defined by

$$\varepsilon = \frac{\varepsilon' E}{\sigma_Y} \tag{3.16}$$

and lengths and areas are normalized with respect to the length and area of bar 1:

$$\ell_i = \frac{\ell'_i}{\ell_1} \tag{3.17}$$

$$A_i = \frac{A'_i}{A_1} \tag{3.18}$$

where ℓ_i is the length of the ith bar and A_i its cross-sectional area. Equation (3.8) becomes:

$$\varepsilon = \begin{cases} \sigma & \text{if } \sigma \leq 1 \\ \sigma + \left(\frac{\sigma - 1}{\Gamma} \right)^q & \text{if } \sigma > 1 \end{cases} \tag{3.19}$$

in which case Γ is the normalized value of K which is defined by

$$\Gamma = \frac{K \sigma_Y^{1/q}}{\sigma_Y E^{1/q}} \tag{3.20}$$

3.3.4 Numerical Results

The actual multibar model used is described by the data of Table 3.1 and is illustrated in Fig. 3.1. The loading cycle was given by $P_{max} - P_{min} = 6.8$. In the initial state the load required for first yield is 4.0. The

stresses in the bars at this load in the initial state is also given in Table 3.1. These stresses show that the stress concentration factor between the 6th and 1st bars is 6. The behaviour of the multibar model was calculated up to failure of all 6 bars for two values of p. In one case p = 25, which is a typical value for this parameter (see for examples some values given by Blackmon et al. (1983)). In the other case a large value of p = 2500 has been selected so that the value of the damage ψ in a bar will remain small until immediately before the bar falls. This gives a close approximation to the model without damage growth, where each of the bars is failed at the number of cycles given by the Manson-Coffin law. A typical value of c was chosen in the Manson-Coffin equation and the value of ε_f was then chosen to give a total lifetime of the whole structure of the order of 100 cycles. The number of cycles at which each bar was calculated to have failed is given in Table 3.2, for each value of p. As can be seen in this table, the structure with negligible damage growth (p = 2500) has a significantly shorter lifetime than the structure with an appreciable growth of damage (p = 25), the difference being of the order of 25% of the p = 2500 value. Except for the first bar, each bar of the p = 2500 structure fails before the corresponding bar of the p = 25 structure, and the percentage difference between these failure times increases from bar 2 to bar 6. The first bar has a shorter life when p = 25 because damage growth slightly increases the plastic

strain amplitude of the bar which tends to decrease the life of the bar, whereas only negligible damage growth occurs when p = 2500 and the plastic strain amplitude remains the same throughout the life of the bar. After the first bar has failed other effects come into play and, although the same arguments apply and the plastic strain amplitude increases in the presence of damage, the subsequent failure of bars is later when p = 25 than when p = 2500.

Selected results of the computations are presented in Figs. 3.5-3.8. The graphs in Figs. 3.5-3.8 display the common feature that they consist of a series of steps. The sudden jumps in the curves correspond to the failure of one of the bars. Thus, the first jump in the graphs at about 11 cycles corresponds to the failure of the first bar (see Table 3.2). The main difference between the results for the two values of p is the difference in the growth of damage. For the curves of stress and strain, etc. in bars 3 and 6 for p = 25 (Figs. 3.5, 3.6) the growth of damage is indicated clearly by the curvature of the graphs apparent between bar failures. On the other hand for p = 2500, each of the sections between bar failures are flat or nearly so (see Figs. 3.7, 3.8). The upper curve in Fig. 3.5(a) shows that between 27 and 40 cycles the stress decreases due to the increase in damage in bar 3. Figure 3.6(a) shows that the stress in bar 6 is increasing between 27 and 40 cycles to compensate for the decrease in bar 3. This is an example of stress redistribution where the stress is transferred (in

accordance with equilibrium) from weaker, or more damaged bars of the structure, to stronger or less damaged bars.

The increase of plastic strain range with the increase in damage is illustrated in Fig. 3.5(b) where the plastic strain at P_{max} is growing faster than that at P_{min}. These graphs also show that each bar ratchets (see Fig. 3.5(b) and Fig. 3.6(b)). This is due to the fact that damage is only used to calculate the stress-strain response on loading from P_{min} to P_{max} (see equations 3.10 and 3.11).

Figure 3.5(c) illustrates the growth in damage in bar 3. This curve is typical of all the bars. The damage stays very small until just before failure when it grows very rapidly. This growth in damage is extremely rapid when p is 2500, so that the damage stays almost zero until the bar fails, when it suddenly becomes unity.

Figure 3.9 shows the displacements of the moving block of the multibar model with p = 25 at the top and bottom of the load cycles. This figure too has steps showing where each bar has failed and ratchetting is displayed as has already been noted for the strain response of each bar.

By careful comparison of Fig. 3.5(b) with Fig. 3.8, it can be seen why the structure has a longer lifetime for the larger value of p. The plastic strain range in bar 3 is greater after the failure of bar 1 in the case p = 2500 than in the case p = 25. The plastic strain amplitude (which is half the range) is used

in (3.4) to calculate the damage growth rate, and it can be seen from (3.4) that an increase in the amplitude leads to an increase in the damage growth rate. The greater plastic strain amplitude in the case p = 2500 is due to a greater stress amplitude. This appears to be due to the fact that there are larger compressive stresses in failed bars when p = 25 than when p = 2500. This means that stress redistribution to the failed bars in compression is greater when p = 25 compared with when p = 2500, and this has the effect of reducing the stress amplitude experienced by the remaining bars.

3.4 Conclusions

The example given in this chapter has been used to compare the predicted lifetimes of a simple structure given by two related laws of damage growth. In one the damage was allowed to grow and to affect the deformation of each individual component before its failure. In the other, damage was used as a failure criterion and did not affect deformation before failure. The results of the study show that, for the structure considered here, the predicted lifetime is increased by 25% when the effects of damage are taken into account. However, the constitutive models may be criticized on several grounds. The damage growth laws implicitly assume that the fatigue limit of the material is the same as the yield stress and also do not take into account the effect of any mean stresses. The proposed method of including the damage in the constitutive laws for cyclic plasticity has inherent

undesirable properties. Under stress controlled cycling the model predicts an increasing ratchetting rate with increasing damage. This behaviour is observed experimentally, but the theoretical ratchetting rate tends to be excessive. In addition, the same properties of the model lead to a continually decreasing mean stress under strain control with the rate of decrease increasing with damage.

Improved constitutive and damage growth laws will be presented in the next chapter which overcome some of these problems. These laws will then be used in a subsequent chapter to repeat the study made in this one.

Bar	Length (normalized)	Area (normalized)	Stress on first yield (normalized)
1	1	1	1
2	1.2	1	5/6
3	1.5	1	2/3
4	2.0	1	1/2
5	3.0	1	1/3
6	6.0	4	1/6

Other parameters:

in equation (3.19) $q = 2$ and $\Gamma = 0.5$.

$\varepsilon_f = 1.5$, and $c = -0.3$, where $\eta_A = \varepsilon_f (N_f)^c$ is the Manson-Coffin equation.

Young's Modulus of failed bar in tension is 10^{-8}xE, where E is the modulus of undamaged material.

Table 3.1 Details of multibar structure.

		Bar Number					
		1	2	3	4	5	6
Value of p	p = 25	11.11	23.01	39.68	64.00	96.39	97.44
	p = 2500	11.71	21.88	33.98	51.54	77.55	78.34

Table 3.2 Calculated numbers of cycles to failure for each bar in multibar model of Table 3.1.

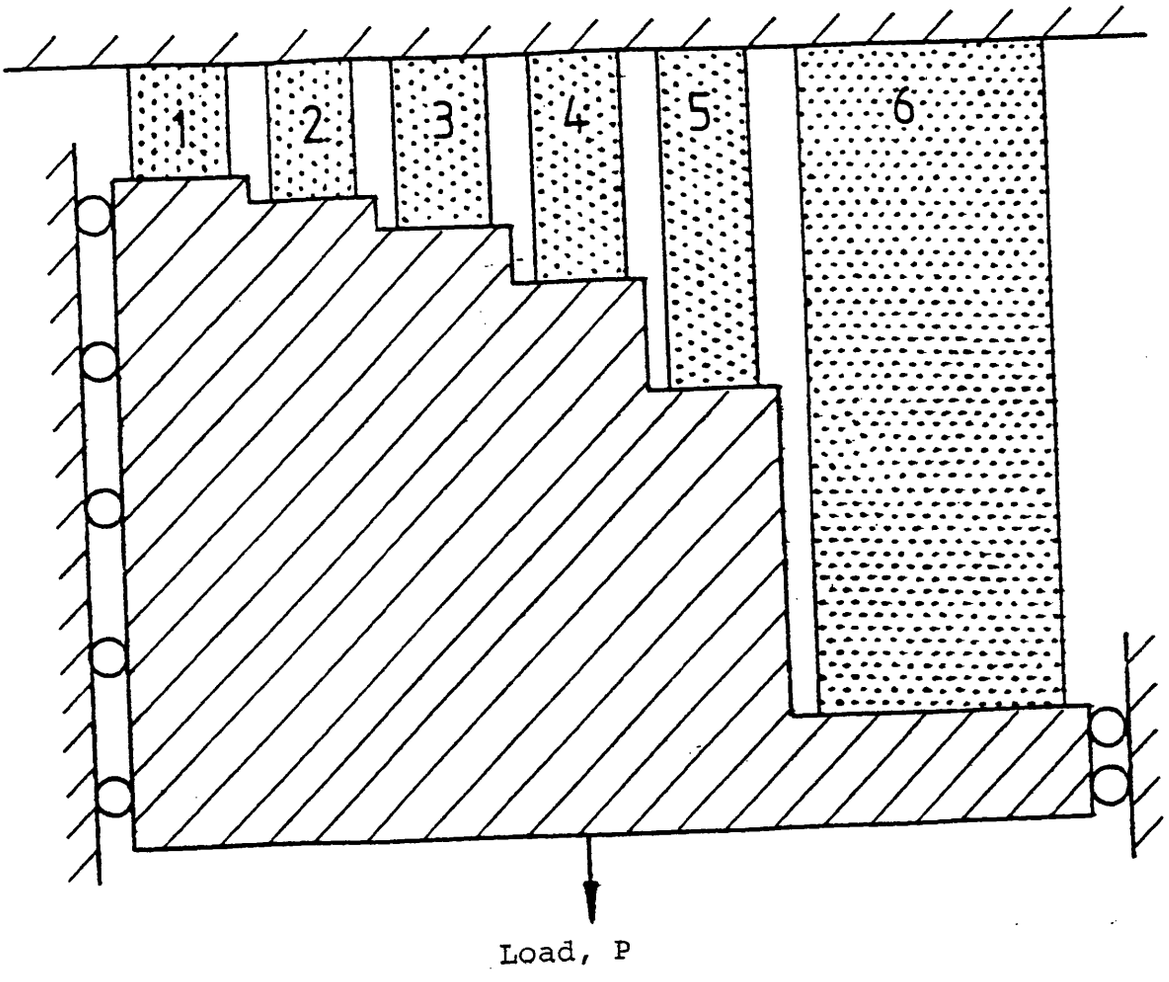

Figure 3.1: An illustration of the 6 bar structure used in the numerical study. Its dimensions are given in Table 3.1.

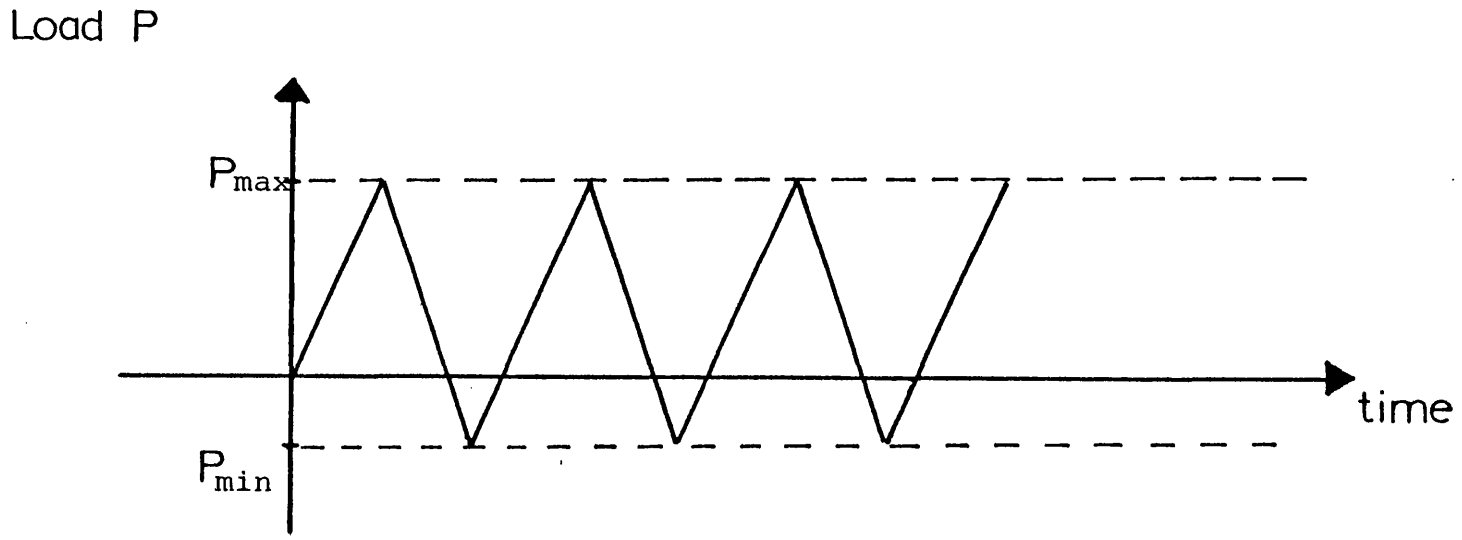

Figure 3.2: Loading applied to multibar structure.

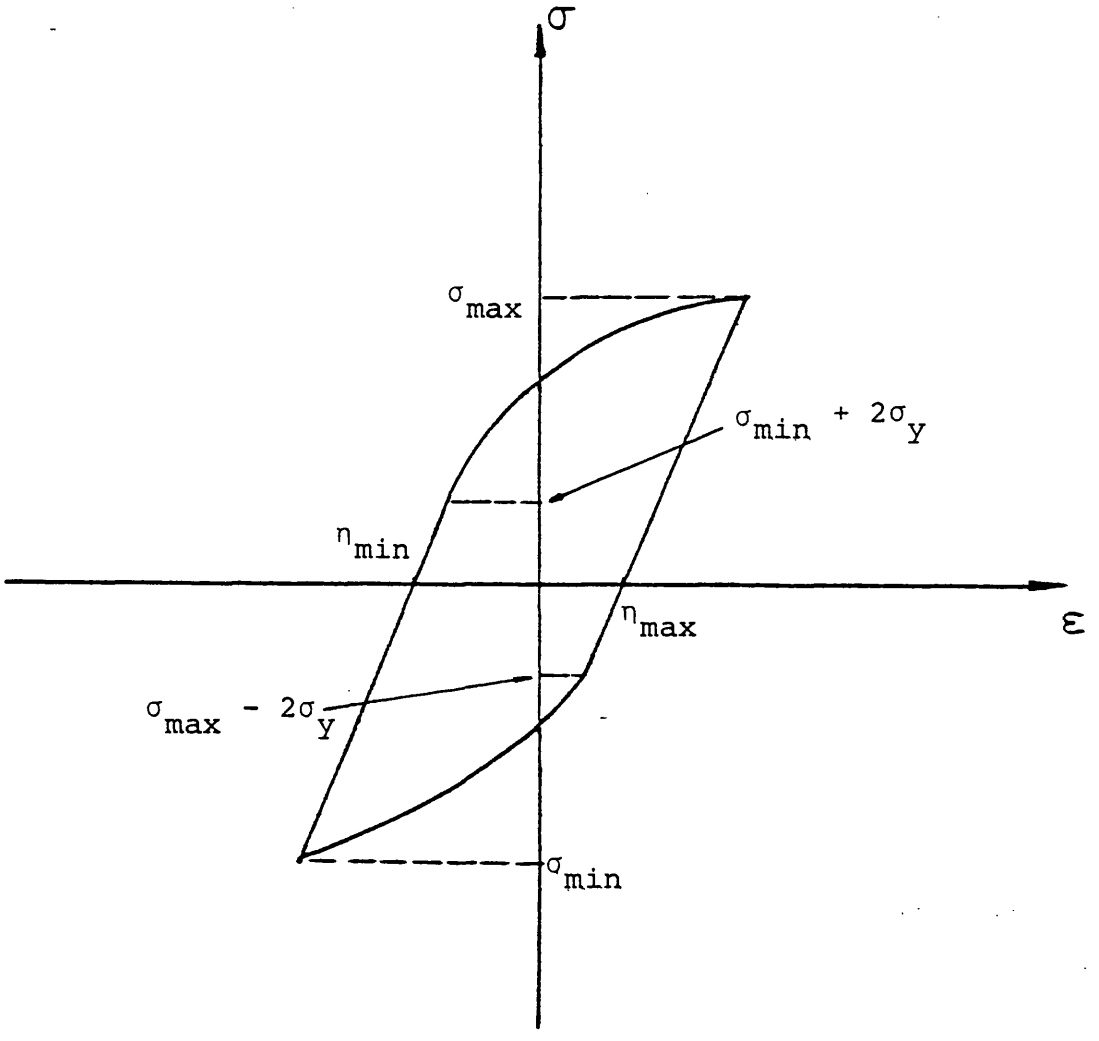

Figure 3.3: Cyclic stress-strain hysteresis loop illustrating the terminology used in equations (3.9) and (3.10).

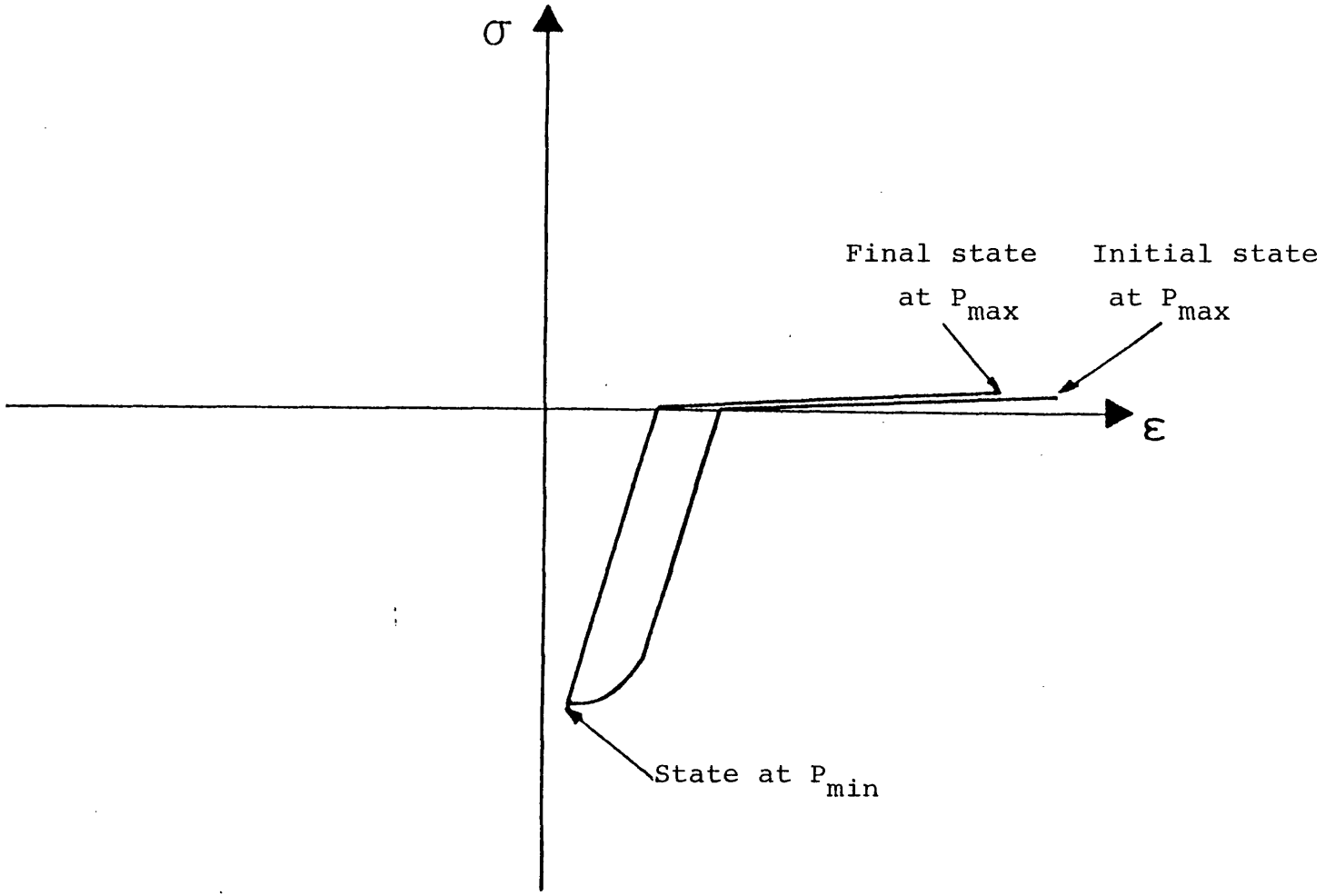

Figure 3.4: An example of the stress-strain behaviour of a failed bar.

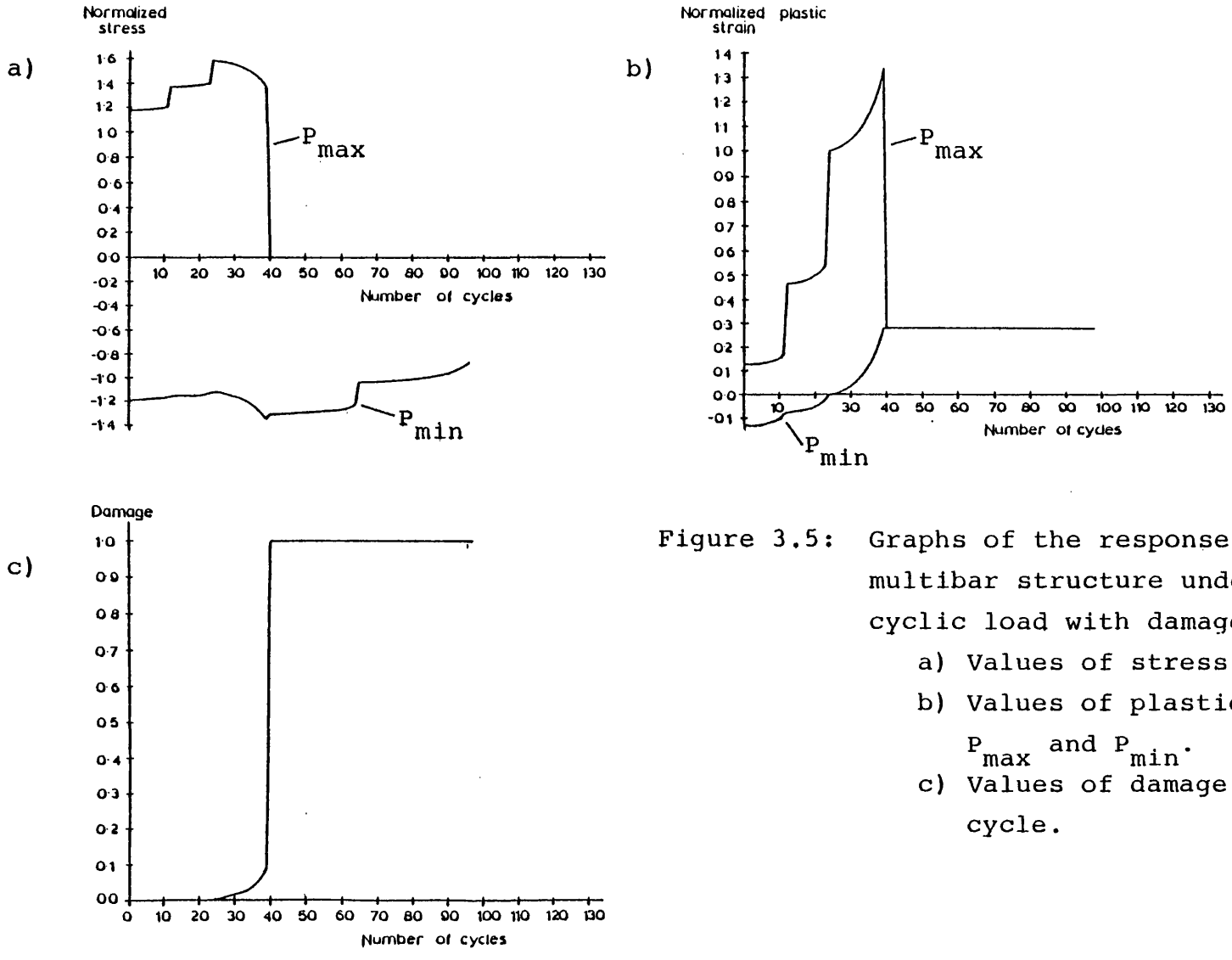

Figure 3.5: Graphs of the response of bar 3 of multibar structure under a symmetric cyclic load with damage (p = 25).

a) Values of stress at P_{max} and P_{min}.

b) Values of plastic strain at P_{max} and P_{min}.

c) Values of damage during each cycle.

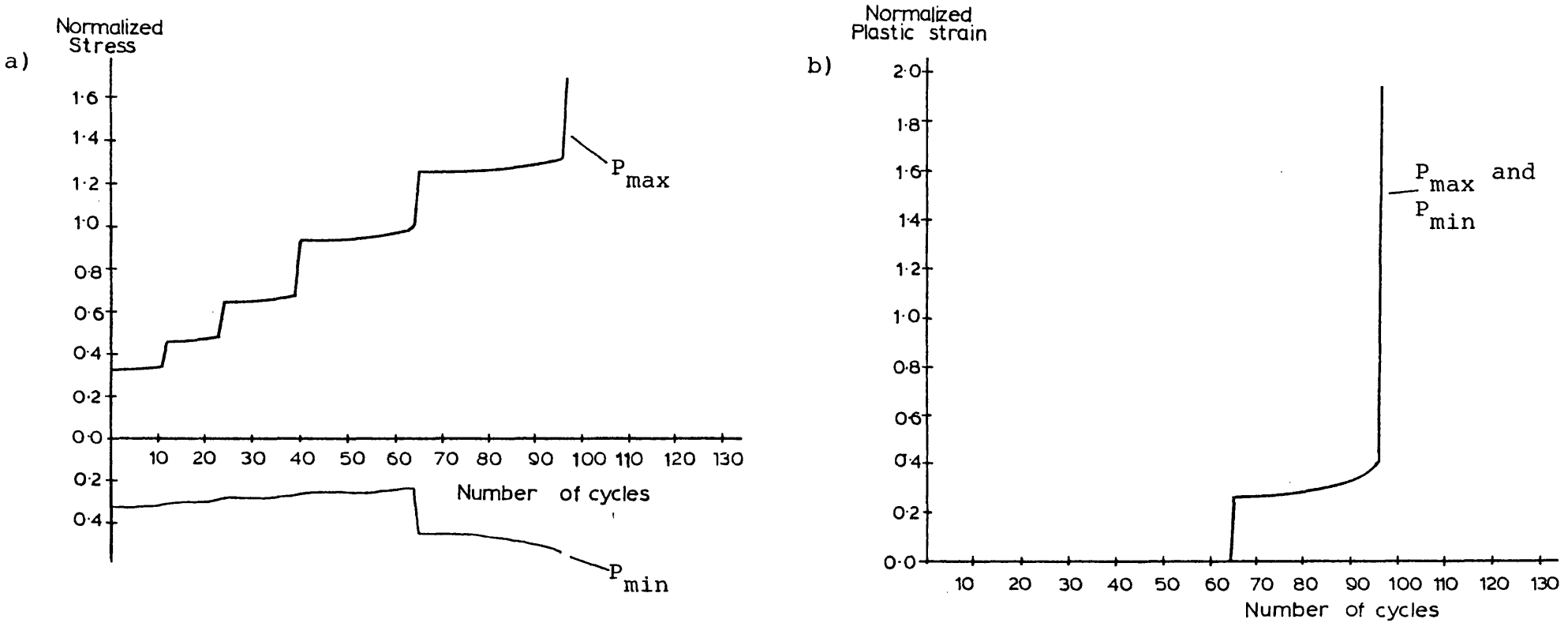

Figure 3.6: Graphs of response of bar 6 of multibar structure under a symmetric cyclic load with damage (p = 25).

a) Stress values at P_{max} and P_{min}.

b) Plastic strain values at P_{max} and P_{min} (in this case they coincide).

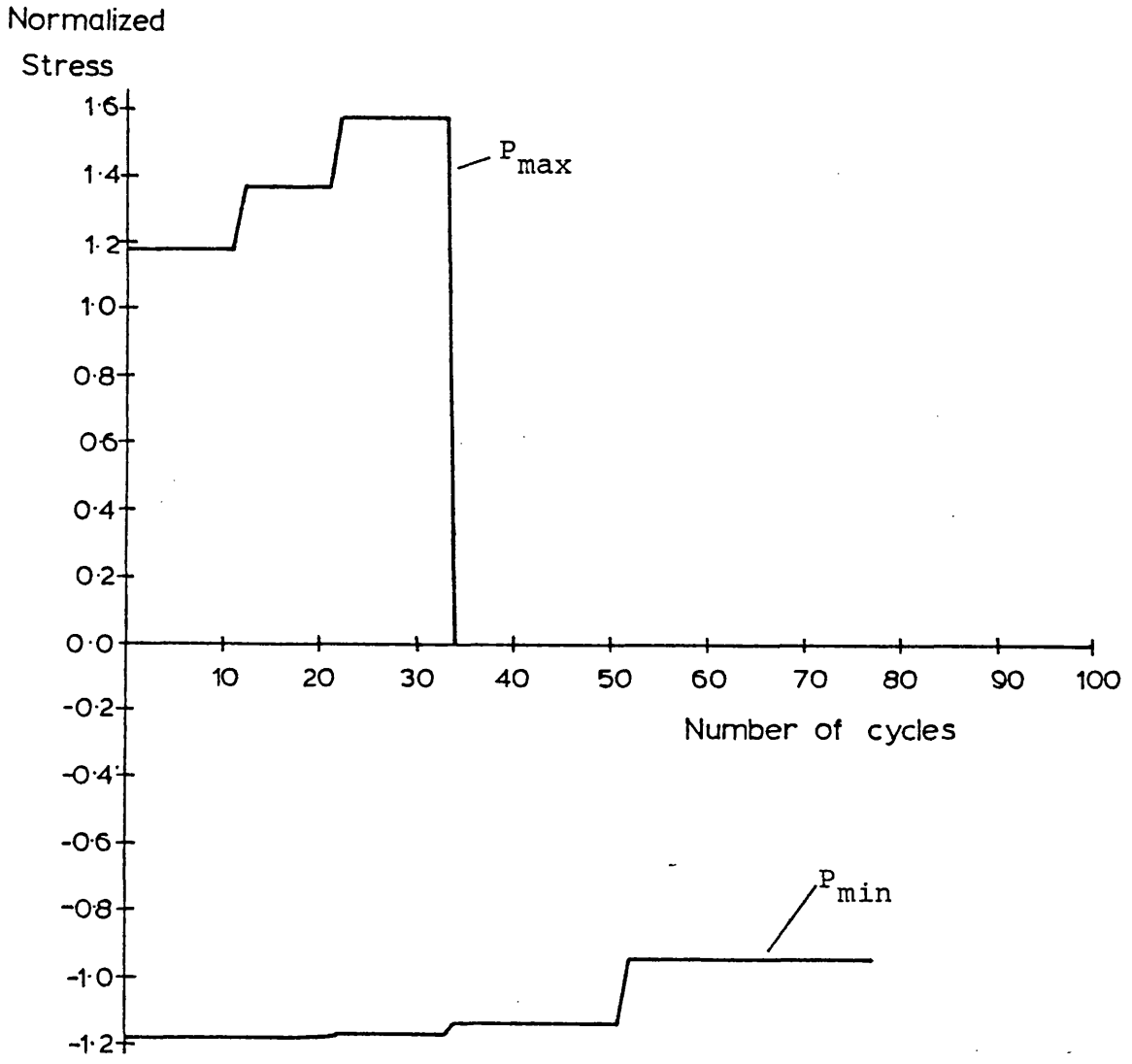

Figure 3.7: Stress reponse in bar 3 at P_{max} and P_{min} with negligible damage growth (p = 2500).

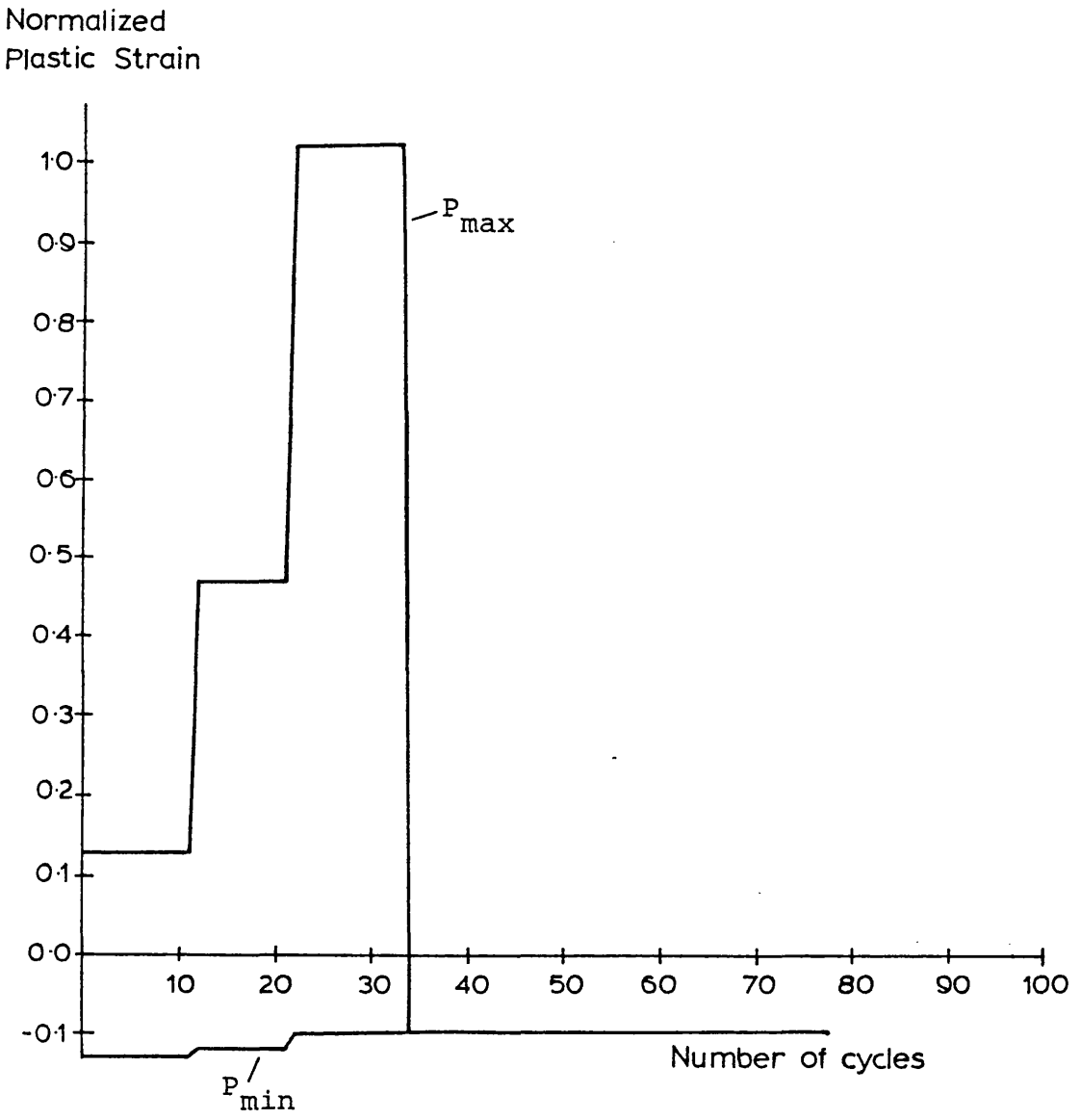

Figure 3.8: Plastic strain in bar 3 at P_{max} and P_{min} with negligible damage growth (p = 2500).

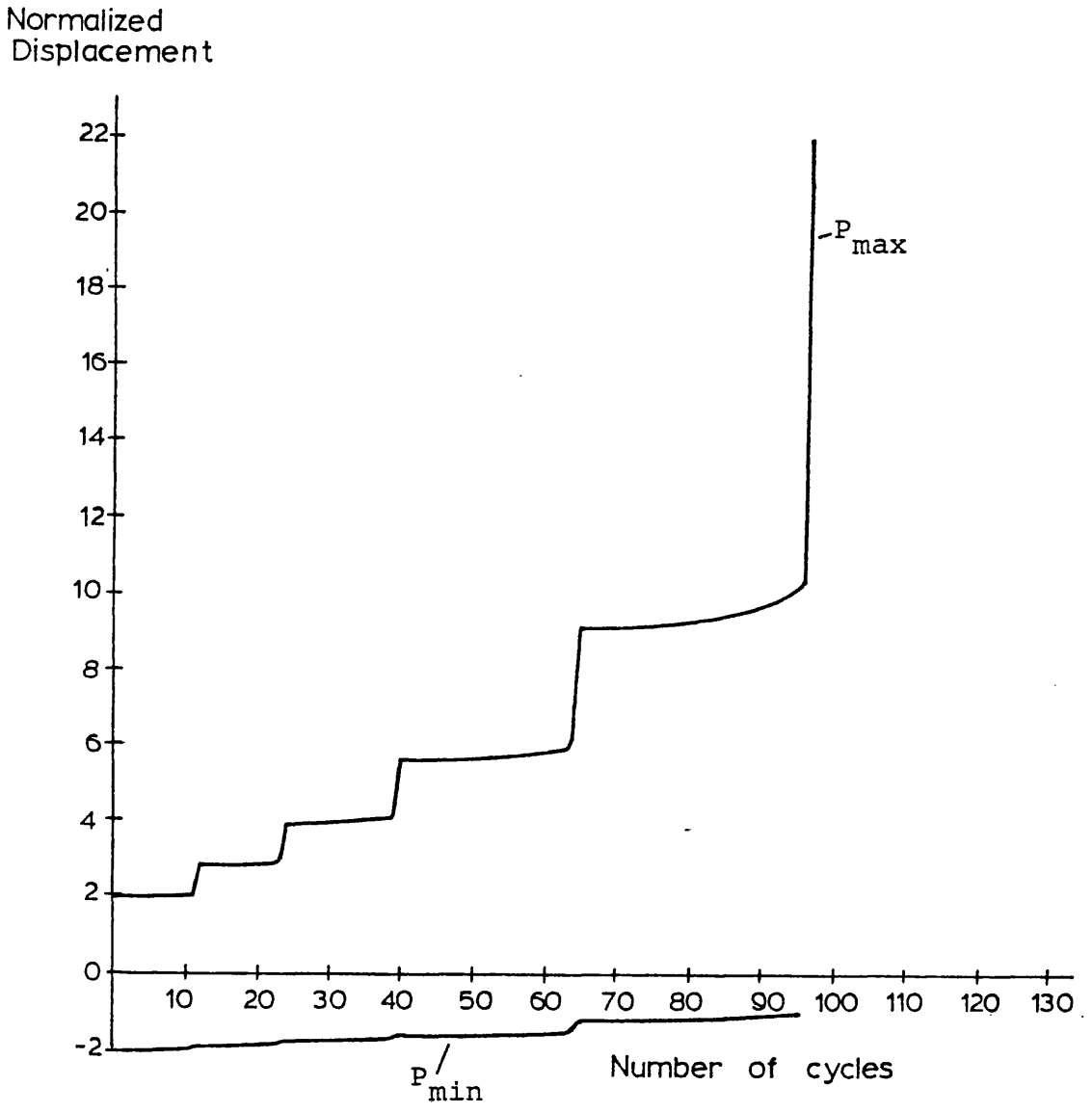

Figure 3.9: Displacement of block in multibar structure at P_{max} and P_{min} with damage (p = 25).

CHAPTER 4

A NON-LINEAR KINEMATIC HARDENING RULE AND DAMAGE EVOLUTION LAW AND THEIR PROPERTIES

4.1 Introduction

The study in Chapter 3 showed that stress redistribution due to the growth of damage can be an important factor in the endurance of structural components subject to fatigue. However, the constitutive model had several undesirable properties. These were discussed in the Conclusions to Chapter 3. The constitutive model studied in this chapter is based on the non-linear kinematic hardening rule, due originally to Armstrong and Frederick (1966), and possesses better properties than the power law model used in Chapter 3. Some of these properties are demonstrated in this chapter, and a method of modelling the effect of damage on the cyclic plastic behaviour of metals is proposed.

The law of damage evolution used in Chapter 3 also had undesirable properties. A more sophisticated law which has been proposed by Chaboche (1978) is introduced and discussed in this chapter. This law is capable of taking into account many of the important factors which affect fatigue life such as mean stress and fatigue limit. However, unlike the law in Chapter 3 it is not easy to convert the law, which is expressed in terms of stress, to one expressed in terms of strain and thus to employ data gathered under strain control to provide the material constants required to make it relevant to real metals.

4.2 The Non-linear Kinematic Hardening Rule and its Properties

4.2.1 Introduction

This model is attributed first of all to Armstrong and Frederick (1966), but has been developed and used extensively by Lemaitre and Chaboche (1985). A pictorial description of the model can be given, Fig. 4.1, in terms of surfaces in deviatoric stress space; the model in its most basic form consists of two surfaces; a yield surface and a limit surface.

The outer limit surface remains fixed and the same size. The inner yield surface moves with changes in plastic strain according to

$$d\underline{\alpha} = \frac{2}{3} C \, d\underline{\eta} - \gamma \, \underline{\alpha} \, dp, \qquad (4.1)$$

where C and γ are material constants and p is the effective plastic strain. It is not obvious that (4.1) leads to the two surface model, but by using the postulates of consistency and the associated flow rule it can be shown that

$$d\underline{\alpha} = \gamma (\underline{\sigma}'_L - \underline{\sigma}') \, dp, \qquad (4.2)$$

Where $'$ denotes deviator and $\underline{\sigma}'_L$ is the point on the limit surface at which the normal is parallel to the normal to the yield surface at $\underline{\sigma}'$. Thus, the motion of the yield surface is along the line joining $\underline{\sigma}_L$ and $\underline{\sigma}$. It can also be shown that the limit surface is given by

$$J_2\ (\underline{\sigma}) = \sigma_y + \frac{C}{\gamma} \quad , \tag{4.3}$$

where J_2 is the 2nd tensor invariant. In the case of the Von Mises yield surface, the hardening modulus is

$$h = C - \frac{3\ \gamma}{2\ \sigma_y}\ \underline{\alpha} : (\underline{\sigma}' - \underline{\alpha}') \quad , \tag{4.4}$$

which gives the model its non-linear characteristics. Some of the properties of the model can now be illustrated for the uni-axial case.

4.2.2 Uni-axial Form of Model

The yield surface has the form

$$f = (\sigma - \alpha)^2 - \sigma_y^2 = 0 \quad . \tag{4.5}$$

In one dimension, the hardening rule (4.1) becomes

$$d\alpha = C d\eta - \gamma \alpha |\ d\eta\ | \tag{4.6}$$

When yielding occurs, let

$$\mu = \text{sign}\ (\sigma - \alpha) \ . \tag{4.7}$$

From this it can be seen that

$$\text{sign}\ (d\eta) = \text{sign}\ (\sigma - \alpha) = \mu \tag{4.8}$$

and hence,

$$|d\eta| = \mu d\eta \tag{4.9}$$

The consistency condition gives

$$df = \frac{\partial f}{\partial \sigma} (d\sigma - d\alpha) = 0 , \qquad (4.10)$$

which implies $d\sigma = d\alpha$. Equation (4.6) can be integrated explicitly for one half cycle beginning at $\eta = \eta_0$ and $\alpha = \alpha_0$ to give the following expression for η and α during that half cycle:

$$\ell n \left[\frac{C - \gamma\mu\alpha_0}{C - \gamma\mu\alpha} \right] = \gamma\mu(\eta - \eta_0), \qquad (4.11)$$

and hence

$$\eta = \eta_0 + \frac{1}{\gamma\mu} \ell n \left[\frac{C - \gamma\mu\alpha_0}{C - \gamma\mu\alpha} \right] \qquad (4.12)$$

From (4.11) it can be shown that

$$\alpha = \frac{C}{\gamma\mu} [1 - \Lambda] + \alpha_0\Lambda \qquad (4.13)$$

where $\Lambda = \exp[-\gamma\mu (\eta - \eta_0)]$. Given the location of the centre of the yield surface to be

$$\alpha = \sigma - \mu\sigma_y ,$$

then

$$\sigma = \frac{C}{\gamma\mu} [1-\Lambda] + \alpha_0\Lambda + \mu\sigma_y \qquad (4.14)$$

Thus, as $\eta \to \infty$ then $\alpha \to \frac{C}{\gamma\mu}$, which defines the limit surface. It should also be noted that the hardening modulus

$$\frac{d\alpha}{d\eta} = C - \gamma\alpha\mu , \qquad (4.15)$$

which from (4.13) becomes:

$$\frac{d\alpha}{d\eta} = [C + \gamma\mu\alpha_0]\Lambda \qquad (4.16)$$

is finite when $\eta = \eta_0$ (i.e. when first yield occurs during a half cycle), so that the first derivative of the stress-strain curve is not continuous at this point.

An example of a stress-strain loop is shown in Fig. 4.2, which is calculated from data for 316 stainless steel.

4.2.3 Relationship between Plastic Strain Range and Stress Range for Stabilized Stress-strain Cycles

The relationship between plastic strain range $\Delta\eta$ and stress range is best derived in terms of α. Let α_{max} be the value of α at the top of a cycle and α_{min} be the value at the bottom, and similarly for η_{max} and η_{min}. The following expression is obtained from (4.13) with $\mu = 1$:

$$\alpha_{max} = \frac{C}{\gamma}(1-\Lambda) + \alpha_{min}\Lambda \qquad (4.17)$$

where $\Lambda = \exp[-\gamma(\eta_{max}-\eta_{min})]$. Similarly

$$\alpha_{min} = -\frac{C}{\gamma}(1-\Lambda) + \alpha_{max}\Lambda \qquad (4.18)$$

Subtraction of (4.18) from (4.17) gives

$$\alpha_{max}-\alpha_{min} = \frac{2C}{\gamma}\left[\frac{1-\Lambda}{1+\Lambda}\right] \qquad (4.19)$$

Since $\alpha_{max} - \alpha_{min} = \sigma_{max} - \sigma_{min} - \sigma_y - \sigma_y = \Delta\sigma - 2\sigma_y$, it can be shown, after some manipulation, that

$$\frac{\Delta\sigma}{2} = \frac{C}{\gamma} \tanh\left[\gamma \frac{\Delta\eta}{2}\right] + \sigma_y \qquad (4.20)$$

4.2.4 Plastic Strain Increment due to Ratchetting Caused by Mean Stress

Suppose that there is a non-zero mean stress $\bar{\alpha} = (\alpha_{max} + \alpha_{min})/2 = \bar{\sigma}$.
Under load controlled cycling this leads to ratchetting or unbounded straining because the distance between α_{max} and its upper limiting value C/γ is different to the distance between α_{min} and its lower limiting value $-C/\gamma$. The ratchet strain can be calculated as follows. Equation (4.12) with $\mu = 1$ gives:

$$\eta_{max} = \frac{1}{\gamma} \ln\left[\frac{C-\gamma\alpha_{min}}{C-\gamma\alpha_{max}}\right] + \eta_{min} \qquad (4.21)$$

and, with $\mu = -1$,

$$\eta_{min} = \frac{-1}{\gamma} \ln\left[\frac{C+\gamma\alpha_{max}}{C+\gamma\alpha_{min}}\right] + \eta_{max} \qquad (4.22)$$

Substitution for η_{min} in (4.21) using (4.22) gives, over one cycle,

$$\eta_{max}^{(2)} = \frac{1}{\gamma} \ln\left[\frac{C-\gamma\alpha_{min}}{C-\gamma\alpha_{max}}\right] + \frac{1}{\gamma} \ln\left[\frac{C+\gamma\alpha_{min}}{C+\gamma\alpha_{max}}\right] + \eta_{max}^{(1)}$$

So that

$$\delta\eta = \eta_{max}^{(2)} - \eta_{max}^{(1)} = \frac{1}{\gamma} \ln\left[\frac{(C/\gamma)^2 - \alpha_{min}^2}{(C/\gamma)^2 - \alpha_{max}^2}\right] \qquad (4.23)$$

or in terms of σ,

$$\delta\eta = \frac{1}{\gamma} \ln\left[\frac{(C/\gamma)^2 - (\sigma_{min} + \sigma_y)^2}{(C/\gamma)^2 - (\sigma_{max} - \sigma_y)^2}\right] \qquad (4.24)$$

It can be seen that if $\bar{\alpha} = 0$ which implies $\alpha_{min} = -\alpha_{max}$ then (4.23) reduces to $\delta\eta = 0$.

4.2.5 Mean Stress Relaxation under Constant Strain Cycling

Now consider a general mean plastic strain $\bar{\eta}$, imposed by plastic strain controlled cycling between η_{max} and η_{min}. Using (4.13) gives, for the upward half cycle,

$$\alpha_{max} = \frac{C}{\gamma}\left[1-e^{-\gamma(\eta_{max}-\eta_{min})}\right] + \alpha_{min}\, e^{-\gamma(\eta_{max}-\eta_{min})}$$

or, in terms of Λ,

$$\alpha_{max} = \frac{C}{\gamma}[1-\Lambda] + \alpha_{min}\,\Lambda \qquad (4.25)$$

Similarly, for the other half cycle,

$$\alpha_{min} = \frac{-C}{\gamma}[1-\Lambda] + \alpha_{max}\,\Lambda \qquad (4.26)$$

Substitution of α_{min} from (4.26) into (4.25) yields, over a whole cycle,

$$\alpha_{max}^{(2)} = \frac{C}{\gamma}[1-\Lambda]^2 + \alpha_{max}^{(1)}\,\Lambda^2 \qquad (4.27)$$

and similarly,

$$\alpha_{min}^{(2)} = \frac{-C}{\gamma}\,[1-\Lambda]^2 + \alpha_{min}^{(1)}\,\Lambda^2 \qquad (4.28)$$

Addition of (4.27) and (4.28) gives the following relationships between mean stresses:

$$\alpha_{max}^{(2)} + \alpha_{min}^{(2)} = \Lambda^2\,(\alpha_{max}^{(1)} + \alpha_{min}^{(1)})$$

$$\bar{\alpha}^{(2)} = \Lambda^2\,\bar{\alpha}^{(1)}\,, \qquad (4.29)$$

or $\quad \bar{\sigma}^{(2)} = \Lambda^2\,\bar{\sigma}^{(1)}\,.$

4.2.6 Some Examples of Ratchetting and Relaxation

The results obtained above in sub-sections 4.2.2-4.2.5 are in terms of α (or σ) and η. If load cycling is stress or plastic strain controlled then (4.12) and (4.14) can be used to calculate the predicted response of the material, and the results of sub-sections 4.2.3-4.2.5 will be valid. However, if (4.14) is rewritten in terms of total strain ε, and σ, then the following expression is obtained:

$$\sigma = \frac{C}{\mu\gamma}\,[1-\Lambda] + \alpha_0\,\Lambda + \mu\,\sigma_y \qquad (4.30)$$

where $\quad \Lambda = \exp\{-\mu\gamma(\varepsilon - \sigma/E - \eta_0)\}$

It is not possible to solve this explicitly for σ and so the results of sub-sections 4.2.3-4.2.5 cannot be derived in terms of σ and ε. However, (4.30) may be solved numerically and thus the results for total strain controlled load cycling may be obtained by

numerical calculation. A computer program was written which used (4.12), (4.14) and (4.30) to study the stress-strain response of the model under various types of loading. The values used for various constants were for 316 stainless steel and they are listed in Table 4.1. Figure 4.3 shows an example of ratchetting under stress controlled cyclic loading, and Table 4.2 gives the values of stress and strain at the top of each cycle. The numerically predicted ratchetting rate is given in the last column of the table. The rate calculated from (4.24) is $\delta\varepsilon = 2.22552 \times 10^{3}$ absolute strain/cycle. Figure 4.4 and Table 4.3 give the results of strain controlled cycling with limits of 0.001 and -0.0002. The 4th column of the table shows that any mean stress does decay and the ratios in the last column show that the decay is exponential. However, the theoretical rates of decay given for plastic strain control by (4.29), and shown in column 3 of the table, do not compare well with the numerically derived values for total strain control given in the last column. However, it may be shown that if the calculations are carried out with the common assumption of plastic strain controlled cycling, then the theoretical and numerically derived results are identical.

Figure 4.5 shows the hysteresis loop obtained for strain controlled cycling with symmetric limits (i.e. $\varepsilon_{min} = -\varepsilon_{max}$). It can be seen from the loops shown that mean stress relaxation takes place. This illustrates the fact that, for the non-linear kinematic hardening model, symmetric limits in the control variable do not imply

that other variables will have symmetric limits. This can also be seen in Fig. 4.2 where the resulting limits in strain are not symmetric. This asymmetry in limits depends on the initial values of α_0 and η_0. For instance, under stress control with zero mean, symmetric limits in plastic strain are obtained when

$$\eta_0 = \frac{1}{2\gamma} \ln \left[\frac{L^2 - (\alpha_{max}^{(1)})^2}{(L - \alpha_0)^2} \right],$$

where $\alpha_{max}^{(1)}$ is the first maximum value of α and $L = C/\gamma$.

4.3 Modelling of Cyclic Plastic Deformation and Damage in Metals Using the Non-linear Kinematic Hardening Rule

4.3.1 Material Behaviour Under Cyclic Loading

In a strain controlled cyclic loading test on a uniaxial specimen, it is observed that the load in tension decreases during the test and eventually becomes zero when the specimen fails. Figure 4.6 shows an idealized stress profile for a uniaxial specimen under strain control. In the figure, the behaviour is simplified by assuming that the stabilized cyclic state is achieved immediately and that there is no initial cyclic hardening or softening. In addition, the stress response in compression is assumed to be constant throughout the lifetime of the specimen. In tension, the decreasing values of stress can be written as $\sigma (1-\psi)$ where σ is the maximum stress of the stabilized cycle and ψ is the damage. The evolution of the damage gives the shape of the upper curve in Fig. 4.6.

This idealized behaviour is the idea which inspired

the model described below. However, the model does not match this ideal exactly, but this is not a serious deficiency since a real metal specimen does not behave in this way and the model reproduces some of the essential features of real material behaviour quite well.

4.3.2 Incorporation of Damage into the Constitutive Laws

In order to follow the evolution of a structural component under cyclic loading, it is necessary to incorporate damage into the constitutive equations to model material weakening, and, in addition, lead naturally to the situation where failure takes place, that is, a state in which the material is incapable of transmitting tensile stress, but is capable of sustaining compressive stress. Damage is usually included into a model by making the hypothesis that the strain is computed from the constitutive equations by replacing σ by $\sigma/(1-\psi)$. Thus, suppose that for undamaged material

$$\varepsilon = F(\sigma) \quad , \tag{4.31}$$

then for damaged material

$$\varepsilon = F\left[\frac{\sigma}{1-\psi}\right] \tag{4.32}$$

For instance, in a damaged linear elastic material, the strain is given by

$$\varepsilon = \frac{\sigma}{(1-\psi)E} \tag{4.33}$$

However, employing this hypothesis directly into the equations for the cyclic state of the material does not reproduce the stress envelope in Fig. 4.6 since the stress in compression would also decay to zero as damage increased to unity. Hence, damage must be included in such a way that only the maximum stress is affected by it. Such a model would provide a consistent link between the damaged and failed states.

In the failed state the material may be thought of as being fissured. A uniaxial model of fissured material can be constructed in the following manner. In compression the material behaves as if it were undamaged. In tension it behaves completely elastically but with a very small value of Young's modulus. This is an approximate model of the behaviour of a no-tension material: the residual strength of the material in tension allows the point at which the stress becomes compressive to be readily determined.

The model of damaged material given in Chapter 3 was relatively crude and led to certain undesirable predictions, but was very simple to use. In that case, damage did not affect elastic behaviour, and only affected the non-linear part of the stress-strain curve. Also, the damage was non-zero in the equations only for the upward portion of the loop (from compression to tension). Since the non-zero damage flattened the non-linear curve, the strain range on the upward part was greater than that on the downward portion (assuming stress-cycling). This leads to ratchetting under stress control when damage is non-zero, and the ratchetting

rate increases with damage.

Further attempts at modelling the effects of damage were made by assuming that damage only acts in tension (similar to the model for fissured material). That is: any non-zero damage is present in the constitutive equation when the stress is greater than zero, but otherwise damage is effectively zero. Under certain conditions, this is in fact equivalent to the previous model under stress-control. With certain types of damage evolution this model predicted unrealistically large ratchetting rates. These difficulties are not overcome by allowing damage to act on Young's modulus or by replacing the original constitutive law by the non-linear kinematic hardening rule. Under strain control these models predict that the mean stress becomes increasingly compressive, and that the minimum stress decreases in an unbounded fashion.

4.3.3 A Model of the Effects of Damage on the Stress-strain Loop

The stress-strain hysteresis loop can be divided into two parts, the upward part beginning at minimum stress and strain and ending at the maximum (ABC in Fig. 4.7), and the downward part beginning at the maximum and finishing back at the minimum (CDA in Fig. 4.7). In the following, the value of the damage in the constitutive equations at any given point will be called the acting damage at that point.

Suppose the damage has a value ψ_0, which remains constant during a cyle of load from minimum to minimum.

In the constitutive equations at the minimum stress-strain point of the cycle, the acting damage is assumed to be zero. This remains so until the stress reaches zero where the acting damage is set to ψ_0. Since increasing the damage makes the material softer, this will have the effect of putting a corner in the stress-strain curve as shown in Fig. 4.8 at point B. The acting damage remains equal to ψ_0 until point D on the downward part is reached at which the total strain of the material is equal to the strain at point B. At D the acting damage is set to zero and this has the opposite effect to the process at B and produces a downturn in the curve which gives the tail around the minimum. This model will form the basis of the treatment presented in later sections.

4.3.4 Implementation for the Non-linear Kinematic Hardening Model

The model proposed above can be represented using the equations discussed earlier for the non-linear kinematic hardening rule. When damage is included in this model, it is assumed that the stress σ is replaced by the efffective stress $\sigma/(1-\psi)$ in the constitutive equations. It is further assumed that α is replaced by its effective value, $\alpha/(1-\psi)$. Thus (4.12) is rewritten:

$$\eta = \eta_0 + \frac{1}{\gamma\mu} \ln \left[\frac{\mu L - (\alpha_0/(1-\psi))}{\mu L - (\alpha/(1-\psi))} \right] \qquad (4.34)$$

where $L = C/\gamma$.

The points at which acting damage changes from one value to another must be treated carefully. There

are four cases and each will now be treated separately, although they are related. Suppose in each of the following that the acting damage is changing from ψ to ψ' at a stress of σ and a total strain of ε.

CASE (i) Elastic-Elastic

Suppose that $|\sigma - \alpha_0| < (1-\psi)\sigma_y$ and also that $|\sigma - \alpha_0| < (1-\psi')\sigma_y$, i.e. that before the damage change the material is elastic and that afterwards the material remains in that state assuming the value of α is constant. Afterwards the total strain is

$$\varepsilon = \frac{\sigma}{(1-\psi')E} + \eta' \quad , \tag{4.35}$$

and so the plastic strain must be redefined as

$$\eta' = \varepsilon - \frac{\sigma}{(1-\psi')E} \tag{4.36}$$

and $\eta_0 = \eta'$. (4.37)

CASE (ii) Elastic-Plastic

Before the damage change the material has not yielded but afterwards it yields. This can only occur if the acting damage increases during the change, thus decreasing the size of the yield surface:

Before $|\sigma - \alpha_0| < (1-\psi)\sigma_y$

After $|\sigma - \alpha_0| > (1-\psi')\sigma_y$.

Again, plastic strain must be redefined as in (4.36). The equation of the curve is now defined using

(4.34). In (4.34) it is assumed that α_0 remains constant, but this entails a change in η_0. Using (4.34) and (4.36) the following is obtained

$$\eta_0 = \varepsilon - \frac{\sigma}{(1-\psi')E} - \frac{1}{\gamma\mu} \ln \left[\frac{\mu L - (\alpha_0/(1-\psi'))}{\mu L - (\alpha'/(1-\psi'))} \right] \quad (4.38)$$

where α' is the new value of α required to ensure consistency is satisfied:

$$\alpha' = \sigma - \mu(1-\psi')\sigma_y \quad (4.39)$$

CASE (iii) Plastic-Elastic

This can only occur when the damage decreases thus increasing the size of the yield surface:

$$\text{Before} \quad |\sigma - \alpha_0| \geq (1-\psi)\sigma_y$$
$$\text{After} \quad |\sigma - \alpha_0| \leq (1-\psi')\sigma_y .$$

In this case α remains unchanged at $(\sigma - \mu(1-\psi)\sigma_y)$, η becomes η' according to (4.36) and η_0 is set to the value given in (4.38).

CASE (iv) Plastic-Plastic

In this final case we have that:

$$\text{Before} \quad |\sigma - \alpha_0| \geq (1-\psi)\sigma_y$$
$$\text{After} \quad |\sigma - \alpha_0| > (1-\psi')\sigma_y .$$

η' is now defined by (4.36), η_0 by (4.38) in which α' is defined by (4.39).

4.3.5 Predicted Stress-strain Curves

A series of these curves for different values of damage is shown in Figs. 4.9 to 4.13. These curves are for strain control between ±0.02 strain and the values of the constants are given in Table 4.1. It can be seen from the curves that the expected fall in the maximum stress as damage increases is reproduced by the model. The minimum stress remains in compression but rises slightly as damage increases. This does not follow the ideal behaviour as was proposed earlier and shown in Fig. 4.6. However, experimentally it is observed that the minimum stress does not remain constant and does in fact rise towards the end of a test (see for example, Raynor and Skelton, 1983). Comparison of the curves, for large damage, with curves taken from the last few cycles of an actual test (see Fig. 4.14) show that the qualitative material behaviour is reproduced very well.

4.3.6 An Incremental Formulation

In the multiaxial case it is not possible to integrate (4.1) to obtain an equation such as (4.13) which describes the stress strain state exactly. Normally (4.1) would be solved incrementally. This approach is also possible for the uniaxial equation (4.6) and this section compares the incremental approach with the one in sub-section 4.3.4.

If damage is ψ, then (4.6) becomes

$$\frac{d\alpha}{(1-\psi)} = C d\eta - \frac{\alpha}{1-\psi} |d\eta| \qquad (4.40)$$

Suppose the acting damage has just changed to ψ', then (4.40) gives the increments in α and η by:

$$\int_{\alpha}^{\alpha+\Delta\alpha} \frac{d\alpha}{C(1-\psi') - \mu\gamma\alpha} = \int_{\eta}^{\eta+\Delta\eta} d\eta \qquad (4.41)$$

where α and η are the values of α and η after the change in acting damage. This gives:

$$\Delta\eta = \frac{1}{\gamma\mu} \ln \left[\frac{\mu L - \alpha/(1-\psi')}{\mu L - (\alpha+\Delta\alpha)/(1-\psi')} \right] \qquad (4.42)$$

Using the previous formulation the following expression is obtained:

$$\Delta\eta = \eta_0 + \frac{1}{\mu\gamma} \ln \left[\frac{\mu L - \alpha_0/(1-\psi')}{\mu L - (\alpha+\Delta\alpha)/(1-\psi')} \right] - \eta \qquad (4.43)$$

If it is assumed that η is defined by (4.36) and α, if necessary by (4.39) then substitution for η_0 from (4.38), gives (4.42). Thus, the two approaches are equivalent provided the definitions of α and η at the damage change are the same.

4.4 Damage Evolution

The expression for damage evolution used here has been proposed by Chaboche (1978). The rate of growth of damage with respect to the number of cycles can be written (see Lemaitre and Chaboche, 1985).

$$\frac{\delta\psi}{\delta N} = [1-(1-\psi)^{\beta+1}]^{\alpha(\sigma_{max},\bar{\sigma})} \left[\frac{\sigma_{max} - \bar{\sigma}}{M(\bar{\sigma})(1-\psi)} \right]^{\beta} \qquad (4.44)$$

where

$$\alpha(\sigma_{max}, \bar{\sigma}) = 1\text{-}a \left\langle \frac{\sigma_{max} - \sigma_1^*(\bar{\sigma})}{\sigma_u - \sigma_{max}} \right\rangle \qquad (4.45)$$

$$\sigma_1^*(\bar{\sigma}) = \sigma_1 + (1\text{-}b\,\sigma_1)\,\bar{\sigma} \qquad (4.46)$$

$$M(\bar{\sigma}) = M_0(1\text{-}b\bar{\sigma}) \qquad (4.47)$$

a, M_0, β are coefficients dependent on temperature,

b is a temperature independent coefficient,

σ_u is the ultimate tensile strength,

σ_1 is the fatigue limit for zero mean stress,

σ_{max} is the maximum stress of a cycle, and

$\bar{\sigma}$ is the mean stress of a cycle.

The angle brackets are defined by $\langle x \rangle = H(x)\,x$, where H is the Heaviside function.

Equation (4.44) has been arrived at empirically to describe the effects of mean stress on the rate of damage growth. The coefficients can be obtained by finding α from experimental data. The fall in stress during a strain controlled load cycling test gives the rate of increase of damage, and this can be fitted to the expression (4.44) to give the value of a in α. If (4.44) is then integrated over the lifetime then it can be shown that:

$$N_f = \frac{1}{(\beta+1)(1-\alpha)} \left[\frac{\sigma_{max} - \bar{\sigma}}{M} \right]^{-\beta} \qquad (4.48)$$

From this the coefficients β and M can be found by fitting this relationship to graphs of Log σ against

Log N_f.

The first factor on the right hand side of (4.44) is to ensure that the hypothesis that the effective stress, $\sigma/(1-\psi)$, should be used in calculating the deformation from the constitutive equations is as accurate as possible. In other words, if the damage is measured from the load drop during a strain controlled test, then the form of that load drop is given by (4.44). The form of the function α given by (4.45) serves several purposes. The inclusion of the ultimate tensile strength is so that the failure of the specimen occurs on the first load up if this stress is attained, since α becomes unbounded if σ_{max} approaches σ_u. If $\sigma_{max} > \sigma_1^*$ then $\alpha < 1$ and damage grows from zero, and the lifetime is given by (4.48). If $\sigma_{max} \leqslant \sigma_1^*$ then $\alpha = 1$ and ψ only increases if $\psi > 0$ initially. That is, if $\psi = 0$ and $\alpha = 1$ then no damage cumulation occurs and life is unbounded. However, if $\psi > 0$ and $\alpha = 1$, then ψ increases and life is finite. Thus, for example, an initial overload nullifies the effect of a fatigue limit. These facts will be demonstrated in more detail in Chapter 5. Finally, since α is a function of σ_{max}, the damage cumulation is non-linear. The consequence of this is that Miner's Law (Miner, 1945) is not obeyed if this damage evolution law is used. This will be demonstrated in the case of creep/fatigue interaction in Chapter 6. The expression for a fatigue limit at different mean stresses (4.46) is based on the standard Goodman law. If b in (4.46) is replaced by $1/\sigma_u$ then the Goodman relationship results. (For

the Goodman law see, for example, Fuchs and Stephens, 1980).

4.5 Discussion

A constitutive model has been presented in this chapter which models the behaviour of metals better than the power law model used in Chapter 3. The model is based on the non-linear kinematic hardening rule which has a natural expression in the multiaxial case and which the constitutive model of Chapter 3 does not have. The uniaxial version of the model displays ratchetting and mean stress relaxation as demonstrated in this chapter, both of which are displayed by real materials but not by the model of Chapter 3.

A model of the effect of damage on cyclic plastic deformation has been proposed in this chapter. When damage is close to one, the model reproduces the shape of hysteresis loops of a specimen close to failure very well. In addition, it does not possess the undesirable properties of unbounded ratchetting rates and unboundedly decreasing mean stress which the method of Chapter 3 possessed.

The damage evolution law introduced in this chapter models some of the essential features of the fatigue behaviour of metals. These include the effect of a fatigue limit, mean stress and the ultimate tensile strength. The accumulation of damage is non-linear in a way that leads to a non-linear interaction between damage growth rates in tests where the loading is varied during the test. This is different to Miner's Law.

In the next chapter, Chapter 5, these models will be used to study again the behaviour of the multibar model used in Chapter 3.

C	30 000 MPa
γ	60
σ_y	300 MPa
E	196 000 MPa

Table 4.1 The values of the constants in the constitutive equations used for the examples in sub-sections 4.2.6 and 5.3.4. They are taken from the book by Lemaitre and Chaboche (1985) and are for 316 stainless steel at 20°C.

σ(MPa)	Cycle Number	ε (absolute)	$\delta\varepsilon$
500	1	1.1065×10^{-2}	
			$(\varepsilon_2 - \varepsilon_1 =)$ 0.2225×10^{-2}
500	2	1.3290×10^{-2}	
			$(\varepsilon_3 - \varepsilon_2 =)$ 0.2226×10^{-2}
500	3	1.5516×10^{-2}	

Table 4.2 Values of stress and strain at the top of successive cycles, and the value of the strain difference for stress cycling between +500 MPa -400 MPa. See Fig. 4.3.

i	Column 1	Column 2	Column 3	Column 4	Column 5
	Stress at top and bottom of successive cycles	Plastic strain at top and bottom of successive cycles	Value of Λ in (4.29) $\Lambda = \exp[\pm\gamma(\eta_1-\eta_2)]$ where η_1 is the value in column 2 on the line above and η_2 is the value in column 2 on the line below. This is the theoretical mean stress relaxation rate in terms of plastic strain	Mean stress, σ, σ is the average of the values on the lines above and below it in column 1	Actual relaxation rate. This is equal to the value in column 4 on the line above divided by the value in column 4 on the line below. It is the rate of relaxation over one half cycle and should be compared with the values on the line above in column 3
	σ_i	η_i	$\eta_i=\exp[\pm\gamma(\eta_{i-1}-\eta_{i+1})]$ sign chosen so that exponent is negative	$\bar{\sigma}_i=\frac{\sigma_{i-1}+\sigma_{i+1}}{2}$	Rate of relaxation $\Lambda_i=\bar{\sigma}_{i-1}/\bar{\sigma}_{i+1}$
1	481.969	7.5410×10^{-3}			
2			1.582	56.365	
3	-369.237	-1.161×10^{-4}			1.4970
4			1.6014	37.651	
5	444.540	7.7319×10^{-3}			1.5020
6			1.5891	25.068	
7	-394.404	1.23×10^{-5}			1.4986
8			1.5973	16.727	
9	427.859	7.8170×10^{-3}			1.5008
10			1.5918	11.145	
11	-405.568	6.9226×10^{-5}			1.4993
12			1.5954	7.4334	
13	420.435	7.8549×10^{-3}			1.5003
14			1.5930	4.9545	
15	-410.526	9.4521×10^{-5}			1.4997
16			1.5946	3.3038	
17	417.134	7.8718×10^{-3}			

Table 4.3 Numerical results corresponding to Fig. 4.4. Shows stress and plastic strains at the top and bottom of each cycle along with Λ in (4.29), mean stress and the ratio of consecutive mean stresses. Cycling was total strain controlled with limits 0.001, and -0.0002.

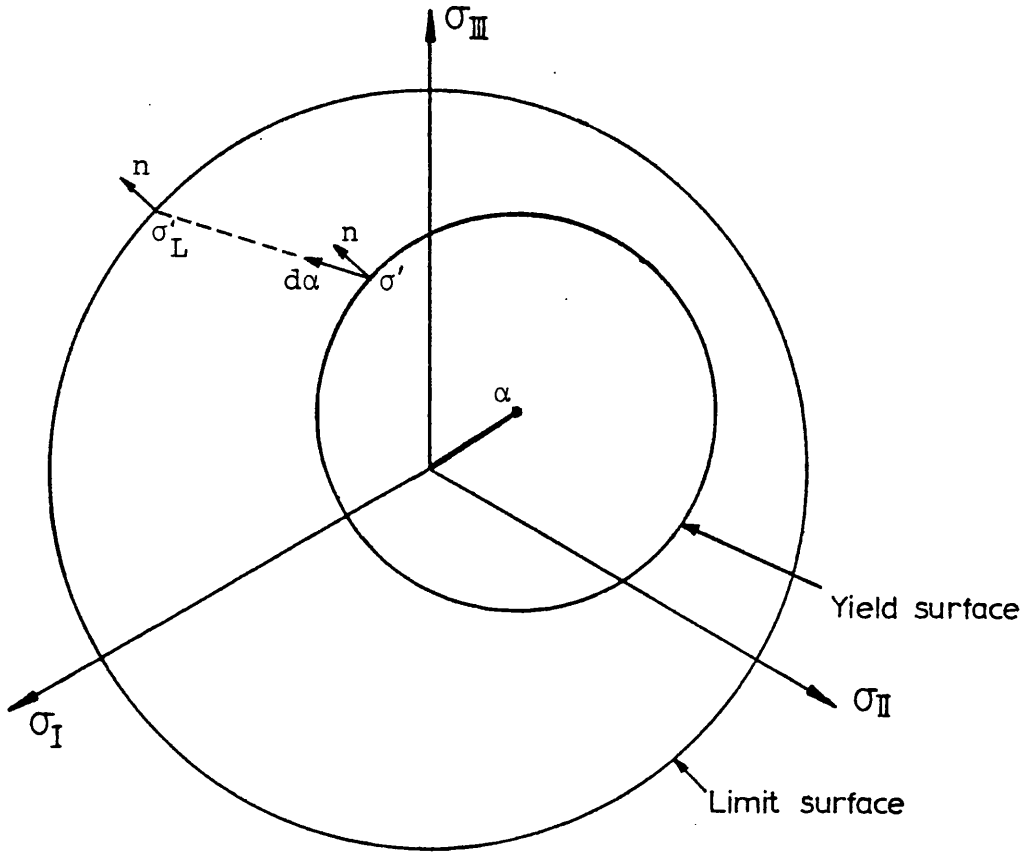

Figure 4.1: Non-linear kinematic hardening model - plastic yield and limit surfaces in the π-plane.

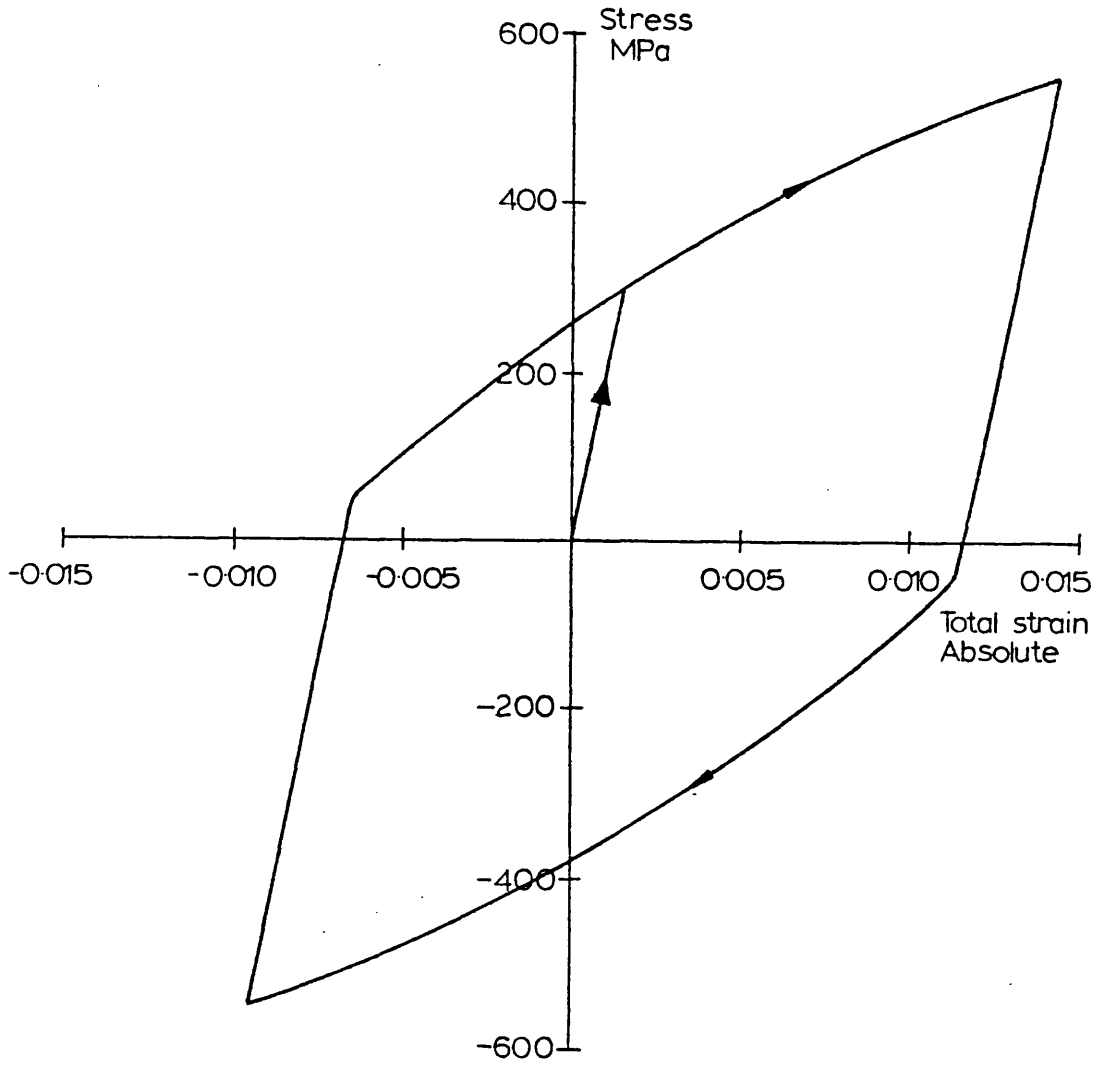

Figure 4.2: Example of predicted stress-strain response of 316 stainless steel at 20°C under stress controlled load cycling between the limits ±550 MPa.

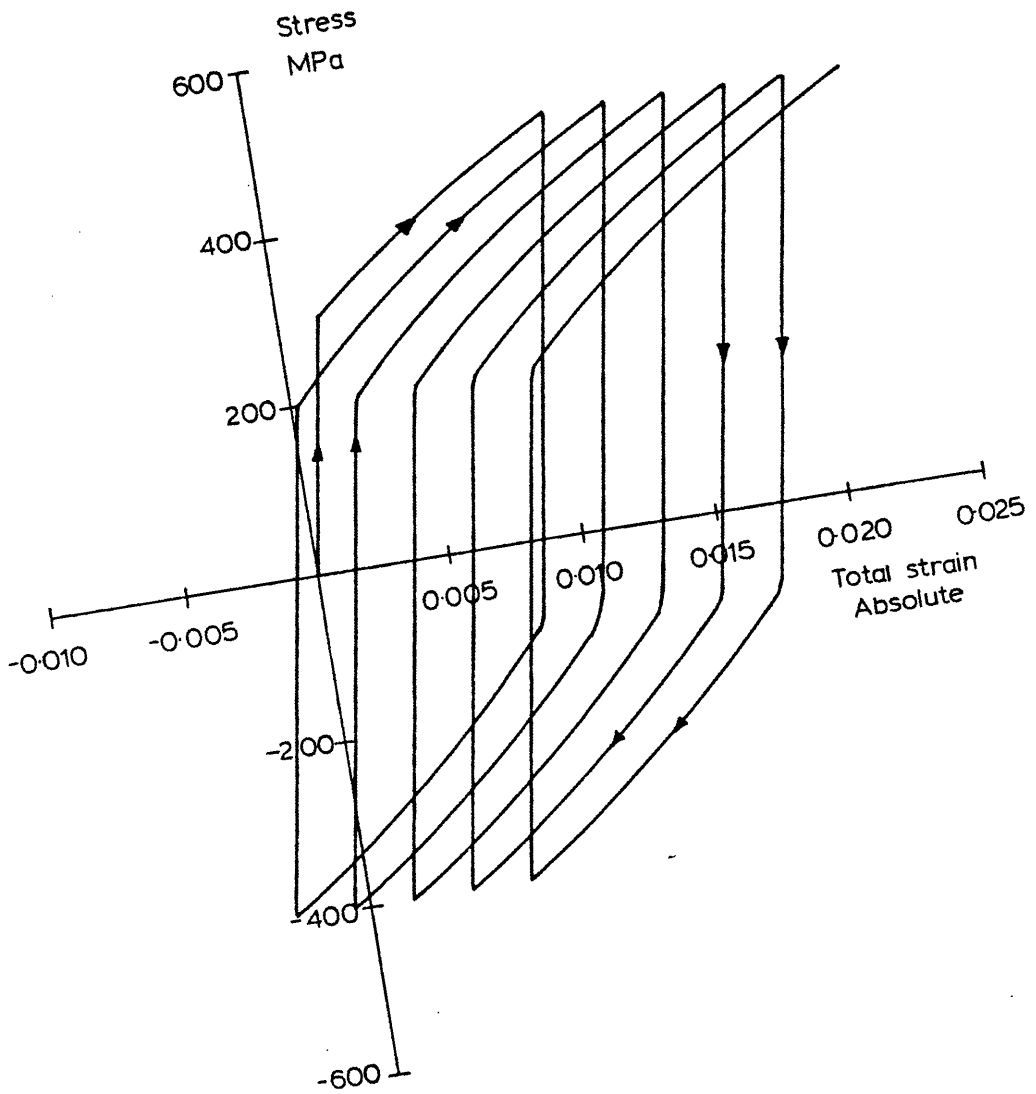

Figure 4.3: Stress controlled load cycling of 316 stainless steel exhibiting ratchetting.

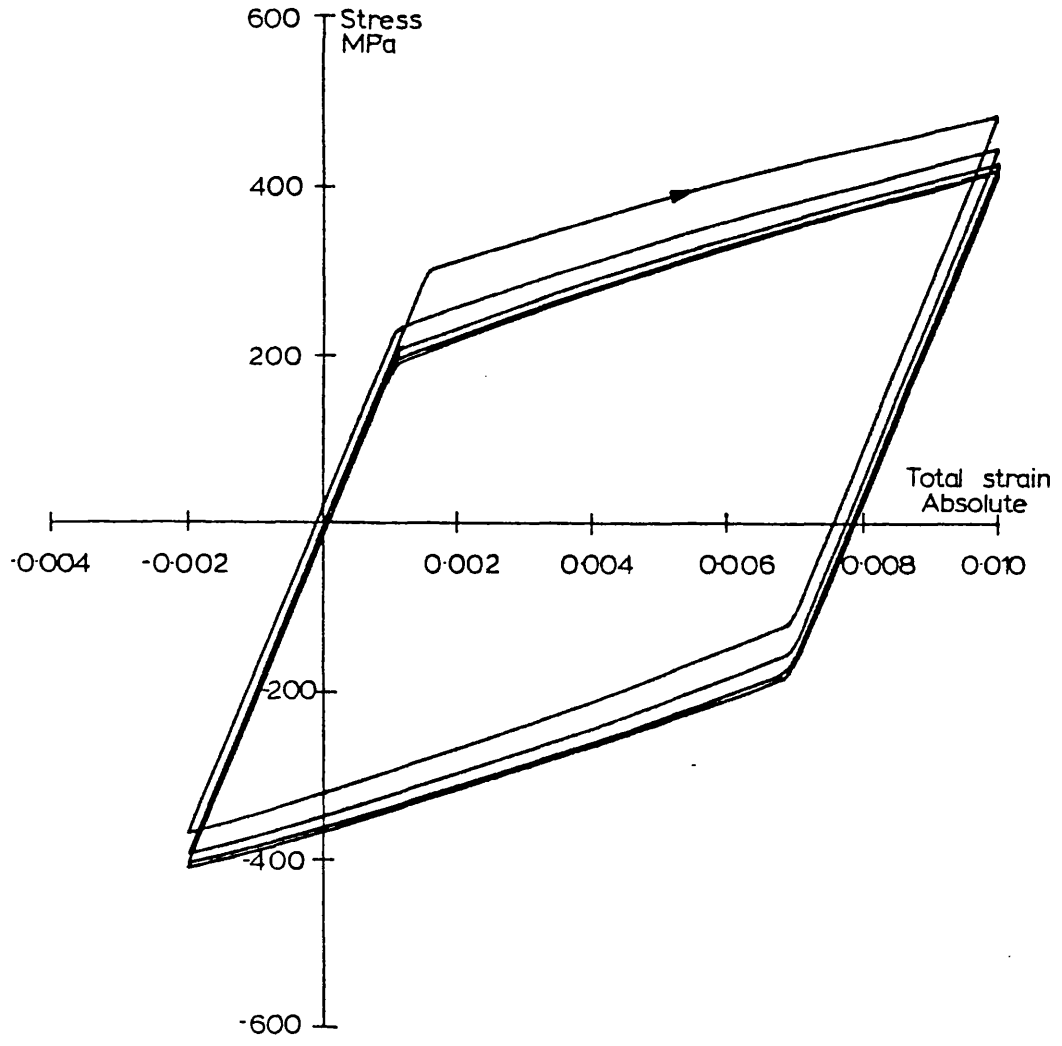

Figure 4.4: Total strain controlled cycling of 316 stainless steel exhibiting mean stress relaxation.

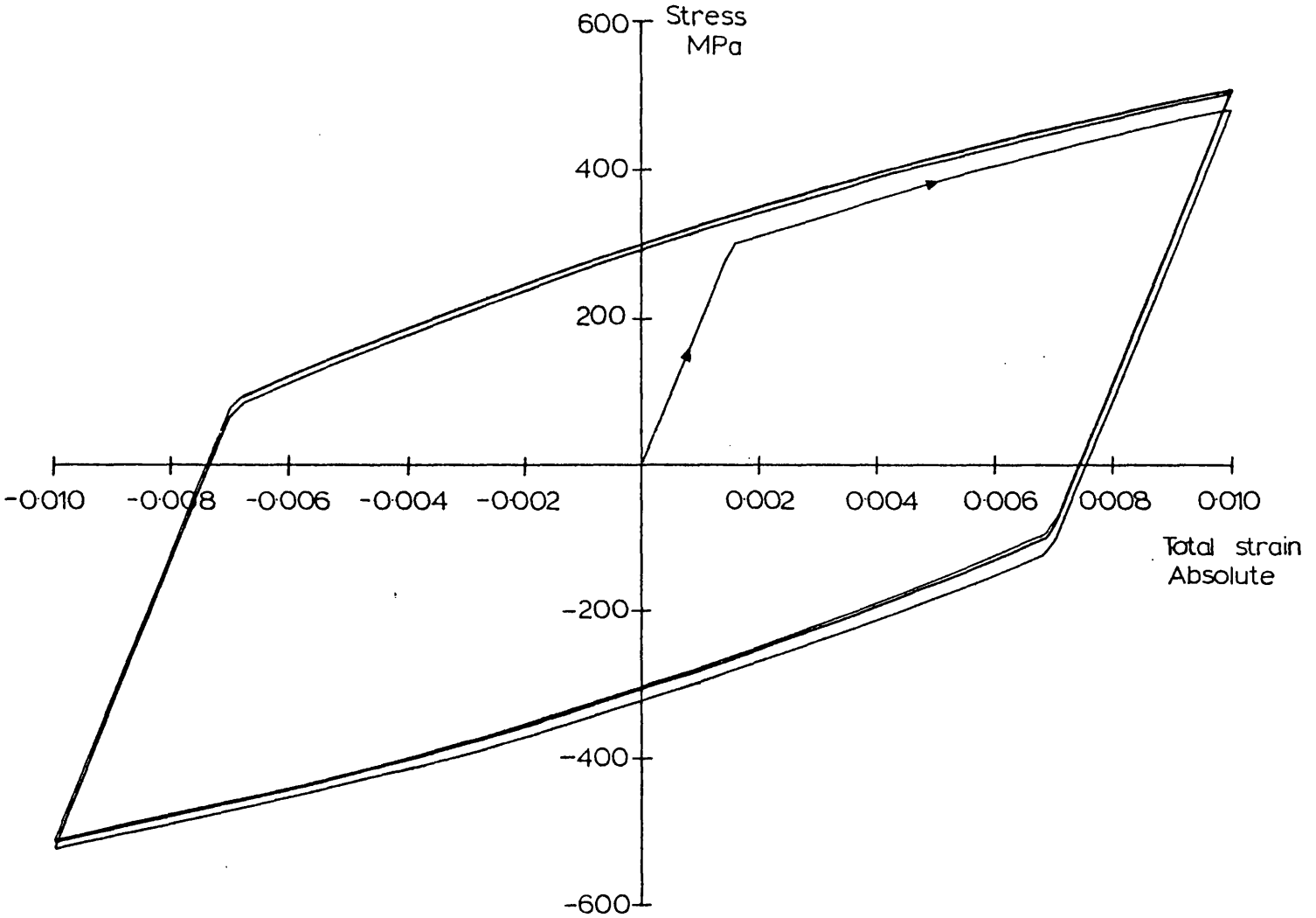

Figure 4.5: Example of predicted stress-strain response of 316 stainless steel at 20°C under strain controlled cycling between the limits ±0.01 .

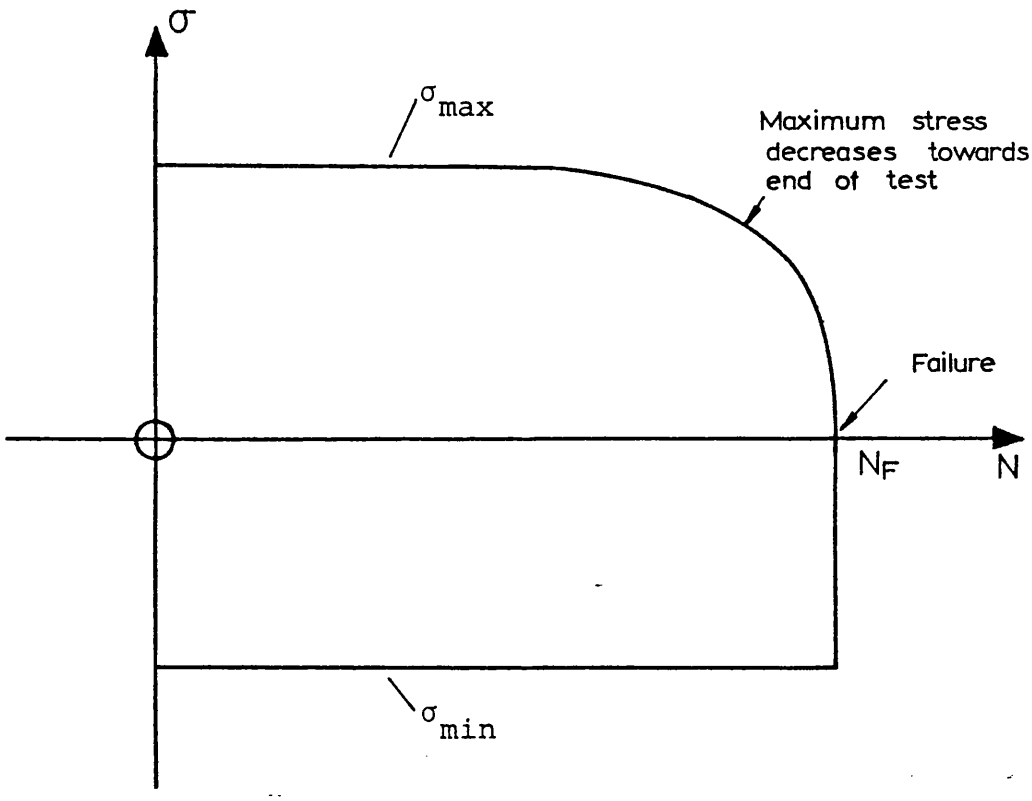

Figure 4.6: Stress response of uniaxial specimen under strain controlled cycling.

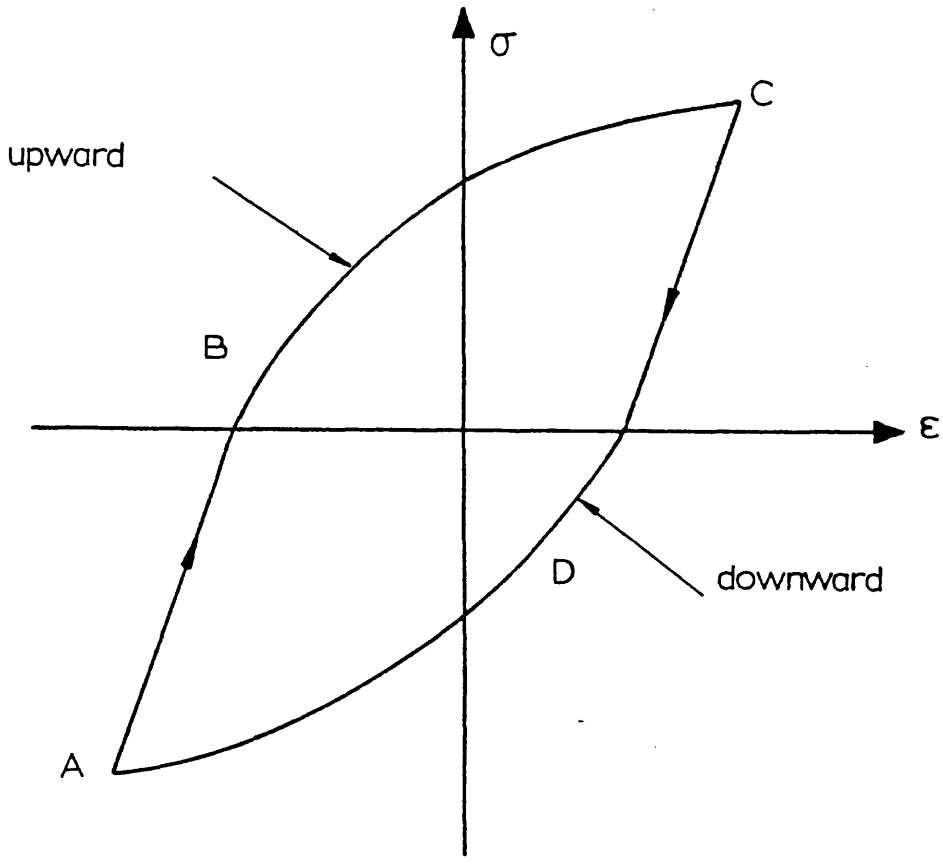

Figure 4.7: Typical stress-strain hysteresis loop.

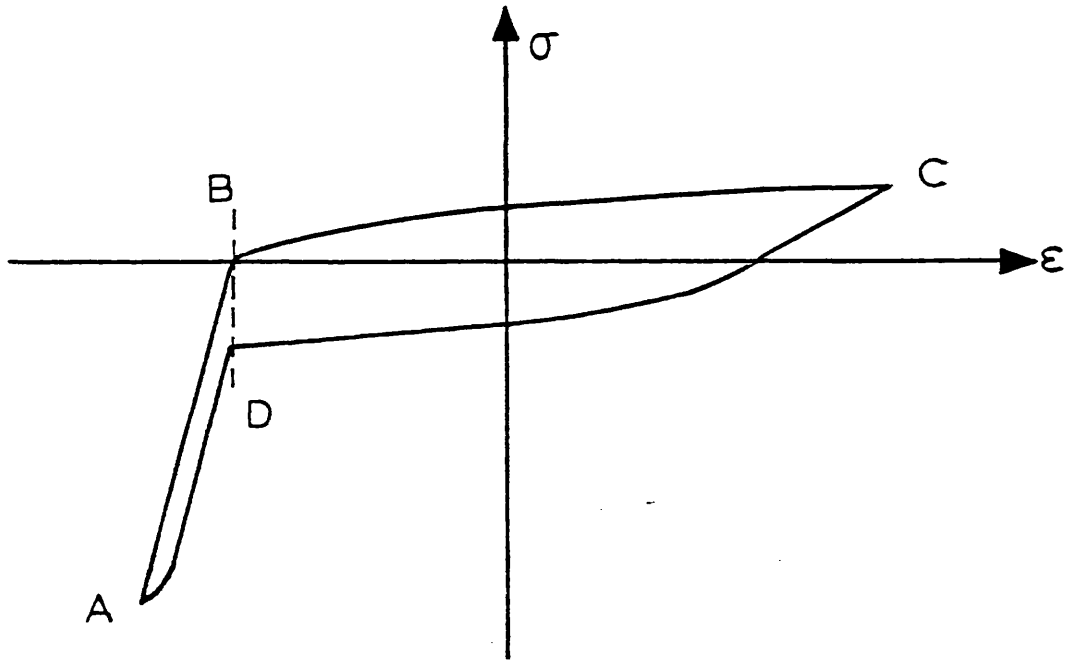

Figure 4.8: Typical stress-strain hysteresis loop when damage is non-zero.

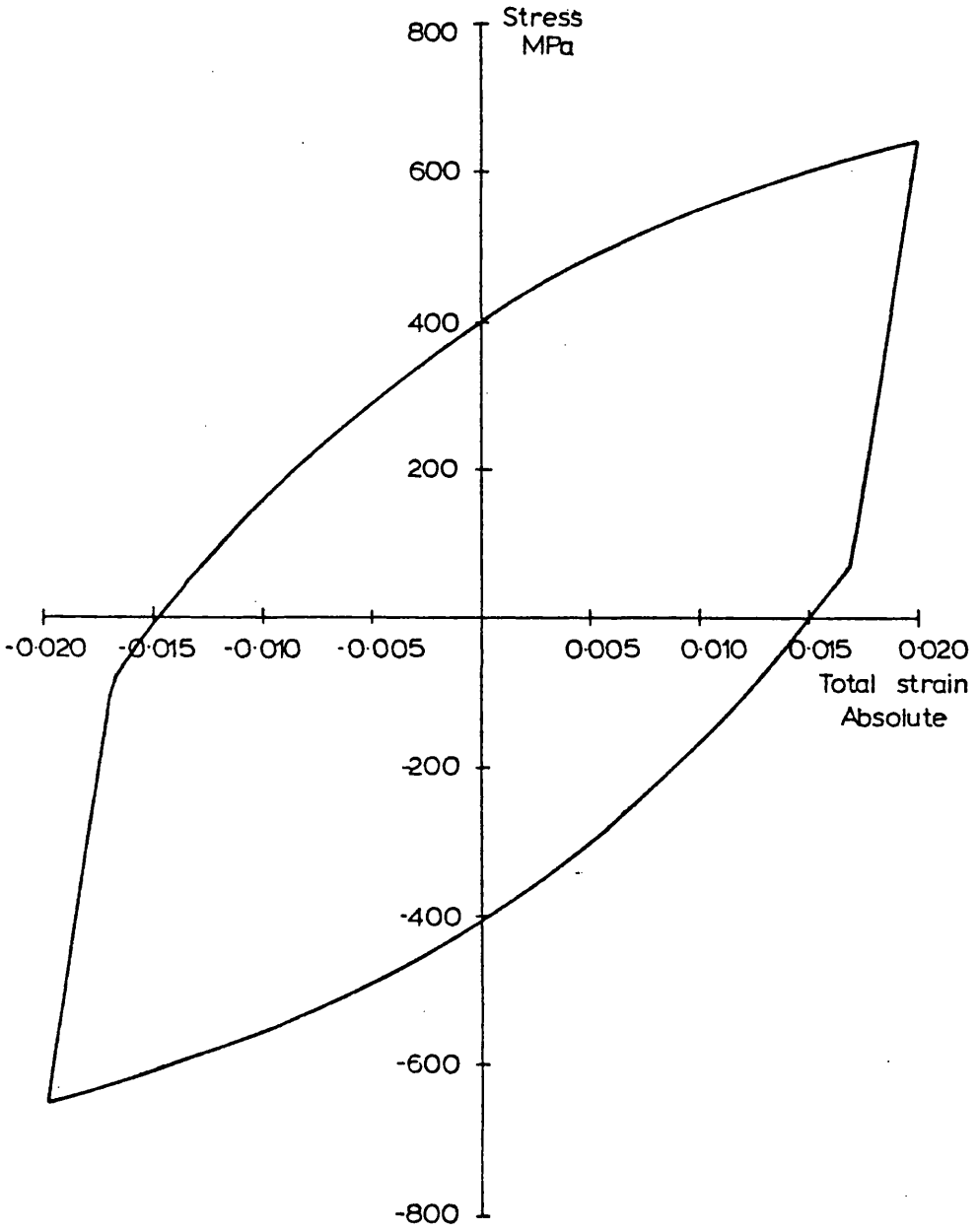

Figure 4.9: Predicted stress-strain hysteresis loop for stainless steel at 20°C with ψ = 0.05 .

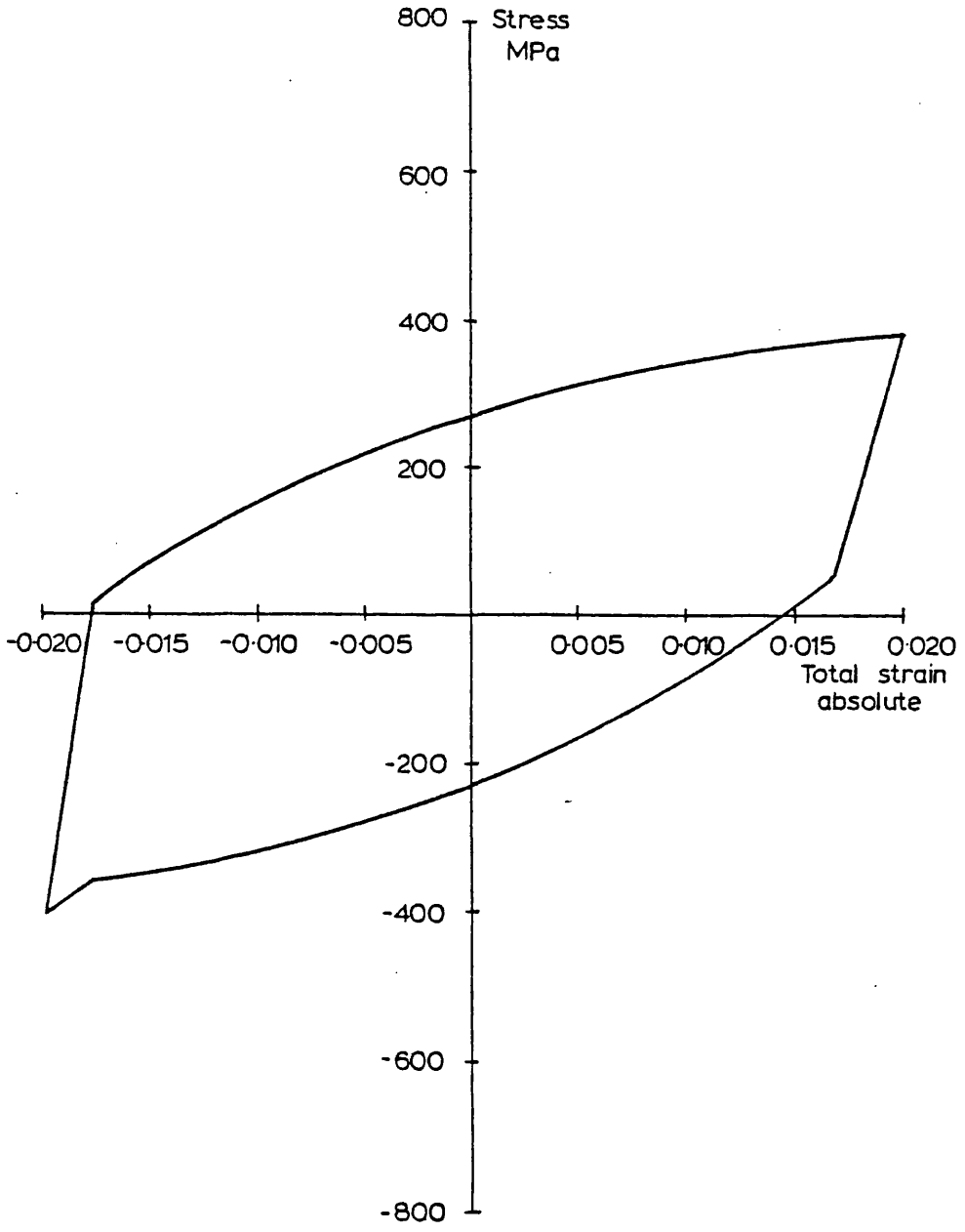

Figure 4.10: Predicted stress-strain hysteresis loop for 316 stainless steel at 20°C with ψ = 0.45 .

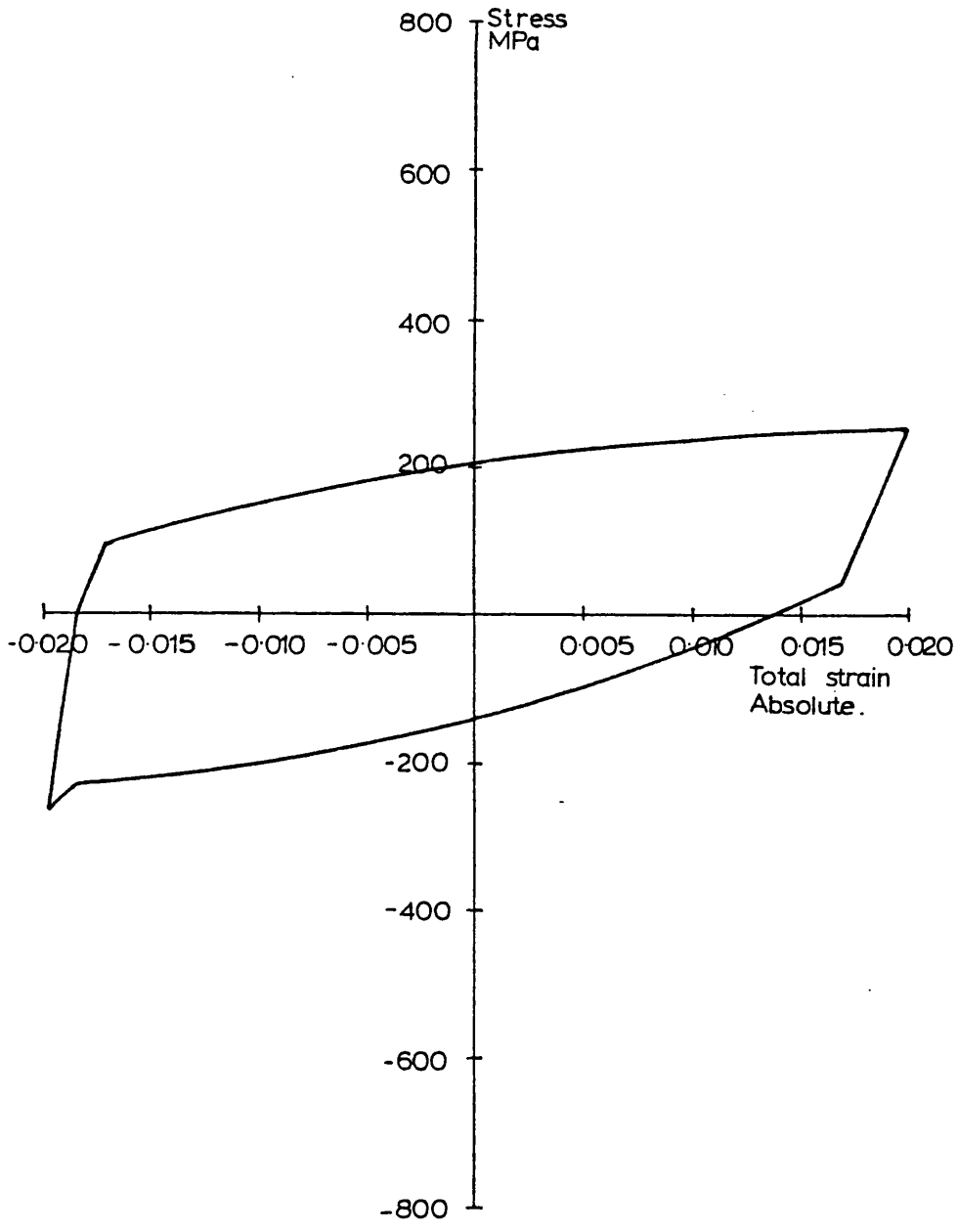

Figure 4.11: Predicted stress-strain hysteresis loop for 316 stainless steel at 20°C with ψ = 0.65 .

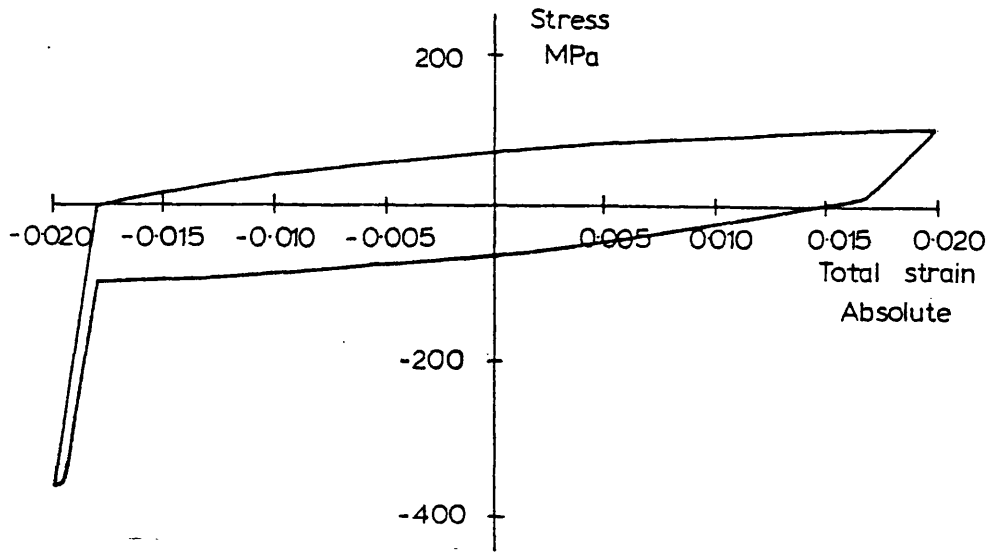

Figure 4.12: Predicted stress-strain hysteresis loop for 316 stainless steel at 20°C with ψ = 0.85 .

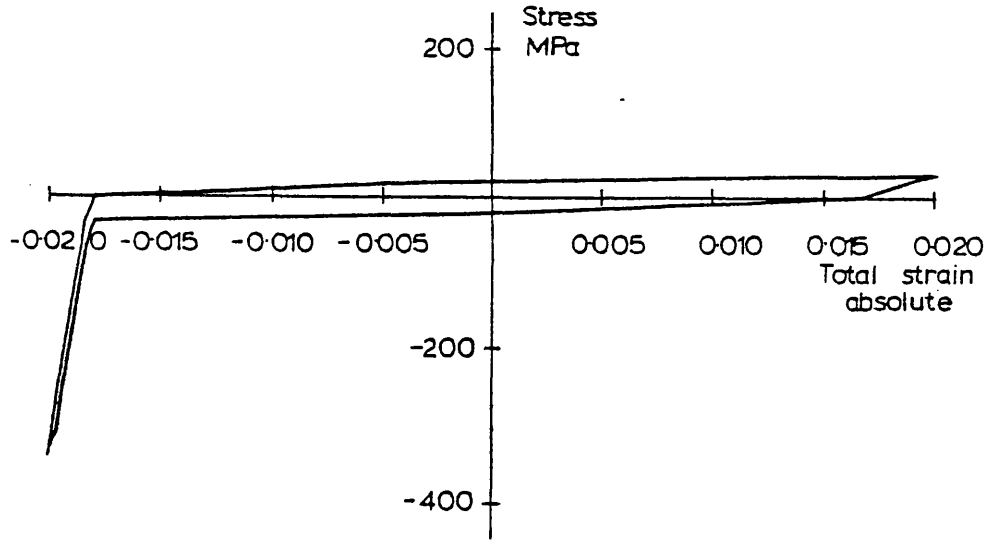

Figure 4.13: Predicted stress-strain hysteresis loop for 316 stainless steel at 20°C with ψ = 0.95 .

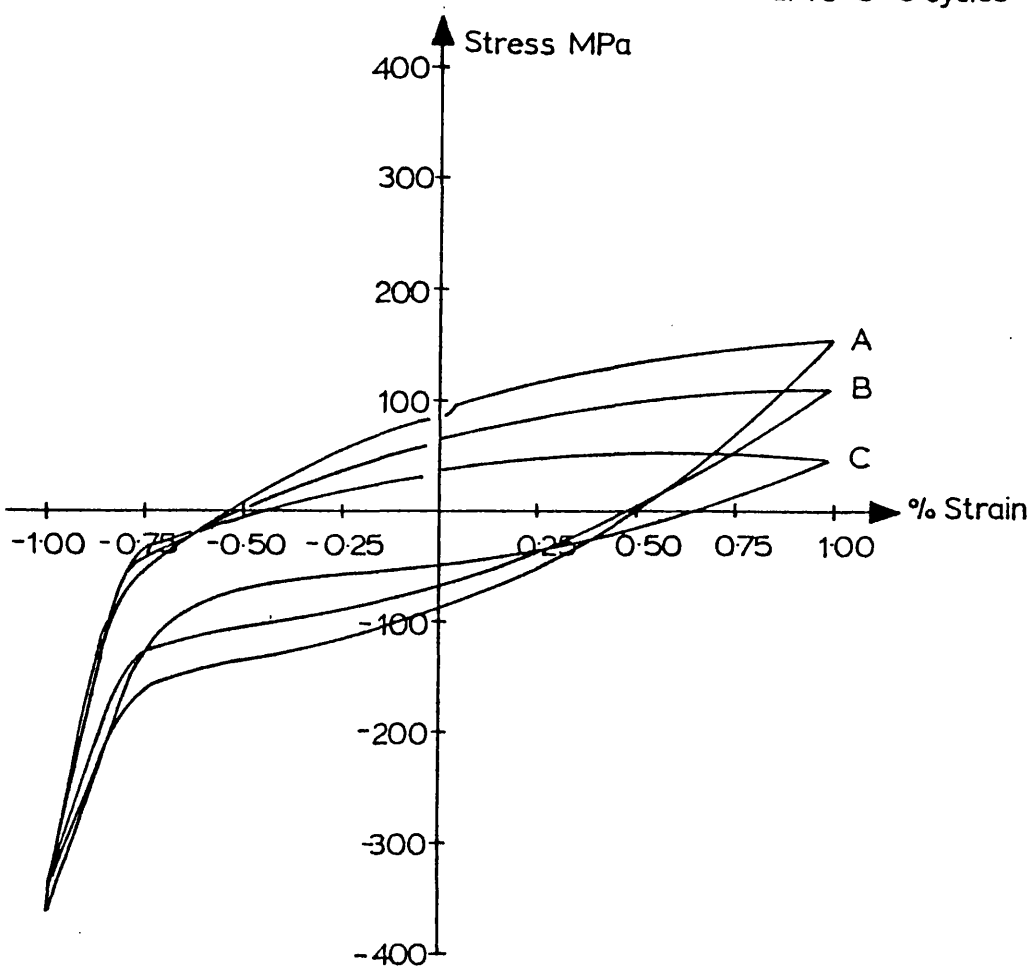

Figure 4.14: Experimental stress-strain hysteresis loops in 316 stainless steel (at 20°C) just before failure (Taylor, 1985).

CHAPTER 5

A STUDY OF STRESS REDISTRIBUTION IN A STRUCTURE DUE TO CUMULATIVE FATIGUE DAMAGE

5.1 Introduction

This chapter consists of a study of a multibar structure similar to that of Chapter 3. The multibar structure itself is the same as before. The constitutive model and damage evolution law are those introduced and described in Chapter 4. The material properties are also different: in this chapter the material is supposed to be 316 stainless steel and not an arbitrary material as used in Chapter 3.

The procedure followed will be similar to that in Chapter 3. Two solutions will be compared: one in which stress redistribution occurs and another in which the bars fail abruptly with negligible damage growth and stress redistribution before failure. In addition, two asymmetrical loadings will be examined: in one there will be a positive mean load in the other a negative mean load.

5.2 The Solution Method

5.2.1 Integration of the Damage Evolution Equations

Damage evolution will be according to equations (4.44) and (4.47) of Chapter 4. For constant σ_{max} and σ_{mean}, (4.44) may be integrated to obtain a relationship between ψ and N. There are two cases for the integration: they are $\alpha = 1$ and $\alpha < 1$. Suppose the lower and upper limits of ψ and N are ψ_1, N_1 and ψ_2, N_2 respectively, then for $\alpha = 1$ the result is

$$(N_2 - N_1)\,\Sigma = \ell n \left[\frac{z_2}{z_1}\right] \qquad (5.1)$$

where

$$z_i = 1-(1-\psi_i)^{\beta+1} \quad \text{for } i = 1,2,$$

and where

$$\Sigma = (\beta+1)\left[\frac{\sigma_{max}-\sigma_{mean}}{M}\right]^{\beta},$$

and for $\alpha < 1$ the result is

$$(N_2-N_1)\,\Sigma = \frac{1}{1-\alpha}\,(z_2^{\,1-\alpha}-z_1^{\,1-\alpha}) \qquad (5.2)$$

On making the assignments $N_1 = 0$, $N_2 = N_f$, $\psi_1 = 0$ and $\psi_2 = 1$ in (5.2), an expression for the total number of cycles to failure for any values of the stress limits for which $\alpha < 1$ is obtained:

$$N_f = \frac{1}{(1-\alpha)\Sigma} \qquad (5.3)$$

A similar assignment of values in (5.1) is not possible since z_1 is zero if ψ_1 is zero. However, setting ψ_1 to zero in (5.1) does give the result that the fatigue life is unbounded if the maximum stress is below the fatigue limit.

Equations (5.1) and (5.2) make it possible to calculate approximately the lifetime for a specimen under varying stresses such as would, for instance, be encountered during a strain-controlled load cycling test or in the presence of stress redistribution in a structure. If it is assumed that the stresses imposed

on the specimen remain constant over R cycles then (5.1) or (5.2) may be used to calculate the approximate increase in damage incurred during those R cycles. From (5.2) the new value of the damage if $\alpha < 1$ is

$$\psi_2 = 1-(1-\theta^{1/(1-\alpha)})^{1/(\beta+1)} \qquad (5.4)$$

where

$$\theta = \frac{R}{N_f} + [1-(1-\psi_1)^{\beta+1}]^{1-\alpha}$$

In the case $\alpha = 1$, damage becomes

$$\psi_2 = 1-(1-\phi z_1)^{1/(\beta+1)} \qquad (5.5)$$

where

$$\phi = \exp(R\Sigma)$$

The new value of damage obtained can now be used to calculate new stress limits from which a new value of damage may be calculated as above. Notice that there is a finite increase in damage in the case $\alpha = 1$ if ψ_1 is non-zero, otherwise the damage remains zero. Thus, once damage has been accumulated there is effectively no fatigue limit. The accumulation of damage may be continued until damage reaches a value of 1. In general this occurs during the step of R cycles and is signalled by certain terms in (5.4) or (5.5) becoming negative or zero at the end of a step. In the case $\alpha < 1$ then the condition is

$$1 - \theta^{1/(1-\alpha)} \leqslant 0$$

By setting to zero the left hand side of this, an expression can be derived for the number of cycles into the step at which the specimen fails:

$$R_f = (1-z_1^{1-\alpha})\, N_f \qquad (5.6)$$

Similarly, for the case of $\alpha = 1$ the failure of the specimen is signalled by

$$1 - z_1 \phi < 0,$$

and failure is given by

$$R_f = -\frac{1}{\Sigma} \ln (z_1) \qquad (5.7)$$

The procedure outlined here is the one which has been used to calculate the damage growth and lifetimes of bars in the multibar model subjected to load controlled cycling. Since the integration is based on the exact integration given in (5.1) and (5.2), the only source of error in this procedure is the assumption that the stress limits remain constant over several cycles. The accuracy of the method may be increased by decreasing the value of R. Values of R less than 1 may even be used but the validity of doing this would be dubious. This highlights the difficulties associated with the fact that a continuous mathematical approach has been used to describe a problem expressed in discrete form.

5.2.2 Solution Without Stress Redistribution

It was seen in Chapter 3 that the presence of damage in one bar of a multibar structure allows stress redistribution to take place. If the damage in a bar is constrained to be as close to zero as possible until the bar fails, then stress redistribution will not have a significant effect on the behaviour of the whole component. A solution in which the damage is kept near to zero for most of the life of a bar can then be compared with the solution in which stress redistribution is allowed to occur and the effect of redistribution on the behaviour and lifetime of a structure can then be examined. A damage evolution law in which the damage is constrained in this way can be obtained by substituting ψ^r for ψ in (4.44), where the power r must be less than one for it to have the desired effect. As an example of the effect that this substitution has on the expressions above, it can be seen that (5.4) becomes

$$\psi_2 = [1-(1-\theta^{1/(1-\alpha)})^{1/(\beta+1)}]^{1/r} \qquad (5.8)$$

where

$$\theta = \frac{R}{N_f} + [1-(1-\psi_1^r)^{\beta+1}]^{1-\alpha}$$

The application of these models to the multibar structure is described in the following section. Several tests are described and the results obtained are discussed in full.

5.3 Analysis of Multibar Structure and Results

5.3.1 Description of Multibar Model Structure

A computer program was written to apply the solution method described in Section 5.2. This was then used to study the theoretical behaviour of a multibar structure for three different cyclic loadings. The multibar structure used was the same as that described in Chapter 3. The lengths and areas of the bars for this structure are given in Table 5.1. Lengths have been normalized by dividing by the length of bar 1 and the areas have been normalized by dividing by the area of bar 1. It should be noted here that, since areas have been normalized but stresses have not, then loads will have units of MPa. Also shown in Table 5.1 are the stresses in the bars when the stress in bar 1 is 300 MPa. The bars were assumed to be made of 316 stainless steel and the temperature of the system was assumed to be constant at 20°C. The properties of the material were the same as those employed in Chapter 4 and were all taken from the book by Lemaitre and Chaboche (1985) and are reproduced here in Table 5.2 which shows the values for the constants in the constitutive laws, eq. (4.6), and the damage evolution laws, eq. (4.44). The cyclic loading cases were chosen to be in the low cycle fatigue region and to show the effect of changing the mean loading. One loading cycle had zero mean and was between the limits -2200 MPa and +2200 MPa. The other loadings had the same range of 4400 MPa but one had a positive mean load of 200 MPa and the other had a negative mean load of -200 MPa.

The value of R, the number of cycles during which

the state of the structure is assumed to remain constant, was taken as 20 in all the tests. Thus, the structure is allowed to perform one cycle and the stress ranges recorded during this cycle are used in (5.4) or (5.5) with R set to 20 to calculate a new value for damage. This value of damage is used for the next cycle of the structure and the total number of cycles for the structure is increased by 20.

As shown in Chapter 4, the properties of the non-linear kinematic hardening rule are such that, as damage increases, the limit and yield surfaces shrink. This means that the limit stress decreases and that, since the constitutive law does not allow stresses to be outside the limit surface, under stress controlled cyclic loading the material is at some point no longer able to support the imposed load. In fact, the constitutive model predicts infinite plastic strain at a stress equal to the limit stress. In order to detect bars in the model for which the load imposed is beyond the limit stress, a limit in total strain of 0.1 absolute (10%) is imposed, and if a bar exceeds this limit then it is failed. Thus, if the stress in a bar increases towards its limit then it would strain unboundedly, but the limit in strain means this would be detected and the bar would fail before the limit surface is attained.

The computer program was used to test the model described above. The results collected for the various loadings described above are now described.

5.3.2 Failure of the Bars

The number of cycles at which each of the bars failed for each of the cyclic loadings is given in Table 5.3. It can be seen from this table that a positive mean loading decreases the life of each of the bars and of the whole multibar structure, and that a negative mean load has the opposite effect of increasing the life of each of the bars and of the whole structure. This is in accordance with what would be expected in practice, where it is well known that a tensile mean stress in a material decreases its fatigue life when compared to a cycle with zero or negative mean stress, but with the same stress range. The differences in the total life of the structures are about 17% of the zero mean life for the positive mean test and about 11% for the negative mean test. These proportions of increase or decrease are greater than the corresponding change in the lifetime of the first bar.

Note that, in one test, bar 6 failed due to the strain exceeding 0.1. This is possibly due to the fact that the structure underwent ratchetting as damage increased in all the bars. It may also be due to the stress in the bar becoming greater than the limit stress, but this is less likely since the damage precipitously becomes unity at the end of the life of the bar and it would be unusual if a large value of damage were to be calculated for the end of a group of R cycles and thus cause the stress limit to be low enough to cause unbounded straining.

A variety of tests were carried out to find out

what effect decreasing the step length, R, has on the failure times of the bars. These tests were carried out for zero mean loading with R = 1, 5, and 10. It was found that decreasing the step length had a varying effect on the different bars. Thus, the life of bar 1 was increased slightly by decreasing R, but the life of bar 6 was decreased. In between these two limits the life of bar 3 changed hardly at all with changes in R. The difference between the life of bar 6 for R = 20 and R = 1 was about 4.3% This can be explained by the fact that decreasing the step length allows more stress redistribution to occur. This effect is important early in the life of the structure since stress is redistributed away from bar 1 to the other bars in the structure. Thus, the stress range in bar 1 decreases and this prolongs its life. On the other hand, the increase in stress in the other bars would decrease their total life and this effect is seen in the decrease in the total life of the structure. Another test was carried out in which the number of cycles performed by the structure after each increase in damage was actually 2 rather than 1. Thus, in this case 2 cycles were actually performed for each 20 cycles of the approximation. This did not have much effect on bars 1, 2 and 3, but tended to reduce the life of the remaining bars of the structure. The magnitude of the decrease in life for the whole structure was about 4% in this case.

In order to remove the effects of stress redistribution, damage was integrated using (5.8) instead

of (5.4) with r = 0.2. The failure times of the bars are shown in Table 5.4 for each of the three cyclic loadings. Comparison of Table 5.4 with Table 5.3 shows that if stress redistribution is negligible, then the number of cycles to failure of each of the bars and of the whole structure is significantly less than if stress redistribution is accounted for. The reduction in life for bar 1 is about 28% of the life given in Table 5.4 in each loading case. The reduction in life for the whole component is about 15% of the life without stress redistribution in the zero mean loading case, about 21% for positive mean loading and about 13% for negative mean loading. This agrees with the result obtained in Chapter 3 where a similar reduction in life was observed if the effects of stress redistribution were ignored. The reason for the increase in life when stress redistribution is taken into account is due to the fact that the maximum stress in a bar decreases as damage increases and this leads to a decrease in the stress range and the mean stress in the bar, which in turn tends to prolong the life of the bar.

5.3.3 Behaviour During Tests

During the running of the program a record was kept of the maximum and minimum values of stress and strain and of the growth of damage in each bar, and of the maximum and minimum values of displacement of the whole structure. These values were subsequently plotted to give a graphical record of the behaviour of the structure during a cyclic loading test.

Two graphs of the maximum and minimum stress values for zero mean loadings are shown in Figs. 5.1 and 5.2. Figure 5.1 shows the stress in bar 3 and Fig. 5.2 shows that in bar 6. In both graphs, the sudden jumps or steps in the maximum stress correspond to the failure of other bars in the structure. Thus, these jumps occur at about 1290, 1720, 2220, 2470 and 2570 cycles. The tensile stress in bar 3 becomes zero at about 2220 cycles which corresponds to its failure. Once all of the bars have failed, the program stops so the failure of bar 6 is not shown explicitly in Fig. 5.2. Less pronounced jumps can be seen in the compression part of Fig. 5.1, which also correspond to the failure of bars 1 and 2. The changes in slope visible on the lower curve of Fig. 5.2 correspond to the points at which the stress in compression of other bars becomes zero. For instance, there is a change in the slope of the curve at about 2460 cycles which is the point at which the lower curve in Fig. 5.1 goes to zero. The change in slope at about 2200 cycles is the place at which the compressive stress in bars 1 and 2 becomes zero and the changes at about 2440 and 2580 cycles correspond to similar events in bars 4 and 5, respectively. Examination of Figs. 5.1 and 5.2 shows that when a bar fails, equilibrium is satisfied by distributing the stress to the other bars. This is the reason for the jumps in the upper curves. However, comparison of the two figures shows that bar 6 supports this extra load, whereas bar 3 only supports a little extra and even this soon decays. In fact, it is bars 5 and 6 which take most of the extra load when

any of the other bars fail. The compressive stress in failed bars becomes zero after a few cycles because of the ratchetting which is taking place. This ratchetting causes the tensile strain to become so large that the fissures in the material stay open and thus it does not support any compressive load.

In the presence of a non-zero mean loading there is an extra effect in addition to those already noted for zero mean loading. The following discussion will be for the case of positive mean loading. The case of negative mean loading is the same in all respects except that decreasing mean stresses are replaced by increasing mean stresses and vice versa, and positive mean values are interchanged with negative mean values. When the loading has a positive mean the stress in bar 1 also has positive mean. After about 100 cycles this has all but decayed to a zero mean stress, as can be seen in Fig. 5.3. A similar effect was observed in bars 2 and 3. In bar 6, however, the initial value of the mean stress increased during these cycles as the stress was redistributed from the bars in which the mean stress was decreasing to zero.

The graphs of plastic strain show similar features to those of stress. Representative examples are shown in Figs. 5.4. and 5.5. Figure 5.4 shows the plastic strain in bar 4 for zero mean loading. Again the jumps in the two curves, especially those in the upper curve, correspond to the failure of the other bars in the structure, as can be seen by comparing their positions with the similar jumps in Fig. 5.2. Figure 5.4 clearly

displays ratchetting with both curves ultimately increasing. In all of the loading cases, bars 4, 5 and 6 exhibited ratchetting similar to this to some degree. Figure 5.5. shows the plastic strain in bar 2 for negative mean loading. This shows how the minimum plastic strain in bars 1 and 2 remains roughly constant throughout the life of the bars, and how the maximum plastic strain increases up to the failure of the bars. This behaviour is exhibited by bars 1 and 2 for all loading cases. Once a bar has failed then no further plastic straining occurs as is displayed in these two figures. Figure 5.5 demonstrates the effect of a non-zero mean loading. In a similar manner as for stress the effects of a non-zero mean loading can be described for both positive and negative means by interchanging increasing and decreasing mean plastic strain. For negative mean loading, all the yielded bars began with negative mean plastic strains and these means decreased as exemplified in Fig. 5.5. Finally, the peak plastic strains attained by each bar just before failure also reflect the mean loading. Thus, the peak strains reached by bar 2 are about 0.008, 0.0047 and 0.0035 for positive, zero and negative means respectively, and this pattern is the same for all of the bars.

An example of the displacement of the structure is given in Fig. 5.6 for zero mean loading. Again, the jumps in the curves correspond to the failure of the bars. Also, ratchetting is clearly displayed. Ratchetting in a positive direction occurs in all the loading cases, but its magnitude depends upon the value of the mean

loading. Thus, ratchetting of the structure is more severe for a positive mean loading than for a negative mean loading. The initial mean displacement is of the same sign as the mean of the loading, but there is no transient period during which this mean changes, as there was with the stresses and plastic strains.

5.4 Conclusions

A relatively complex material model has been used to solve a fatigue problem for a simple structure. The demonstration showed that the model successfully reproduces the experimentally observed load drop in specimens subjected to cyclic loading. The expected effect of non-zero mean loading on lifetimes of components has also been shown to be exhibited by the model. In addition, the importance of taking into account the effects of stress redistribution on life has been demonstrated. The numerical method used has been shown to be accurate even when large step lengths are used. This property will be important when the techniques are combined with the finite element method where each step would require large amounts of computer processing time. It is evident from this chapter that continuum damage mechanics offers a convenient method of modelling the complete behaviour of a component subjected to fatigue loading, although the accuracy of the predictions of this particular model have not been tested by reference to experimental results. It is now intended to extend this approach to the study of creep-fatigue behaviour of structures by including a creep model with the fatigue model.

Bar Number	Length (normalized)	Area (normalized)	Elastic stress (MPa)
1	1.0	1	300
2	1.2	1	250
3	1.5	1	200
4	2.0	1	150
5	3.0	1	100
6	6.0	4	50

Table 5.1 Description of multibar model used in tests. The elastic stresses given are those when bar 1 first yields.

σ_y (MPa)	300
C (MPa)	30000
γ	60

(a) Constants used in constitutive law, equation (4.6), Chapter 4.

σ_ℓ	222
σ_u	760
β	5
b	0
a	0.9
M_0	1700

(b) Constants used in damage evolution law, equation (4.44), Chapter 4 (units in MPa).

Table 5.2 Material constants for 316 stainless steel at 20°C.

	Bar number					
Loading (MPa)	1	2	3	4	5	6
-2200 → +2200	1293	1719	2219	2471	2572	2635
-2000 → +2400	1258	1679	2046	2234	2306	2354
-2400 → +2000	1310	1739	2279	2775	2976	3080*

*
A star indicates that the failure was due to the bar exceeding the limit of 10% total strain.

Table 5.3 Cycle number at which each bar fails for three loading cases.

	Bar number					
Loading (MPa)	1	2	3	4	5	6
-2200 → +2200	1007	1396	1868	2117	2204	2282
-2000 → +2400	972	1353	1681	1836	1893	1940
-2400 → +2000	1023	1420	1900	2413	2612	2735

Table 5.4 Cycle number at which each bar fails for three loading cases for the no damage solution.

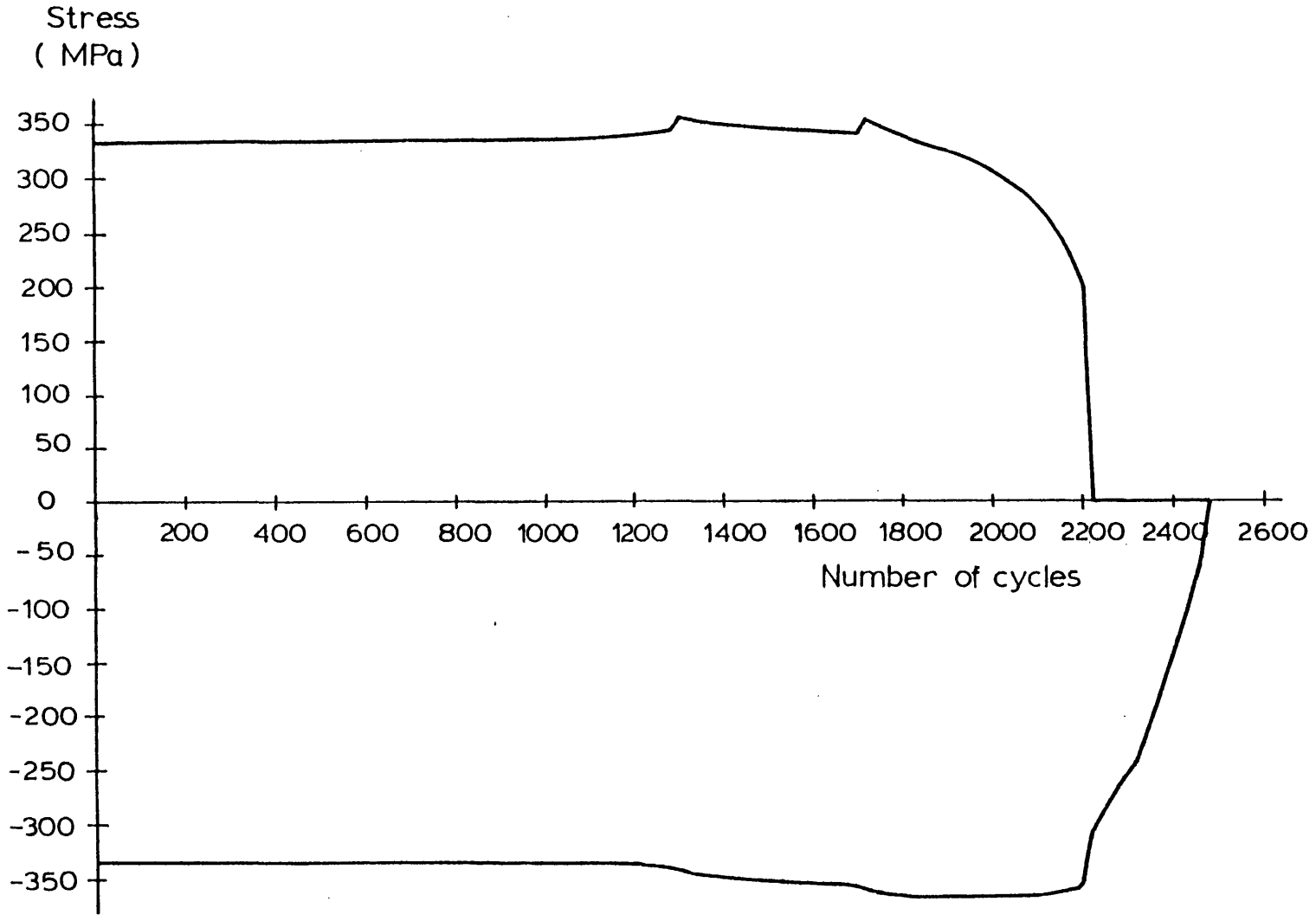

Figure 5.1: Maximum and minimum values of stress in bar 3 under a cyclic load between ±2200 MPa.

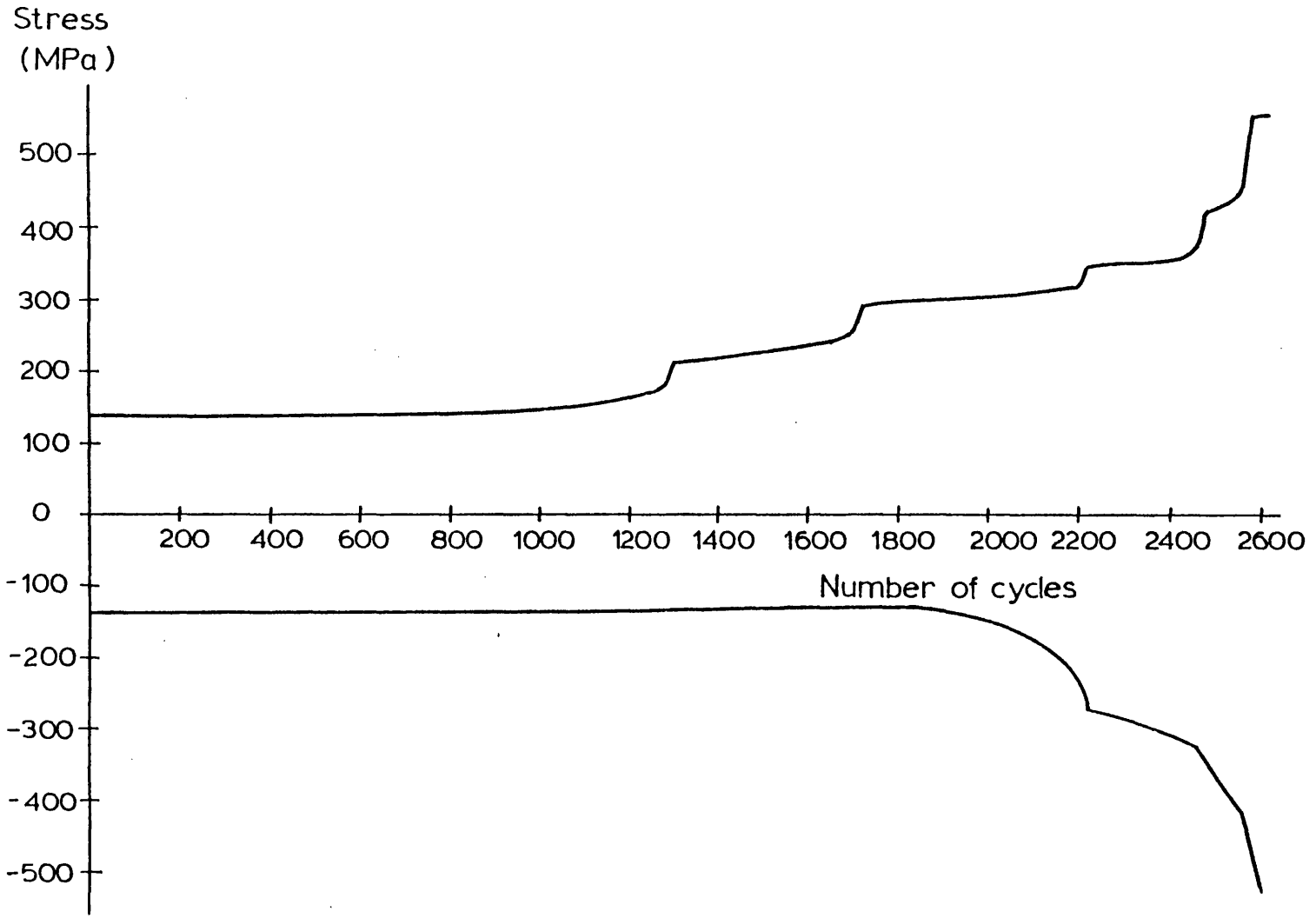

Figure 5.2: Maximum and minimum values of stress in bar 6 under a cyclic load between ±2200 MPa.

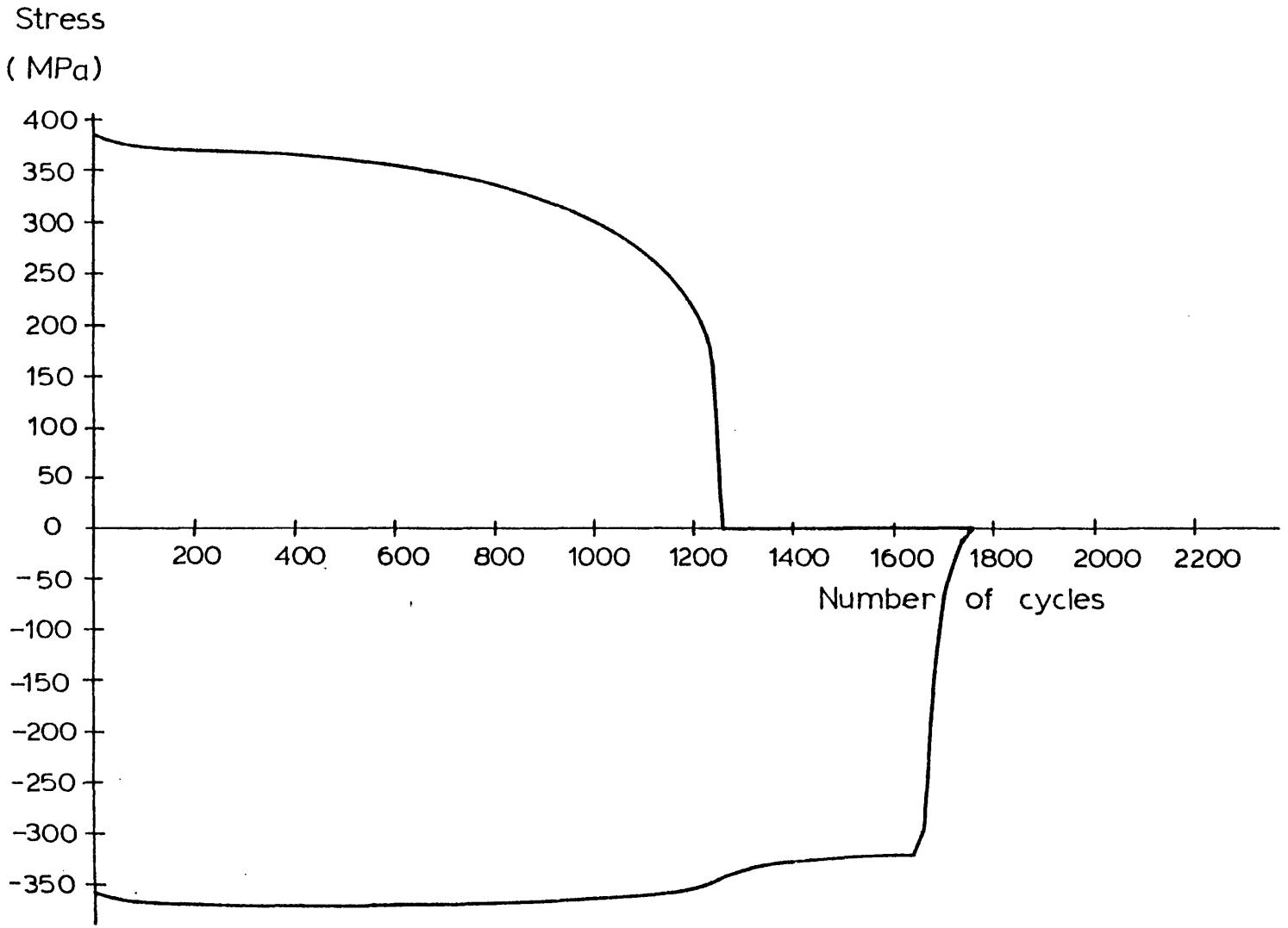

Figure 5.3: Maximum and minimum values of stress in bar 1 under a cyclic load between -2000 and 2400 MPa.

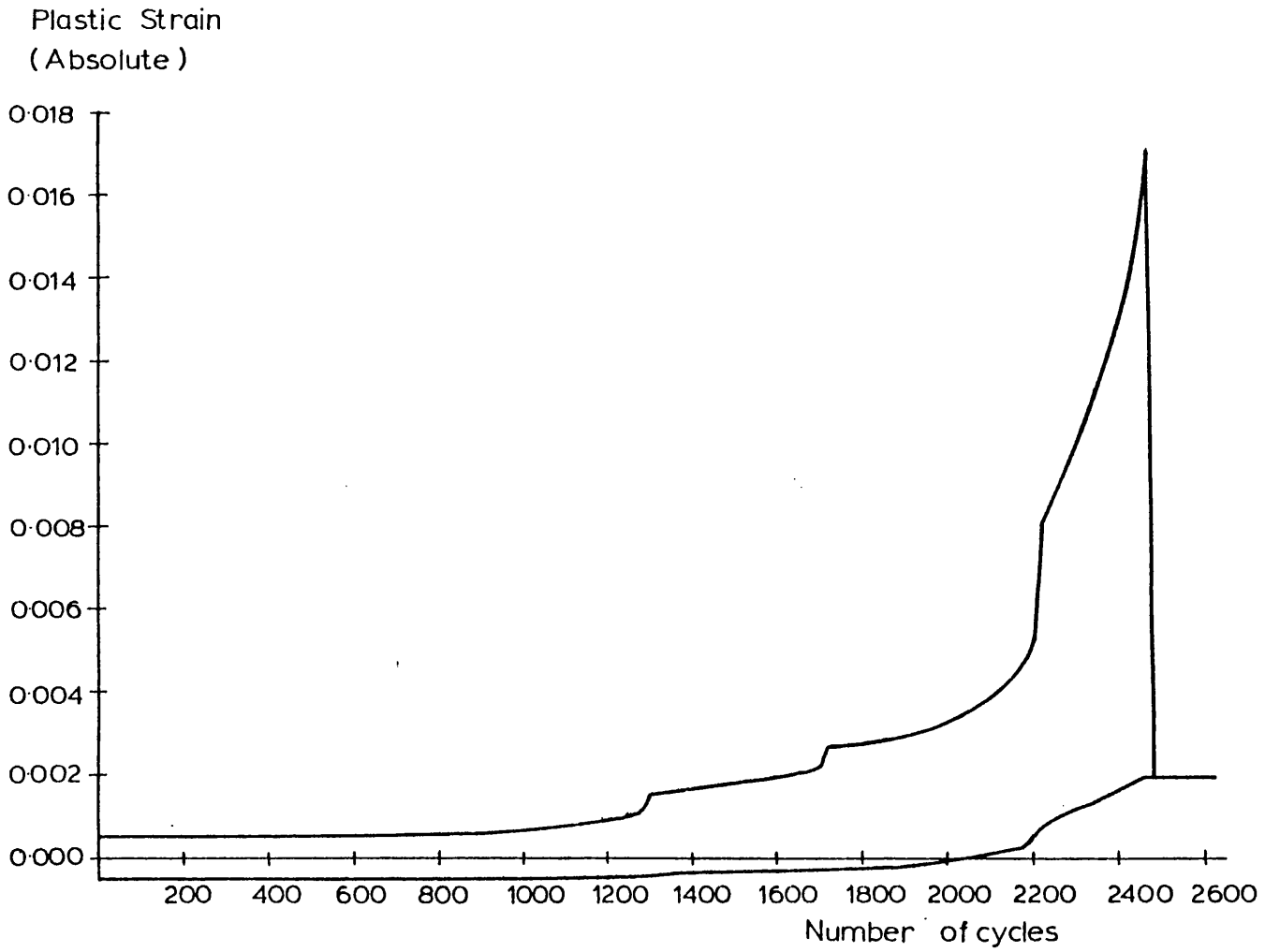

Figure 5.4: Maximum and minimum values of plastic strain in bar 4 under a cyclic load between ±2200 MPa.

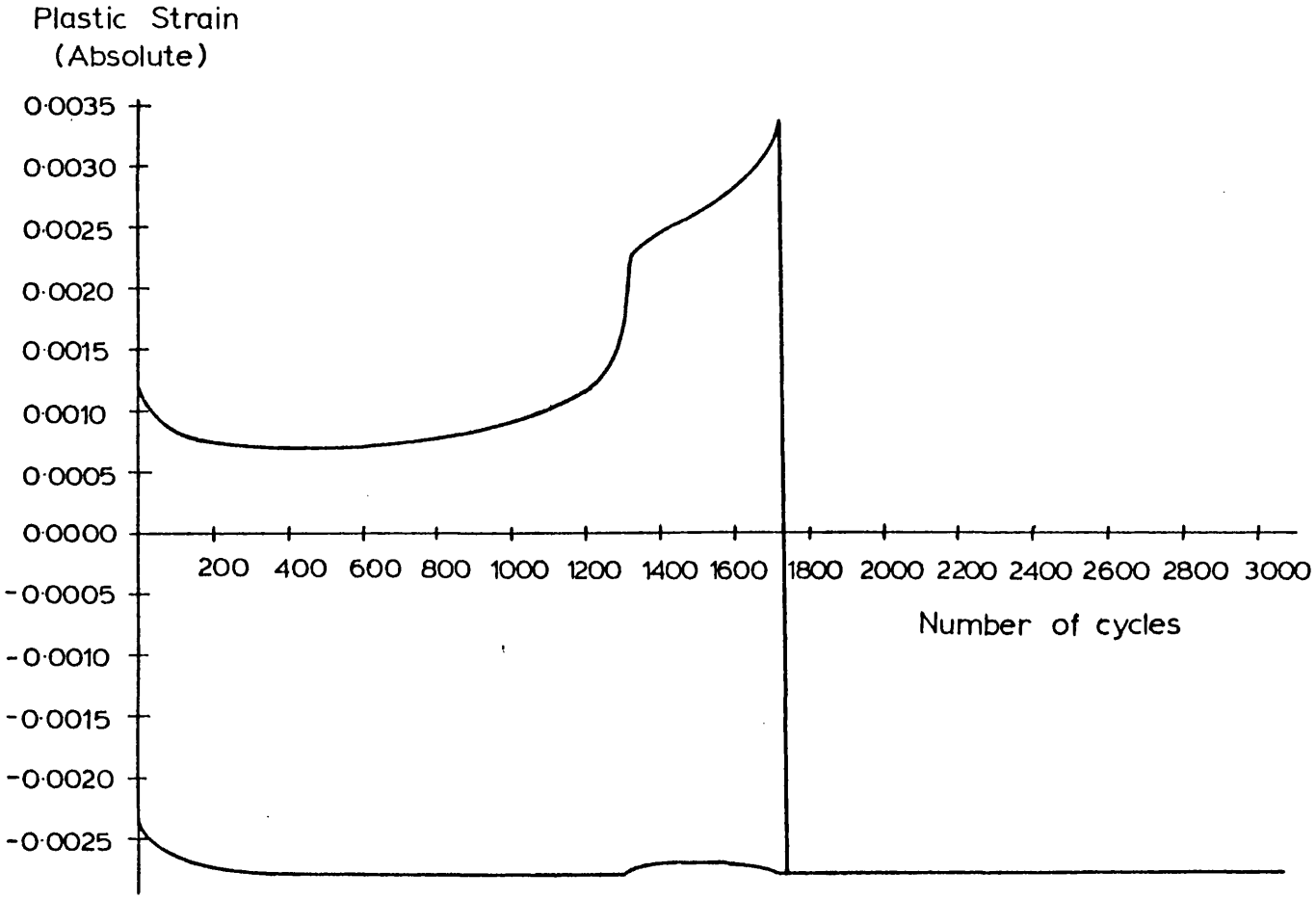

Figure 5.5: Maximum and minimum values of plastic strain in bar 2 under a cyclic load between -2400 and +2000 MPa.

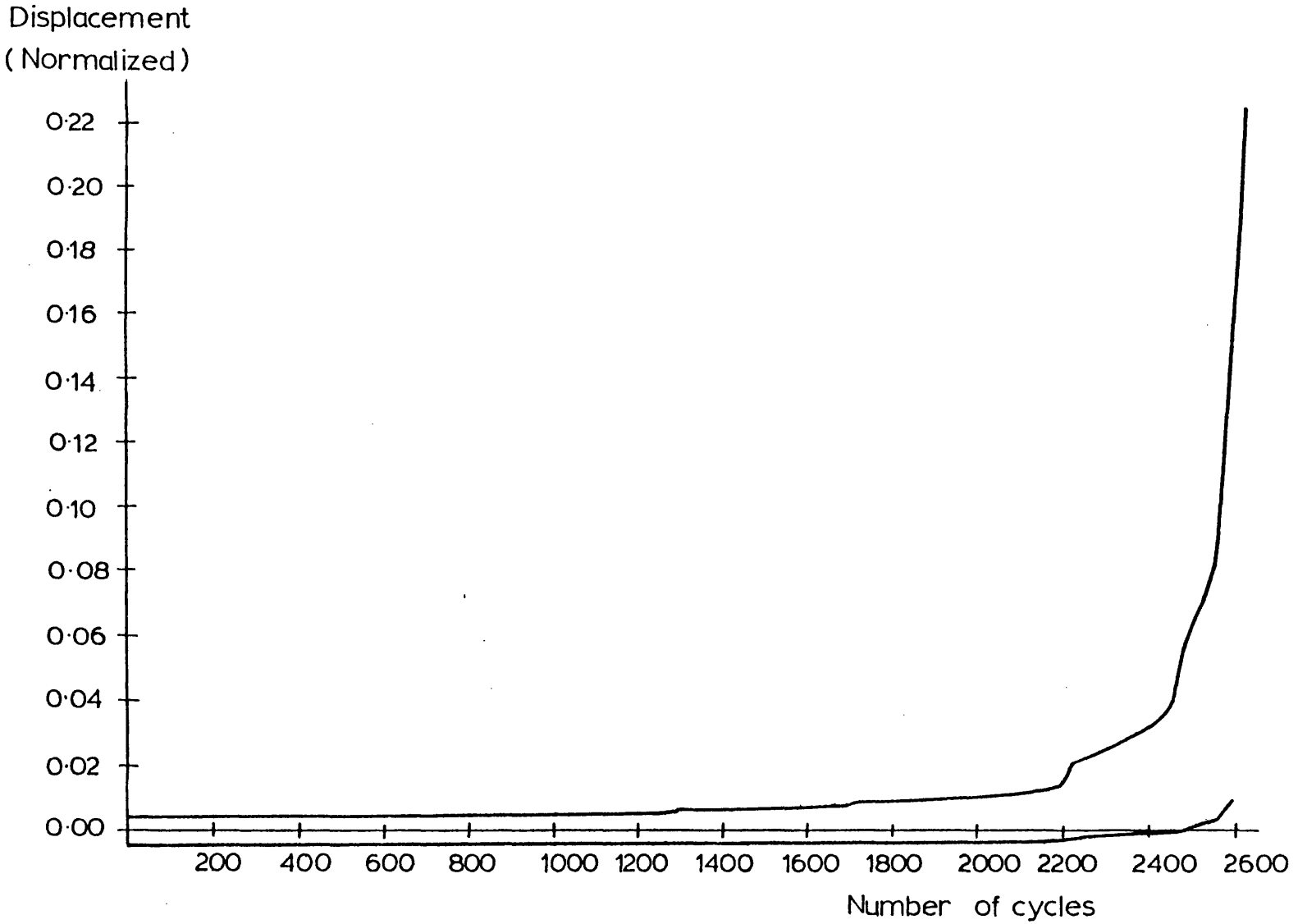

Figure 5.6: Maximum and minimum values of displacement of multibar structure under a cyclic load between ±2200 MPa.

CHAPTER 6

A UNIAXIAL MODEL OF DEFORMATION AND RUPTURE UNDER CREEP-FATIGUE CONDITIONS AND ITS APPLICATIONS TO MATERIAL MODELLING AND STRUCTURAL PROBLEMS

6.1 Introduction

In previous chapters a model has been developed for uniaxial plasticity and fatigue failure. This includes the effect of damage on cyclic plastic deformation and a law for damage evolution. These have been used to study the behaviour of multibar structures under cyclic loading. The concept of damage is not usually used for predicting fatigue failure, but is more normally applied to creep rupture. In this chapter a model for creep deformation will be added to that of plastic deformation and a rule will be given for the interaction of creep and fatigue damage. In this way, the foundations are laid for the study of creep-fatigue deformation and rupture. Also in this chapter experimental data which are available in the literature will be used to construct a model of copper. This material was chosen because of the availability of information on its behaviour and because it is used in the specimens in a series of tests on a simulated two bar structure. The predictions of the model can then be compared with the results of the tests. Since the loading in these tests is thermal, the solution methods can be extended to study the effect of fluctuating thermal gradients on components; with and without mechanical loads.

This chapter is organised as follows. Firstly, the creep laws are described. Then the model of the deformation and rupture behaviour of copper is constructed. Following a discussion of creep-fatigue interaction, the predictions obtained using this model are compared with the experimental results on the behaviour of a two bar structure. The final section consists of studies of other multibar structures under fluctuating thermo-mechanical loading.

6.2 A Uniaxial Model for Deformation under Creep-fatigue Conditions

Cyclic plasticity is described by the non-linear kinematic hardening rule which was introduced in Chapter 4. The damage evolution law is given by the Chaboche law, also given in Chapter 4. The laws relating to creep are described in this section.

6.2.1 Creep

The creep behaviour is assumed to obey a simple Norton power law

$$\frac{dv}{dt} = A\sigma^n, \qquad (6.1)$$

where σ is the stress, v is the creep strain and A and n are constants. This law only describes the secondary portion of the total creep curve. A description of the tertiary portion and of failure may be achieved by the introduction of creep damage, ω (Kachanov, 1958). The evolution of creep strain can then be described by the following equation:

$$\frac{dv}{dt} = A \left[\frac{\sigma}{1-\omega} \right]^n \qquad (6.2)$$

6.2.2 Creep Damage Evolution

A simple form of damage evolution relationship will be used here:

$$\frac{d\omega}{dt} = B \left[\frac{\sigma}{1-\omega} \right]^\nu \qquad (6.3)$$

where B and ν are constants. This equation can be integrated for constant stress to give the time to rupture at that stress:

$$t_r = \frac{1}{B(1+\nu)\sigma^\nu} \qquad (6.4)$$

The constants B and ν can be found directly from uniaxial rupture data. Equation (6.3) is a relatively simple form of the damage evolution law and may be improved. It is the shape of the tertiary portion of a creep curve that is governed by damage growth and hence by (6.3). However, the actual shape obtained by simultaneous integration of (6.2) and (6.3) does not necessarily match very well the shape of experimentally obtained tertiary creep curves. The description of tertiary creep may be improved by the inclusion in (6.3) of an additional material constant. However, the experimental data that will be used in a later section only provides enough information for the calculation of the constants B and ν and does not allow the calculation of the additional material constant. Thus (6.3) will be used here for the description of creep damage growth. The effect of the extra constant on the behaviour

of structures will be demonstrated in a later section.

6.3 Fitting the Model to Experimental Data

The above sections give the basic description of a material model which includes the effects of both creep and fatigue. In principle it can be used to predict the life and deformation of uniaxial components such as single specimens or multibar model structures. However, in order to be able to apply it to real specimens, it is necessary to obtain the values of the various coefficients for the material in question. A description of how this has been done for copper is contained in the next section.

6.3.1 Availability of Data

The authors are not in possession of sufficient experimental data, which has been collected from a single batch of material in a consistent manner, to calculate the coefficients accurately. Much data does indeed exist, but most of it was originally obtained for a specific purpose and does not contain enough information to enable the calculation of all the coefficients that are required by the model proposed here. For example, since fatigue damage is a measure of the weakening of the material during a fatigue test, it is necessary to observe the load drop that occurs during a strain controlled cyclic test, or some other effect of damage such as changes in electrical resistance or the speed of sound in a specimen (Lemaitre and Chaboche, 1985), in order to obtain some of the constants required for the damage evolution law. However, fatigue tests have generally been carried out to construct

graphs of strain or stress amplitudes against number of cycles to failure and so information on parameter variation during a test is not available. Also, it is often the case that extensive experiments have been performed to study, say, the creep properties of a material, but similar tests have not been performed to determine the fatigue properties of the same material at the same temperature.

One of the most complete sets of experimental data that the author is aware of is for OFHC copper. In addition to this, some experiments have been carried out which simulated multibar structural models with two copper bars under creep-fatigue conditions. This provides results against which the predictions of the theoretical model may be compared. The experimental data used here is not ideal since it represents a large range of temperatures and of batches of material. The effect of differing batches of material would be impossible to quantify and so, for the purposes of this investigation, it is assumed that the properties of the copper are insensitive to changes in preparation and composition. For most of the data it is not possible to estimate the effect of temperature because tests were carried out for only one temperature. Since data on copper was collected by the different experimenters at different temperatures, it is necessary to assume that the material properties of copper are independent of temperature. Since the behaviour of metals actually varies significantly with temperature, it is evident that agreement between theory and experiment will be qualitative rather than quantitative. This difficulty

is most accute for cyclic plasticity tests; but, as will be shown in a later section, creep data is available for different temperatures. Wherever possible, cyclic plasticity data has been used for a temperature which is compatible with the dominant creep temperature under consideration. The data sources are now listed and discussed.

A modest independent program of testing for fatigue properties was carried out in-house and a few of these results were employed. The cyclic stress-strain curve, and the elastic properties, for copper at 150°C was found in these tests and these were used here to obtain the plasticity properties of copper. Megahed and Ponter (1979) have published the results of some creep tests on copper at 250°C and 300°C and this provided the information for the creep part of the model. Finally, a paper by Lemaitre and Plumtree (1979) contains a graph of strain range against cycles to failure and a graph of damage against number of cycles for OFHC copper at 540°C. This was used to find the fatigue constants.

The spread of temperatures at which experimental results have been collected is large, and the variation in preparation and in composition of the material may also be large. In addition to these difficulties the data is not necessarily in a form which can easily be used to fit it to the model. This is especially true in the case of fatigue. The methods by which the constants were obtained are now described for each aspect of the model. The values determined are listed in Table 6.1.

6.3.2 Elasticity Constant

The cyclic plasticity properties of OFHC copper were studied in tests carried out in house; from these the values of Young's modulus was found to be 90 GPa.

6.3.3 Plasticity Constants

The yield stress was obtained from a cyclic stress strain curve and is 15 MPa. This value of the yield stress is a little low when compared with the monotonic value or with a value that is observed in an individual stress-strain hysteresis loop at a particular strain amplitude. Copper has been shown to be a non-Masing material (Fenn, 1979) which implies that cyclic stress strain hysteresis loops at particular stress amplitudes cannot be constructed from the general cyclic stress-strain curve. In particular, the yield stress for a hysteresis loop will be different for different stress amplitudes (Fenn, 1979). However, fitting the model to a cyclic stress-strain curve in this way enables it to represent the behaviour of the material over a wide range of levels of stress.

In order to model the complete stress-strain curve it is necessary to find the values of two more constants. These are C and γ in equation (4.6). C/γ was shown in Chapter 4 to be the limiting value of the absolute value of α which can be found from the limiting value of stress and a knowledge of the yield stress. The limit stress was obtained from a monotonic stress-strain curve for copper at 300°C, which is found in Pascoe (1961). This provided a convenient method of fixing the value of the stress limit for a temperature of 300°C, in the absence

of any cyclic data at this temperature. A temperature of 300°C was chosen because it is the temperature at which the creep tests by Megahed and Ponter (1979) were performed.

The remaining parameter, γ, was obtained as follows. The cyclic stress-strain curve was represented as a series of points which could be plotted, by computer, on the same graph as a theoretical curve for a given value of γ and a fixed value of C/γ, previously determined. The value of γ was varied until an acceptable fit was achieved. Two graphs of the final fit are shown in Fig. 6.1; one is for low strain values ($<1.5\%$) showing the difference between the actual and fitted curve in detail and the other is for large strains ($<10\%$), showing how the curve lies in comparison with the limit stress.

6.3.4 Ratchetting Data

The cyclic creep or ratchetting behaviour of copper has been studied by two groups of authors (Feltner and Sinclair, 1963, and Megahed et al., 1980) who give experimental data. Since the non-linear kinematic hardening rule predicts ratchetting under a non-zero mean cyclic stress (Chapter 4), then this data should offer an additional check on the validity of the model fitted to the experimental data discussed above. Also, in the absence of direct information of the shape of the hardening curve it could also provide another method of calculating the plasticity constants. However, both of these suggestions turn out to be impractical. If the values of the plasticity constants, which were found by the method above, are used to calculate the ratchet rates for the tests reported

in Feltner and Sinclair (1963) and Megahed et al., (1980), then the theoretical rates are found to be about two orders of magnitude too large. The experimental and theoretical rates are compared in Table 6.2. The table shows experimental ratchet rates published in Megahed et al., (1980) and theoretical rates calculated from

$$\frac{d\varepsilon}{dN} = \frac{1}{\gamma} \ln \left[\frac{L^2-\alpha^2_{max}}{L^2-\alpha^2_{min}} \right] \qquad (6.5)$$

where $L = C/\gamma$ and α_{max} and α_{min} are the maximum and minimum values of α during a cycle. The values of the constants required in (6.5) were taken from Table 6.1. The three negative theoretical values that occur in Table 6.2 are due to the fact that the stress range is less than 30 MPa which is twice the yield stress. This means that the method of calculation produces a value of α_{min} greater than α_{max}, and hence a negative rate according to (6.5). The fact that (6.5) predicts ratchetting rates which are much larger than those observed experimentally has been noted by Chaboche and Rousselier (1983). They suggest that the problem can be overcome by introducing an extra kinematic variable into the description of non-linear kinematic hardening. This has been investigated by the present author and a considerable reduction of theoretical ratchetting rates can indeed be achieved in this way. However, this makes the calculation of stress and plastic strain very difficult, even for the uniaxial case, since the equations cannot be solved directly, as they can be for a single variable. Also, since it is envisaged that this rule can be used

to solve multiaxial problems, the considerable extra computation required in order to use more than one kinematic variable in the multiaxial case is considered to be prohibitive. Another difficulty with this approach is that it does not overcome restrictions imposed by the model on the variation of ratchet rate with stress amplitude or mean stress. This difficulty will be discussed in the next paragraph.

As discussed earlier, it should be possible to calculate the plasticity constants by fitting the model to the experimental ratchetting rates. However, when this is done, it is found that the predicted stress-strain curve becomes unrealistic and tends towards a shape characteristic of perfect plasticity. Also, even though the predicted ratchet rates are of the correct order of magnitude, the variation of the ratchet rate with stress amplitudes or mean stress was much smaller than the experimentally observed variations and this remains insensitive to both the number of kinematic variables and to changes in the parameters used to describe each variable. In other words, if ratchet rate is plotted against stress amplitude on logarithmic axes then the slope of the theoretical line is much smaller than the slope of the experimental line found in Megahed et al., (1980), and the slope of the theoretical line cannot be changed without affecting the magnitude of the ratchetting rates.

However, these factors are not considered sufficient reason for rejecting the kinematic hardening rule for use in modelling plasticity. The plasticity model

considered in Chapter 3 does not predict ratchetting behaviour in the absence of damage and the non-linear kinematic hardening model is considered to be more realistic. Also, it is possible that the model can be extended to make the prediction of ratchetting more accurate.

The ratchetting behaviour of the model has been illustrated in Chapter 4. The variation of the magnitude of the theoretical ratchetting rates with respect to stress amplitude is shown in Fig. 6.2 for a range of values of mean stress. The available experimental data (Megahed et al., 1980) plotted on the same axes, produces a set of linear characteristics, each line having the same slope and being displaced by an amount dependent upon the mean stress. It can be seen in Fig. 6.2 that the theoretical rates follow this pattern for intermediate values of stress amplitude for each value of the mean stress. However, as already noted, the quantitative agreement between theory and experiment is poor.

6.3.5 Isothermal Creep and Creep Damage Constants

These are the four constants required in equations (6.2) and (6.3), namely A, B, n and ν. Their values were taken directly from those calculated in Megahed and Ponter (1979). The constants A and n can be obtained from minimum creep rate data. The original data is displayed in Fig. 6.3 which is from Megahed and Ponter (1979). Failure data affords the constants B and ν and again the original data as presented in Megahed and Ponter (1979) is shown in Fig. 6.4. The only differences between the values of

the parameters as given by Megahed and Ponter and in this report reside in the units - all the constants here have been expressed in S.I. units - and in the temperature dependence, which has been neglected here for the reasons stated in an earlier sub-section. However, unlike the other sources of data, information on the temperature dependence of the creep properties is available and, in a later section, will be added to the basic model which is being constructed here. The values of the constants are presented in Table 6.1. In addition, when the stress in (6.3) is negative, $d\omega/dt$ is taken to be zero; this is in line with observations made in compression creep tests.

6.3.6 Fatigue Damage Constants

These constants were the most difficult to calculate and hence are probably the most in error. Some estimates and assumptions were made because of the lack of information, and so the model may not represent the true behaviour. The constants to be determined are those in equations (4.44) to (4.47). The value of the ultimate tensile strength was taken as the limiting value of stress given by the plasticity equation. Thus it is equal to $C/\gamma + \sigma_y$. The fatigue limit was taken to be 2/3 times the yield stress; this choice is essentially arbitrary, and is based on the value found in several other metals. However, it is often difficult to demonstrate the existence of a fatigue limit at all in some cases, so the choice of this value was retained because it is comparatively low. Thus, the effect of a fatigue limit can be examined

but at the same time it does not have a significant effect on the growth of damage at large stress amplitudes.

There is no information on the effect of mean stress on the fatigue limit or on the parameter M for this material. However, (4.46) is basically the Goodman law for the variation of the endurance limit with mean stress. The actual form of the Goodman law is obtained from (4.46) by replacing b by $1/\sigma_u$. Hence this is the value that the parameter b is set to in this model.

The number of cycles to failure for a constant stress amplitude cyclic load test is given by

$$N_f = \frac{1}{(1-\alpha)(\beta+1)} \left[\frac{\sigma_{max}-\sigma_{mean}}{M} \right]^{-\beta} \qquad (6.6)$$

which is obtained by integration of (4.44). A graph of the logarithm of total strain amplitude against the logarithm of the number of cycles to failure is given by Lemaitre and Plumtree (1979). However, the relationship in (6.6) requires a knowledge of the stress amplitude. This problem was overcome by using the elasticity and plasticity relations previously found. From these laws a value of σ_{max} was calculated for a value of total strain amplitude taken from the graph in Lemaitre and Plumtree (1979) by assuming that σ_{mean} is zero. Two points were taken from the straight line that appears on the graph in Lemaitre and Plumtree (1979) and these provided a linear relationship between the logarithms of stress and number of cycles to failure. This procedure assumes that the relationship between stress and strain was the same for the two very different tests.

The coefficient β is constant but α varies according to (4.45). Since the value of a and thus the variation of α with stress was unknown at this point, it was assumed that α remained constant. Hence the slope of the straight line obtained above affords a value for β. This method of finding β is not accurate for at least two reasons. Firstly, the assumption that α remains constant. The size of the inaccuracy due to this will depend on the size of the constant a. When a value for a has been calculated, it will be shown how the variation of α affects the prediction of fatigue lifetimes by the model. The second reason for a discrepancy results from the load drop associated with a strain controlled cyclic loading test. The results for lifetime in Lemaitre and Plumtree (1979) were obtained by keeping the total strain range constant but the stress range varies during each test. However, the conversion from total strain range to stress range using the plasticity laws, and then using this to construct a stress-life curve, implicitly assumes that stress remains constant throughout life. This difficulty can best be overcome by using the results of experiments with stress control, but, since such results are not available to the author, it was necessary to use the method described above. It is possible to convert between a strain-life curve and a stress-life curve by using an accurate numerical simulation, but this would require knowledge of the very material constants which are being sought.

Lemaitre and Plumtree also publish in their paper (1979) a graph of $\log(1-\psi)$ against $\log(1-N/N_f)$. Each of

the fatigue data points on this graph was transferred to a graph with $\log(1-(1-\psi)^{\beta+1})$ as the ordinate and $\log(N/N_f)$ as the abscissa. A straight line was drawn to follow the points corresponding to the last stages of life of the specimen as shown in Fig. 6.5. The slope of this curve should be equal to $1/(1-\alpha)$. The value of total strain amplitude for which the results in the original graph in Lemaitre and Plumtree (1979) were obtained was converted to a stress amplitude by using the stress-strain curve. The value of the stress amplitude gives a value for the maximum stress which can then be substituted into (4.45) to obtain a value for a.

Finally, it can be seen from (6.6) that the intercept of the straight line log(stress)-log(life) curve, which was found earlier, with the life axis is equal to

$$\log\left[\frac{M^{\beta}}{(1-\alpha)(\beta+1)}\right]$$

Since α and β had already been found, it was possible to calculate a value for M. Notice, however, that this again assumes that α remains constant. The value of α used to find M was that at which the value of a was previously calculated.

The original straight line stress-life curve calculated from the straight line strain-life curve in Lemaitre and Plumtree (1979) can now be compared with the actual curve obtained using the expressions in (4.44)-(4.47). Figure 6.6 shows the straight line and the calculated curves for three different values of mean stress. The point at which the zero mean stress curve

meets the straight line for constant α corresponds to the value of stress at which the value of α was calculated: i.e. to the value of stress for which the experimental results for Fig. 6.5 were obtained. Figure 6.6 shows that the assumptions made lead to a large overestimation of life by the model at low stress levels compared with the experimental results. It is conceivably possible to improve the correspondence of theory and experiment by removing the assumption that α remains constant and by finding α and β simultaneously. However, this would be an extremely complicated and time consuming procedure since, for each trial value of β, it would be necessary to refer to a graph of $\log (1-(1-\psi)^{\beta+1})$ against $\log(N/N_f)$, such as the one in Fig. 6.5, and to fit a straight line to the experimental points in order to find a value of α. It would perhaps be possible to automate this process in order to make it practical, but the effort required would not be justified since it would not constitute a general method. A better theoretical model could be obtained if better experimental data were available. In particular, if the load drop data from several fatigue tests were available, then it would be possible to use a more general curve fitting method to obtain both α and β without the necessity of assuming that α is constant.

6.4 Creep-fatigue Interaction

In previous sections a constitutive model for metals has been described and the coefficients of this model have been calculated for copper. It is implicit in the

model described that the effects of creep and fatigue are independent of each other. However, it is known from experiments that when they are both significant there is some interaction between them. The next sub-section describes the interaction between creep and fatigue in terms of a relationship between creep and fatigue damage. Some of the consequences of this relationship are then examined.

6.4.1 Damage Interaction

Creep and fatigue damage occur simultaneously when a component is subjected to cyclic loads at high temperatures. The prediction of the life of a specimen or component under these conditions is complicated by the fact that the two processes interact with each other in some way. For example, the creep life of a component is reduced if some fatigue damage is allowed to occur. Continuum damage mechanics provides a convenient method of modelling this interaction. In general, the evolution of damage in a material is described by rate equations such as

$$d\omega = f(\sigma, t, \omega, \psi)\, dt,$$
$$d\psi = g(\sigma, N, \psi, \omega)\, dN, \qquad (6.7)$$

where ω is the creep damage, ψ is the fatigue damage, N is the number of cycles and f and g are functions which describe the evolution of creep and fatigue damage respectively. It is convenient to make the assumption that ω and ψ are the same internal variable. If this

is denoted by D then this can be expressed by

$$D = \omega + \psi \qquad (6.8)$$

Equation (6.7) can now be rewritten as

$$d\omega = f(\sigma , t, D)\, dt,$$
$$d\psi = g(\sigma , N, D)\, dN, \qquad (6.9)$$

and so

$$dD = f(\sigma , t, D)\, dt + g(\sigma , N, D)\, dN \qquad (6.10)$$

Using these equations predictions can be made of the lifetimes of specimens under given loadings.

This hypothesis has been used by several authors in the prediction of lifetimes for specimens subjected to combined creep and fatigue conditions. The predictions have compared favourably with experimental results. The paper by Lemaitre and Plumtree (1979) contains such a study, as does a paper by Blackmon et al (1983). Chaboche (1981) has also published some results. These studies clearly show that the reduction in fatigue lifetime due to the occurrence of creep during the cyclic loading is predicted very well by the concepts of damage mechanics in conjunction with the interaction hypothesis described above.

In these studies the emphasis has been upon varying the frequency of cyclic loads. A very high frequency leads to pure fatigue loading, but if the frequency is lower

then timescales are extended and hence creep becomes more important. This is one of the many ways in which creep can be introduced into a cyclic loading test and this and other examples are illustreated in Fig. 6.7. One of the more common ways is to introduce dwell periods during which the load is held constant, as shown in Fig. 6.7(c). For the present report it will be supposed that the loading can be divided up into blocks and this is shown in Fig. 6.7(d). Each block has a fatigue component which is essentially time independent, during which the load is cycled at high frequency, and a creep component, during which the load is held constant for a certain period of time. This type of loading is used because it is representative of that which occurs in the nuclear power generation industry where plant operates under load for long periods of time with cyclic loads being imposed when it is shut down periodically for maintenance or inspection.

The model described above for OFHC copper, and the values of the coefficients found were used in a theoretical study of the effect of block creep and fatigue loading on the total lifetime of a specimen. The results of this are now presented.

6.4.2 Sequence Effects

The model was used in a study of the effect of the sequence in which the different types of loading are applied. Thus, there are two types of loading: (i) a load dwell followed by cyclic loading, and (ii) a period of cycling followed by a load dwell. These will be referred to as creep first and fatigue first loading respectively.

In each case a set amount of the first type of loading is applied and then the second type of loading is applied until failure occurs. For example, creep first loading involves applying a load dwell for a certain time t, followed by cycling to failure. The number of cycles required for failure is denoted N and it is assumed that the period of cycling does not take any time. These loading cases may be thought of as block loading with a single block being applied over the whole lifetime. The effects of these loadings may be summarized by plotting a graph of t/t_f against N/N_f where t_f is the time to failure if the load dwell is held fixed throughout the life of the specimen, and N_f is the number of cycles to failure under the pure cyclic loading. The symbols t and N are the actual time and number of cycles respectively at which the specimen fails. Examples of these graphs are shown in Fig. 6.8. The first graph is for a creep first loading. Note that t/t_f is plotted along the horizontal axis. This is because for creep first loading the time t is the independent variable. Graphs such as these may be interpreted by noting the following points. The point (0, 1) corresponds to an initial dwell period of zero time and therefore to a pure cyclic loading with failure occurring at N_f. The point (1, 0) corresponds to an initial dwell period equal to t_f and therefore to failure wholly due to creep. For values of t in between 0 and 1, the graph shows the effect on the number of cycles required for failure after different periods of initial load dwells. For example, the graph shows that if even a relatively small amount of creep is allowed to take place before

applying a cyclic load, then the remaining life of a specimen under pure fatigue loading is substantially reduced. For instance, a dwell time of 10% of the total creep life results in the remaining life under cyclic loading being reduced by almost 80% of the total fatigue life. This reduction in remaining life can be explained by examining the damage evolution for creep and fatigue. Creep damage grows much more quickly in the early stages of the life of a component under pure creep loading than does the fatigue damage under pure fatigue loading. In the latter case it is not until late in the life that the damage becomes appreciable. Thus, the relatively quick growth of creep damage in the early stages of creep life means that the material degradation is as bad in the early stages of creep life as it is in the late stages of fatigue life and so, according to the damage interaction rule described above, the remaining life under fatigue is greatly reduced. The second graph in Fig. 6.8 shows the results obtained for fatigue first loading. Note that N/N_f is now plotted as the horizontal axis since it is now the amount of initial cycling that is specified for each test. The graphs shows that the initial period of cyclic loading does not have the same effect on the remaining creep life as creep does on the remaining fatigue life. For example, the remaining creep life is only reduced by 10% of the total life even after an initial period of cyclic loading for 80% of the fatigue life. This is again due to the shapes of the damage evolution curves for creep and fatigue damage. Thus, it is not until quite late in the fatigue life that enough damage has been

accumulated to cause the creep life to be significantly affected. This is simply the reversal of the argument given for creep first loading. In fact, the curve in Fig. 6.8(b) is the same shape as that in Fig. 6.8(a), but with the one being obtained from the other by reflection in the line from (0, 1) to (1, 0).

6.4.3 Block Loadings

The situation with regard to block loading programs is a little more complicated but similar effects can be demonstrated. The terms used to describe a block are schematically illustrated in Fig. 6.7(d). The interaction of creep and fatigue loading may be studied by varying the amounts of the two types of loadings within each block. The amounts of each loading type are not allowed to vary freely within a block, but the amount of creep or fatigue loading is fixed for each block and the other type of loading is varied. When failure occurs, the total time and number of cycles which have been accumulated are recorded. In this way graphs like those in Fig. 6.8 may be constructed for block loadings. For example, Table 6.3 gives the results obtained for 10 hours of load dwell per block. These results are plotted in Fig. 6.9 where they are also compared with the graph obtained for creep before fatigue (Fig. 6.8(a)). This shows that, in general, the presence of creep damage reduces fatigue life with respect to the pure fatigue life, but that, since the loading is in blocks, more cycles are required for failure than in the two level test.

6.5 An Example - The Two Bar Structure with Mechanical Loading and Superimposed Thermal Cycling

In their paper (1979), Megahed and Ponter report the results of several tests carried out on a two bar structure, shown in Fig. 6.10(a), at high temperature. Each of the bars was made from copper and the load consisted of a fixed mechanical load with cyclic thermal strain occurring in one of the bars. The model which has been developed above for copper may be assessed by comparing its predictions with the results of these tests. The previously written computer program, for solving problems in multibar structures, may be used for modelling this two bar structure and the predictive ability of the model may be examined. The computer program could only solve multibar problems involving cyclic plasticity, hence it had to be adapted so that it would be capable of solving creep problems as well. In addition, further modifications were made to the program so that it could solve a problem in which the applied strains are thermal and are not applied uniformly to all of the bars in a structure. The methods by which these additional requirements for the program are satisfied are discussed below. Also discussed are several other aspects of the model and solution procedure such as temperature dependence, primary strains and creep ductility.

6.5.1 The Method of Calculating Creep Strain and Creep Damage

The evolution of creep strain and damage are described by the rate equations (6.2) and (6.3). These must be

numerically integrated simultaneously with respect to time to give the actual strains and damage values. The method employed here is an Euler method with time step control which is described in a paper by Hayhurst and Krzeczkowski (1979). Details of how it was employed in the present case are given in Appendix C. This appendix also contains details of how the equilibrium of a multibar structure is satisfied in the presence of creep strains.

The effect on a structure of any change in creep strain is calculated before the change in damage is calculated. The damage change is calculated by the Euler method from (6.3), using the same time step that was used in calculating the change in creep strain. Once the new value is found, a check is made to see if the bar has failed due to damage becoming greater than or equal to unity. If a bar does fail then the time at which it fails is ascertained by liner interpolation and the stress and plastic strain are recalculated to reflect the new state of the bar.

A change in damage causes a change in the effective value of both Young's modulus and the hardening modulus and hence also a change in the elastic and plastic strains. The changes in these strains are computed from the constitutive equations and the effect of this is treated in the same manner as creep or thermal strains.

6.5.2 Thermal Straining

A change in thermal strain is treated in the same way as a change in creep strain and details are given in Appendix C. In order to simplify the computation

required to solve the temperature cycling problem, it was assumed that the change in temperature is instantaneous so that no creep straining occurs during the heating and cooling phases. This is not a realistic assumption to make since Megahed and Ponter (1979) report that the cooling of one of the bars by 50°C took about 1 hour to complete in their tests. However, the time-variation of temperature in a bar during heating or cooling was not reported by Megahed and Ponter, and so it was necessary to make an assumption about the time-variation used in the theoretical model.

The introduction of thermal strains into the model introduces a problem with the numerical solution of multibar problems. The equilibrium solution procedure operates using the assumption that the residual forces decrease monotonically to zero, and that the strain increments in all the bars are of the same sign during each iteration. If the plastic strain in one bar is of the opposite sign to that in another bar, then the procedure overestimates the amount of plastic strain in one of the bars. In a two bar structure the result is that both bars unload and the stress in each bar does not lie on the yield surface. The effect of this problem is small because the overestimation of plastic strain is not very great when compared with the total amount of plastic straining and it was observed that this situation occurred infrequently. Also, the effect of this can be minimized by restricting the amount by which the thermal strain in each bar is allowed to change. It was found that a satisfactory value for the restricted strain

change is given by the elastic strain that corresponds to a change of stress equal to the yield stress.

6.5.3 Temperature Dependence of Model

As already noted, the coefficients for a model of copper listed in Table 6.1 were calculated on the assumption that they were independent of temperature. The data published by Megahed and Ponter (1979) and shown in Figs. 6.3 and 6.4 demonstrates that for creep this is not the case, and that the difference in creep rates and creep lifetimes is quite significant even for a difference of only 50°C. The tests on two bar structures performed by Megahed and Ponter were creep dominated and so it was deemed necessary to include the effects of temperature on the creep properties of the model so that the predictions of lifetime would be as accurate as possible. The temperature dependence follows the Arhenius law for both creep and damage rates and so (6.2) and (6.3) are now written as

$$\frac{dv}{dt} = A_0 \exp\left[\frac{-Q_c}{R\theta}\right]\left[\frac{\sigma}{1-\omega}\right]^n \qquad (6.11)$$

and

$$\frac{d\omega}{dt} = B_0 \exp\left[\frac{-Q_r}{R\theta}\right]\left[\frac{\sigma}{1-\omega}\right]^\nu \qquad (6.12)$$

where A_0, B_0, Q_c and Q_r are material constants, R is the universal gas constant and θ is the absolute temperature. The values of the additional constants are listed in Table 6.1.

6.5.4 Primary Creep

The numerical model does not take into account the creep strains that are accumulated at the beginning of a creep test. These strains are known as primary strains and occur during a relatively short period after a load is first applied to a material at high temperature. It was found during trials that the numerical model predicted a transient excursion in the stress envelope which occurred during the first few cycles. This stress excursion does not appear in the experimental results and so the reason for this difference was sought. It was found that the excursion could be altered by the inclusion of an initial plastic strain in one of the bars. This led to the conclusion that initial primary strains could be such that the excursion in stress was not observed in the experimental tests. Thus, it was discovered that by including a rapid accumulation of creep strain at the beginning of a computation, the stress excursion could be eliminated. The results obtained showed the success of this procedure to be strongly insensitive to the form of model used for primary creep.

6.5.5 Creep Ductility

Equation (6.3) may be written with an extra parameter as follows:

$$\frac{d\omega}{dt} = B \frac{\sigma^{\nu}}{(1-\omega)^{\phi}} \qquad (6.13)$$

The extra parameter, ϕ, controls the shape of the tertiary portion of the creep curve and allows it to be changed

without affecting the theoretical rupture time of a uniaxial specimen. The shape of the tertiary creep curve governs the rate and amount of stress redistribution that takes place in a structure during the last stages of life and so has an effect on the total lifetime of the structure. Hence, the value of a ϕ will influence the lifetime of a structure. Goodall and Ainsworth (1977) have proposed a parameter λ called creep ductility which depends on ϕ and which is a measure of the amount of tertiary creep straining that a material is capable of. λ is defined by

$$\lambda = \frac{1+\phi}{\phi-n+1} , \qquad (6.14)$$

where n is the same as in (6.2). High creep ductility ($\lambda > 7$) implies that stress redistribution readily occurs whereas low creep ductility ($\lambda < 3$) results in a relatively small amount of stress redistribution. Therefore, a greater value of λ leads to a longer structural lifetime than a smaller value.

The effect of creep ductility on stress redistribution in the two bar structure and the consequent effect on life is shown in Fig. 6.11. The figure shows the stress envelope of the shorter bar for two values of ϕ, namely ϕ = 6.1 and 10. These correspond to the values 16.9, and 2.5 of λ respectively. Also shown in Fig. 6.11 are the calculated lifetimes of the shorter bar in hours. It can be seen that greater creep ductility leads to the maximum stress becoming lower quite early in the lifetime of the structure. This difference in maximum stress increases

with time at first but eventually, because damage growth is retarded by the relative decrease in maximum stress, the material with the higher maximum stress (ϕ = 10) fails before that with the lower (ϕ = 6.1).

From these results it can be seen that creep ductility can have an important effect on the lifetime of a thermo-mechanically loaded structure, although it was found that it was not as important as the effect due to temperature change on creep strain rates. Thus, the extra parameter ϕ was incorporated into the constitutive model but, since no data on its exact value is available, its value was set equal to that of ν for the subsequent studies.

6.5.6 Comparison of Model Predictions with the Experimental Results

Two of the tests that Megahed and Ponter carried out were chosen for comparison with the numerical model. The specifications of these tests are given in Table 6.4 and the structure is illustrated in Fig. 6.10. The structure consisted of two bars, both with the same cross-sectional area and with bar 2 twice the length of bar 1. The thermal loading was applied by changing the temperature of bar 1 periodically. In both tests the temperature in bar 1 was held constant for 3 hours at a time. The base temperature for the experiment was 300°C and the temperature change was -50°C. The difference between the two tests was the value of the steady mechanical load: In test 1 it was about 52 MPa and in test 2 about 62 MPa (the loads have been divided by the area of the bar 1). The results published by Megahed and

Ponter (1979) consist of a trace of the stress in bar 2 and a trace of the total strain in bar 1. The envelopes of these original plots are shown in Figs. 6.12-6.15 alongside the predictions of the numerical model.

Figure 6.12 shows the stress in bar 2 during the first test. The upper stress variation in this bar is very well reproduced by the model. The theoretical envelope displays a flat upper curve which remains at an almost constant level. The lower curve displays the rapid increase in level just before the failure of the other bar at the end of the test. In the theoretical curve this increase towards the end is due to the rapid growth of damage in the other bar just before it fails. It can be seen that the behaviour of the experimental specimen, which is due to the weakening effect of grain boundary cavities, is well modelled by continuum damage mechanics. The time to rupture is predicted with an error of less than 25%. This is not very accurate but is not surprising since it can be seen that the actual levels of stress in the bar are not predicted very accurately either. This is because in the theoretical calculations it was assumed that the temperature change took place instantaneously. However, Megahed and Ponter (1979) report that the temperature changes took place over relatively long periods. For instance, they report that the drop in temperature of 50°C took about an hour to complete which is a third of the time during which the temperature was supposed to be constant. However, they do not give details of how the temperature in the bar varies with time, and so it would be difficult to overcome this problem

by modelling the actual temperature variation. An exploratory study showed that trying to take the elapse of time into account during the temperature change did reduce the predicted stress range in line with what is observed in the experiments. Figure 6.13 shows the total strains for this test. The theoretical calculations reproduce the behaviour of the bar very well.

Figures 6.14 and 6.15 show the equivalent results for the second test which is the same as the first except that the applied constant mechanical load is higher than in the first. Again, the theoretical stress range (Fig. 6.14) is larger than the experimentally observed range. However, in this case the lifetime of the first bar is underestimated. In Figure 6.15 it can be seen that the total strain variation is reproduced quite well but that the level of strain at any time is consistently underestimated.

6.5.7 Discussion

The model described in previous sections has been used here to provide theoretical predictions for a series of tests carried out on two bar structures by Megahed and Ponter. The model has reproduced the qualitative features of the experimental results very well. The theoretical model has been shown to reproduce the effects of stress redistribution due to the growth of damage towards the end of the life of the structure. However, the predictions of the lifetime of the structure have not been as good. This is presumably because some of the details of the tests have not been copied by the model.

In particular, the most important difference is the exact time-variation of the temperature in the bars when the temperature is changed from one level to another. This would have a significant effect on the stress envelope and hence on the creep strain and damage rates. A less significant inaccuracy in the model is that the stress-strain curve was found for a different batch of copper under different conditions. Thus, the cyclic stress-strain curve of the material used in the experiments is possibly quite different from that assumed by the model. This should make a difference, but it was found that the predictions of the model were relatively insensitive to variations in the shape of the stress-strain curve.

It was found that, for these types of tests where the temperature varies and the failure is creep dominated, it is important to take into account the dependence of creep properties on temperature. It was found that estimates of lifetime can be significantly altered by assuming that these properties do not vary with temperature. In addition, it has been demonstrated that creep ductility influences lifetime and hence should be taken into account. Although this has been demonstrated for the two bar structure it should be taken into consideration when making lifetime predictions for any structure.

In this section, the capabilities of the model have been demonstrated by comparing its predictions with some tests carried out on a two bar structure. The multibar model structure may be used to model more complex components where the stresses in the region of interest

are essentially uniaxial in character. Thus, it is of interest to study the behaviour of other structures under other loading conditions using this model. These further studies are carried out in the next section.

6.6 Predicted Behaviour of Other Structures

In this section, the behaviour of various multibar structures under various loading histories are studied. The loading history used in the previous section, where the mechanical load is relatively large, is studied here, but there are also components which operate under creep-fatigue conditions for which the mechanical load is low and it is of interest to study the predictions of the model for this case. These components are associated with heat transfer problems where a high temperature gradient through the component thickness is encountered. Under on-load conditions there is a large temperature change through the surface layer of the component with the bulk of the section remaining at an approximately uniform temperature. Under off-load conditions an approximately uniform temperature distribution is found throughout the cross-section of the component. Cycling between these two states is frequently encountered and this situation may be modelled using the constitutive model described above and the multibar model.

This situation is simulated by a purely thermal loading. This was firstly applied to a two bar model and the results of this test are presented below. After this it was applied to a six bar model structure. This enabled the study of the effect of a thermal gradient in the

component in more detail by introducing a temperature gradient from bar to bar. The effect of a stress concentration in a component may be studied using a multibar model and this can be done in better detail using a structure with more than the two bars used in the previous section. A six bar structure has already been used in Chapters 3 and 5 to study the effect of stress redistribution due to fatigue damage. This is used again here to study the effects of a stress concentration on the creep-fatigue behaviour of a structure and the results of this are also presented in the next sub-sections. Each of the structures used in these studies is described in detail in the relevant sections.

6.6.1 Two Bar Model Structure with Zero Mechanical Load

The previous section has dealt with the response of a two bar structure subjected to a fixed mechanical load and a cycled temperature. Here the load is removed and the behaviour of a two bar structure under a pure thermal load is examined. Under these conditions the simple structure is representative of a component whose surface is subjected to a temperature cycle.

Initially, numerical experiments were carried out on the same structure that was used in the last section. However, it was found that it was impractical, simply by imposing a large temperature jump, to induce in the structure stresses which were large enough to result in reversed plasticity. Since the stresses induced were not very large it took a large number of temperature cycles to accumulate enough damage to cause rupture of any of

the bars, and this in turn lead to the use of a large amount of computer time. The low stresses induced in the thermally loaded bar were due to the low stiffness of the rest of the structure. When the thermal strain in bar 1 changed, the other bar tended to yield and the strains were allowed to become quite large without significant changes in the stresses. The low rate of damage growth was due in part to the low stresses, but another factor was the dependence of the creep properties on temperature. Large temperature changes resulted in extremes of creep behaviour. At the lower temperature, bar 1 was in tension and creep damage accumulated. However, if the temperature change was a large one then the lower temperature would be such that the rate of damage growth was very slow. At the higher temperature, bar 1 is in compression and the damage in this bar did not increase. One way to increase the stiffness of the structure is to increase the area of bar 2 so that it remains elastic under most conditions and another is to decrease its length. This causes the stress in the first bar to become relatively large, even for small temperature changes. Thus, changing the structure also means that the temperature can be higher when bar 1 is in tension and this results in increased damage growth rates. The results obtained from one particular structure are now described.

In the structure that was used, both bars have the same length and the area of the bar 2 was ten times that of the bar 1, as is illustrated in the inset to Fig. 6.16. This meant that for moderate temperature excursions bar

2 did not yield and that it was possible to raise the stresses in bar 1 to relatively high levels. This structure is a simple model of a component without a stress concentration and with a surface layer which is subjected to a cyclic temperature variation. This surface layer yields due to the stresses induced by the thermal strains, but the body of the component, which is protected by its surface remains at the base temperature, does not yield.

A temperature cycle between the limits 300°C and 400°C was applied to bar 1 of this structure. The timing of this temperature cycle was the same as that used in the experiments reported above and consisted of a holdtime of 3 hours at each temperature, as shown in Fig. 6.10. The response of bar is illustrated by Figs. 6.17-6.18. One of the surprising features of these graphs is that the evolution of the plotted quantities is, in each case, almost linear with respect to time. Another feature is the magnitude of the plastic strains in bar 1, which reach values of almost 6% at failure.

The almost linear evolution of the response of the bars is due to the rate of damage growth and to how the level of stress changes it. This interaction between stress and damage is governed by equation (6.13). The graphs in Figs. 6.17-6.18 were obtained using a set of coefficients for which $\phi = \nu = 6.1$ and so the effect of stress on damage growth rate and that of damage on stress exactly balance each other. The damage in bar 1 is shown in Fig. 6.16. The two curves in this figure are the total damage and the fatigue damage and hence the difference

between the curves is the creep damage. It can be seen that the damage growth is almost linear. Fatigue damage is not apparent until about 1100 cycles. There is a bend in the curves at around 1900 cycles but its cause is not clear; it is possibly due to the increase in fatigue damage. The growth of fatigue damage is very small in the early stages of life and it is not until quite late in the total life of a specimen that it becomes significant. Since fatigue damage is governed by a separate equation from (6.13) it will result in a different rate of damage growth and it may be this that causes the change in the slope of the curves. However, the growth in fatigue damage depends upon the stress amplitude and this is decaying as the test proceeds, as can be seen in Fig. 6.17 and this may mean that the fatigue damage does not continue to grow faster.

The linear evolution of the stress envelopes is shown in Fig. 6.17. The two curves are the minimum and maximum values of the stress that are attained in bar 1 during the temperature cycles. The upper curve is the stress which occurs when the temperature of the bar is 300°C, and the lower curve when the temperature is 400°C. The slope of the stress envelopes is directly related to the slope of the damage curve in Fig. 6.16. Hence, there is a change in the slope of the curves at around 1900 cycles which corresponds to that in the damage curve at the same place. If the value of ϕ is different to that of ν in (6.13) then the damage growth curve becomes non-linear with a sudden increase in damage as the time approaches that for rupture. This means that the stress

envelopes also become non-linear, as is illustrated in Fig. 6.19 which shows the stress envelopes that are obtained if $\phi = 10$. Figure 6.19 also shows that the lifetime of the bar is decreased at this value of ϕ. $\phi = 10$ corresponds to a creep ductility of $\lambda = 2.5$ according to (6.14), whereas $\phi = 6.1$ corresponds $\lambda = 16.9$. These results are thus in accord with the statements which were made about the effect of creep ductility on lifetime.

Figure 6.18 shows the plastic strains in bar 1 for this test. Here again the curves are the envelopes of the maximum and minimum values and the lower curve is the higher temperature. Two changes of slope occur, one at 1000 cycles and the other at 1700 cycles. It can be seen that the plastic strains become quite large at failure. This is due to equally large creep strains in the opposite sense, which is in turn due to the temperature dependence of the creep rate. When the temperature is at a maximum the stress in bar 1 is negative, due to a positive thermal strain and the creep strain is accumulated in the negative sense. Conversely, when the temperature is at a minimum the stress is positive and the creep strain rate is positive. However, the creep rate is greater at the greater temperature than it is at the lower temperature and so the overall creep strain is negative. In order to satisfy the compatibility requirement of the structure, large positive plastic strains accumulate to compensate for the negative creep strains, while the total strain remains very small.

It is clear from Fig. 6.16 that the fatigue component

of the total damage is actually quite small compared with the creep damage component and in the examples studied so far, creep damage has been the dominant factor in any failure. This is because the stresses that are produced by pure thermal strain changes are not great enough to cause fatigue damage to accumulate significantly enough to cause failure due to low cycle fatigue. In addition, the temperature dependence of creep means that if large temperature variations are used to cause a large stress change, then the creep life at the higher temperature is extremely short and again the creep damage accumulation greatly predominates over fatigue damage. The effect of increasing the fatigue component can be investigated by altering the constants describing the fatigue damage evolution so as to reduce the fatigue life at the stress levels which are of interest. This was done for the two bar structure used here and it was found that the stress behaved in a similar manner to that shown in Fig. 6.19, even though the parameters ϕ and ν were equal.

The structure under pure thermal loading will never fail completely due to rupture of the second bar. This is simply because all of the stresses in the structure are due to those induced thermally in bar 1 and once this has failed, then the stresses in the structure become zero and no further damage is caused in bar 2.

6.6.2 Six Bar Model Structures

A component with a region of stress concentration can be modelled by a multibar structure with the lengths and areas of the bars chosen so that the variation of

stress from bar to bar simulates the variation of stress at the stress concentration. This was the idea behind the six bar example model which has been used in Chapters 3 and 5, to investigate stress redistribution in structures where fatigue damage occurs. The same six bar model is employed here to examine the combined effects of a cyclic thermal gradient and a steady mechanical load on a simple component with a stress concentration. A further six bar structure will be used after that to study the effects of a temperature gradient alone.

In each of the cases described below the temperature of the structure is initially uniform throughout and equal to the base temperature of θ_0 . A thermal gradient is applied by assuming that the temperature excursion varies in magnitudes linearly between bars 1 to 5 from the maximum to zero. Thus, if a temperature excursion of $\Delta\theta$ is applied to the structure, then the temperature in the ith bar is

$$\theta_i = \theta_0 + (5-i)\ \Delta\theta\ , \qquad i = 1,2,3,4,5 \qquad (6.15)$$

The temperature in bar 6 remains at θ_0 . This temperature distribution is illustrated in Fig. 6.20(a).

The first case consisted of the six bar structure used in Chapters 3 and 5 with an applied positive mechanical load and a cyclic temperature applied according to (6.15). The size of the mechanical load in this case was 220 MPa (divided by the area of bar 1) and $\Delta\theta$ = 50°C. The lengths and areas of the bars in the structure are summarized in Table 6.5 and the structure is illustrated

in Fig. 6.20(b). The temperatures in each of the bars when the temperature excursion $\Delta\theta$ has been applied are also listed in Table 6.5, as are the failure times that were calculated for each bar (due to a difficulty with the computer program the failure time of bar 6 was not calculated). The temperature cycle was 6 hours long with 3 hours at each temperature, as in Fig. 6.10. The behaviour of this model had similarities to that of the two bar structure under similar conditions. However, due to the larger number of bars, extra details of the behaviour became apparent. Bars 1 and 2 behaved in a similar manner to the bar 1 of the two bar structure. The stress in bar 1 is shown in Fig. 6.21. As this figure shows, the upper envelope curved down towards the end of the life of the bar and meets the lower envelope which has remained at an approximately constant level. As in the two bar structure, the upper envelope corresponds to the lower temperature (300°C) and the lower envelope to the higher temperature (350°C). Bars 5 and 6 of this structure behaved in a similar manner to bar 2 of the two bar structure. This is illustrated by the results shown in Figs. 6.12 and 6.14. However, bars 3 and 4 display different stress histories. Figure 6.22 shows the stresses in bar 3. It can be seen from this that stress redistribution causes both the maximum and minimum stresses to decay throughout the life of the bar with a sudden drop in stress, which completes the decay, taking place during the final few cycles. Bar 4 seems to have a behaviour which is intermediate between that of bars 1 and 6 (see Fig. 6.23). The lower envelope increases at about the same rate as

the upper envelope decreases and so the envelopes actually cross each other at about 125 cycles.

The sequence of failure of the bars was generally from 1 to 6, although under certain conditions other sequences were observed. Also, as can be seen in Table 6.5, it was observed that the bars failed in quick succession after the first failure. There are two possible reasons for this. One is that the load on each of the remaining bars is increased by the failure of any of the bars because equilibrium must be satisfied. The second is that the positive mechanical load causes the structure to creep throughout its life and to accumulate creep damage. Thus, once the first failure has occurred, the bars have all suffered appreciable damage and it does not take much more to complete the accumulation of damage and for failure to occur.

The second case is that in which the applied mechanical load is zero. A different structure was used to study this loading history as was the case with the two bar structure. This new structure consisted of six bars all of equal length and the areas of the bars were equal apart from bar 6 which had an area 6 times that of the rest (see Fig. 6.20(c)). This was so that the total area of the bars was the same as that of the two bar structure studied under zero load. The temperature cycle was applied to each of the bars according to (6.15) with $\Delta\theta$ = 100°C. Again the hold time was 3 hours at each temperature. The damage in bar 1 increased linearly from 0 to 1 in a similar manner to bar 1 of the two bar structure and so the stress envelopes were similar to

those shown in Fig. 6.17. The stress envelopes of the other bars also varied approximately linearly, although bar 4 had a lengthy period at the beginning of the test during which the stresses slowly rose, before settling down to a more linear evolution, as can be seen in Fig. 6.24. In fact, the evolution of damage in bar 4 did not become completely linear until after the failure of bar 3 at about 13,500 cycles. The stress envelope corresponding to the lower temperature in bars 2-6 had a short period of decay just before the failure of bar 1 and a sudden increase when bar 1 actually failed. Figure 6.24 also shows the jumps in the stress envelopes at the points at which bars 1-3 failed. After the failure of a bar, the stress envelopes in the remaining bars changed slope slightly and then continued to evolve linearly. This is illustrated best in Fig. 6.25 which is a plot of stress envelopes for bar 3. The stress in most of the bars decayed gradually to zero, but in bars 3 and 4 it remained quite high for a relatively long time, as can be seen in Figs. 6.24 and 6.25. This meant that fatigue damage began to grow in these bars. This is shown in Fig. 6.26 where the total and fatigue damage in bar 4 is plotted. The figure shows that the fatigue damage grew continually from when it became significant at about 1,500 cycles. The point at which bars 1-3 failed are picked out by changes in slope of the curves at around 2,600, 4,500 and 13,500 cycles.

Unlike the previous case there is a large number of cycles between the failure of each bar. There are two reasons for this. The first is because the load is

zero, the maximum stresses in the bars on average decay due to the increase in damage in the bars. Secondly, since the load is generated by thermal strains, on failure of a bar the loads in the remaining bars decrease; and since the magnitude of the temperature cycle decreases from bar 1 to bar 4, the thermal load decreases as these bars successively fail. As in the case of the two bar structure with bars of equal length, failure of the whole structure never occurs because bars 5 and 6 are held at the base temperature θ_0.

The results obtained here for the zero load case illustrate how the surface of a component, which is exposed to changes in temperature, can become damaged and cracked. In the material used for these tests the process appears to be comparatively slow and is creep dominated. The model employed here can clearly be used for predicting the time over which this surface cracking takes place, especially if the actual temperature variation is known.

6.7 Summary and Discussion

A model of the high temperature behaviour of a metal has been presented which includes both the time independent and time dependent properties of a material: i.e. those of creep and plasticity. The plasticity model is a kinematic hardening law with non-linear hardening curve which displays ratchetting and stress relaxation. The constitutive law for creep is relatively simple but can easily be extended to include the effects of primary creep and variable creep ductility. The growth of damage

due to both creep and cyclic plasticity is also included so that predictions of the deformation of a component close to failure and of the time of failure can be made.

Published data has been used to construct a model of the behaviour of copper at high temperatures. It was discovered that the available data is incomplete and could only be used to make qualitative assessments. In order that it should be possible to model materials in the manner proposed here, it is therefore necessary that a consistent program of material testing should be carried out beforehand. The testing should be done with this end in view so that sufficient information is retained from the experiments to be able to calculate all of the coefficients required by the model.

Published experimental results on a simulated two bar structure were then used to test the ability of this model to predict real material behaviour and the failure of a structure. The qualitative agreement between the model and the experimental results was very good. The model correctly predicted the effect of the growth of damage in one of the bars on the strain and stress envelopes towards the end of the life of the structure. The quantitative predictions were not very accurate. However, this was due mainly to the lack of information on the way in which the temperature changed during the thermal cycling.

Finally, the model was used to study the behaviour of a range of multibar structures under various conditions. A two bar and a six bar model were used to investigate the behaviour of a component subjected to

cyclic thermal loads on its surface, but with no mechanical load. Each structure behaved similarly; in each case it was predicted that the surface bars would damage and fail after about 2,500 cycles under the conditions which were imposed. The damage evolution when $\phi = \nu$ in (6.13) in both cases was essentially linear. In the six bar structure, stress redistribution between the bars meant that damage evolution was not linear in all of the bars all the time. However, once bars 1-3 had failed, then the damage evolution in bar became linear. When the creep ductility in the two bar structure was changed by using a different value for ϕ, then the damage evolution became non-linear and the life of bar 1 was substantially reduced. In each structure, plastic and creep strains accumulated steadily throughout life, but the total strains and the overall displacement of the structure remained small because there was no overall load. For the six bar structure, the number of cycles between the failure of each bar increased as the bars failed. This is because the stresses induced in the structure became less severe, since the thermal strains were not as great in the remaining bars. The zero mechanical load conditions correspond to models of practical situations where a component is subjected to a cyclic temperature gradient at its surface. The failure of the bars is analogous to the surface cracking of these components known as craze-cracking.

A six bar model which has been used before was used and was subjected to combined mechanical and thermal loading. This structure demonstrated the effects of a

stress concentration. Its behaviour was similar to the two bar structure that Megahed and Ponter used since the loading conditions are similar. The feature of the behaviour of this structure that cannot be seen in the two bar case is that the bars fail in very quick succession. This is because there is a positive mechanical load, and hence when one bar fails the remaining bars suffer a sudden increase in load. Also, the mechanical load means that all of the bars are undergoing creep damage throughout the initial period before the first failure and are consequently already relatively close to failure. This also means that the overall displacement of the structure steadily increases throughout the life of the structure.

The model has been shown to be capable of modelling very complex loading situations. However, it has been found that it is important to specify the precise loading conditions in as much detail as possible, especially for thermal loading, in order that the predictions of lifetime are accurate. In spite of this, it is expected that it will provide a very powerful design tool when used within a finite element package.

Name		Value
Elastic:	E	90 000 MPa
Plastic:	σ_y	15 MPa
	C	24520.8 MPa
	γ	102
Creep:	A	1.827×10^{-15}
	n	6.68
	B	2.355×10^{-13}
	ν	6.10
	A_0	1.025×10^{-9}
	B_0	3.363×10^{-3}
	Q_c	15062 J mol^{-1}
	Q_r	26604 J mol^{-1}
	R	8.314 J $K^{-1} mol^{-1}$
Fatigue:	σ_ℓ	10 MPa
	σ_u	254.5 MPa
	β	2.671
	b	0.00393
	a	0.0438
	M_0	1526

Table 6.1 Coefficients for the model of OFHC copper. The nominal temperature is 300°C where temperature dependence is not explicit.

Stress limits		dε/dN (absolute units)	
σ_{min} (MPa)	σ_{max} (MPa)	Experiment ($\times 10^{-6}$)	Theory ($\times 10^{-4}$)
0.0	193.0	1.81	77.56
0.0	206.8	8.32	98.88
0.0	220.6	46.0	128.53
0.0	234.4	166.00	175.02
22.1	220.6	29.60	126.55
55.2	220.6	8.05	120.18
110.3	220.6	1.09	97.83
165.5	220.6	0.40	47.64
84.2	105.3	1.23	-3.41
63.2	105.3	2.28	3.95
42.1	105.3	3.25	9.21
107.6	129.1	4.13	-4.50
64.6	129.1	8.62	13.67
43.0	129.1	9.70	19.16
21.5	129.1	13.12	22.76
132.1	154.1	6.98	-6.01
88.0	154.1	18.98	20.04
44.0	154.1	24.72	33.85
22.0	154.1	32.7	37.59
22.0	154.1	33.80	37.59

Table 6.2 Comparison of theoretical and experimental ratchetting rates. The experimental data come from Megahed et al., (1980).

Number of cycles per block	Failure	
	Cycles	Time (hours)
0	0	585
1	46	460
2	78	390
3	104	340
5	140	280
7	168	240
8	177	220
10	198	190
20	260	130
30	297	90
40	322	80
50	348	60
60	364	60
80	400	50
100	426	40
130	465	30
160	499	30
200	545	20
300	647	20
500	850	10

Table 6.3 Failure in terms of number of cycles and time for block loading with creep loading fixed at 10 hours per block.

	Mechanical Load, P/A (MPa)	θ_0(°C)	$\Delta\theta$ (°C)	Time at θ_0 (hours)	Time at $\theta_0 + \Delta\theta$ (hours)
Test 1	51.73	300	-50	3	3
Test 2	62.34	300	-50	3	3

Table 6.4 Loading of the two bar structure for experimental tests shown in Fig. 6.10(a).

Bar Number	Length	Area	High Temperature (°C)	Failure time (hours)
1	1.0	1	350.0	886.5
2	1.2	1	337.5	902.9
3	1.5	1	325.0	909.3
4	2.0	1	312.5	920.0
5	3.0	1	300.0	923.3
6	6.0	4	300.0	-

Table 6.5 Dimensions of the six bar structure shown in Fig. 6.20(b) and the temperatures and failure times of the bars.

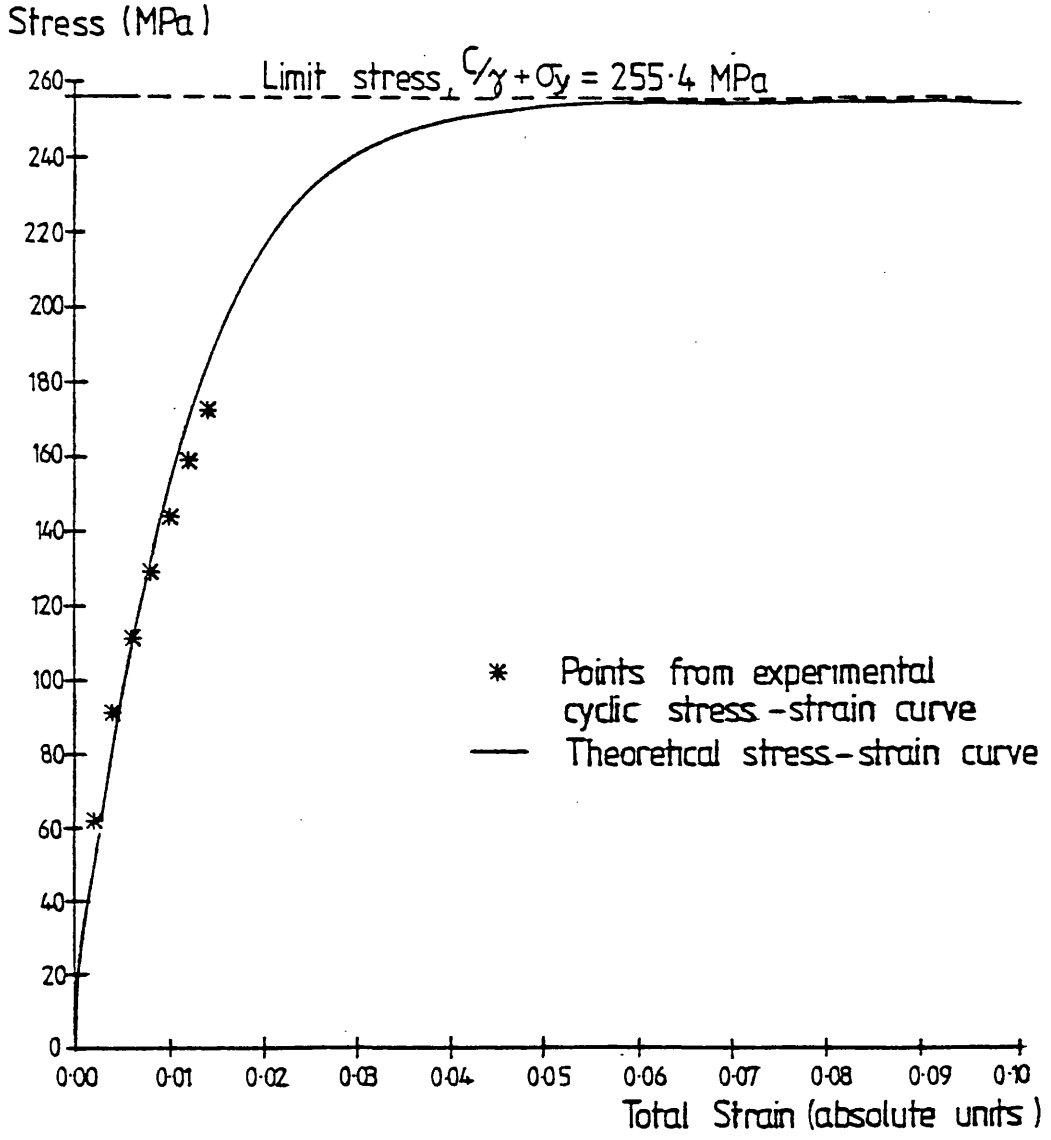

a) Total strain up to 10%.

Figure 6.1: Comparison between points taken from an experimental cyclic stress-strain curve and the theoretical curve fitted to them.

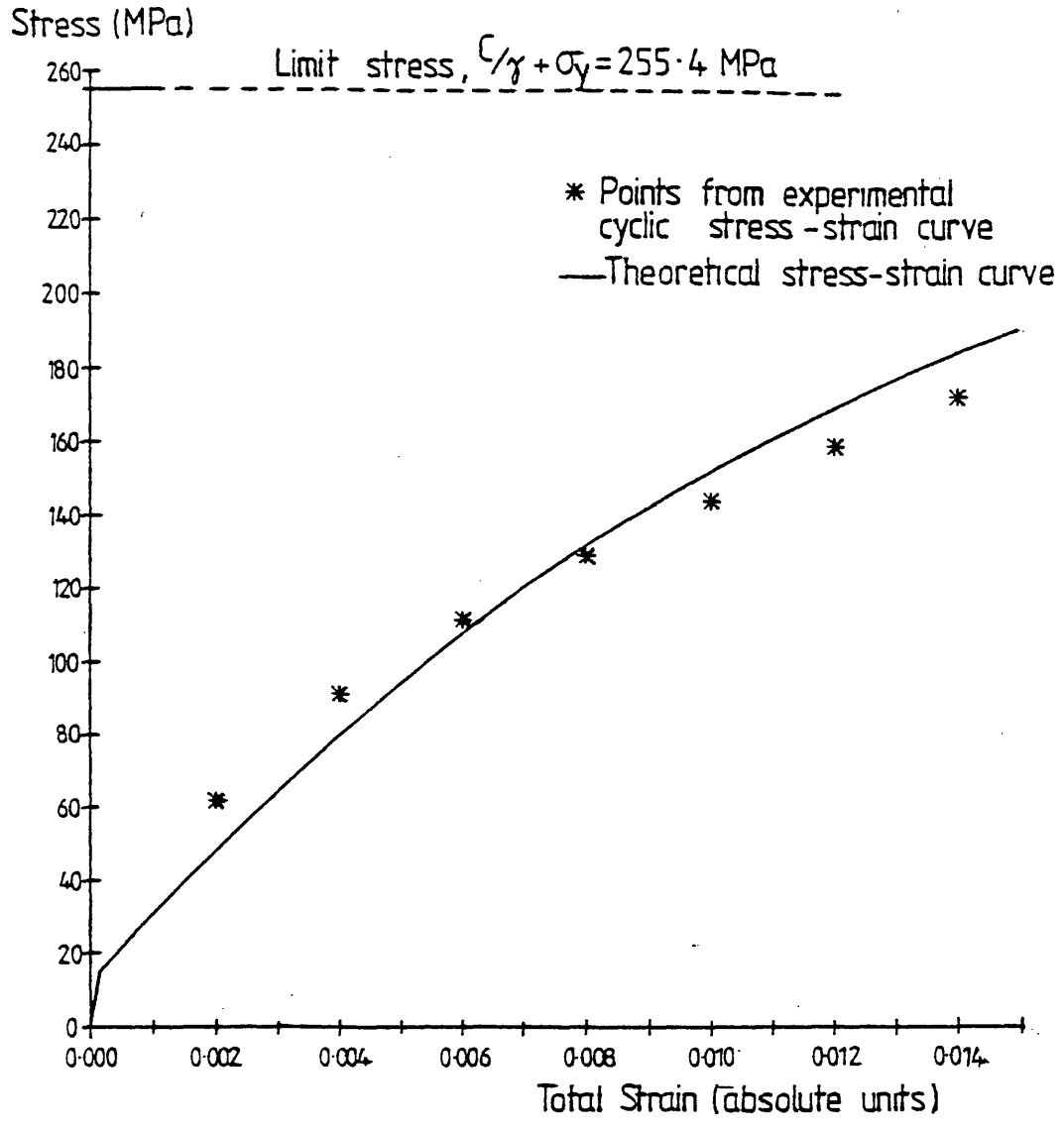

b) Total strain up to 1.5%.

Figure 6.1: continued

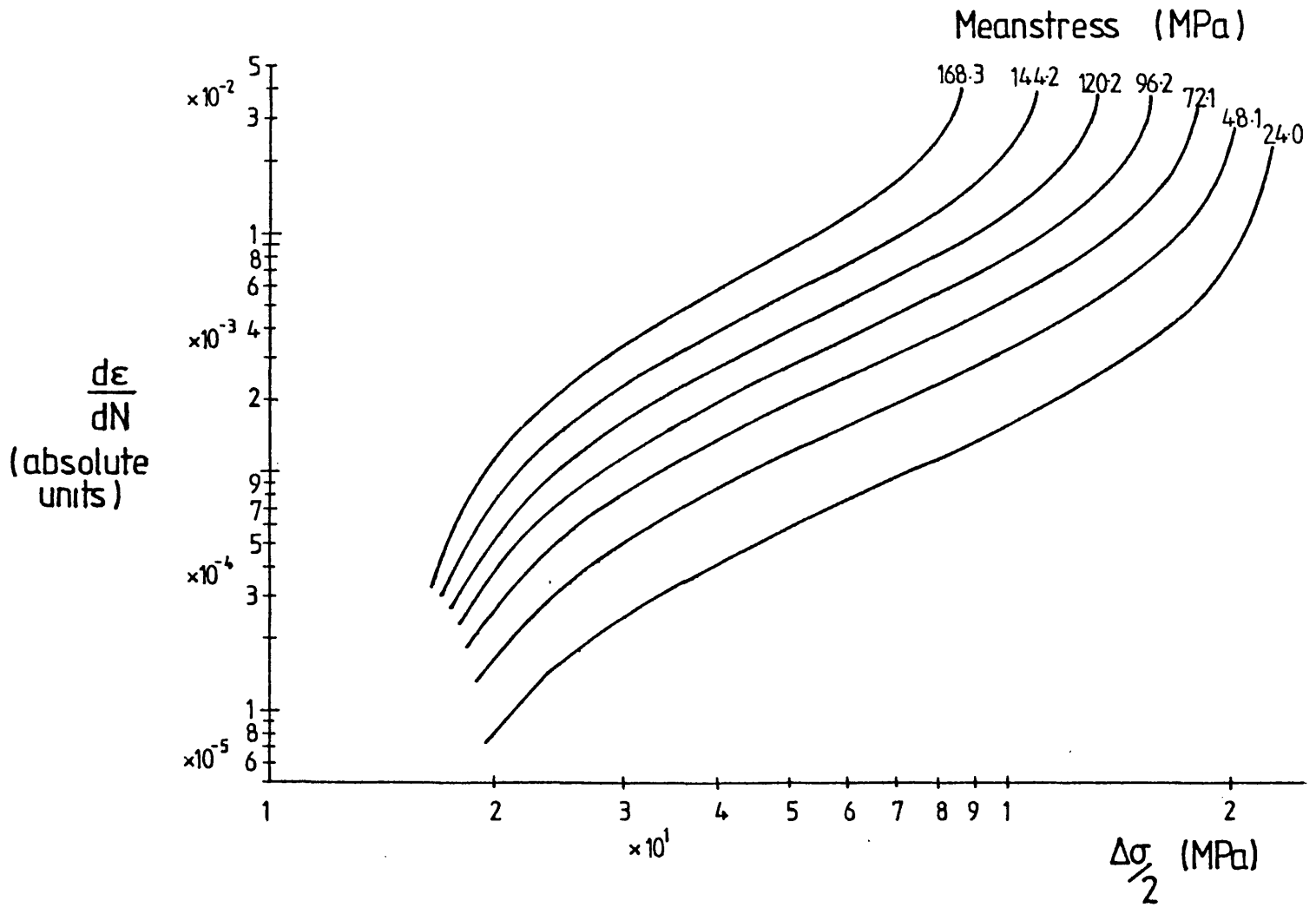

Figure 6.2: Graph of log(ratchet rate) against log(stress amplitude) for a series of values of mean stress, according to equation (6.5).

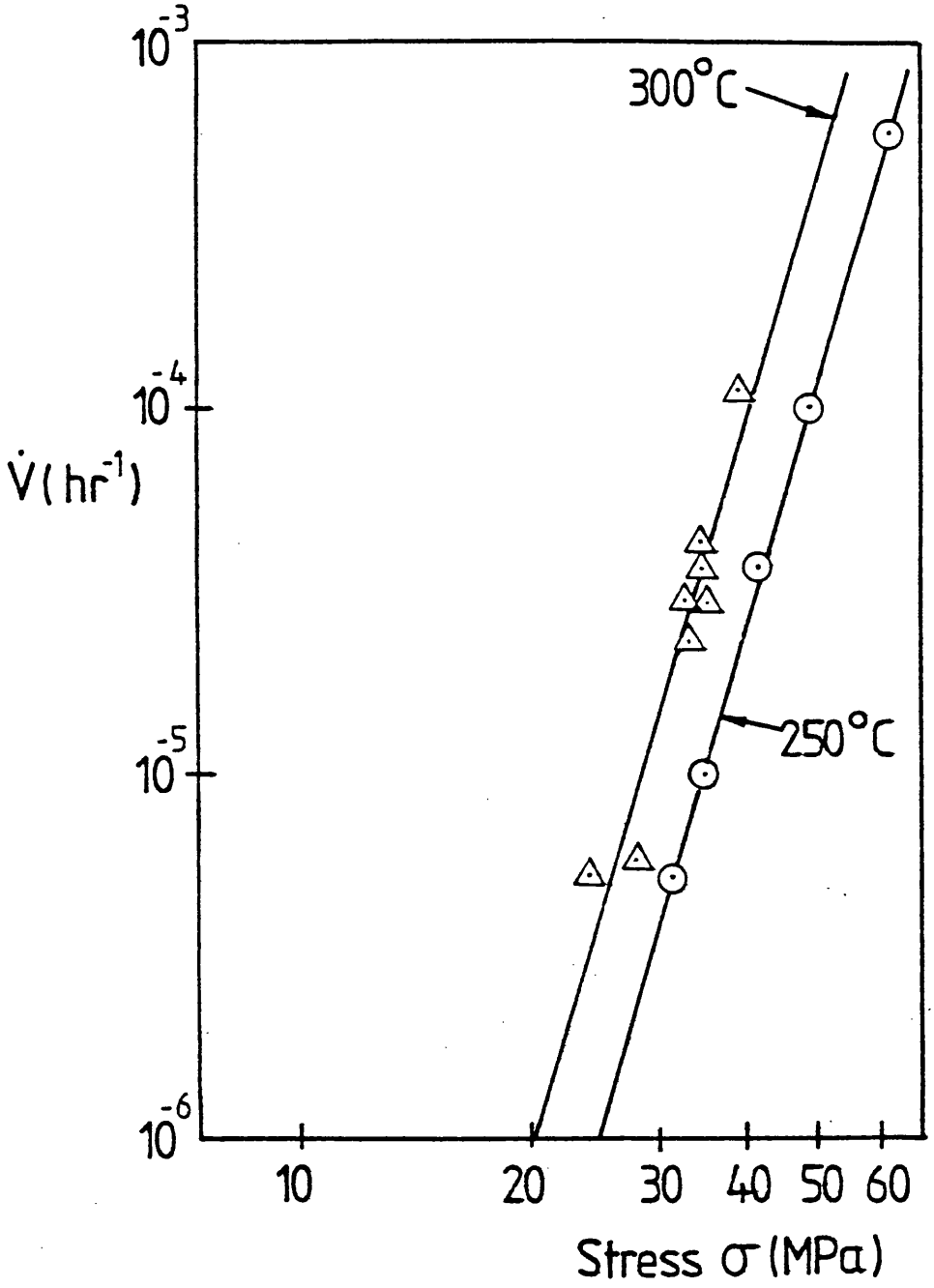

Figure 6.3: Experimental steady state creep rates for copper at 300°C and 250°C.

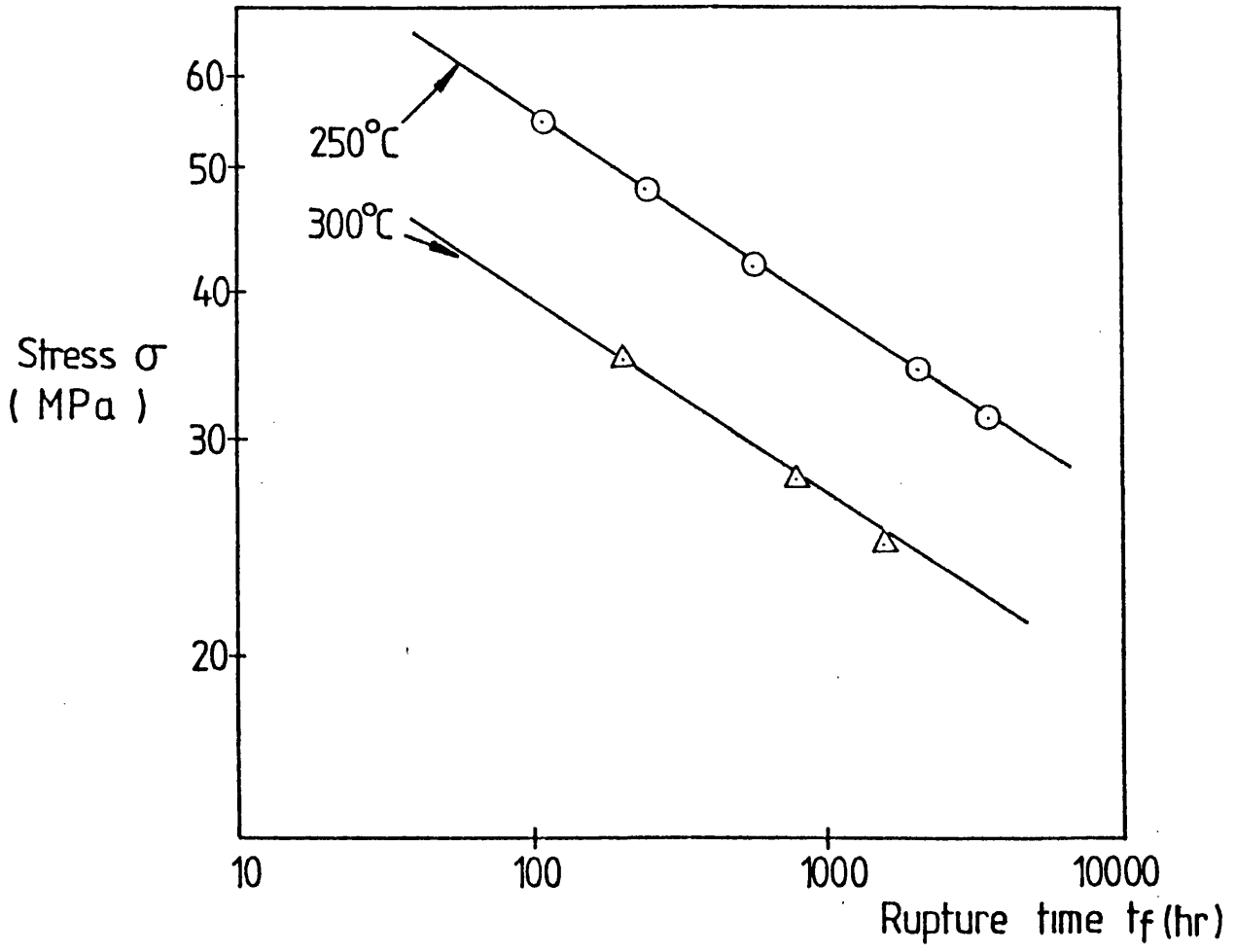

Figure 6.4: Log σ - log t_f plot of experimental data for copper at 300°C and 250°C.

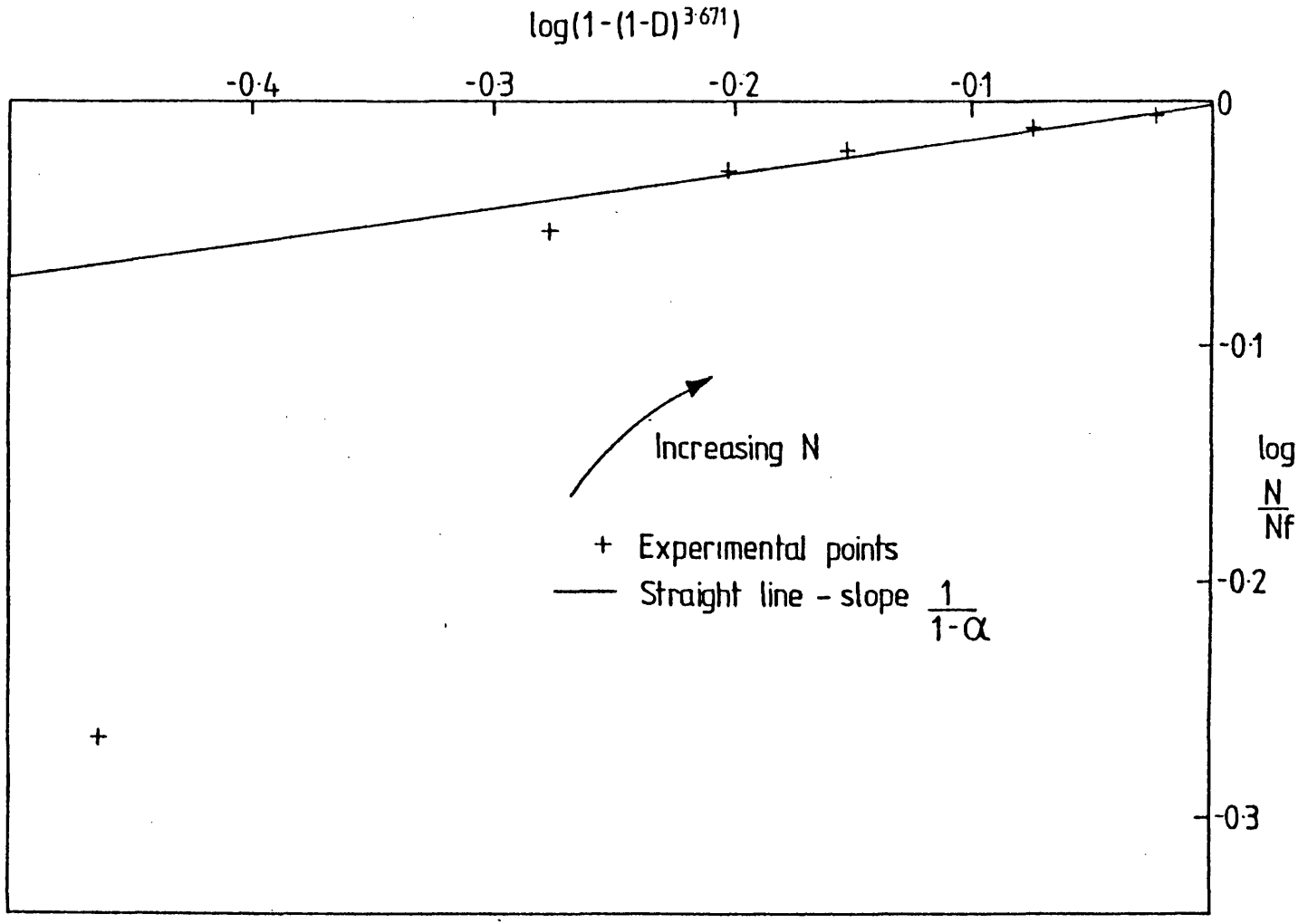

Figure 6.5: The relationship between the experimental points from Lemaitre and Plumtree (1979) and the straight line used to obtain the value of α.

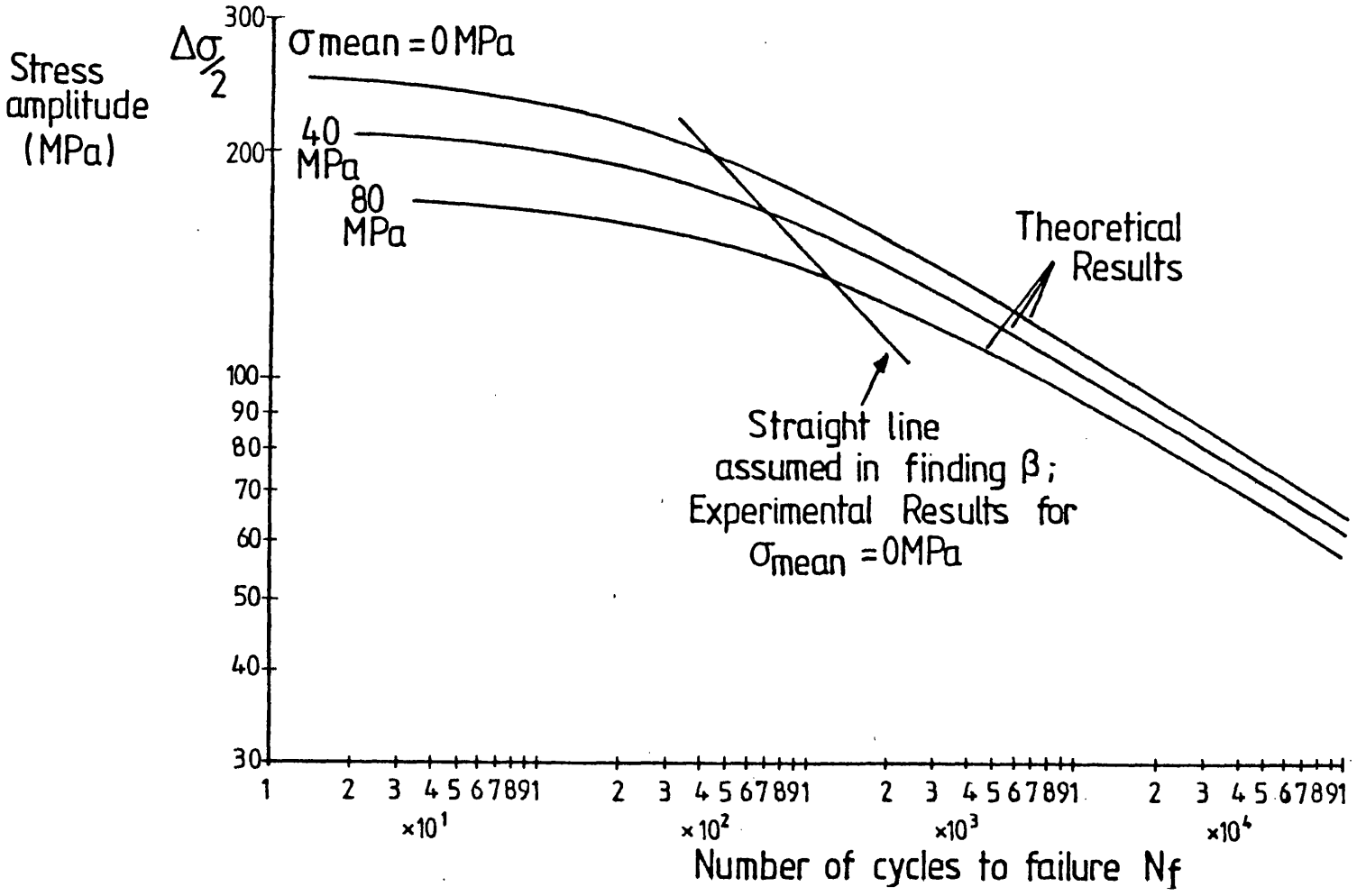

Figure 6.6: Curves of log(stress amplitude) against log(cycles to failure) for different mean stresses. The straight line has been calculated from the original experimental data in Lemaitre and Plumtree (1979).

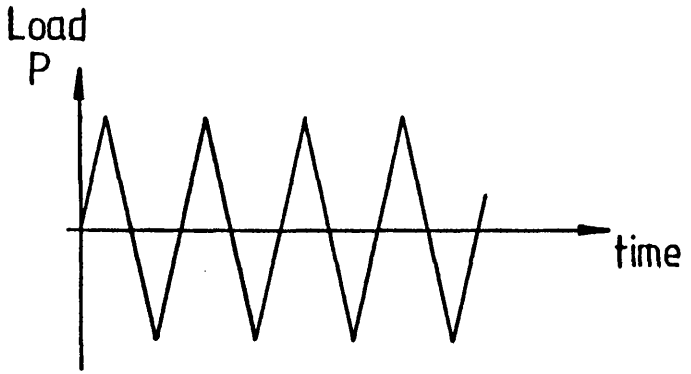

(a) Fast cyclic load leading to pure fatigue failure.

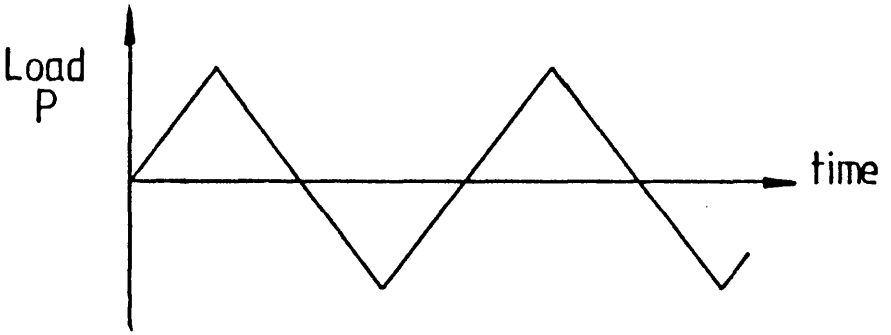

(b) Slow cyclic loading leading to creep/fatigue failure.

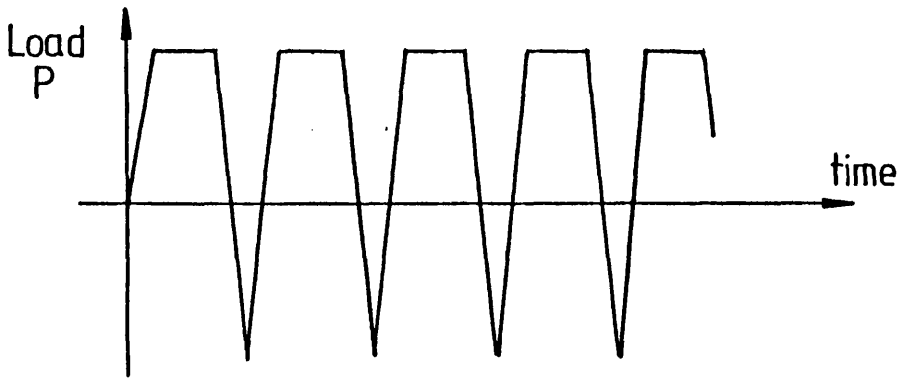

(c) Cyclic loading with tensile dwells.

Figure 6.7: Possible loading sequences for creep and fatigue tests.

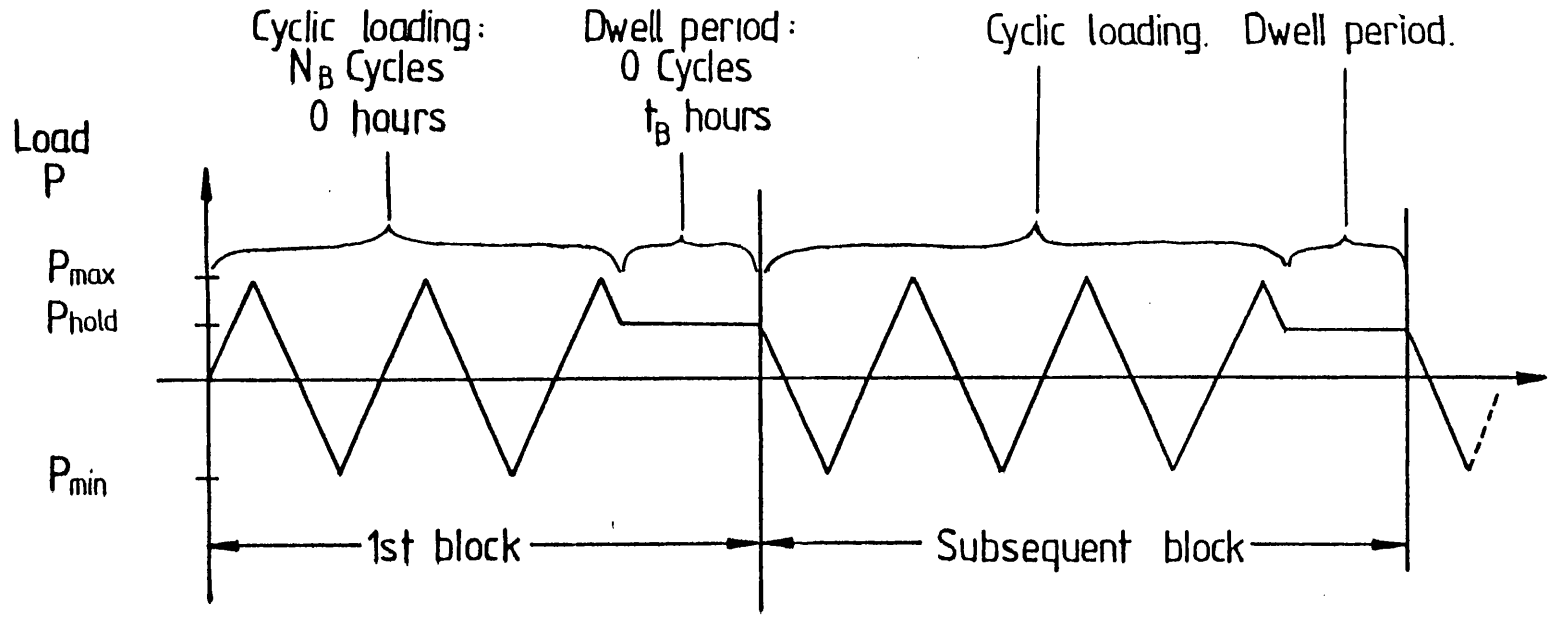

(d) Schematic diagram of a block loading program with N_B cycles and t_B hours dwell per block.

Figure 6.7: Continued.

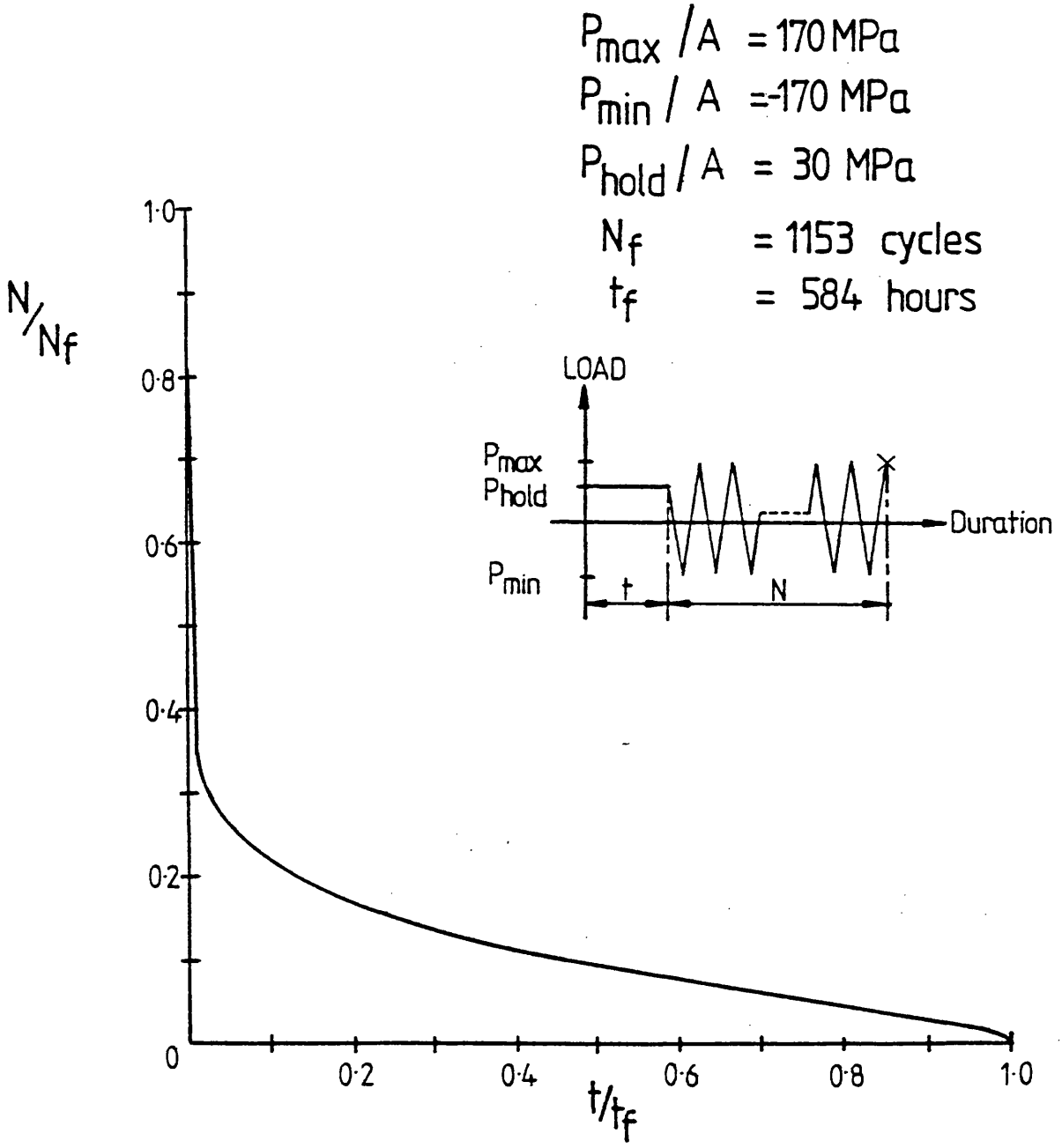

a) Load dwell for time t before cycling until failure occurs (creep first loading).

Figure 6.8: Effect of the sequence of creep and fatigue loading on time and cycles to failure.

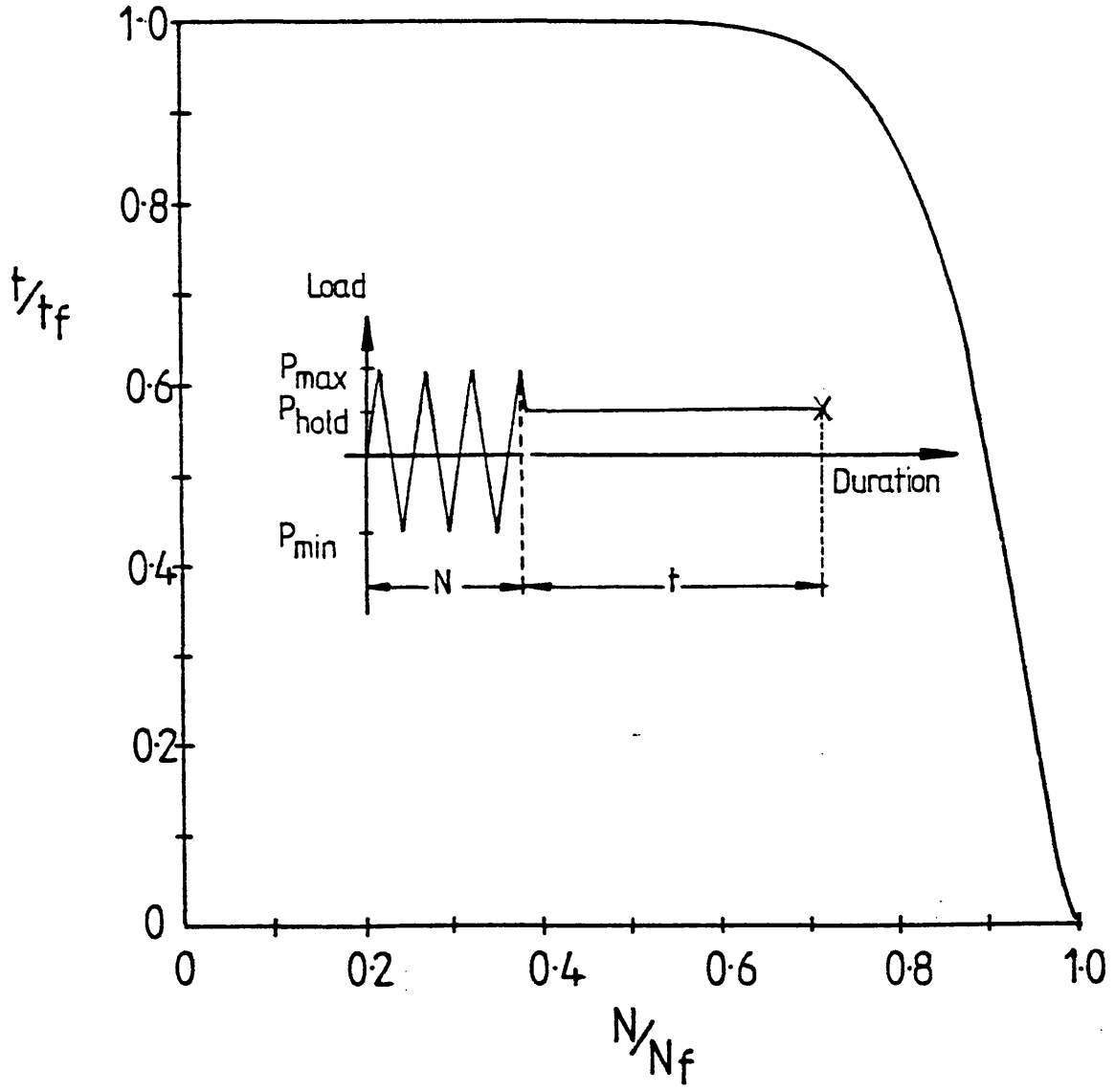

b) N cycles before tensile dwell until failure occurs (fatigue first loading).

Figure 6.8: Continued.

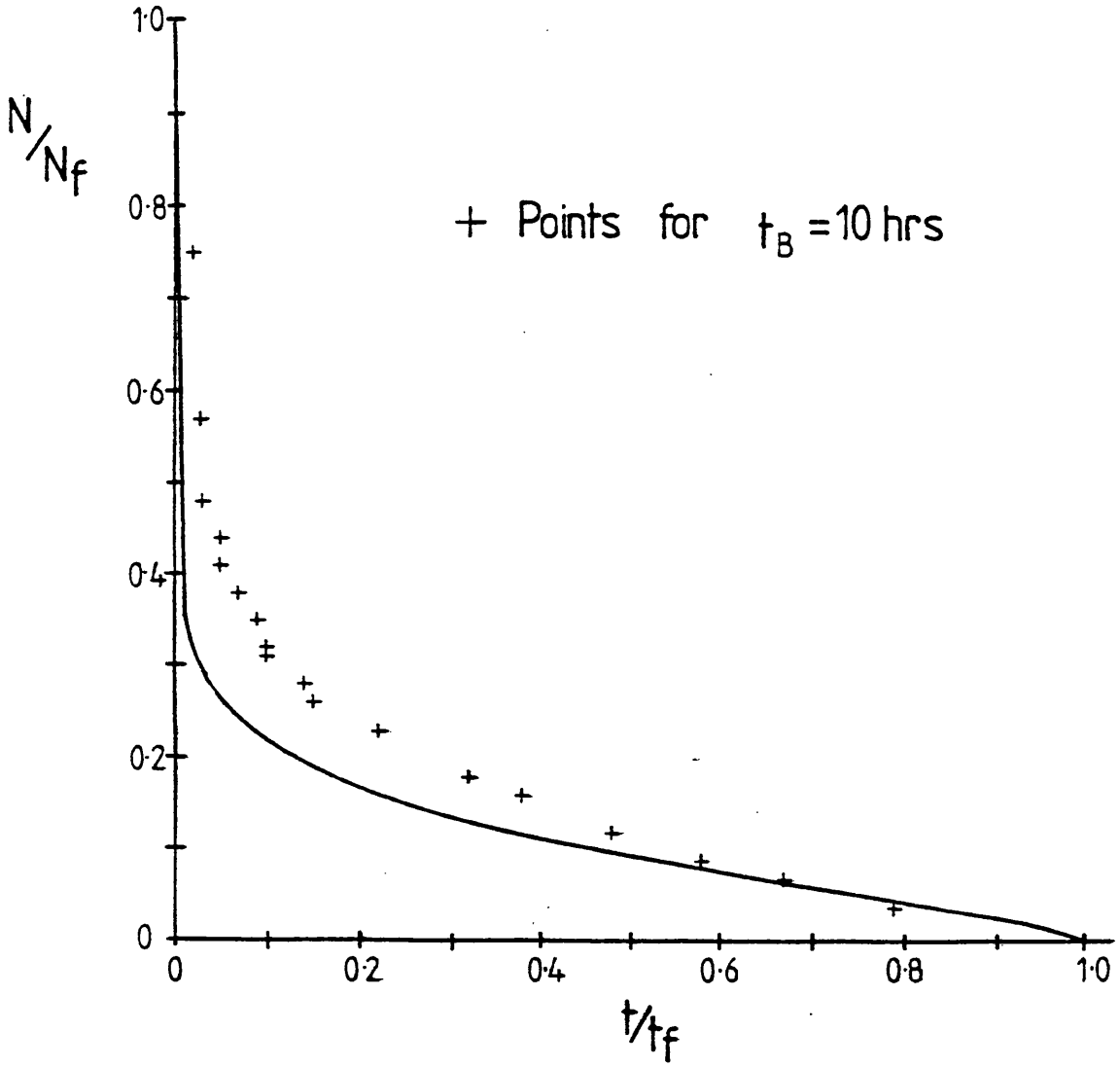

Figure 6.9: Comparison between curve in Fig. 6.8(a) and failure points for block loading with t_B=10hrs.

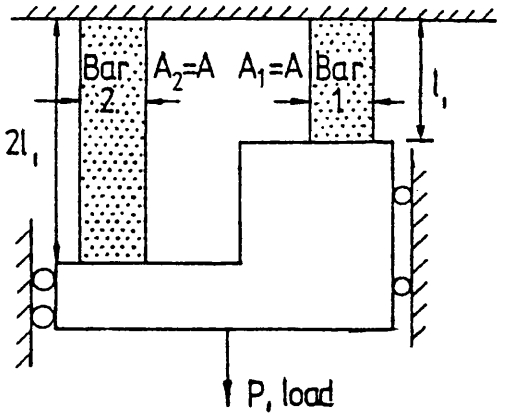

a) Two bar structure.

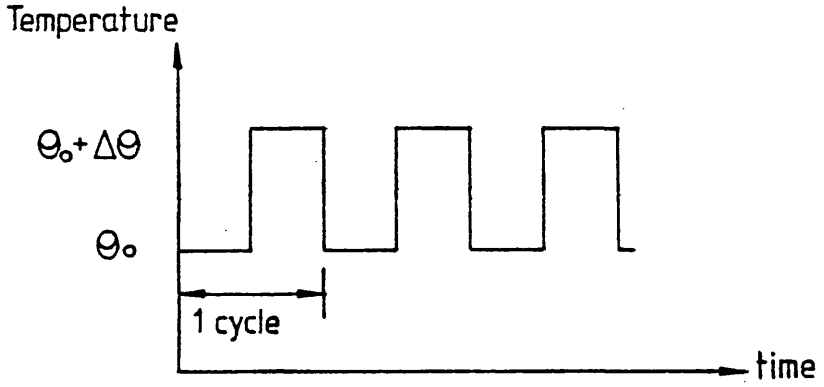

b) Applied temperature history.

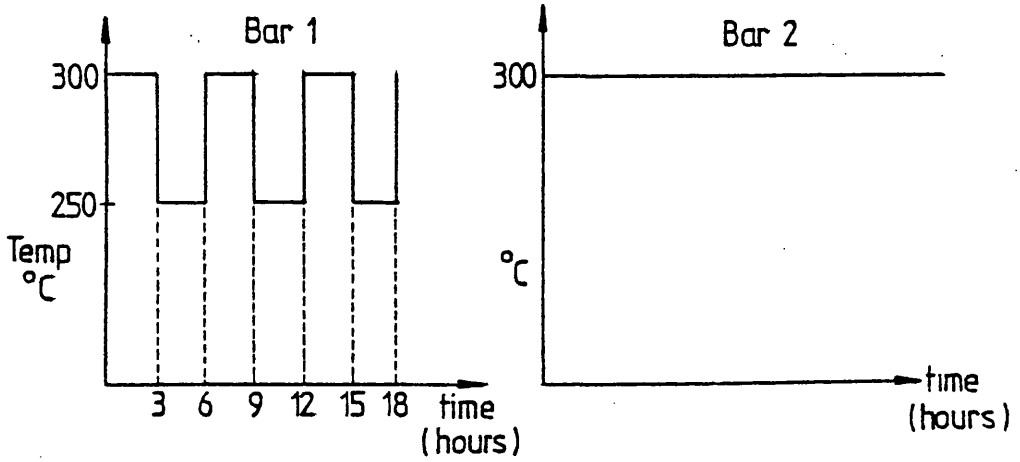

c) Temperature histories for each bar of 2 bar structure.

Figure 6.10: Two bar structure and its loading.

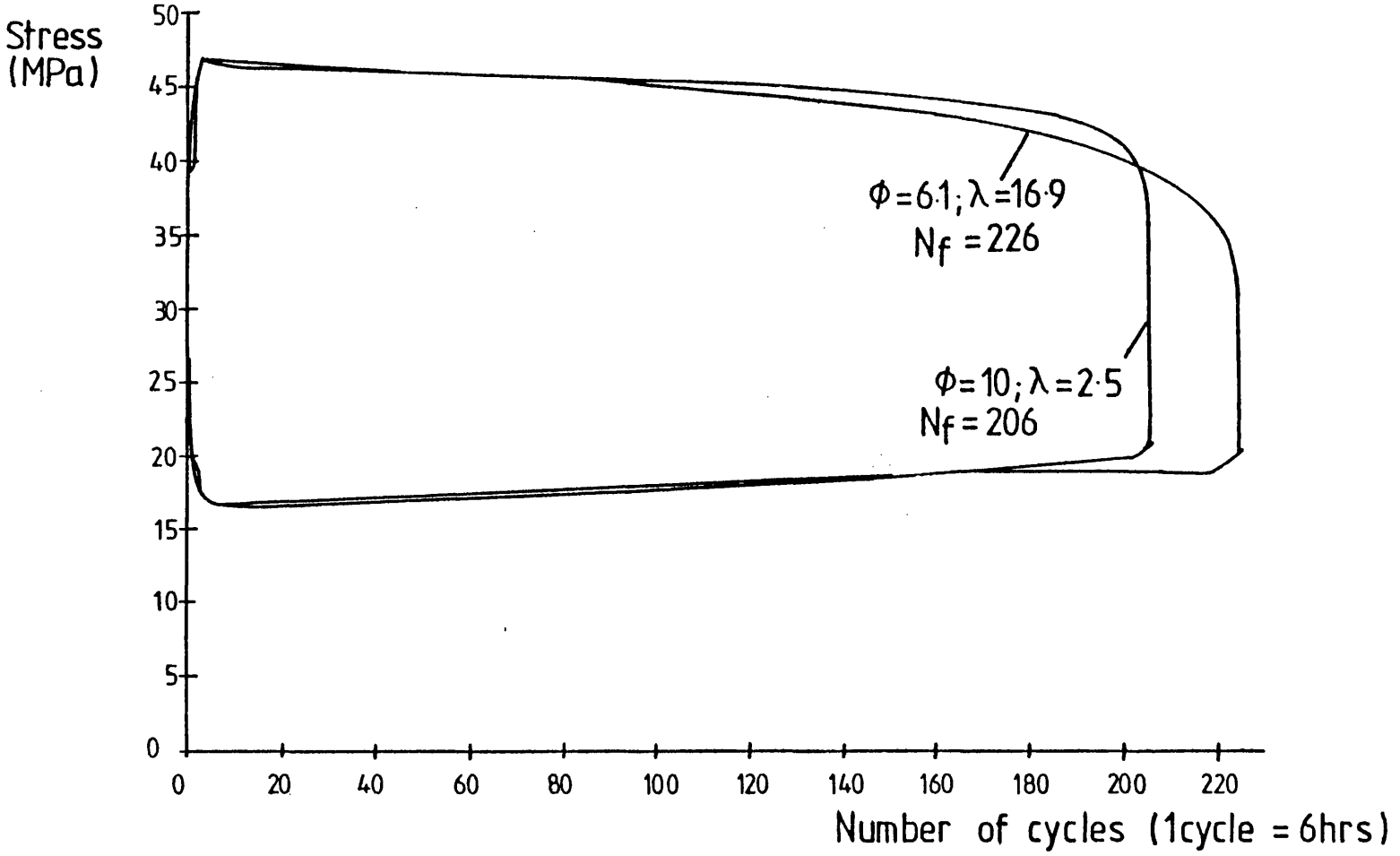

Figure 6.11: Stress envelopes for bar 1 in 2 bar structure for two different values of creep ductility.

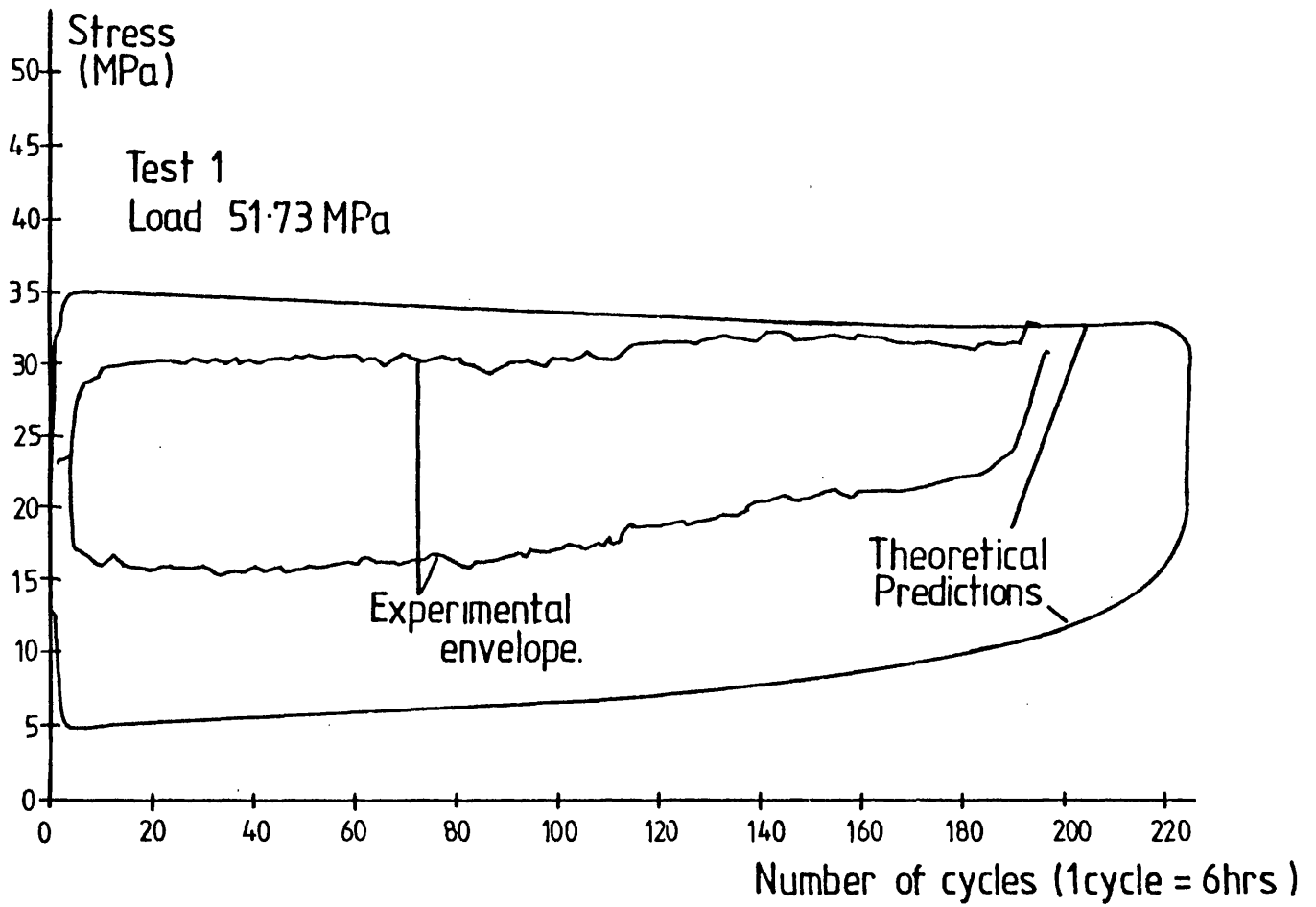

Figure 6.12: Comparison between the experimental and theoretical stress envelopes for bar 2 in test 1.

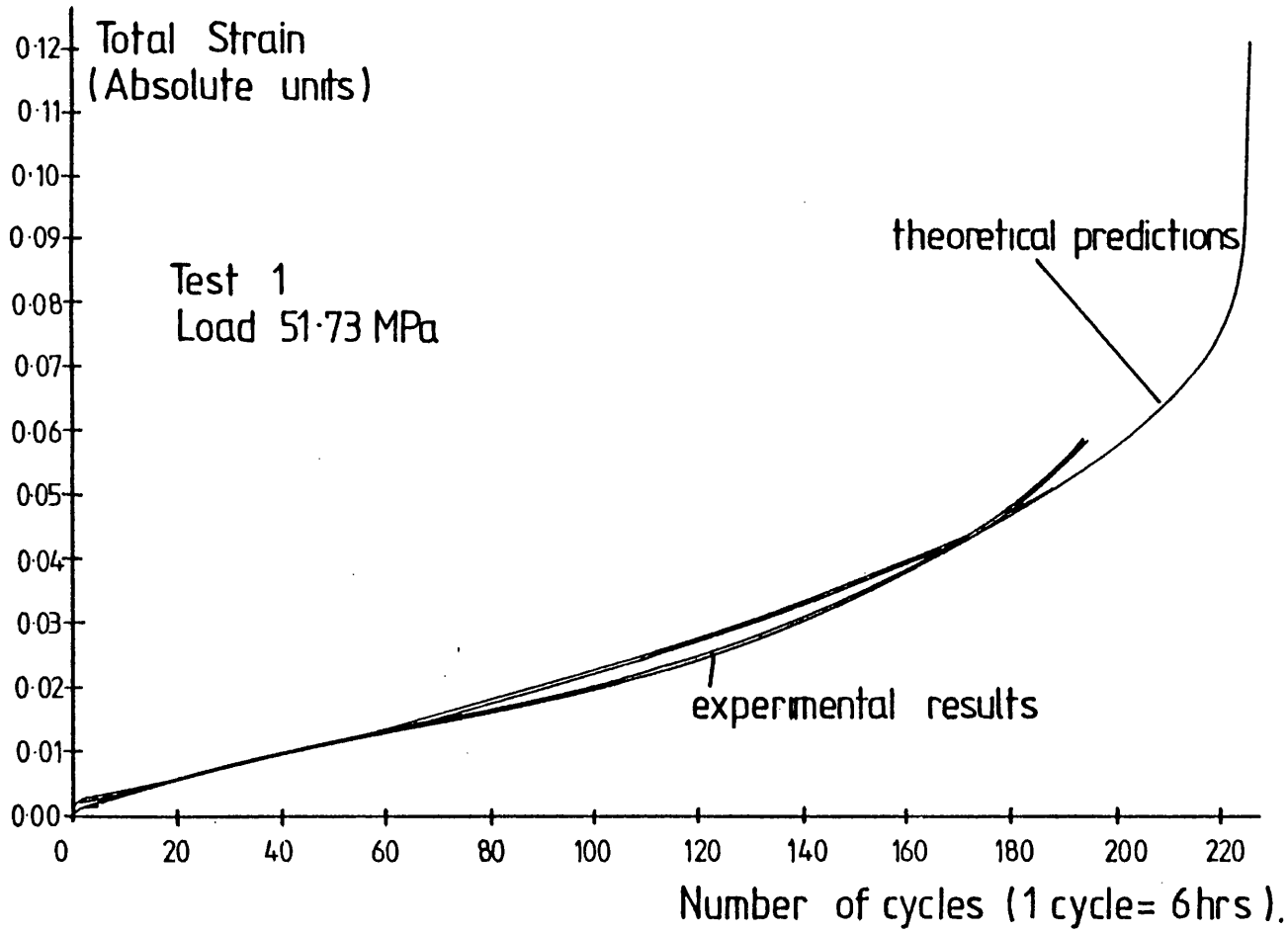

Figure 6.13: Comparison between the experimental and theoretical total strain envelopes for bar 1 in test 1.

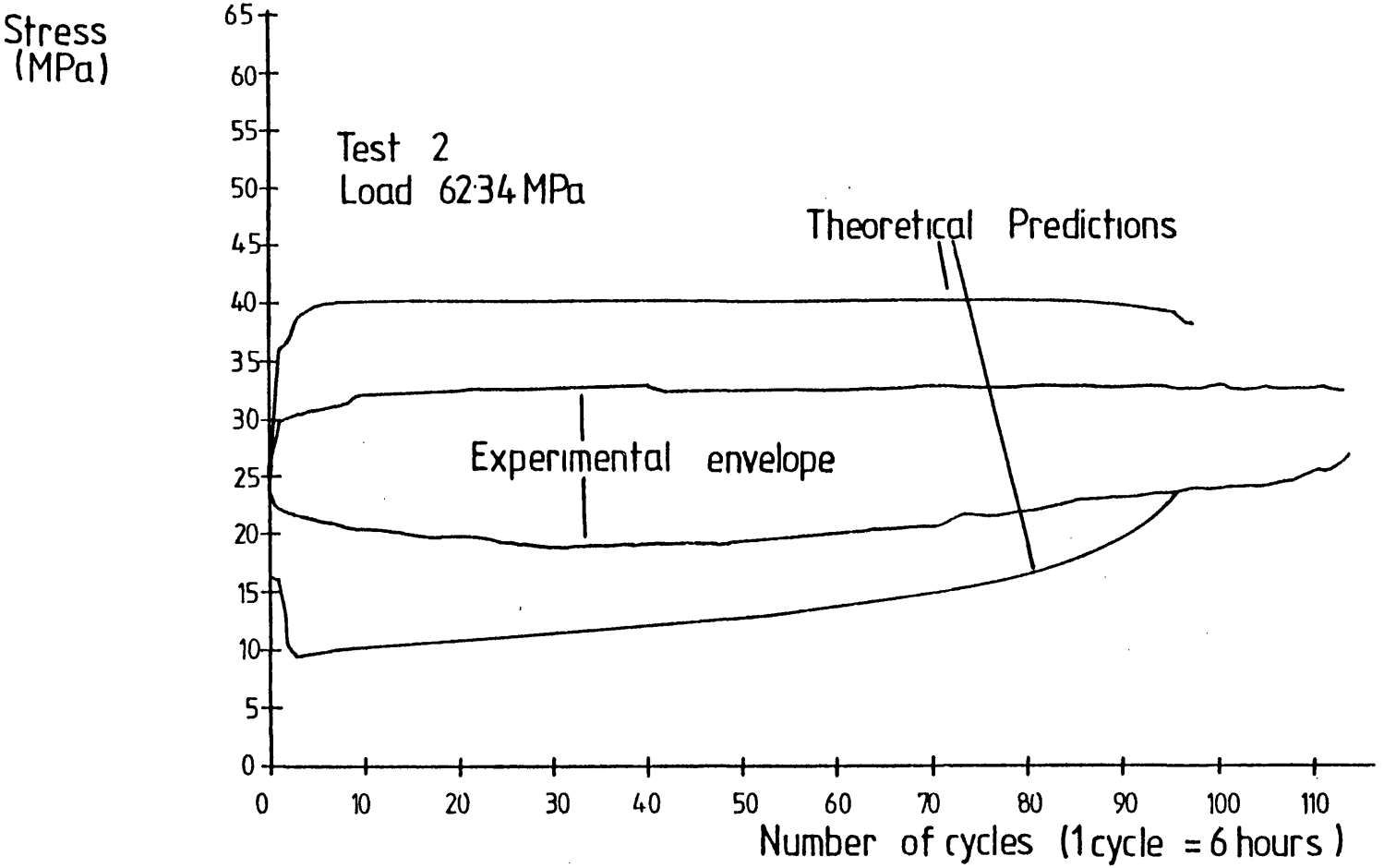

Figure 6.14: Comparison between the experimental and theoretical stress envelopes for bar 2 in test 2.

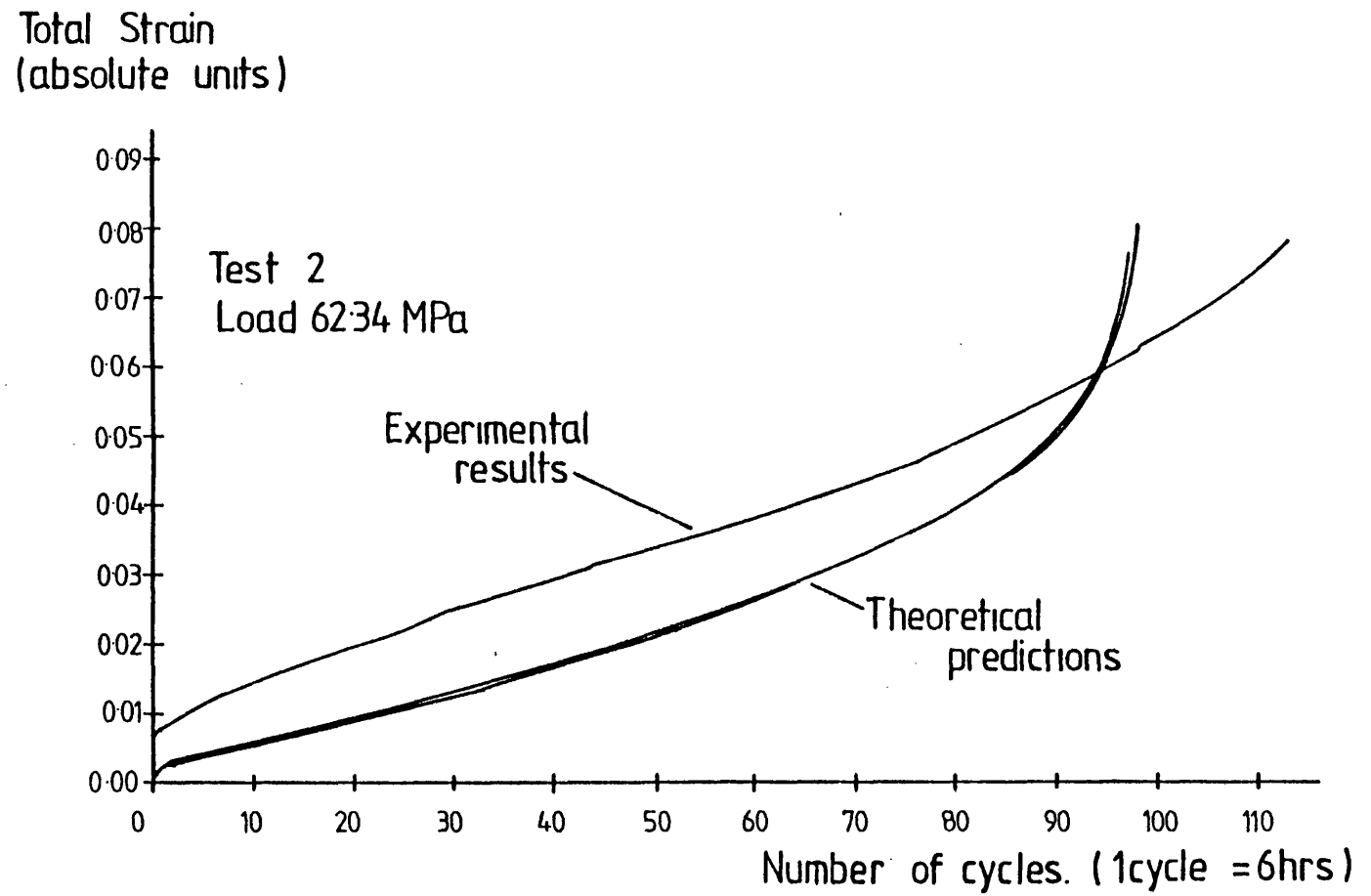

Figure 6.15: Comparison between the experimental and theoretical total strain envelopes for bar 1 in test 2.

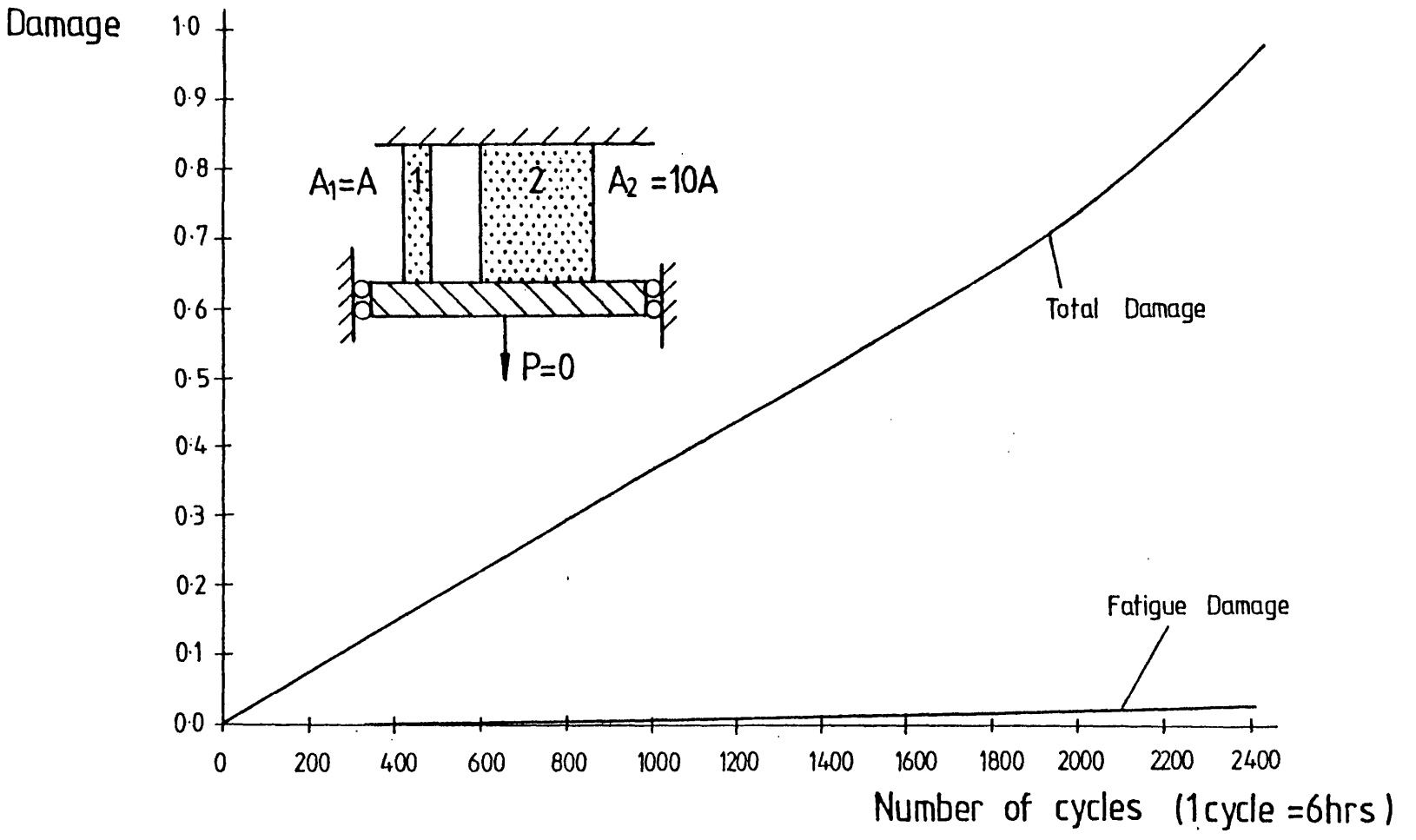

Figure 6.16: Total and fatigue damage in bar 1 of a 2 bar structure subjected to thermal cycling ($\Delta\theta$ = 100°C, θ_0 = 300°C) and zero mechanical load.

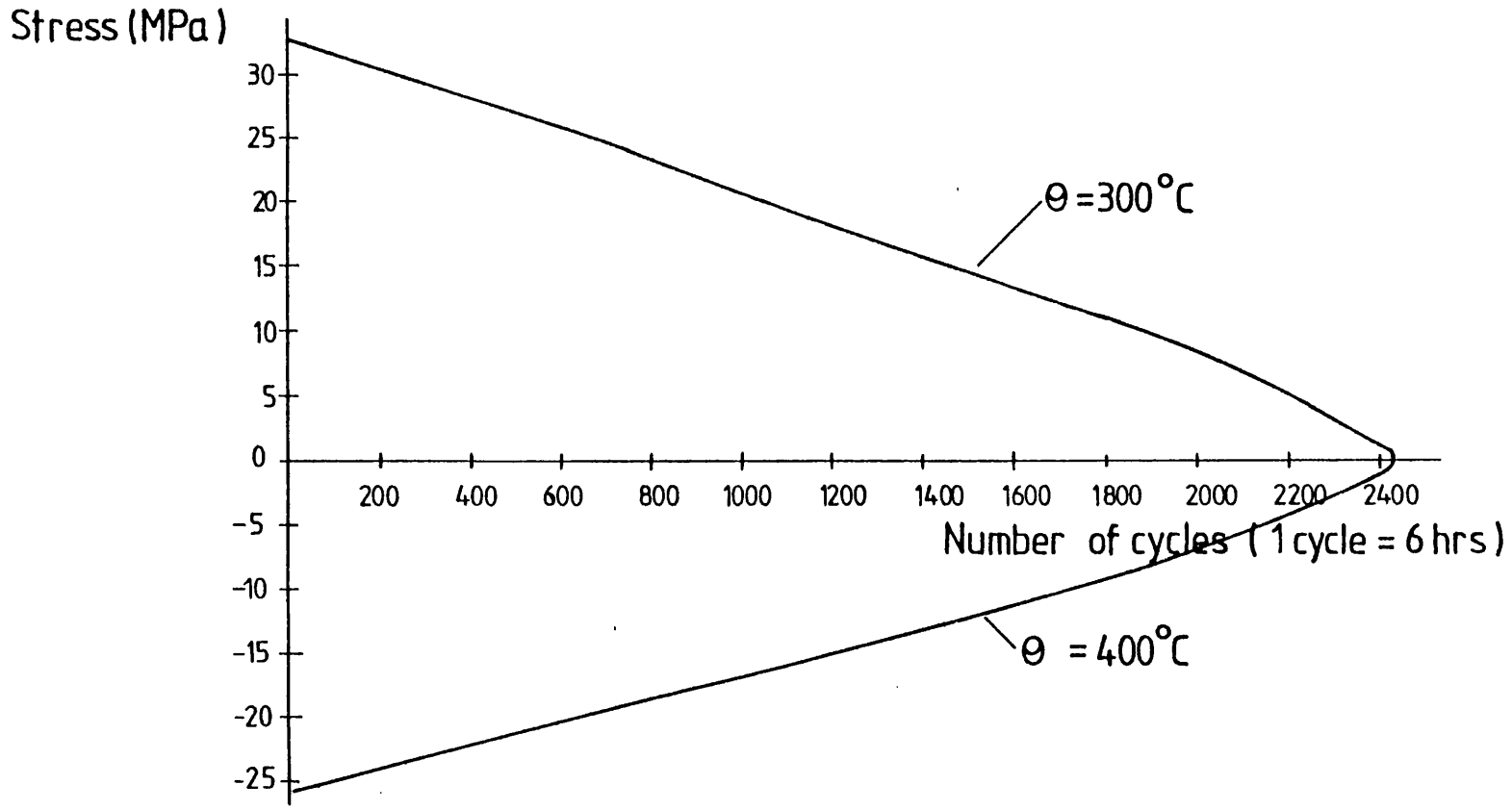

Figure 6.17: Stress envelopes for bar 1 of a 2 bar structure subjected to thermal cycling and zero mechanical load.

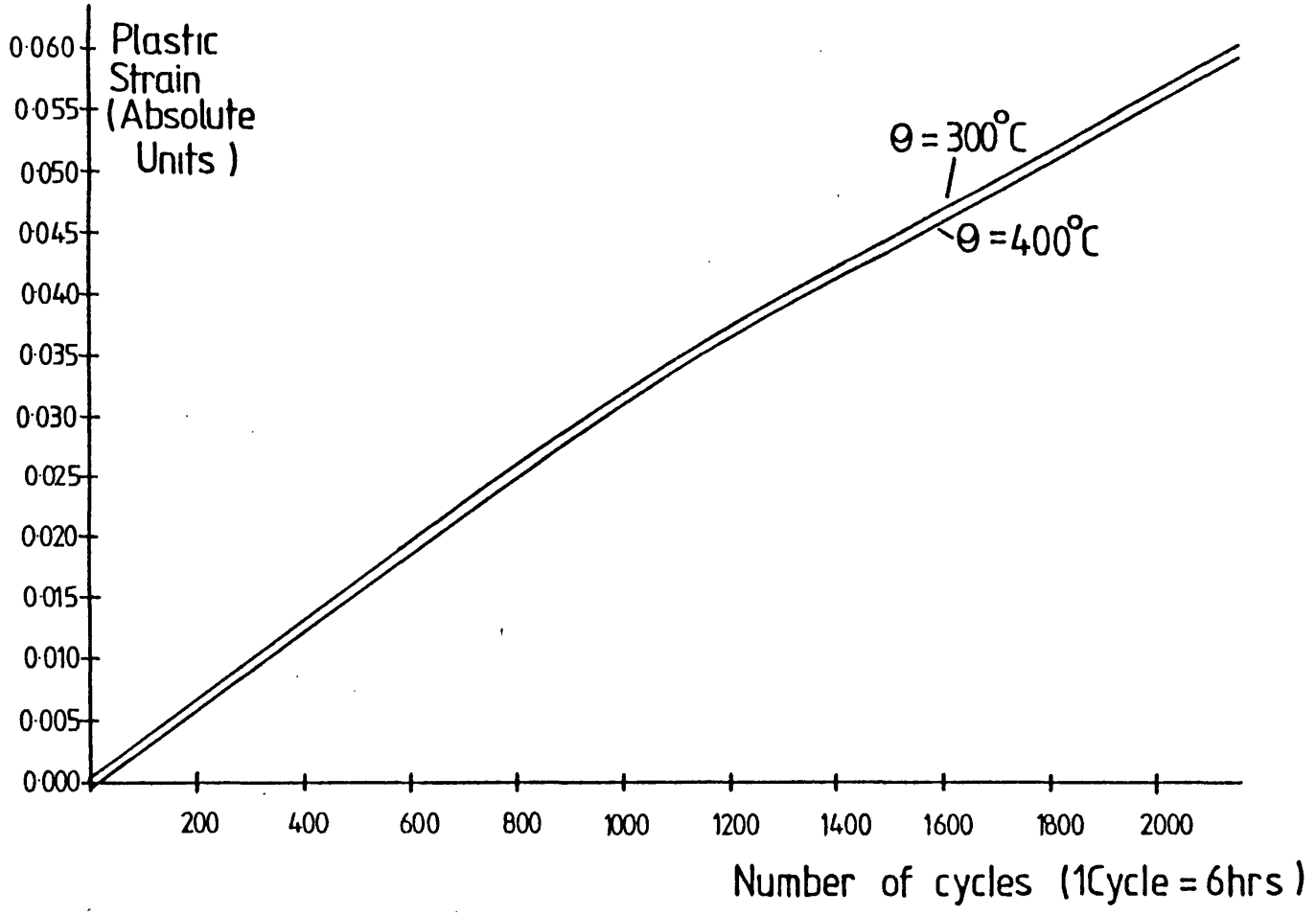

Figure 6.18: Plastic strain envelopes for bar 1 of a 2 bar structure subjected to thermal cycling and zero mechanical load.

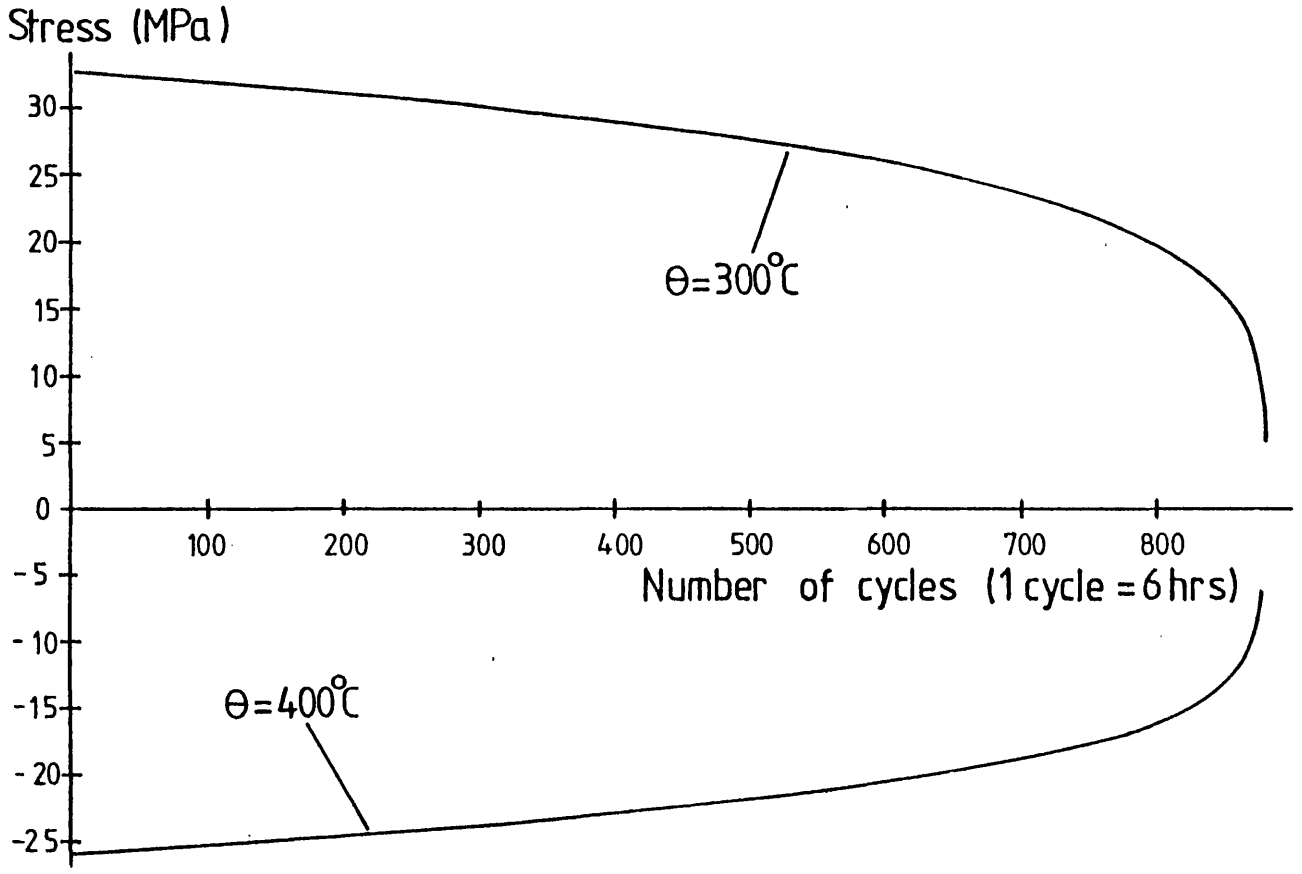

Figure 6.19: Stress envelopes for bar 1 of a 2 bar structure subjected to thermal cycling and zero load when ϕ = 10.

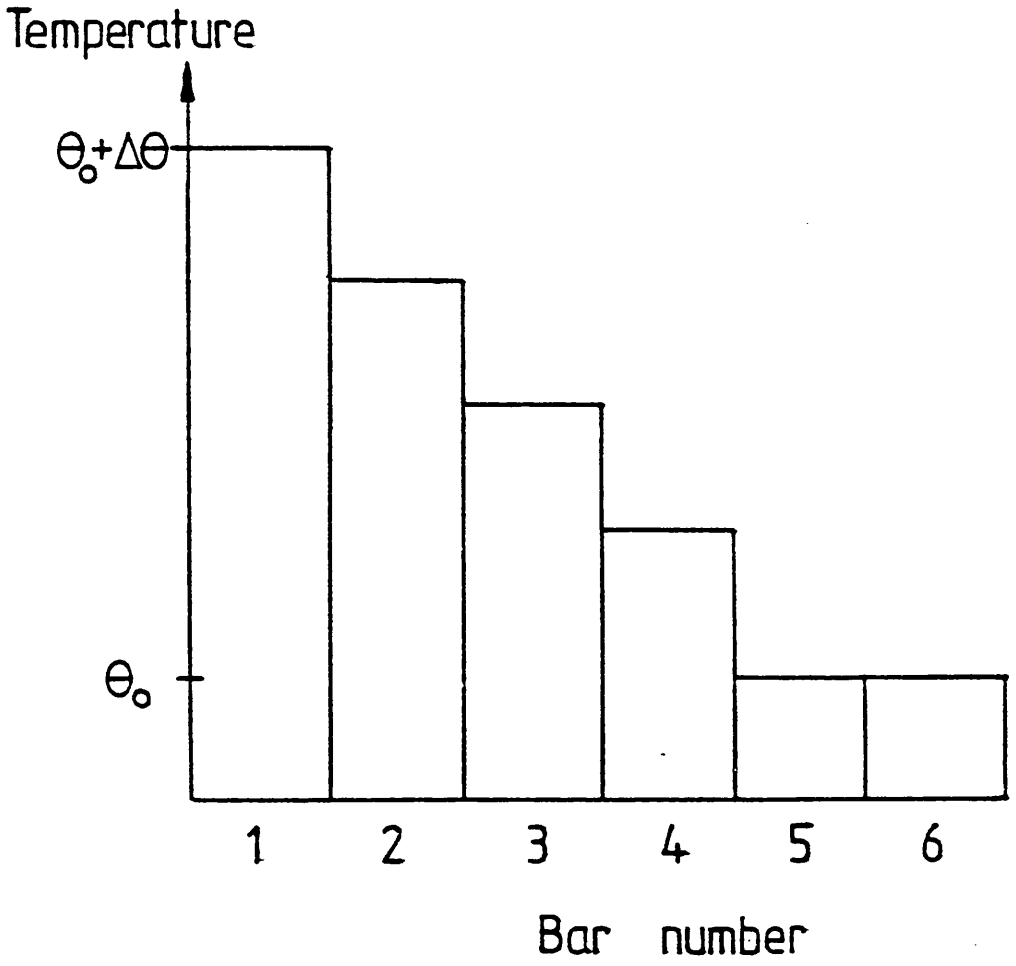

a) The temperature distribution through the structures according to equation (6.15).

Figure 6.20: Two 6 bar structures and the temperature distribution through them when a thermal gradient is applied.

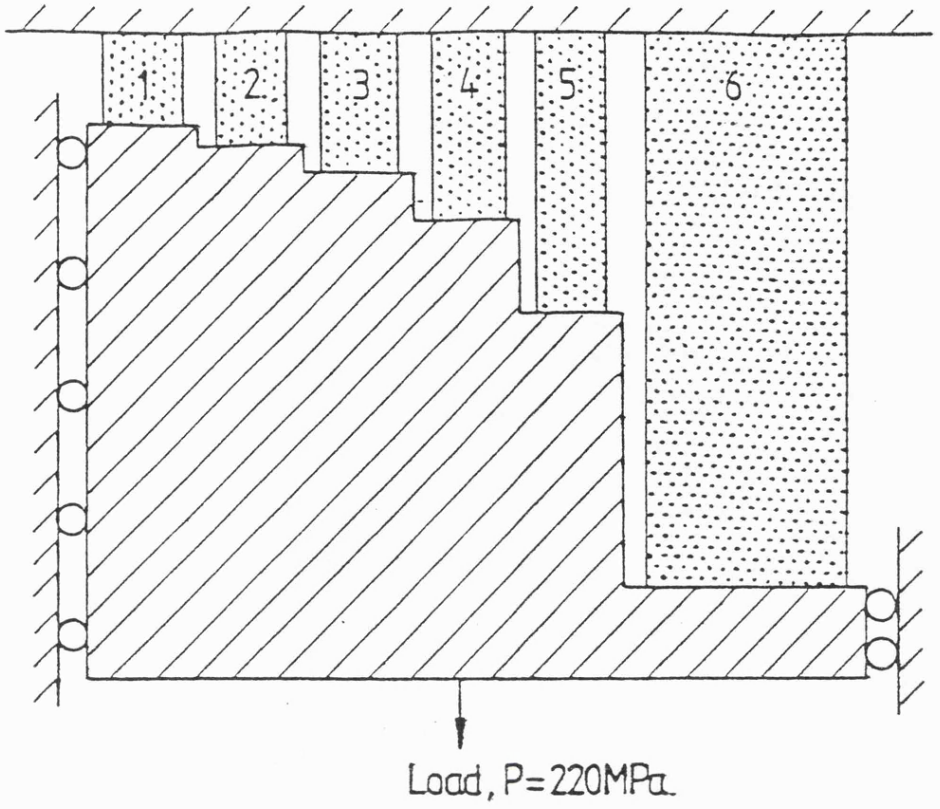

b) A 6 bar structure with a stress concentration. Its dimensions are given in Table 6.5.

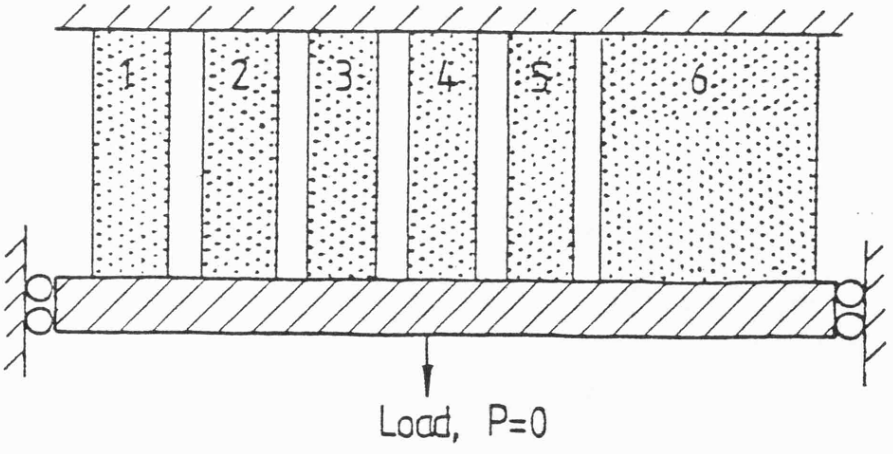

c) A 6 bar structure without a stress concentration.

Figure 6.20: Continued.

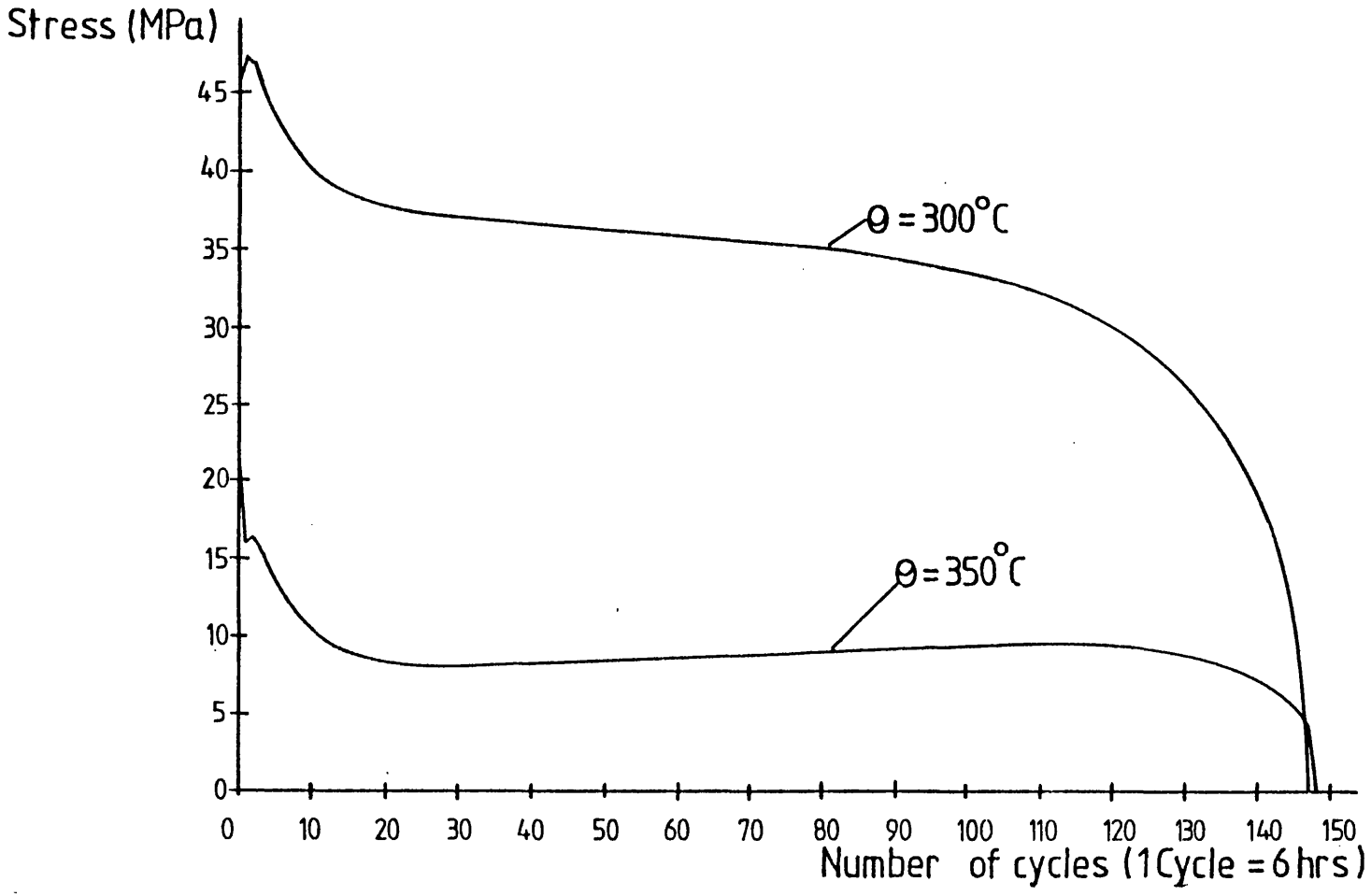

Figure 6.21: Stress envelopes for bar 1 of a 6 bar structure subjected to thermal cycling and a steady mechanical load.

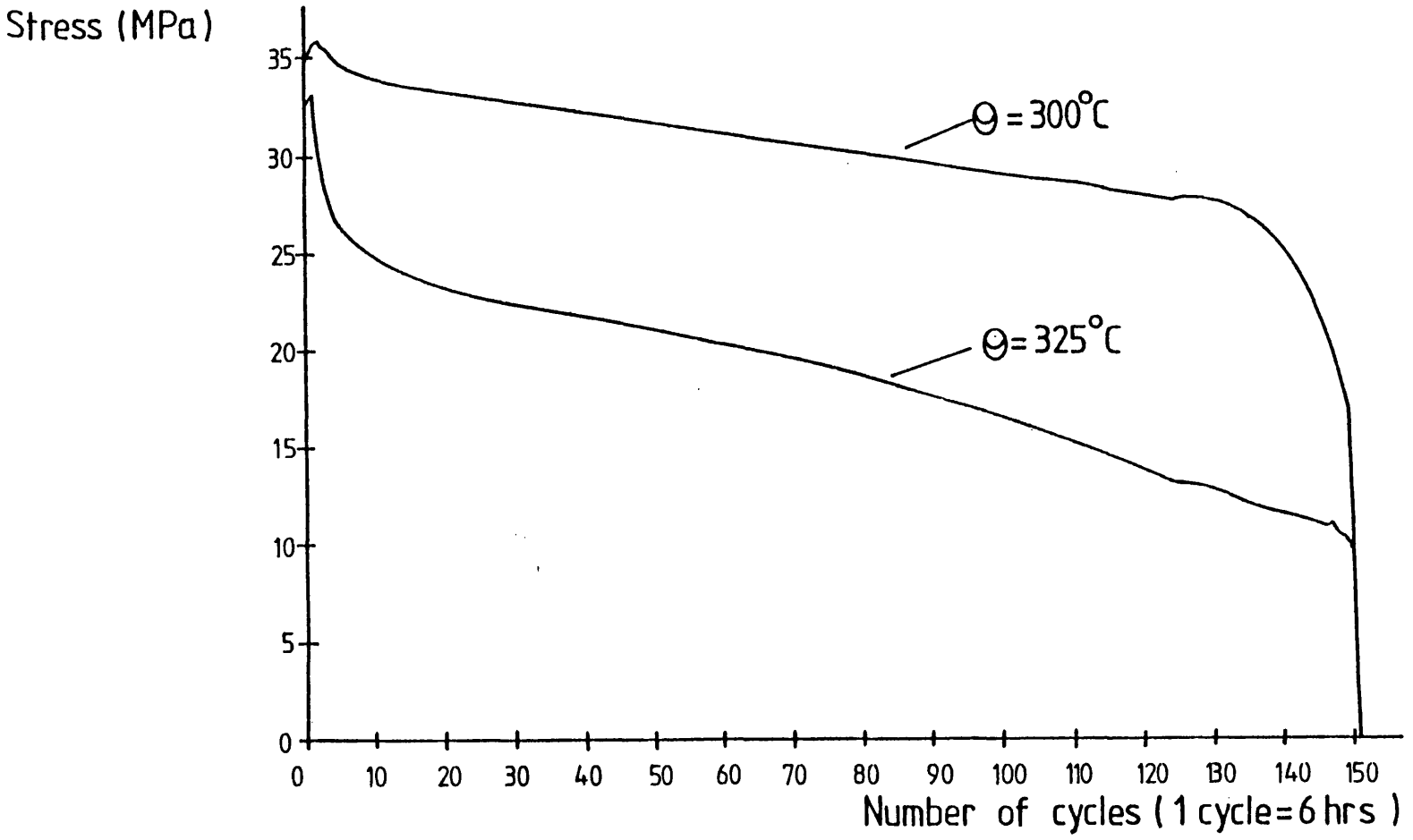

Figure 6.22: Stress envelopes for bar 3 of a 6 bar structure subjected to thermal cycling and a steady mechanical load.

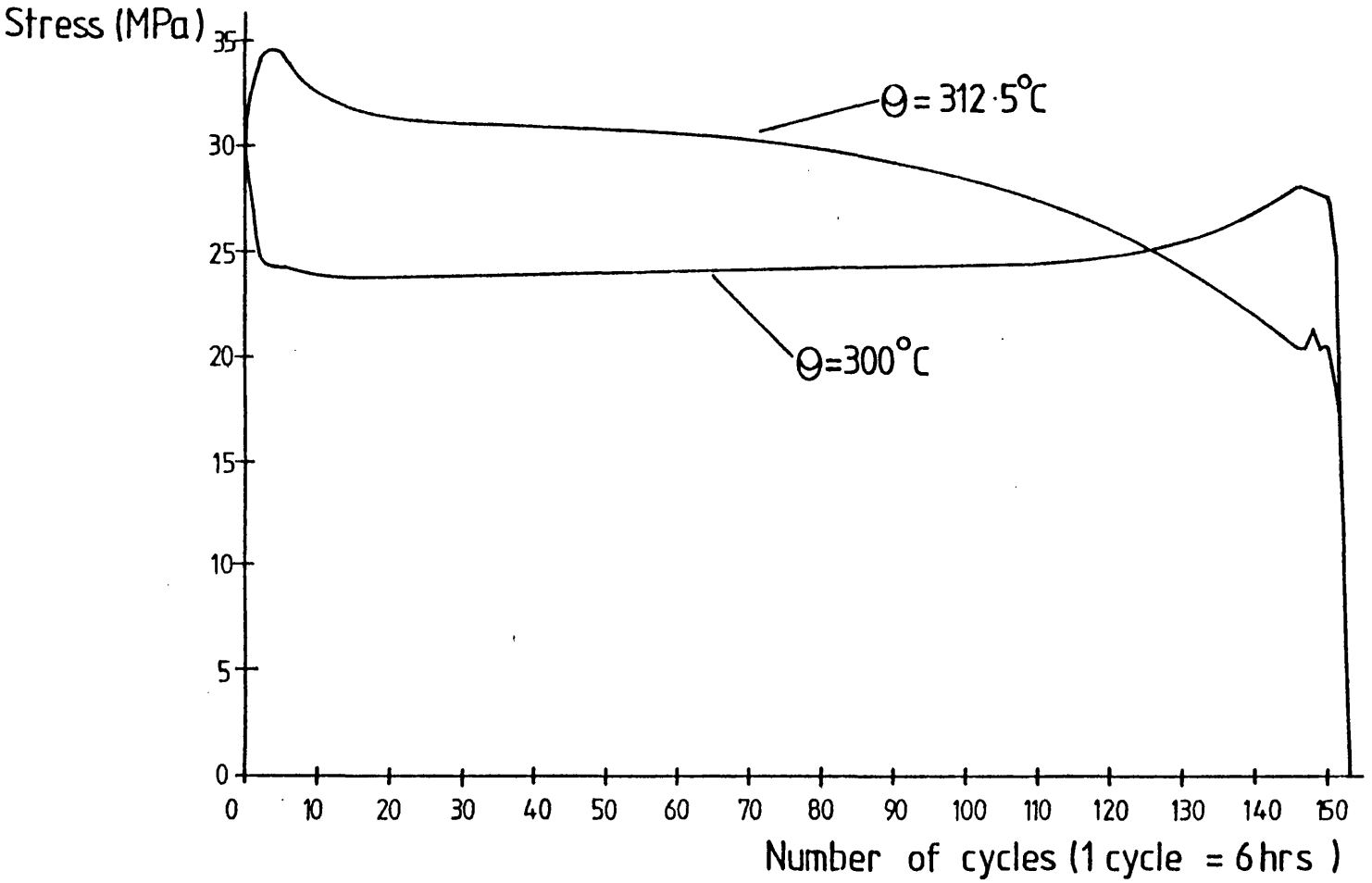

Figure 6.23: Stress envelopes for bar 4 of a 6 bar structure subjected to thermal cycling and a steady mechanical load.

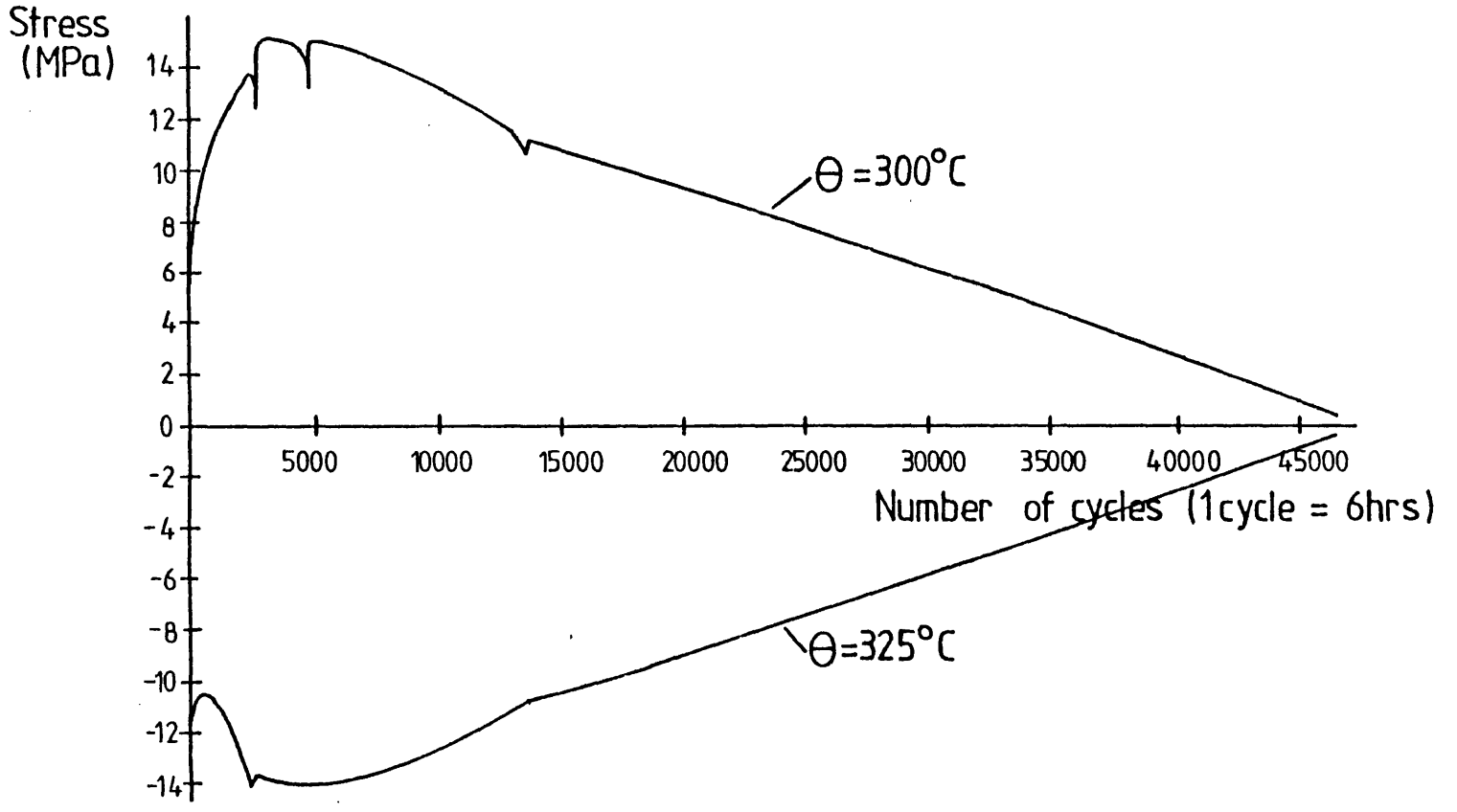

Figure 6.24: Stress envelopes for bar 4 of a 6 bar structure subjected to thermal cycling and zero mechanical load.

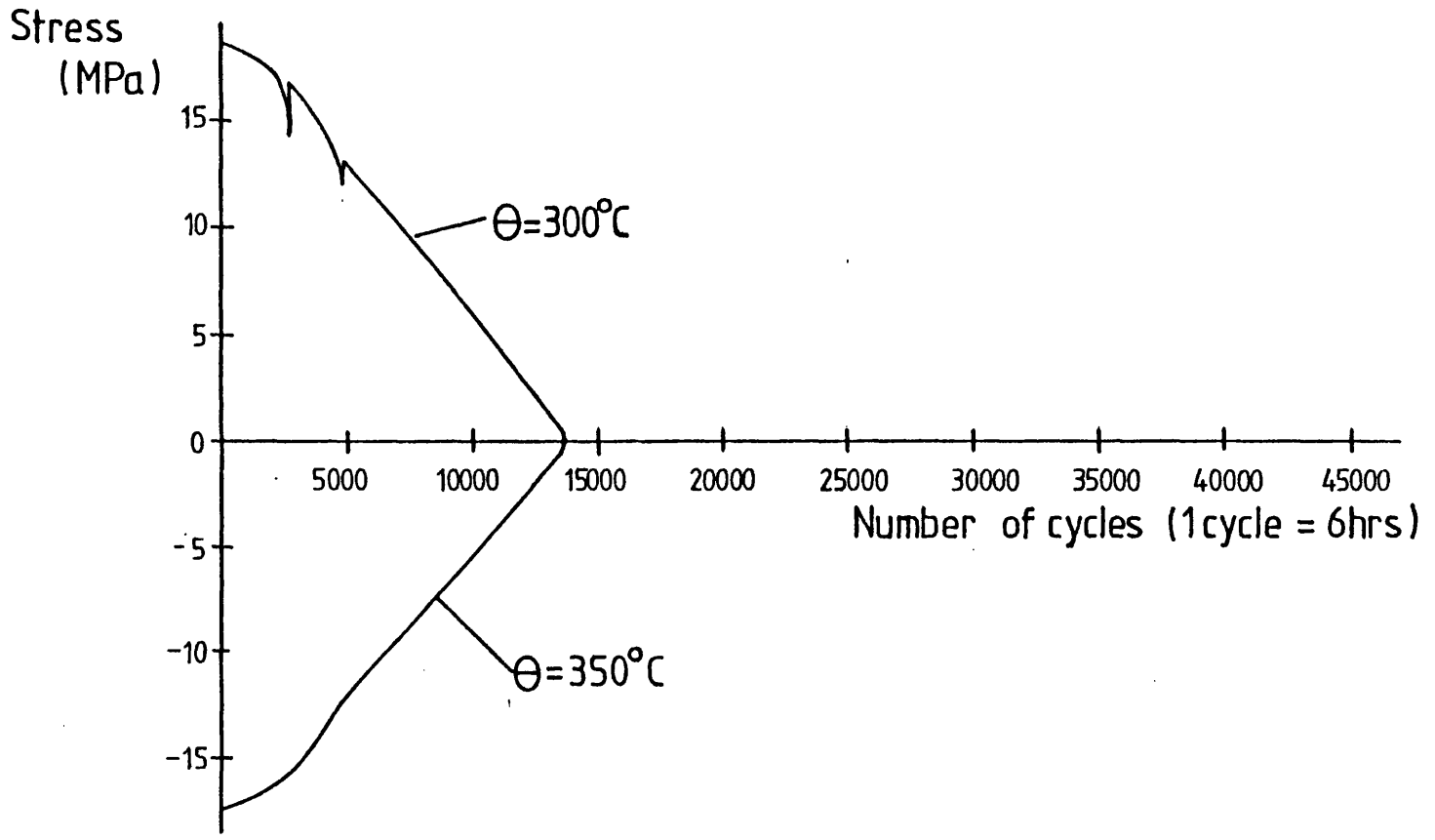

Figure 6.25: Stress envelopes for bar 3 of a 6 bar structure subjected to thermal cycling and zero mechanical load.

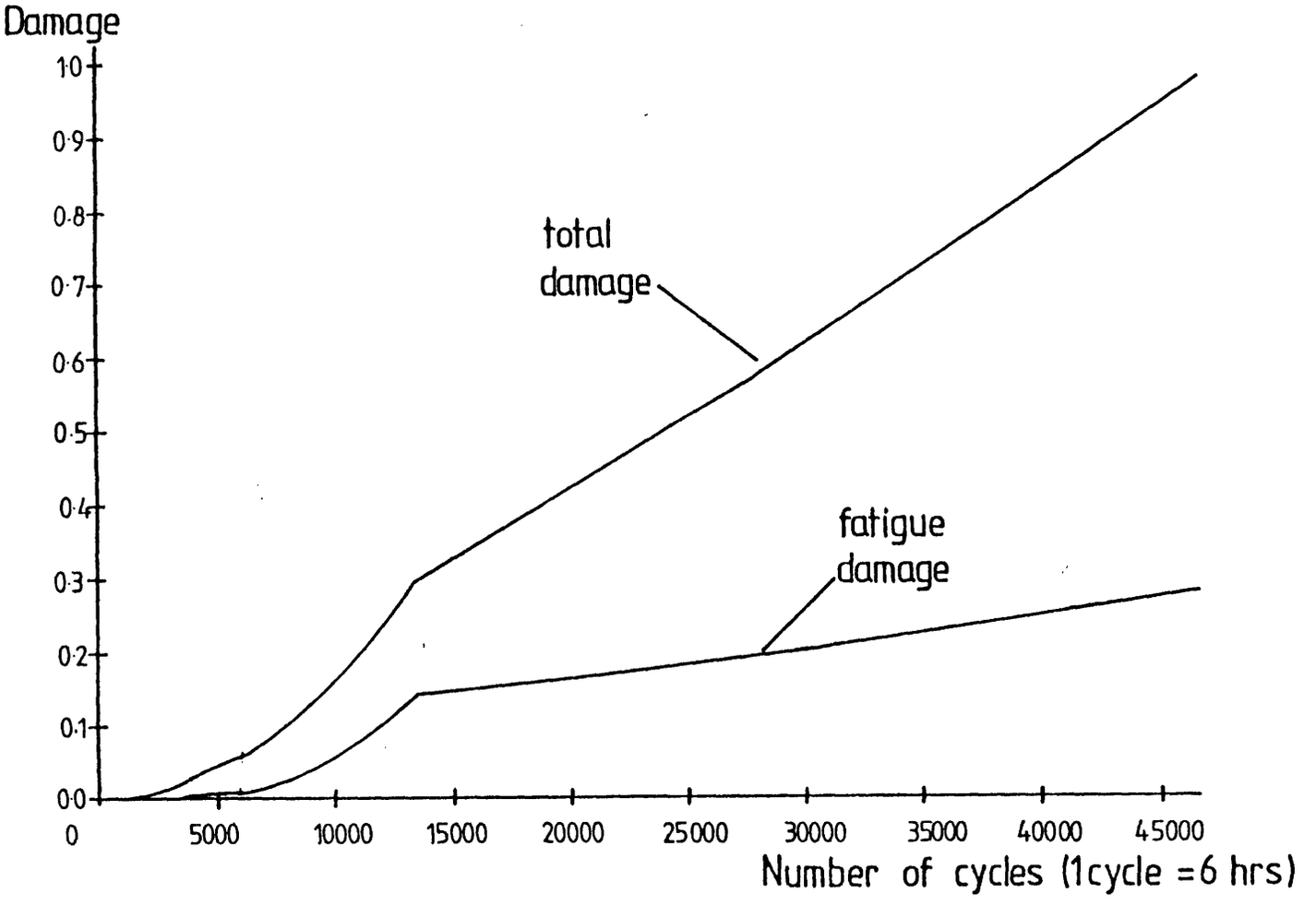

Figure 6.26: Total and fatigue damage in bar 4 of a 6 bar structure subjected to thermal cycling and zero mechanical load.

CHAPTER 7

MULTIAXIAL PLASTICITY AND FINITE ELEMENT TECHNIQUES FOR NON-LINEAR PROBLEMS

7.1 Introduction

In previous chapters the constitutive laws have been restricted to uniaxial laws. This was so that structural calculations would be relatively easy to carry out. However, most applications are multidimensional and require structural and material models that reflect this fact. The step from uniaxial to multiaxial solution techniques is substantial and separated into two parts: (i) the constitutive laws must be expressed in a multiaxial form and methods must be developed for dealing with them numerically, and (ii) techniques for solving structural problems in many dimensions must be developed. In this chapter, a review of multiaxial plasticity models will be given and the constitutive law of Chapter 3 will be extended to a multiaxial law within this framework.

The solution of multidimensional structural problems is often effected using the finite element method. Within this context there is a large choice of techniques available for solving problems involving non-linear material behaviour, such as plasticity. A review of some of these techniques is presented in this chapter. Several methods have also been proposed for the integration of the multiaxial plasticity laws; a review of these is also presented.

Two techniques finding structural equilibrium are chosen from those available and, along with a method

for integrating the constitutive equations devised by the author, are used to solve a two bar plasticity problem by the finite element method. The results are compared with the more reliable solutions obtained using the methods of Appendix A. The chapter ends with some discussion and conclusions.

7.2 Multiaxial Plasticity Models

7.2.1 General Review

Many models for describing plastic behaviour in metals have been proposed. These are usually based on the idea of a yield surface which is a surface bounding a region in stress space. If the material is in a stress state which is in the interior of this region, then it behaves elastically. States of stress outside the yield surface are not permitted by the model. When the stress point describing the state of stress in the material touches the yield surface and tries to move outside it, then plastic straining occurs. For perfect plasticity the yield surface remains fixed and does not change size or shape, thus the stress cannot take a value which is outside the surface. If the material hardens, then the stress is allowed to go beyond the region defined by the current yield surface but the surface must change, either its shape, size or position, in order to keep the stress point on or inside the new yield surface. Computationally, it is easier to assume that the yield surface changes its size or position rather than its shape. If the yield surface only changes its size as the material hardens during plastic straining, it is

called isotropic hardening. If the yield surface only moves without change of shape, then this is called kinematic hardening.

Isotropic hardening is simpler to implement in a computer program than kinematic hardening which, amongst other things, requires an additional parameter giving the current position of the yield surface in stress space. However, isotropic hardening does not predict the Bauschinger effect which is important for describing cyclic plasticity where the stress is cycled between upper and lower values. The isotropic model predicts that the yield stress in compression is minus the yield stress in tension. Also, since the yield surface changes size to accommodate the stress point, it predicts that, if the cycling is between fixed stress values, the material will behave completely elastically after the first cycle. The kinematic model, however, predicts that the yield stress in compression depends on the amount of plastic straining in tension, and also can reproduce the experimentally observed hysteresis loop in the stress-strain plane and which is characteristic of cyclic plasticity. For these reasons a kinematic hardening model will be used. (The previous uniaxial models have all been kinematic hardening models.)

For kinematic hardening, it is necessary to specify the direction of motion of the yield surface. Prager proposed that the yield surface should move in the direction of the normal to the yield surface at the point at which the stress point touches the surface. Shield and Ziegler (1958) studied this rule and found that its

application in subspaces of full stress space can cause the yield surface to change its size or shape and also that the direction of motion is not necessarily along the normal to the surface. Subsequently, Ziegler (1959) proposed an alternative hardening rule which did not suffer from these drawbacks of Prager's rule and which was equivalent to Prager's rule in subspaces including those commonly used, such as plane stress. For these reasons, the Ziegler hardening rule is used in this chapter. The mathematical formulation of these concepts will now be listed and briefly described.

The yield surface used is that named after Von Mises. The equation for this surface in stress space can be written

$$F(\sigma_{ij}) = (3/2)S_{ij}S_{ij} - \sigma_y^2 = 0 \qquad (7.1)$$

where S_{ij} is the deviatoric stress tensor and σ_y is the uniaxial yield stress. The assumption of a kinematic hardening model can be represented by including the position tensor, α_{ij}, of the centre of the yield surface in equation (7.1). Thus, the equation for the yield surface becomes

$$F(\sigma_{ij}-\alpha_{ij}) = (3/2)(\sigma_{ij}-\alpha_{ij})'(\sigma_{ij}-\alpha_{ij})'-\sigma_y^2 = 0 \quad (7.2)$$

where the prime ($'$) indicates that the deviator of the tensor is to be used.

The direction of plastic straining (the flow rule) is given by the associated flow rule,

$$d\eta_{ij} = \lambda \frac{\partial F}{\partial \sigma_{ij}} \qquad (7.3)$$

The factor λ is obtained by comparing the plastic strain η_{ij} with an equivalent uniaxial value of plastic strain η_e. The value of η_e corresponding to any value of η_{ij} is given here by the work equivalent plastic strain which is defined by

$$\eta_e = \int d\eta_e \ , \qquad \text{where}$$

$$d\eta_e = \frac{1}{\sigma_y} (\sigma_{ij} - \alpha_{ij}) d\eta_{ij} \qquad (7.4)$$

Using (7.3) and (7.4) it can be seen that

$$\lambda = \frac{\sigma_y d\eta_e}{(\sigma_{ij} - \alpha_{ij}) \frac{\partial F}{\partial \sigma_{ij}}} \qquad (7.5)$$

The direction of movement of the yield surface (hardening rule) is given by the rule due to Ziegler (1959) and can be written

$$d\alpha_{ij} = \mu(\sigma_{ij} - \alpha_{ij}) \qquad (7.6)$$

The factor μ in this equation is calculated by relating the multiaxial stress-strain state to the uniaxial hardening curve via η_e. The relationship is assumed to be

$$d\alpha_{ij} = C \frac{d\eta_e}{\sigma_y} (\sigma_{ij} - \alpha_{ij}) \qquad (7.7)$$

where $C = \frac{d\sigma}{d\eta_e}$ is the slope of the uniaxial hardening curve.

7.2.2 Constitutive Laws

The value of C in (7.7) is given by the slope of some uniaxial hardening curve. The position on the uniaxial curve is given by the accumulated equivalent plastic strain, η_e. The particular uniaxial curve used in this chapter is based on the constitutive laws in Chapter 3 (equations (3.9) and (3.10)). This law provides a better approximation to the observed cyclic stress-strain behaviour of metals than the more usual bilinear stress-strain curve (which is obtained from (3.9) and (3.10) by setting q = 1).

However, for general loading paths in many dimensions, there is no consistent method for using these uniaxial laws other than for the bilinear curve. This is overcome here by assuming that the loading is proportional and regular, meaning that the loads change monotonically between two extreme values. Initially, η_e is assumed to be zero and is reset to zero at first yield each time yielding occurs after a reversal of the load. This enables hysteresis loops to be modelled and allows for elastic unloading to be realistically treated.

7.3 Finite Element Techniques

7.3.1 Introduction

The finite element method has been successfully applied to solving problems in many areas, including solid mechanics. A standard introduction to the method is the book by Zienkiewicz (1977). The usual displacement

method approximates the displacements in a solid body by expressing them in terms of the displacements at a certain set of points, called nodes. The relationship between the forces and displacements at the nodes is given in terms of the stiffness matrix K, and may be written $\underline{f} = K\underline{a}$, where $\underline{f}$ and $\underline{a}$ are vectors of the forces and displacements, respectively, at the nodes.

The particular type of element used here is the constant strain triangle. The author has carried out an investigation into other element types (Lavender and Hayhurst, 1986) and has found that higher order elements give better results when solving an elastic problem. However, constant strain triangles are a lot simpler to use because stress and strain are constant within each element.

Two types of non-linear finite element solution methods were investigated, namely elasto-plastic methods and visco-plastic methods. When a non-linear structural problem is formulated in terms of a finite element approximation, a system of non-linear equations is obtained. There are many methods in existence for the solution of such systems of equations and these have been applied to solving structural problems: they are usually called elasto-plastic methods. However, since plasticity in metals is dependent on loading history, the traditional methods need to be adapted to take this into account. The elasto-plastic methods also neglect the fact that plastic strains may change with time, i.e. plastic strains are assumed to develop instantaneously within a material. For this reason they are often called

time independent solution methods. An alternative approach is given by the visco-plastic methods which are based on the fact that plastic strains can be modelled as visco-plastic strains which change with time at a finite strain rate upon the application of stress. This formulation of the finite element problem leads to a system of ordinary differential equations which are solved using a method designed for the solution of initial value problems. These two categories of method will now be described and some remarks on their use will be presented.

7.3.2 Visco-plastic Methods

These methods have been studied and developed by Zienkiewicz and Cormeau (1974). An outline of the method is presented here, for more details see Owen and Hinton (1980) or Zienkiewicz and Cormeau (1974). The method assumes that the inelastic strains are visco-plastic strains. The total strain rate is accordingly decomposed thus

$$\dot{\underline{\varepsilon}} = \dot{\underline{\varepsilon}}_e + \dot{\underline{\varepsilon}}_{vp} \qquad (7.8)$$

The yield condition states that visco-plastic straining only occurs when $F(\underline{\sigma} - \underline{\alpha}) > 0$. The strain rate is given by

$$\dot{\underline{\varepsilon}}_{vp} = \gamma \langle \phi(F) \rangle \frac{\partial F}{\partial \underline{\sigma}} \qquad (7.9)$$

where the angle brackets $\langle\ \rangle$ denote,

$$< \phi\ (F) > = \begin{cases} \phi\ (F) & F > 0 \\ 0 & F \leq 0 \end{cases} \qquad (7.10)$$

In these equations γ is known as the fluidity parameter and scales the strain rate, but when time independent plasticity is being modelled it is essentially arbitrary. ϕ is a positive monotonic increasing function which governs the change in strain rate and is also arbitrary when used for modelling time independent plasticity. The last term gives the direction of the inelastic strain rate and, in this case, is the normal to the yield surface. The method of solution involves solving the system of differential equations that results from this formulation. The inelastic strain rate decays and the process is halted when it is less than a given tolerance. As can be seen from these equations, a strain rate of zero corresponds to the satisfaction of consistency.

The differential equations are normally solved by an Euler method. The simplest is the usual explicit method. This only requires the inversion of the elastic stiffness matrix and is equivalent to an initial strain type of procedure (Zienkiewicz and Cormeau, 1974). More sophisticated methods, such as implicit Euler, require the inversion of a stiffness matrix for each time step of the solution process. The advantage of implicit methods is that larger time steps than those for the explicit methods can be used without the solution becoming unstable. Fuller discussions of these methods can be found in publications by Zienkiewicz (1977) and by Owen and Hinton (1980).

One advantage of the visco-plastic method is that

the consistency condition is satisfied automaticaly by the method of solution, which is not the case with the elasto-plastic methods. Also, it is not explicitly necessary to find the point where the stress point first touches the yield surface as is the case with most other methods.

The visco-plastic method was promising because the formulation is simple and is similar to that used in an existing program for solving creep problems (Hayhurst et al., 1984a). This is the reason why researchers in France have used a visco-plastic formulation for numerical work (see for example Chaboche and Rousselier, 1983). However, the principal disadvantage compared to the elasto-plastic methods is that it can be very slow to converge when a non-linear hardening curve is required. It was found that a very stiff system of differential equations resulted when differing parts of a structure were on different parts of the hardening curve with widely differing slopes. In particular, the slope of the hardening curve varies from infinity at the yield point to very small at large strains. It was found that the stiffness of the equations made it impossible to use conventional methods, such as Euler, for economically solving the differential equations; it was concluded that the special techniques required could not be developed within the timescale of the project. The elasto-plastic methods are not affected by this stiffness of the differential formulation and the solution technique was much more accurate and economical than the visco-plastic method.

7.3.3 Elasto-plastic Methods

An elasto-plastic procedure can be divided into two main parts. One part consists in the solution method for the system of non-linear equations and, since the satisfaction of equilibrium of stresses and forces in the structure is a central part of this process, this part is often referred to as an equilibrium solver. It is usually based on the Newton-Raphson method for solving systems of non-linear equations. The other part consists in the use of an appropriate constitutive law which allows the stresses to be calculated from the strains. The discussion will now continue by looking at the equilibrium solvers, after which the methods for solving the constitutive equations will be described and discussed.

7.3.4 Equilibrium Solvers

Equilibrium solvers usually involve iterative methods, often based on the Newton-Raphson method. The Newton-Raphson method itself can require a lot of computer time because it involves the inversion of large matrices for every iteration. Other methods based on this one employ ways of reducing the work required to obtain a solution, such as by using approximations to the true tangent matrix used by the Newton-Raphson method or by changing the calculated displacement increments in order to accelerate convergence. A general procedure for Newton methods can be written down. The differences between particular methods occur in the way the tangent matrix is evaluated.

In order to illustrate these methods, suppose a

structure to be modelled by a finite element mesh with a vector of displacements at the nodes, $\underline{a}$, and a vector of the nodal forces, $\underline{f}$, equivalent to the external forces acting on the structure.

Let

$$\underline{\psi}(\underline{a}) \equiv \underline{P}(\underline{a}) + \underline{f} \equiv \int B^T \underline{\sigma}\, dV + \underline{f} = 0 \qquad (7.11)$$

where $\underline{\sigma}$ is the vector of stress components in each element, B is the matrix connecting displacements at the nodes with strains in the elements and $\underline{\psi}$ can be thought of as the vector of residual forces acting on the mesh at the nodes. If we have an approximate solution $\underline{a}_k$, then in general $\underline{\psi}(\underline{a}_k) \neq 0$. Let $\underline{a}_0$ be the solution at a load $\underline{f}$. If another load increment is applied, $\Delta\underline{f}$, then from (7.11)

$$\underline{\psi}(\underline{a}_0) = \Delta\underline{f} \qquad (7.12)$$

The iteration scheme can be written

$$\left.\begin{aligned} \Delta\underline{a}_{k+1} &= K_*^{-1}\,(\underline{a}_k)\ \underline{\psi}\ (\underline{a}_k) \\ \underline{a}_{k+1} &= \underline{a}_k + \Delta\underline{a}_{k+1} \end{aligned}\right\} \quad k = 0,1,2,\ldots \qquad (7.13)$$

(In $\underline{\psi}$ the value of $\underline{\sigma}$ is found from $\underline{a}$ using the constitutive equations.) The way K_* is defined determines the nature of the scheme and some specific methods are now discussed.

Initial Stress

Here K_* is the elastic stiffness matrix

$$K_*(a) = K = \int B^T D\ B\ dV \qquad (7.14)$$

where D is the elasticity matrix.

Modified Newton-Raphson

K_* is set to be tangent matrix at the start of the load increment.

$$K_*(\underline{a}) = K_T(\underline{a}_0) = \int B^T D_{ep}(\underline{a}_0)\ B\ dV \qquad (7.15)$$

where $D_{ep} = \frac{d\underline{\sigma}}{d\underline{\varepsilon}}$ calculated from the constitutive equations.

Newton-Raphson

K_* is calculated for each iteration from

$$K_*(\underline{a}) = K_T(\underline{a}) = \int B^T D_{ep}(\underline{a})\ B\ dV \qquad (7.16)$$

7.3.5 Acceleration and Other Methods

One of the first acceleration methods for the solution of finite element equations was proposed by Nayak and Zienkiewicz (1972). The method can be used to improve the convergence of the initial stress method by multiplying the initial stress displacement increment by a matrix which is calculated to improve the speed of convergence of the method. The author has not used this method since, more recently, other methods have been proposed

and studied which are claimed to perform better; they are simpler to use and less expensive since they require less storage. In particular, the author has used a method proposed by Crisfield (1979) which has been shown to be a member of a group of acceleration techniques called Secant Newton methods (Crisfield, 1984). This method improves the convergence of the modified Newton method by scaling the displacement increment by an appropriate factor. The method was found to be reliable and its use resulted in some savings on processor time as compared with the full Newton-Raphson method, but, as will be shown, there is not always a satisfactory saving and, in some cases, the method fails even to converge. Generally, accelerated methods are not as robust as the full Newton procedure and it is necessary to use them circumspectly if convergence is to be obtained for all required solutions.

Another group of methods, which are now receiving more attention in the literature for the solution of finite element equations, are the quasi-Newton methods (Matthies and Strong, 1979). In these methods the inverse tangent stiffness matrix is updated more simply and cheaply than by inverting an updated stiffness matrix. These methods have been used successfully in optimization work but have not been used extensively in finite element work because they can suffer from slow, or difficult, convergence just like the accelerated methods discussed above. They do, however, belong to the Newton family of techniques described above.

7.3.6 Choice of Method

Two methods were selected from those described above for evaluation. The Newton-Raphson method was selected because of its reliability and because it is the basic method from which all the rest are derived. Thus, it can be used as a standard method against which others can be compared. The other method chosen was one of the secant Newton methods due to Crisfield (1979). This method is simple to use and is simple to implement in an existing finite element solver based on a Newton type equilibrium solver. In addition, it does not require large amounts of computer storage and so does not make the computer code appreciably larger. Details of the version of this method used by the author are given in Appendix D.

7.3.7 The Integration of Constitutive Equations

The constitutive equations are usually based on a relationship of the form

$$d\underline{\sigma} = D_{ep}\, d\underline{\varepsilon} \qquad (7.17)$$

Since this is a relationship between infinitesimal quantities, it must be integrated to be applicable to the finite strain increments encountered in a finite element solution. There are many methods which have been proposed for the calculation of $\Delta\underline{\sigma}$ using equation (7.17), but in most cases the expression for D_{ep} is basically the same and the difference between methods occurs in the procedure for integrating equation (7.17). The exact form of the expression for D_{ep} is governed by the type

of constitutive laws from which it is derived. In the present case, kinematic hardening is assumed and the hardening rule is that due to Ziegler (1959). Thus, a standard derivation (see for example Owen and Hinton, 1980) produces

$$D_{ep} = D - \frac{D\underline{a}\ \underline{a}^T D}{\underline{a}^T D\underline{a} + C/\mu^2} \qquad (7.18)$$

where $\mu = \dfrac{\sigma_y}{(\underline{\sigma} - \underline{\alpha})^T \underline{a}}$ and $\underline{a} = \dfrac{\partial F}{\partial \underline{\sigma}}$

Most of the methods for evaluating equation (7.17) are based on the Euler algorithm for integrating ordinary differential equations. However, there is the added complication that there are additional plasticity laws that are required to be satisfied. In particular, the consistency condition has to be satisfied by the solution. Usually this condition is not satisfied if $\Delta\underline{\sigma}$ is calculated directly from equation (7.17), and its value must be adjusted in some way in order to satisfy consistency. Some of the methods described in the literature will now be described and discussed.

For each of the following descriptions let $\underline{\sigma}_I$ be the initial stress point, $\underline{\sigma}_T$ and $\underline{\sigma}_A$ be intermediate points and $\underline{\sigma}_F$ be the final calculated stress point. Also, let $\Delta\underline{\varepsilon}$ be the given total strain increment.

Tangent Stiffness - Radial Return

This method is described in detail by Schreyer et

al (1979) and is used by Owen and Hinton (1980). If $\underline{\sigma}_I$ is not on the yield surface then a purely elastic increment is applied which brings the stress to a point $\underline{\sigma}_c$ which does lie on the surface. $\underline{\sigma}_c$ can be written

$$\underline{\sigma}_c = \underline{\sigma}_I + pD\Delta\underline{\varepsilon} \tag{7.19}$$

where p is a scaling factor $0 \leqslant p \leqslant 1$. For the remainder of the stress increment, $(1-p)D\Delta\underline{\varepsilon}$, plastic straining occurs. D_{ep} is evaluated at $\underline{\sigma}_c$ and used to give

$$\underline{\sigma}_T = \underline{\sigma}_c + D_{ep}(1-p)\Delta\underline{\varepsilon} \tag{7.20}$$

In general, $\underline{\sigma}_T$ does not lie on the yield surface so it is scaled radially to give $\underline{\sigma}_F$ which does satisfy consistency:

$$\underline{\sigma}_F = r\,\underline{\sigma}_T \tag{7.21}$$

where r is a scalar such that $F(r\underline{\sigma}_T, \underline{\alpha}) = 0$.

Secant Stiffness - Radial Return

A particular version of this for perfect plasticity is described by Krieg and Krieg (1977) and a version was used in a past version of the ABAQUS (1983) code. It is given its full generality by Zienkiewicz (1977). Suppose that $\underline{\sigma}_c$ lies on the yield surface as in the tangent stiffness method and that $\underline{\sigma}_T$ is an elastic trial stress where

$$\underline{\sigma}_T = \underline{\sigma}_c + (1-p)\, D\, \Delta\, \underline{\varepsilon} \qquad (7.22)$$

D_{ep} can be evaluated at any stress point $\underline{\sigma}_A$ between $\underline{\sigma}_c$ and $\underline{\sigma}_T$:

$$\underline{\sigma}_A = r\underline{\sigma}_c + (1-r)\, \underline{\sigma}_T \qquad (7.23)$$

where r is a scalar $0 \leqslant r \leqslant 1$. (Hence the tangent stiffness method is a special case of the secant stiffness method r = 1.) A new value of stress can now be calculated in the same manner as in equation (7.20), but again, in general, will not lie on the yield surface and consistency can again be satisfied by a radial return procedure. The particular methods used by Krieg and Krieg (1977) and ABAQUS (1983) use a value of r of 1/2 in equation (7.23).

Implicit Euler Method

This method is used by a more recent version of ABAQUS (1984). The technique requires that D_{ep} be evaluated at the final stress point $\underline{\sigma}_F$ and so some iterative method is required to solve a system of non-linear equations in order to find $\underline{\sigma}_F$. The Newton-Raphson procedure is the method used in ABAQUS since it is the most robust available (ABAQUS, 1984).

Elastic Predictor - Radial Corrector

This method is described by Schreyer et al (1979), who ascribe it to Mendelson, and the special case of perfect plasticity is discussed by Krieg and Krieg (1977)

where it is called the radial return method. It does not fit into the same class as the methods described so far, since it is not based upon equation (7.18). The elastic trial stress is found by

$$\underline{\sigma}_T = \underline{\sigma}_I + D\Delta\underline{\varepsilon} \qquad (7.24)$$

For this method, it is not necessary to find $\underline{\sigma}_c$ where the stress point meets the yield surface. Various assumptions are made (Schreyer et al., 1979) which lead to the result that the final stress deviator is a scalar multiple of the trial elastic stress deviator. The scalar factor is adjusted to allow the final stress value to satisfy consistency.

Subincrementation

The accuracy of these methods can be improved by using smaller step lengths, i.e. by splitting $\Delta\underline{\varepsilon}$ up into smaller subincrements. Each of the methods described above can be applied to each of the subincrements of strain and the total stress increment is obtained by addition of the resulting subincrements of stress. There are several different formulae that have been suggested for the number of subincrements that are required for any particular value of $\Delta\underline{\varepsilon}$. Examples are given in Schreyer et al. (1979), Krieg and Krieg (1977), and the ABAQUS (1983) manual.

7.3.8 Choice of Method

The method used by the author is basically a tangent

stiffness method. The satisfaction of the consistency condition is a little more complicated than radial return. The predicted increment in stress is scaled by a scalar factor r, but at the same time, the elastic strain is adjusted to take this into account, which in turn changes the amount of plastic strain contained in the total strain increment. The constitutive equations are used to relate the stress and strain increments and this is combined with the equation of the yield surface to give a scalar function of the factor r which is zero when the scaled stress increment satisfies the consistency condition. A root finding algorithm is then used to find a value of stress which gives a zero of this function. Subincrementation has not been used in the present program. The details of this method and its implementation are set out more fully in Appendix E.

This method has been selected and developed in order that a non-linear hardening curve may be modelled accurately. In fact, the method reproduces exactly a non-linear uniaxial hardening curve when it is used in solving problems where a uniform uniaxial stress is present. It also provides a way of satisfying plasticity laws in conjunction with the consistency condition.

This method and the equilibrium solvers selected above will now be used to solve a finite element problem. A particular structure will be used for which it is possible to obtain accurate solutions to plasticity problems which can then be compared with the finite element results.

7.4 An Example - The Two Bar Structure

The two-bar model is shown in Fig. 7.1. The bars are assumed to obey the uniaxial constitutive laws as discussed in sub-section 7.2.2. Solutions for this model were obtained very accurately by using the computer program described in Chapter 3. These numerical solutions were used as a benchmark to test the accuracy and efficiency of other numerical techniques. The model will be referred to as the 'ideal model'. In order to test the finite element solution procedure that has been proposed, the two-bar model was itself modelled by a finite element mesh. This mesh effectively consisted of two meshes representing the bars with common nodes at one end in order to simulate the attachment to the common block, as shown in Fig. 7.2. The element used was the 3-noded constant strain triangle. In the example studied, one bar was selected to be twice the length of the other and the cross-sectional areas of the bars are equal. This model does not exactly reproduce the ideal two-bar model. This is due to the fact that the axial (y-direction) stresses in the two bars are different and so the Poisson strains in the perpendicular or x-direction are different. This induces stresses in the x-direction in each bar due to the interaction at the common nodes. The stresses in the x-direction in turn have corresponding Poisson strains in the y-direction which changes the y-stress by a small amount. Thus, at equilibrium, the y-stresses in the finite element model will be slightly different from those predicted by the ideal two-bar model.

A series of tests was used to evaluate the effectiveness of the methods chosen to solve plasticity problems. These tests will now be described and the results presented and discussed.

7.4.1 Results of Numerical Studies

A series of trials was performed using the mesh shown in Fig. 7.2. Different material properties, numerical methods, and loading sequences were used in the trials to test the various methods. Only one material property was varied between tests. This was the parameter q in the constitutive equations (3.9) and (3.10) and it was given values of 2, 7 and 10. This was done because it was observed that, in general, it is the slope of the hardening curve that affects the convergence of the numerical methods tried. The constitutive laws were assumed to be normalized according to equation (3.19) and the parameter Γ was set to 0.5. Poisson's Ratio is required in order to calculate the elastic D-matrix and its value was set to 0.5. Two equilibrium solvers were tried: the full Newton-Raphson and the secant Newton method described by Crisfield (1979). The maximum applied load was either at a level at which only one bar yields or at one which caused both bars to yield - the values selected were, in terms of normalized load, respectively 1.5 and 2.4. (Normalized loads are defined such that a load of unity causes the shorter bar to have a stress equal to the yield stress.) The loads were either applied in one step or several equal steps (called, respectively, one-shot and incremental loading). The average values

of the y-stress and y-plastic strain in a group of elements close to the fixed ends of the bars were calculated and compared with the results from the ideal two-bar model. The values of stress and strain were taken from near the fixed ends of the bars so that any effects due to the interaction of the common nodes at the other end would be negligible. Values were not taken from the very end of the meshes so that there were no effects due to the boundary conditions in the results. The location of the elements from which the stress and strain values were taken is shown on the meshes in Fig. 7.2. The results of the tests are presented in Table 7.1-7.3.

7.4.2 Discussion of Results

The results presented in Table 7.1 show that the errors in y-stress in all of the tests were less than about 0.3%. The y-stress errors in the elastic finite element (FE) solution, which are solely due to the Poisson effects discussed earlier, are about 0.4%. Thus, the errors in y-stress in the FE solution are mainly due to Poisson effects. As further evidence of this, it can be seen from Table 7.1 that the FE values of stress derived using FE techniques are greater than the corresponding expected values in the long bar, and that the opposite is true for the shorter bar. This effect can also be accounted for by Poisson effects. It should be noted that, if the absolute error in one bar is added to that in the other, the result is very close to zero, thus demonstrating that equilibrium is closely satisfied by the solutions obtained. The error in y-stress is not

significantly affected by the method used to obtain the FE solution. This can be seen by the fact that it did not make much difference to the results whether Newton or secant Newton methods were used or whether the loading sequence was a one-shot or an incremental one.

The CPU times shown in Table 7.2 also indicate that there is no significant difference between results obtained by the Newton or the secant Newton methods in terms of total CPU time required to obtain a solution. Thus, although the secant method took less time per iteration than the Newton method, it took more iterations to converge to a solution. The one-shot loading sequence uses less CPU time than the corresponding incremental sequence. There are, however, exceptions to these general remarks in the case of q = 10. Here, the one-shot loading sequence using the secant Newton method failed to converge at all, and, with the same problem, the full Newton-Raphson method used significantly more CPU time than the incremental sequence. Also, there was a more significant saving by using the secant method over the Newton method. These differences can, in part, be explained by the fact that there are relatively large strains in the bars when q = 10 compared with those at q = 2 and 7. The program incorporates a limit on the total strain increment that is allowed during any iteration of the equilibrium solver. This was included into the program in order to ensure that divergence, which was observed when large strain increments were allowed, does not occur. Thus, if the strains are large compared with this limit, then this becomes a determining

factor upon the number of iterations required to reach the necessary strains. Hence, it can be seen that the number of iterations for the two numerical methods is about the same and, since the secant method requires less time per iteration than the Newton method, the former uses less computer time to obtain a solution than the latter.

The errors in plastic strain (Table 7.3) are on the whole larger than those in stress. As with stress, the finite element value is less than the theoretical value in the longer bar and the opposite is true in the shorter bar. The pattern of error is not as uniform as for stress, with the errors being greater for larger values of q than for smaller values. However, the errors can be explained mostly in terms of Poisson effects - if the errors in stress are substituted into the constitutive equations, then the calculated error in plastic strain is of the same order as that recorded in the table.

7.5 Discussion and Conclusions

In this chapter, methods for solving many dimensional structural problems with nonlinear material behaviour have been reviewed. A selection of these techniques were developed and used to solve a simple finite element problem. The results showed that the chosen techniques gave accurate results. However, the number of loading cycles that may be performed is limited because the method requires a lot of computational effort.

The particular equilibrium solvers chosen were Newton-Raphson and Crisfield's accelerated modified

Newton method. On the whole, the Newton-Raphson method was more robust, always converging to a solution, whereas Crisfield's method occasionally failed to converge. It has been seen that Crisfield's method converges more slowly than the Newton-Raphson method and this meant that its use did not afford a significant saving on the amount of computer time required. However, Crisfield's method was found to be easy to use and could well provide savings when used in the solution of problems requiring larger meshes where the inversion of the stiffness matrix is much more costly.

These methods are two elasto-plastic methods. They were used in preference to visco-plastic methods because these latter were found to be impractical in the present case. However, visco-plastic methods could still be efficient in other situations. The difficulties that were encountered were due to the nature of the hardening curve and not to the methods themselves. Their advantage is that they could provide a uniform solution method for both plasticity and creep problems and, in addition, deal with time dependent plasticity or visco-plasticity. These possibilities have been exploited by researchers at ONERA in France where a computer program has been developed to use visco-plastic methods in modelling many aspects of material behaviour, including creep and plasticity (see for example, Chaboche and Cailletaud, 1986).

The constitutive law used in this chapter suffers from the same problems as its uniaxial precursor; for example, a lack of ratchetting or relaxation. Also, the

extension to a multiaxial law in this chapter does not cater for general loading paths and would give an unrealistic response for many paths. The non-linear kinematic hardening rule of Chapter 4 has a natural multiaxial extension and will be used in the next chapter.

The method of integrating the constitutive law was developed by the author to deal with a non-linear hardening curve in many dimensions. It is an extension of the uniaxial method used in Chapter 3 for solving multibar problems. However, the multiaxial method proved to be very cumbersome to run. As outlined in Appendix E, there are many situations that must be dealt with and it was found that situations can occasionally arise that are not covered by these procedures and new procedures must then be found. Notice, however, that the problem of spurious unloading is a problem for other methods too.

In the next chapter, the multiaxial non-linear kinematic hardening rule will be used to look at ways of incorporating damage and failure into multiaxial models.

Procedure	Value of Parameter q in Constitutive Equations					
	2		7		10	
	Bar 1	Bar 2	Bar 1	Bar 2	Bar 1	Bar 2
2AD	-3.335×10^{-3} (-2.089×10^{-1})	3.334×10^{-3} (1.664×10^{-1})	-1.410×10^{-2} (-8.023×10^{-2})	1.413×10^{-3} (7.668×10^{-2})	-1.213×10^{-3} (-6.848×10^{-2})	1.350×10^{-3} (7.382×10^{-2})
2AI	-3.053×10^{-3} (-1.913×10^{-1})	3.052×10^{-3} (1.523×10^{-1})	-1.384×10^{-3} (-7.874×10^{-2})	1.386×10^{-3} (7.521×10^{-2})	Failed to converge	
2ND	-3.334×10^{-3} (-2.089×10^{-1})	3.333×10^{-3} (1.663×10^{-1})	-1.384×10^{-3} (-7.871×10^{-2})	1.391×10^{-3} (7.549×10^{-2})	-1.200×10^{-3} (-6.770×10^{-2})	1.309×10^{-3} (7.159×10^{-2})
2NI	-3.309×10^{-3} (-2.073×10^{-1})	3.308×10^{-3} (1.651×10^{-1})	-1.426×10^{-3} (-8.111×10^{-2})	1.432×10^{-3} (7.772×10^{-2})	-1.027×10^{-3} (-5.794×10^{-2})	1.152×10^{-3} (6.300×10^{-2})
1AD	-2.739×10^{-3} (-3.020×10^{-1})	2.738×10^{-3} (2.039×10^{-1})	-2.038×10^{-3} (-2.434×10^{-1})	2.037×10^{-3} (1.442×10^{-1})	-1.790×10^{-3} (-2.179×10^{-1})	1.789×10^{-3} (1.252×10^{-1})
1AI	-2.713×10^{-3} (-2.991×10^{-1})	2.712×10^{-3} (2.019×10^{-1})	-2.025×20^{-3} (-2.419×10^{-1})	2.025×10^{-3} (1.433×10^{-1})	-1.786×10^{-3} (-2.175×10^{-1})	1.786×10^{-3} ($1,250\times10^{-1}$)
1ND	-2.739×10^{-3} (-3.020×10^{-1})	2.738×10^{-3} (2.039×10^{-1})	-2.038×10^{-3} (-2.434×10^{-1})	2.037×10^{-3} (1.442×10^{-1})	-1.789×10^{-3} (-2.179×10^{-1})	1.789×10^{-3} (1.252×10^{-1})
1NI	-2.718×10^{-3} (-2.997×10^{-1})	2.717×10^{-3} (2.023×10^{-1})	-2.012×10^{-3} (-2.403×10^{-1})	2.012×10^{-3} (1.424×10^{-1})	-1.763×10^{-3} (-2.147×10^{-1})	1.763×10^{-3} (1.234×10^{-1})

KEY TO TABLE

The terminology in the procedure column of each table is defined as follows:

First Character	2 -	Two bars yielded at maximum load
	1 -	One bar only yielded at maximum load
Middle Character	N -	Newton-Raphson method
	A -	Secant Newton method
Last Character	D -	Load applied in equal steps (6 steps for 2 bars yielded, 3 steps for 1)
	I -	Load applied in 1 step

Table 7.1 Errors in normalized stress calculated at maximum load after 1 full load cycle. Values are the absolute error $(\sigma_C-\sigma_T)$ and, in parentheses, the percentage error $100(\sigma_C-\sigma_T)/\sigma_T$, where σ_C is the finite element value and σ_T the accurate value.

Procedure	Value of parameter q in constitutive equations		
	2	7	10
2AD	31 (0.140)	96 (0.166)	222 (0.159)
2AI	21 (0.161)	180 (0.198)	Failed to converge
2ND	35 (0.248)	106 (0.268)	310 (0.262)
2NI	12 (0.267)	77 (0.267)	343 (0.263)
1AD	11 (0.096)	11 (0.097)	11 (0.096)
1AI	6 (0.093)	6.5 (0.085)	7 (0.085)
1ND	16 (0.210)	14 (0.220)	14 (0.219)
1NI	5 (0.199)	5 (0.195)	5.5 (0.198)

KEYS TO TABLE

The terminology in the procedure column of each table is defined as follows:

First Character:
- 2 - Two bars yielded at maximum load
- 1 - One bar only yielded at maximum load

Middle Character:
- N - Newton-Raphson method
- A - Secant Newton method

Last Character:
- D - Load applied in equal steps (6 steps for 2 bars yielded, 3 steps for 1)
- I - Load applied in one step

Table 7.2 C.P.U. times (in seconds) required for finite element calculations over one load cycle. Numbers in brackets are the C.P.U. times (in seconds) per iteration.

Procedure	Value of Parameter q in Constitutive Equations					
	2		7		10	
	Bar 1	Bar 2	Bar 1	Bar 2	Bar 1	Bar 2
2AD	-1.586×10^{-2} (-1.116)	2.682×10^{-2} (0.6653)	-2.382×10^{-1} (-1.295)	4.535×10^{-1} (1.180)	-3.597×10^{-1} (-4.682×10^{-1})	2.736 (1.761)
2AI	-1.452×10^{-2} (-1.022)	2.455×10^{-2} (0.6090)	-2.338×10^{-1} (-1.272)	4.449×10^{-1} (1.157)	Failed to converge	
2ND	-1.586×10^{-2} (-1.116)	2.682×10^{-2} (0.6652)	-2.337×10^{-1} (-1.271)	4.466×10^{-1} (1.162)	-9.13×10^{-1} (-1.19)	2.50 (1.61)
2NI	-1.573×10^{-2} (-1.107)	2.661×10^{-2} (0.6600)	-2.407×10^{-1} (-1.309)	4.598×10^{-1} (1.196)	-1.016 (-1.322)	2.300 (1.480)
1AD	--	7.544×10^{-3} (1.603)	--	9.169×10^{-3} (3.506)	--	9.11×10^{-3} (4.25)
1AI	--	7.473×10^{-3} (1.587)	--	9.113×10^{-3} (3.484)	--	9.09×10^{-3} (4.25)
1ND	--	7.545×10^{-3} (1.603)	--	9.170×10^{-3} (3.506)	--	9.11×10^{-3} (4.25)
1NI	--	7.487×10^{-3} (1.590)	--	9.053×10^{-3} (3.461)	--	8.98×10^{-3} (4.19)

KEY TO TABLE

The terminology in the procedure column of each table is defined as follows:

First Character: 2 - Two bars yielded at maximum load
1 - One bar only yielded at maximum load

Middle Character: N - Newton-Raphson method
A - Secant Newton method

Last Character: D - Load applied in equal steps (6 steps for 2 bars yielded, 3 steps for 1)
I - Load applied in 1 step

Table 7.3 Errors in normalized plastic strain calculated at maximum load after 1 full load cycle. Values are the absolute error $(\eta_C-\eta_T)$ and, in parentheses, percentage error $100(\eta_C-\eta_T)/\eta_T$, where η_C is the finite element value and η_T the accurate value.

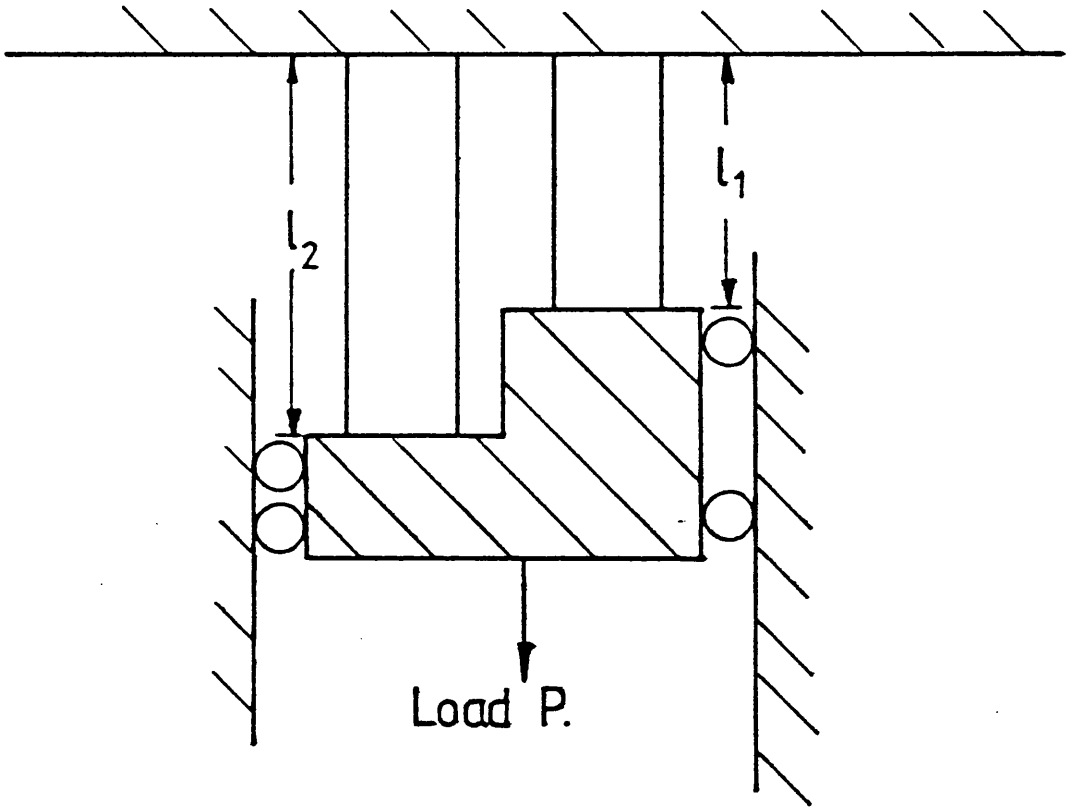

Figure 7.1: Two bar model structure.

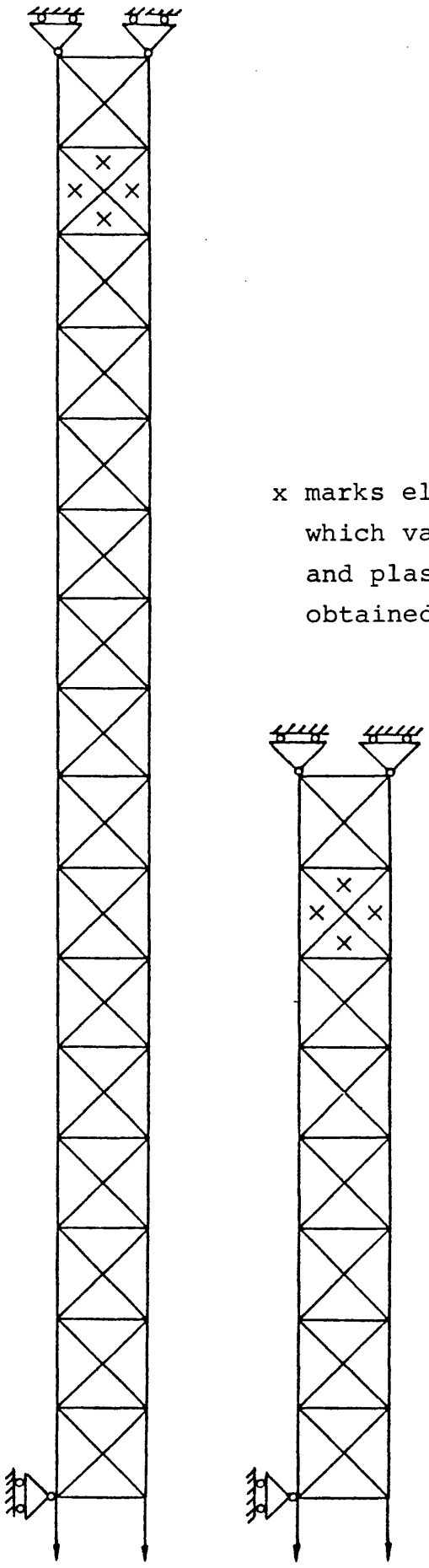

x marks elements from which values of stress and plastic strain were obtained.

Figure 7.2: Finite element mesh for 2 bar structure.

CHAPTER 8

THE USE OF DAMAGE AND FAILURE IN MULTIAXIAL PROBLEMS

8.1 Introduction

Solution methods for non-linear finite element problems were examined in Chapter 7. Also, the constitutive law of Chapter 3 was extended to a multiaxial law. In this chapter, the non-linear kinematic hardening rule will be used in its multiaxial form. Methods for incorporating the effects of damage on deformation into the multiaxial laws are suggested and tested on two simple examples.

8.2 A Model of Multiaxial Behaviour

In Chapter 4, a model was proposed for the behaviour of damaged material. In this model the value of damage being used in the constitutive equations varied according to the position of the stress-strain state of the material on the hysteresis loop. In this section, a proposal is made as to how the original model may be extended to multiaxial cases. Sub-sections 8.2.1 and 8.2.2 give the details of the proposed multiaxial model and 8.2.3 gives the multiaxial damage evolution law that will be used.

8.2.1 Damage in More Than One Dimension

Damage is often directional in nature; for example when it represents fissuring or cracking due to fatigue. A full representation of this directionality would involve the use of some form of damage tensor (Chaboche, 1981).

However, there is no accepted form for a damage tensor and the matter is still the subject of research. Also, the use of a damage tensor leads to complications when the effect on constitutive laws is considered and this is not only computationally difficult and expensive, but is also still a matter for research. In the case of creep, Leckie and Hayhurst (1974) have found that a single scalar damage variable which acts isotropically is adequate for a description of creep rates in many multiaxial situations. In view of this, it will be assumed here that fatigue damage is a single scalar variable, ψ , which acts isotropically. Hence the effective stress hypothesis becomes this: for a damaged material, σ_{ij} is replaced by $\sigma_{ij}/(1-\psi)$ in the constitutive equations.

A further problem is the definition of the points at which the acting damage is changed. The model in Chapter 4 relied on the change of stress from compression to tension. Clearly, similar rules based on tension and compression are not immediately applicable in many dimensions.

The method proposed is that, for each load cycle, a fixed direction is chosen. The components of stress and strain in this direction are then treated as if they were uniaxial stress and strain in the uniaxial model proposed in Chapter 4. Thus, when the stress component along this direction becomes zero, then the acting damage is set to the current value of damage. When the strain component in this direction subsequently returns to the value it had when the acting damage was changed, then

the acting damage is reset to zero. The choice of this fixed direction is based on the orientation of the plane in which fissuring is expected to occur.

8.2.2 Damage and the Multiaxial Non-linear Kinematic Hardening Rule

The multiaxial non-linear kinematic hardening rule is represented by

$$d\alpha_{ij} = \frac{2}{3} C\, d\eta_{ij} - \gamma \alpha_{ij}\, dp \ , \qquad (8.1)$$

where all the terms are the same as they were defined in Chapter 4.

When damage is included isotropically in (8.1), it becomes:

$$\frac{d\alpha_{ij}}{1-\psi} = \frac{2}{3} C\, d\eta_{ij} - \gamma \frac{\alpha_{ij}}{1-\psi} dp \qquad (8.2)$$

During a change in the value of the acting damage, the values of η_{ij} and α_{ij} must be redefined in order to maintain constant stress and total strain. Before the damage change,

$$\varepsilon_{ij} = D^{-1}_{ijk\ell}\ \sigma_{k\ell} + \eta_{ij} \ , \qquad (8.3)$$

and afterwards,

$$\varepsilon'_{ij} = \tilde{D}^{-1}_{ijk\ell}\ \sigma'_{k\ell} + \eta'_{ij} \qquad (8.4)$$

Continuity of stress and strain over the change is maintained by setting:

$$\varepsilon'_{ij} = \varepsilon_{ij} \qquad (8.5)$$

$$\sigma'_{ij} = \sigma_{ij} \ ,$$

and thus

$$\eta'_{ij} = \varepsilon'_{ij} - \tilde{D}^{-1}_{ijk\ell}\ \sigma'_{k\ell} \qquad (8.6)$$

The change in the value of α_{ij} is found as follows. The effect of the change in damage is to change the size of the yield and limit surfaces in stress space since they are effectively magnified by a factor of $(1-\psi)$ in the presence of damage, ψ. Thus, if the material is yielding after the change then the new value of α_{ij} must satisfy

$$f\left[\frac{\sigma_{ij} - \alpha'_{ij}}{1-\psi'}\right] = 0 \qquad (8.7)$$

where f is the yield function. It is assumed that α'_{ij} is on the line joining α_{ij} to σ_{ij}, hence

$$\alpha'_{ij} = \alpha_{ij} + \lambda(\sigma_{ij} - \alpha_{ij}) \qquad (8.8)$$

where the scalar λ is chosen so that (8.7) is satisfied. In summary, there are two possibilities that occur when the acting damage is to be changed:

either $f\left[\frac{\sigma_{ij} - \alpha_{ij}}{1-\psi'}\right] > 0$ in which case α'_{ij} is set

according to (8.7) and (8.8),

or

$$f\left[\frac{\sigma_{ij}-\alpha_{ij}}{1-\psi'}\right] \leqslant 0 \text{ in which case } \alpha'_{ij} = \alpha_{ij}$$

8.2.3 Multiaxial Damage Evolution

The form proposed here is a generalization of the uniaxial equation given in Chapter 4 and is taken from Lemaitre and Chaboche (1985). It does not have widespread experimental support, but it does use some standard empirical results such as Sines' Criterion for the fatigue limit in the multiaxial case.

In the case where the damage is isotropic, the damage evolution rate is given by the following series of equations:

Let

$$A_{II} = \frac{1}{2} \underset{t}{\text{Max}} \underset{t'}{\text{Max}} J_2 (\sigma_{ij}(t) - \sigma_{ij}(t')) \qquad (8.9)$$

where t and t′ are parameters describing points within a stress cycle. Then

$$\frac{\delta\psi}{\delta N} = [1-(1-\psi)^{\beta+1}]^{\alpha} (A_{II}, \bar{\sigma}_H, \sigma_{eqM}) \left[\frac{A_{II}}{M(\sigma_H)(1-\psi)}\right]^{\beta} \qquad (8.10)$$

where

$$\alpha(A_{II}, \bar{\sigma}_H, \sigma_{eqM}) = 1-a \left\langle \frac{A_{II}-A^*_{II}(\bar{\sigma}_M)}{\sigma_u - \sigma_{eqM}} \right\rangle \qquad (8.11)$$

$$A^*_{II}(\bar{\sigma}_H) = \sigma^*_{\ell} (1-b\bar{\sigma}_H), \quad \text{(Sines' Criterion)} \qquad (8.12)$$

$$M(\bar{\sigma}_H) = M_0 (1-b\bar{\sigma}_H) \qquad (8.13)$$

$\bar{\sigma}_H$ is the average hydrostatic stress over a cycle, and

σ_{eqM} is the maximum value of J_2 (σ_{ij}) during cycle.

The coefficients σ^*_ℓ, σ_ℓ, b, a, σ_u, β are the same as those used in the uniaxial case. It can be seen that this damage rate law depends exclusively on the maximum effective stress range.

8.3 An Example - The Multiaxial Behaviour of a Material Element in Plane Stress

The behaviour of the uniaxial version of the non-linear kinematic hardening model has been studied in detail in Chapter 4. In this section, the behaviour of the multiaxial version is studied for two selected loading cases under plane stress conditions. Plane stress is of interest because much multiaxial fatigue testing is done under various types of biaxial loading. This includes tests under tension-torsion conditions, where a thin-walled tube is subjected to combined axial and torsional strains and where a material element in the gauge length of the specimen is essentially under plane stress conditions. Tension-torsion tests are the motivation for the two linear, fully reversed cyclic straining paths which have been chosen to test the model. These straining paths are illustrated in Fig. 8.1. Paths similar to these have been used by Socie et al. (1985) in conducting experiments into the tension-torsion fatigue behaviour of Inconel 718. The first path in Fig. 8.1 consists of cycling the shear strain whilst keeping the axial strain constant and positive. The second reverses the roles of shear and axial strain: the shear

is constant whilst the axial strain is cycled.

However, although many tests have been carried out on tension-torsion specimens in order to study the multiaxial fatigue properties of materials, the author is not aware of any experimental data on the complete deformation and load histories for these tests. Hence, there is little experimental evidence with which to compare the theoretical predictions of this model. However, the model also predicts lifetime and, since there is plenty of experimental data on failure under multiaxial conditions, this provides one way in which the model may be compared with experiment.

The multiaxial version of the non-linear kinematic hardening rule cannot be solved explicitly, and numerical methods have to be employed. One suggested method is described in detail in Appendix B. This is based on the implicit Euler methods mentioned in Chapter 7 and is used here to study the response of the model to the cyclic strain paths shown in Fig. 8.1.

The evolution of fatigue damage was included in the numerical model and was calculated according to (8.9-8.13). The coefficients required for these equations were for 316 stainless steel at 20°C and were taken from the book by Lemaitre and Chaboche (1985). These values are listed in Table 8.1. The method of using equations (8.9-8.13) was as follows: during each cycle the damage was assumed to remain constant. For each cycle its was assumed that there are two points during the cycle at which the stress took on an extreme value in terms of the Von Mises equivalent stress. At one of the extreme

points of the cycle the value of the stress was stored and at the other the increase in damage was calculated, based on the stress values at these two points. The increase in damage over one cycle was calculated by integrating (8.10) for one cycle.

8.3.1 The Orientation of Fissures and its Action on Deformation

The plane along which fissures would be supposed to form was determined in advance. In general there are two possible planes: (i) the plane of maximum shear strain; and (ii) the plane perpendicular to the maximum principal tensile stress. Often cracks or fissures grow in the plane perpendicular to the direction of maximum principal tensile stress. However, in the case of low cycle fatigue in pure torsion, cracks often propagate along the maximum shear planes (Brown and Miller, 1979). It is in general not easy to predict the directions in which cracks will grow and this matter is still the subject of much research. Thus, the fissure planes used in this investigation were determined on the basis of what is observed in low cycle tension-torsion fatigue experiments.

For the strain paths used here it was found that there was a transient period, lasting a few cycles (less than 10), during which any mean stresses relaxed to zero. It was found to be desirable to allow the fissured plane to affect the deformation only once the stress had relaxed and the stable cyclic state had been attained.

8.3.2 Example 1 - Cyclic Axial Strain with Constant Shear Strain

The cyclic strain path for this test is the one shown in Fig. 8.1(a). In obtaining values of stress for the damage evolution equations it was assumed that the points A and B were the extreme points of each cycle. The initial loading was from the origin to $\gamma = 0.01$, and this produced a shear stress in the element. A graph of the shear stress over the first few cycles with respect to the imposed axial strain is shown in Fig. 8.2. As can be seen, the shear stress relaxes to zero very quickly. This is in accordance with experimental observations not reported in the literature, although the author is not aware of any experimental data with which the theoretical results can be directly compared. The fact that the shear stress relaxes to zero in this case is a property of the non-linear kinematic hardening model. The more usual bilinear kinematic hardening model shows some relaxation over the first quarter cycle, but thereafter the shear stress remains constant at a non-zero level.

This relaxation means that after a few initial cycles the stresses induced are the same as in a uniaxial push-pull test. One of the stress-strain hysteresis loops obtained for moderate value of damage is shown in Fig. 8.3. This is similar to those obtained earlier for the uniaxial version by solving the equations exactly. The direction of cracking was taken to be perpendicular to the axial strain since, after the first few cycles, this is the direction perpendicular to the maximum principal tensile stress and hence is the plane in which cracks

grow in uniaxial push-pull tests.

The envelopes of maximum and minimum axial stress are shown in Fig. 8.4. This illustrates the load drop in tension due to the increase in damage. The stress in compression remains relatively stable right up until failure at about 260 cycles. The differences between the results obtained in this test and a uniaxial test for the same axial strain range are very small indeed; the difference in lifetime amounts to less than 0.1%.

8.3.3 Example 2 - Cyclic Shear Strain with Constant Axial Strain

The strain path for this test is illustrated in Fig. 8.1(b). As with the previous test, the stress component not directly affected by the component of strain being cycled - in this case the axial stress - relaxes to zero very quickly. The plot of axial stress against shear strain over the first few cycles is very similar in shape to the plot in Fig. 8.2.

The fissure plane in this case is again perpendicular to the axial direction. This represents crack growth along planes of maximum shear which is the main type of crack growth in pure torsion specimens under low cycle fatigue conditions. Under these conditions cracks also grow in a plane parallel to the axis. However, the model of cracking being used here only caters for one fissure plane to be present in the material at once.

The envelopes of maximum and minimum shear stress are shown in Fig. 8.5. In this case both the positive and negative stresses remain constant for most of the

lifetime of the test. The only variation of the levels of the envelopes occurs during the first few cycles and this is due to mean stress relaxation. Thus, in this case the model predicts that there is no load drop during the test and that failure occurs suddenly when damage reaches unity. This behaviour is not what would be expected since, as damage increases, the stresses would be expected to decrease. The reason for this is that, according to the proposed model, the material is assumed to be uninfluenced by damage during the stable cyclic part of the test. The material is assumed only to be influenced by damage when the stress component across the assumed fissure plane becomes positive. Examination of the stress path after the initial period of cycling shows that the stress across either of the planes perpendicular and parallel to the axis is always zero and never becomes positive. Hence, according to the rule for incorporating damage into the constitutive laws, the damage does not affect any of the stress-strain hysteresis loop.

8.3.4 Discussion

This last result is not completely satisfactory since a load drop would be expected towards the end of the test, just before failure. The behaviour of the model is due to the fact that damage is assumed not to influence deformation because the stress does not become positive across the fissure plane. A possible way to overcome this would be to use a different fissure plane, say at 45° to the axis. The stresses and strains across this

plane cycle between positive and negative values and this would give similar results to the first example which is shown in Fig. 8.4. However, the stress envelopes in this case are not symmetric about the horizontal axis and, since the stress states at each end of the cycle are symmetric, then symmetric shear stress envelopes would be expected. This symmetry would be preserved if two orthogonal cracking planes, each inclined at 45° to the axis, were used. In this case damage would influence deformation throughout the test and a symmetrical load drop would be expected. However, there is a fundamental problem with a symmetrical load drop. This would imply that the stress range would decay to zero as the damage increased. According to the damage evolution equations this leads to unlimited life for the specimen, which is not the case.

It is possible that the assumption that scalar damage affects all components of stress to the same degree is a cause of these difficulties. However, the symmetry of the stress states induced by shear strain cycling suggests that the stress range will tend towards zero as damage increases, whatever the configuration of fissures or whatever the nature of the effect of damage on the stress. These considerations call into question the validity of using this method to calculate the damage growth in a specimen under strain controlled tests, since the damage evolution equations considered here have been derived from stress controlled tests. This approach assumes that any stress state encountered during strain controlled tests is equivalent to the same situation

in a stress controlled test.

For these reasons, it might be better to use a law for damage growth that depends on the strain range rather than the stress range. However, there has apparently been no work carried out into finding such a growth law for damage. Chaboche and Lesne (1986) have suggested one possible formulation, but do not give details on the exact form the equations would take. Most work in multiaxial fatigue has been directed towards obtaining failure criterion (for example, one review is presented by Brown and Miller, 1973). It is relatively simple to take a failure criterion and adapt it to a damage based approach. However, this would say nothing about the actual deformation or stress drop during the life of the specimen. There is scope, then, for further work in this area in order to develop a damage growth law which depends on strain, gives the correct failure criterion, and in addition predicts the deformation history of a specimen given the loading history. A possible approach to this is outlined below (a similar approach is given by Lemaitre and Chaboche (1985) for the Manson-Coffin criterion).

A multiaxial failure criterion usually depends on reducing the multiaxial stress or strain state to an equivalent uniaxial value of stress or strain. Suppose that the failure criterion is Q, where Q is a function of either the stress or strain state. The simplest assumption about damage evolution is that it is linear, and this may be written

$$\frac{\delta\psi}{\delta N} = \frac{1}{Q} \qquad (8.14)$$

When this is integrated between the limits

$$\psi = 0, \quad N = 0, \quad \text{and}$$
$$\psi = 1, \quad N = N_f$$

then (8.14) becomes the original failure criterion

$$N_f = Q \tag{8.15}$$

This gives a linear damage growth rate whenever Q is constant. Thus, if Q is a function of strain, the maximum stress would decay linearly to zero during a strain controlled cyclic loading test. This particular formulation is sufficient for predicting lifetimes under constant stress or strain cycling conditions, but, as pointed out by Lemaitre and Chaboche (1985), it is not sufficient to predict lifetimes of tests in which the controlling quantity is varied during the test. It has also been pointed out by Chaboche (1981) that the damage growth rate must be a function of both the failure criterion and of the stress or strain level. He terms this non-separability. The new damage growth law that results from this may be written

$$\frac{\delta\psi}{\delta N} = \frac{\psi^{\alpha}}{(1-\alpha)} \quad \frac{1}{Q} \tag{8.16}$$

where α is also a function of stress or strain state. This type of equation is sufficient to predict the remaining life of a specimen under a given load, given its previous history. However, it may not accurately

model the deformation of the specimen using the concept of effective stress. However, the predicted remaining life is unaffected by any one-to-one transformation of the damage variable. If it is required that the rate of growth of damage governs the deformation history then this last fact may be used to reproduce the deformation history without affecting the predictive capabilities of the damage growth law. The transformation that Lemaitre and Chaboche (1985) recommend is that $\psi \rightarrow 1 - (1-\psi)^{(\beta+1)}$ where β is a constant. This leads to a damage growth law

$$\frac{\delta\psi}{\delta N} = \frac{[1 - (1-\psi)^{\beta+1}]^{\alpha}}{(1-\psi)^{\beta}\,(1-\alpha)(1+\beta)}\,\frac{1}{Q} \qquad (8.17)$$

This is basically the law that has been used earlier. Using this it is possible to give a damage formulation to any failure criterion expressed in the form $N_f = Q$. However, the full power of this formulation may only be realised if the function α is also specified. It may be set to a constant, but this leads to a linear damage cumulation law or Miner's law which has been shown to be inadequate. Several forms of α have been suggested, but most of these are based upon stress. Chaboche and Lesne (1986) have also suggested a strain based expression for α which is of the same form as (8.11), but they do not validate it with experimental evidence. Nevertheless, there is a multitude of possibilities for Q. One example would be the Manson-Coffin criterion for low cycle uniaxial fatigue. This may be written as

$$Q = (\Delta\eta/C)^{-\gamma} \qquad (8.18)$$

where $\Delta\eta$ is the plastic strain range and C and γ are constants. For multiaxial conditions the uniaxial strain may be replaced by an equivalent strain. For example, a particularly simple criterion that is a combination of two criteria that are used in the ASME design codes has been proposed recently by Brown and Buckthorpe (1985). In the case of low cycle fatigue, their criterion may be written

$$Q = (\varepsilon_{eq}/C)^{-\gamma} \qquad (8.19)$$

where again C and γ are constants (not necessarily the same as in (8.18)) and ε_{eq} is an equivalent strain amplitude which is defined as

$$\varepsilon_{eq} = A\,\varepsilon_{eq(R)} + (1-A)\,\varepsilon_{eq(T)} \qquad (8.20)$$

where

$$\varepsilon_{eq(R)} = \frac{1}{1+\nu}\left[\varepsilon_1 + \frac{(\varepsilon_1+\varepsilon_2+\varepsilon_3)\nu}{(1-2\nu)}\right] \qquad (8.21)$$

$$\varepsilon_{eq(T)} = \frac{\varepsilon_1-\varepsilon_3}{1+\nu} \qquad (8.22)$$

where $\varepsilon_1 \geq \varepsilon_2 \geq \varepsilon_3$ are the principal strain amplitudes. The subscripts R and T in these equations refer to the Rankine and Tresca failure criteria respectively. The parameter A in (8.20) is material dependent and can be written

$$A = 1 - (\varepsilon_0/\varepsilon_{eq(T)})^{\frac{1}{2}} \qquad (8.23)$$

where ε_0 is a material constant which can be expressed

$$\varepsilon_0 = (1/q-1)^2\ 2q\ \varepsilon_\ell \qquad (8.24)$$

where ε_ℓ is the uniaxial fatigue limit, and $q = t/b$, where t is the torsional fatigue strength and b is the bending fatigue strength.

This last formulation is suitable for strain controlled tests but is not necessarily valid for stress controlled tests. For example, it is observed experimentally that any mean stress has an affect on life and it is not clear that this formulation adequately accounts for this.

8.4 Conclusions

A few of the properties of the non-linear kinematic hardening rule and of a proposed method for incorporating damage have been investigated in this chapter. However, the models of fissured material and the damage evolution laws have been shown to be inadequate. Some improvements have been suggested, but these can only be assessed by reference to experimental information about how damage affects deformation. This is apparently not available and so a programme of multiaxial testing is necessary to provide the information which is required for improvements to be made to the models.

Name	Value
σ_u	760.0 MPa
a	0.9
β	5.0
σ_ℓ	222 MPa
b	0.00132
M_0	1700.0

Table 8.1 Values of constants in damage evolution laws, equations (8.9) - (8.13) for 316 stainless steel at 20°C.

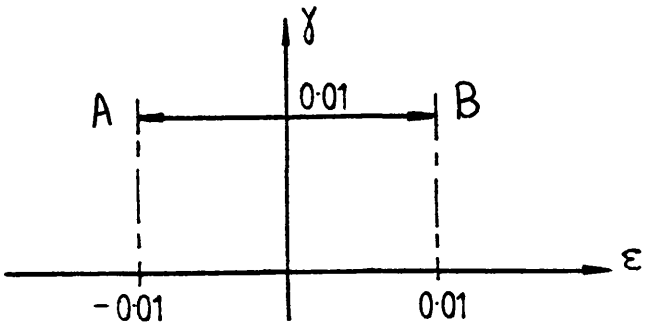

a) Shear strain held constant.

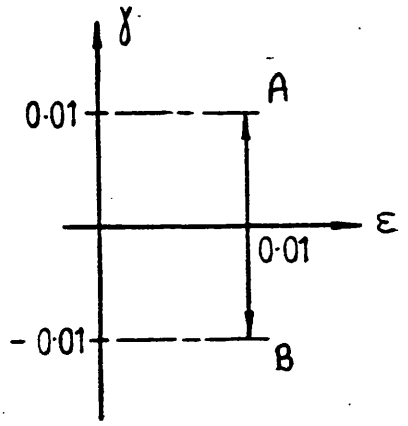

b) Axial strain held constant.

Figure 8.1: Two multiaxial cyclic loading paths used to test the model of multiaxial cyclic plastic behaviour.

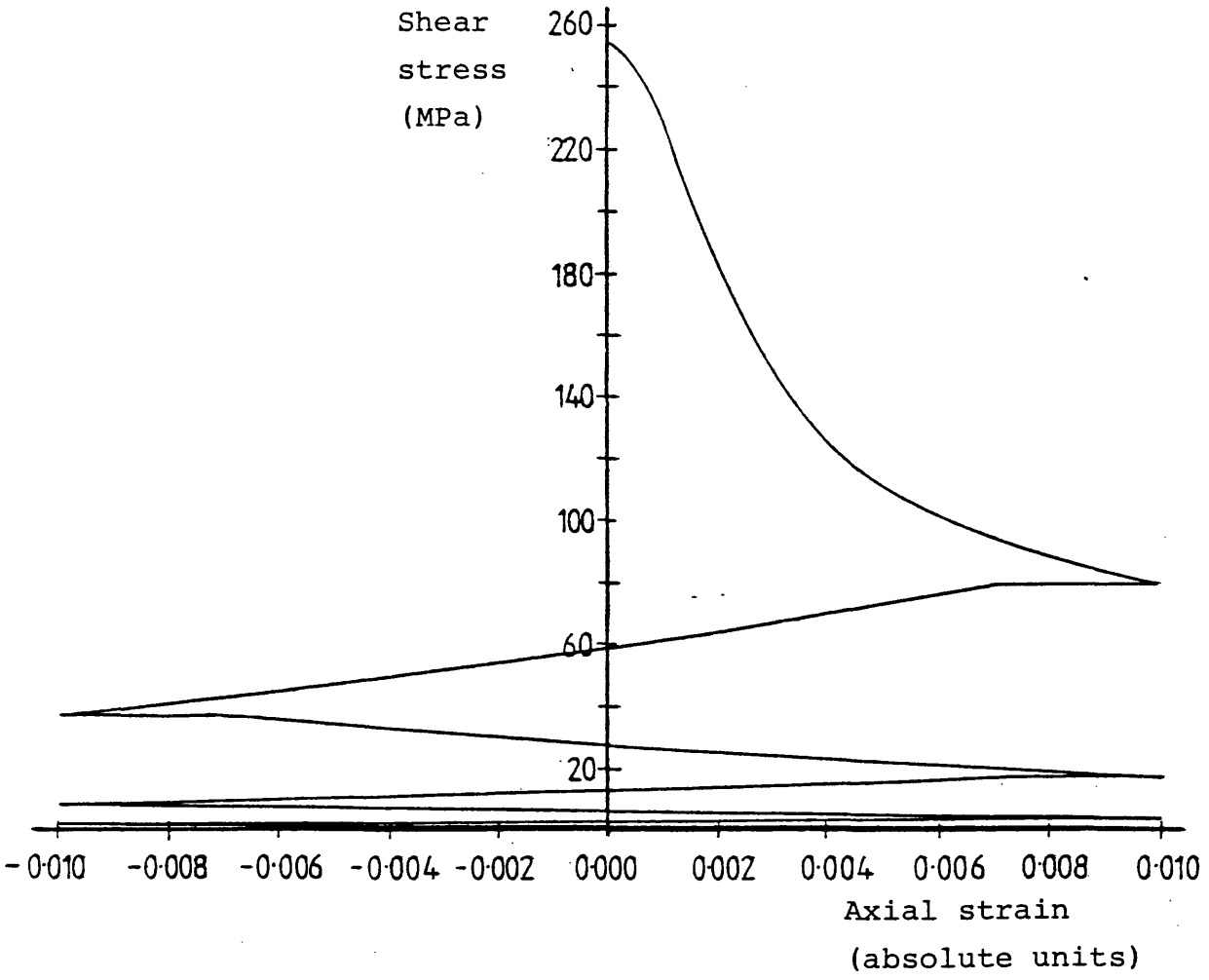

Figure 8.2: Relaxation of shear stress to zero under axial strain cycling.

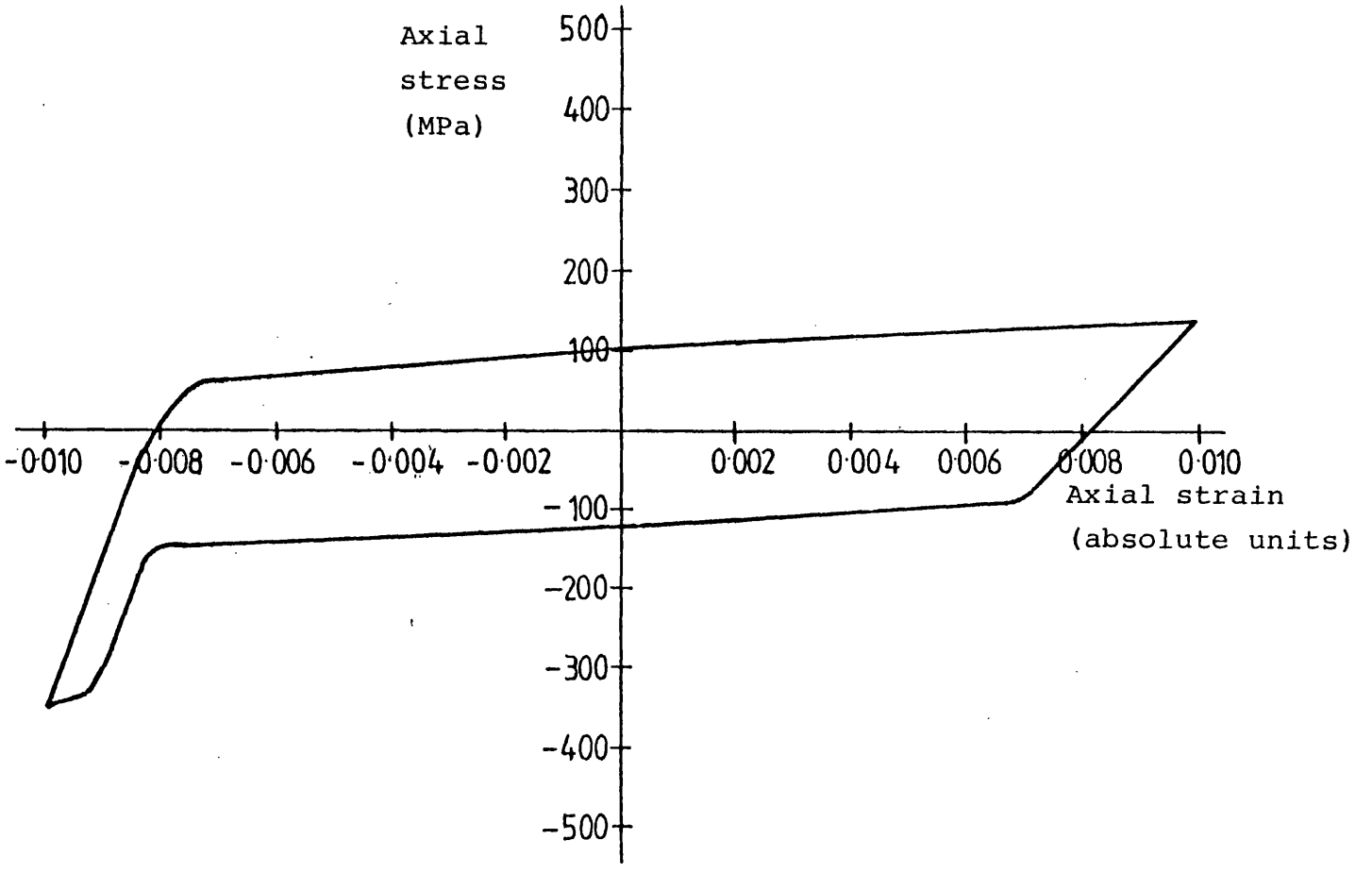

Figure 8.3: Stress-strain hysteresis loop for axial strain cycling when ψ = 0.614 .

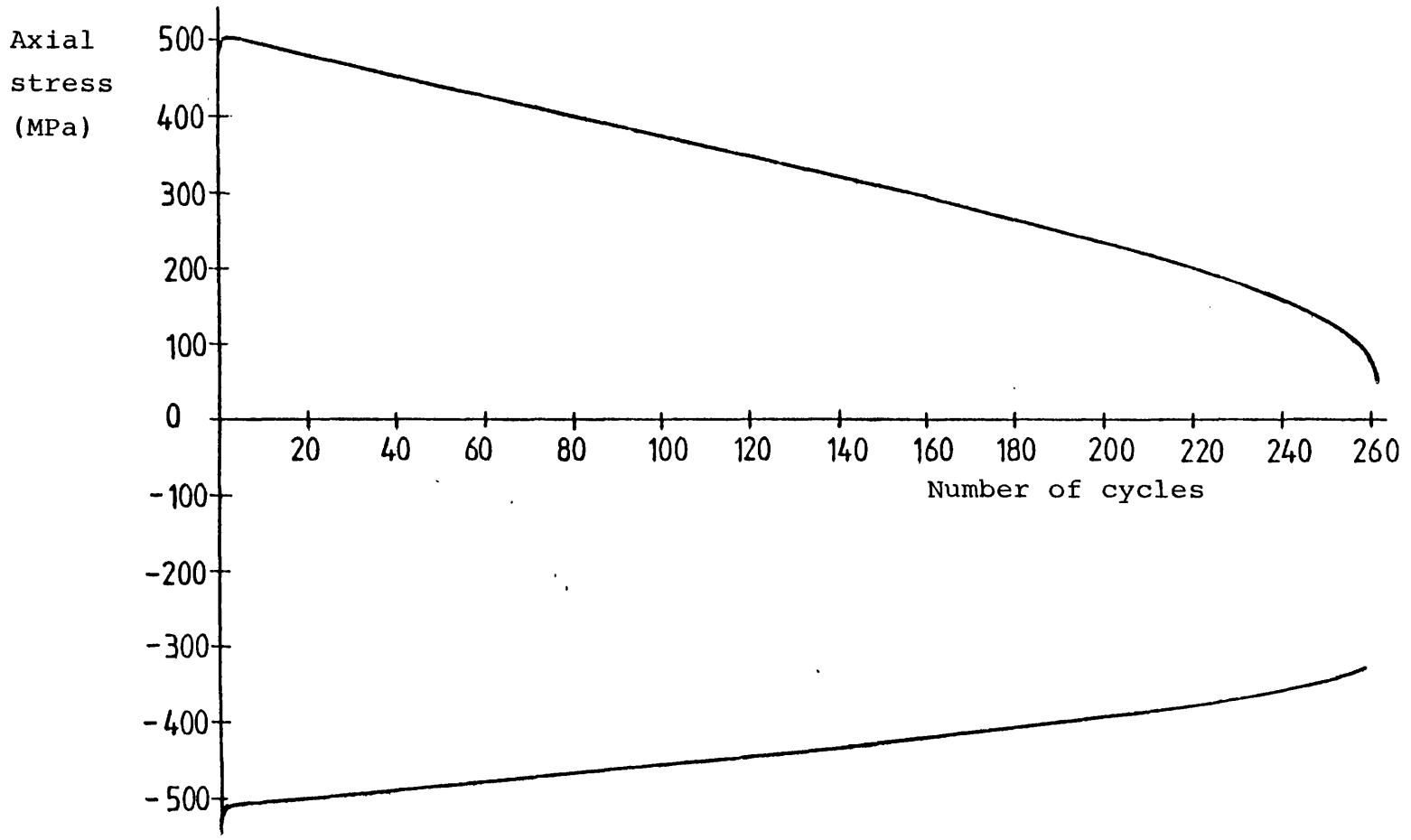

Figure 8.4: Envelopes of maximum and minimum axial stress during axial strain cycling.

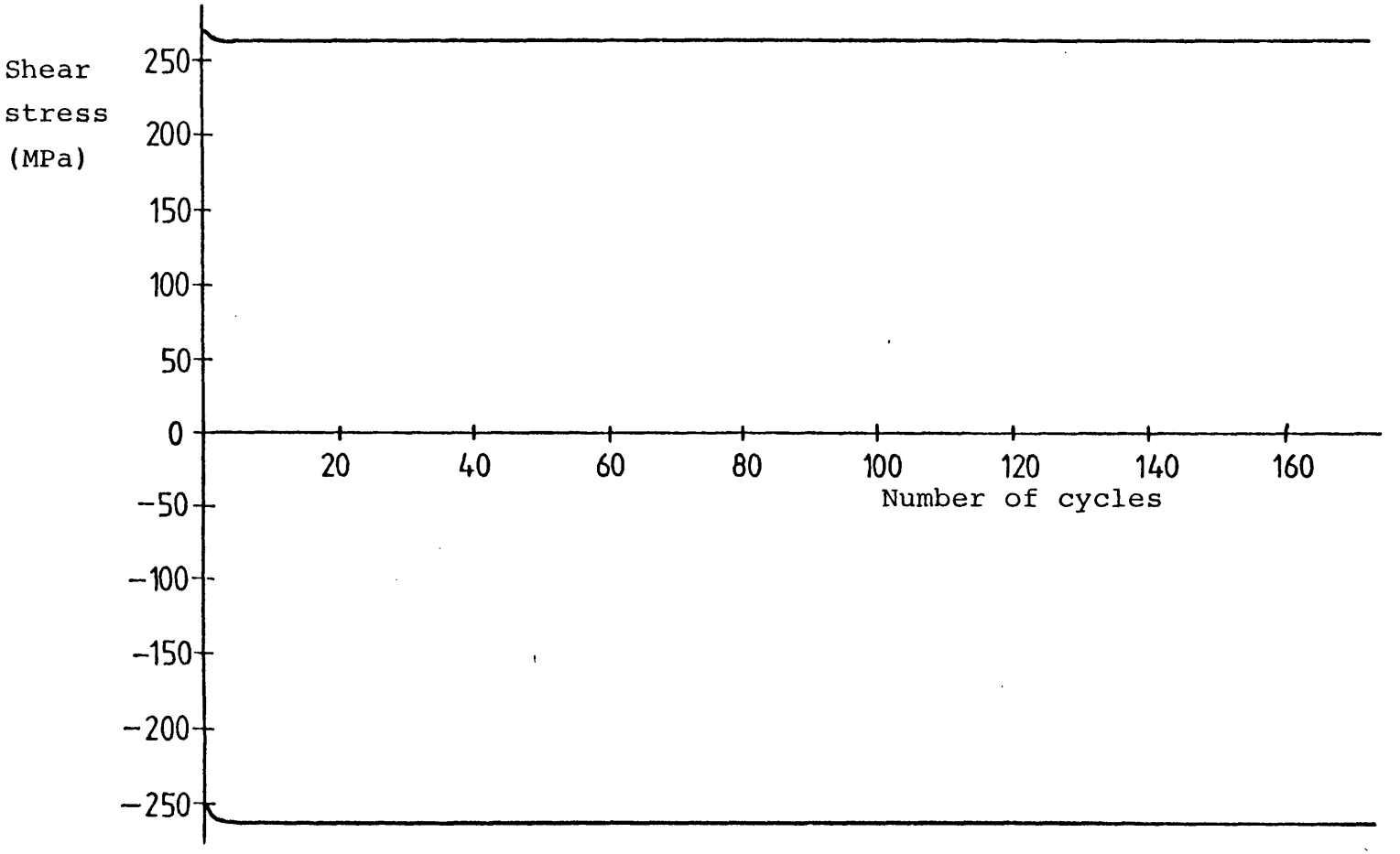

Figure 8.5: Envelopes of maximum and minimum shear stress during shear strain cycling.

CHAPTER 9

CONCLUSION

9.1 Discussion and Conclusions

The purpose of the work reported here has been to introduce a continuum damage mechanics model of fatigue behaviour into a solver for structural problems and to combine it with a creep model which is already available. Experience was, therefore, necessary in carrying out structural calculations that involved cyclic plasticity and damage growth. The basis of this is represented by the work involving multibar model structures. The final chapters showed how the damage and plasticity concepts may be introduced into finite element solvers. In parallel with this has been the study of constitutive models and their ability to reproduce actual material behaviour. These too have been developed from uniaxial models into multiaxial ones.

In a structure, the stress redistributes whenever a part of it becomes weaker than the remainder. The effect of this is to decrease the stress acting on the weakened area and this usually decreases the rate of further weakening, allowing the structure to last longer than would be expected if this were not taken into account. For instance, a stress concentration will tend to be diminished and this will prolong life, as has been observed for creep (Leckie and Hayhurst, 1974). In the case of fatigue, it was demonstrated in Chapters 3 and 5 that the magnitude of this effect can be up to 25% of life.

The cyclic thermal loading used in Chapter 6 was not originally envisaged for this work, but was introduced so that the model could be compared with a particular set of experimental results. It was shown that the model reproduced the qualitative behaviour observed in the experiments but did not predict life very well. In addition, it was possible to examine the behaviour of structures under conditions that have not been extensively studied previously, namely under thermomechanical and pure thermal loading. The results obtained showed that the presence of a mechanical load can have a significant effect on the life and mode of failure of the structure and that creep ductility also plays an important role.

It appears that, for thermal loading, the exact profile of the time-variation of the temperature is important in determining the stresses that occur in the structure. This is because the slower the variation, the more stress redistribution that occurs due to creep, and hence the lower the peak stresses.

The definition of inelastic strain when the magnitude of the damage changes was not straightforward. The solution used here was to change the value of the plastic strain so as to preserve continuity in stress and total strain. The author considers this to be an arbitrary procedure, and that, by using a better crack closure model or by examining the role of cavities and dislocations, a better solution to this may be found.

Another of the aims of this work has been to examine the need for carrying out cycle by cycle calculations in predicting the life of components subjected to low

cycle fatigue. The results of Chapter 7 indicate that this would in general require very powerful computers, but the multibar calculations show that accuracy may be maintained even if 'step lengths' of several cycles are used. This has not been demonstrated for creep-fatigue, but there is no reason to suppose that similar methods are not feasible in this case too.

The testing of nonlinear finite element methods has shown that the full Newton-Raphson method is competitive when compared with an accelerated modified Newton method. However, the accelerated method was found to be easy to implement and the amount of computer time required for one iteration was much less than that for the Newton-Raphson method. Hence, an accelerated method could be more economical for solving large, well-behaved problems.

The integration of the constitutive laws is an important part of a finite element plasticity solver. The method developed by the author turned out to be difficult to use because it was necessary to deal with many special cases. The implicit method, which was used in Chapter 8, gave accurate results as long as step lengths were small enough and it also proved to be relatively robust.

Of the two constitutive laws that were tried, the nonlinear kinematic hardening rule was shown to be very versatile. The other law, a power law hardening curve, lacked ratchetting and relaxation behaviour and, above all, did not possess a natural extension to a multiaxial law. However, nonlinear kinematic hardening possessed

all these properties and can also be modified to display other features of material behaviour such as cyclic hardening. The multiaxial version provides a description of hardening which does not require special loading conditions or arbitrary rules for linking it with uniaxial behaviour.

9.2 Future Work

The models which have been developed in this thesis are at a point at which they may be incorporated, without much difficulty, into a finite element solver. However, improvements are needed in the way in which damage is incorporated into the multiaxial constitutive laws. Some experimental data on how a material behaves before failure takes place would be required as a guide to how this could be accomplished. Also, a suitable multiaxial failure criterion and damage growth law must be chosen. However, it is important that the models constructed in this way are not so complicated that the calculations required would be too difficult or expensive.

Although the ratchetting and relaxation behaviour of the nonlinear kinematic hardening model is a strong point in its favour, the magnitude of the effect is much greater than is observed in experiments. It may be possible to improve this aspect of the model by allowing the limit surface to move. This proposal would also enable the modelling of the initial ratchetting rates as well as the steady state rates. Another aspect of this is the ratchetting behaviour of the model when damage is present. This was not studied, but may be important since

the life of a multibar structure was found to be sensitive to the magnitude of the compressive stresses that were generated in damaged and failed bars. The improvement of the constitutive model may be continued by incorporating the initial cyclic hardening into the model, especially if it has a significant effect on life as Chaboche and Cailletaud (1986) claim.

Finally, as remarked in Chapter 7, the combining of creep and plasticity as different aspects of viscoplasticity, and thus unifying the solution methods, should lead to a streamlined solution procedure.

APPENDIX A

A NUMERICAL METHOD FOR SOLVING PROBLEMS INVOLVING NON-LINEAR MATERIAL BEHAVIOUR IN MULTIBAR STRUCTURES

A multibar model consists of n parallel uniform bars. The bars are each fixed at one end and are loaded at the opposite end so that the axial displacement, s, is the same in all the bars. The problem to be solved is that of finding, given s and the constitutive laws for the bar material, the stresses and strains which satisfy equilibrium and compatability.

Let the length of the bar i be l_i and its cross-sectional area be A_i. The solution procedure entails evaluating the tangent stiffness of the structure and using this in a Newton-Raphson scheme to find the equilibrium state.

A.1 Elastic Solution

Suppose that the total strain in bar i is ε_i and the stress is σ_i. The condition of compatability of displacements gives

$$s = \varepsilon_i \, l_i \, , \quad \text{for } i = 1,2,\ldots,n \qquad (A.1)$$

Equilibrium requires that

$$P = \sum_{i=1}^{n} A_i \, \sigma_i , \qquad (A.2)$$

where P is the applied load. If the bars are linear elastic then

$$\sigma_i = E \varepsilon_i \quad , \qquad i = 1, \ldots, n$$

where E is Young's modulus, and so, by (A.1),

$$\sigma_i = Es/l_i \tag{A.3}$$

Thus, given s, the stress in each bar may be calculated. Substitution of (A.3) into (A.2) allows (A.2) to be put into the form $P = Ks$ where

$$K = E \sum_i A_i/l_i \tag{A.4}$$

is the stiffness.

A.2 Elasto-plastic Solution

The solution of the equilibrium problem can be written as the solution of

$$\Psi(s) = 0 \tag{A.5}$$

An iterative solution to this may be written:

$$s^{(0)} = s_0$$

$$s^{(k+1)} = s^{(k)} - \Psi(s^{(k)})\, K_T^{-1} \qquad k=1,2,\ldots, \tag{A.6}$$

where s_0 is the initial value of the displacement and where

$$K_T = \frac{d\Psi}{ds} \tag{A.7}$$

is the tangent stiffness.

In the case of a multibar structure, Ψ may be written

$$\Psi \equiv P - \sum_i A_i \sigma_i \qquad (A.8)$$

The stresses may be evaluated using the usual assumption that

$$\varepsilon_i = e_i + \eta_i \quad , \qquad (A.9)$$

where e_i is the elastic and η_i the inelastic strain in bar i. Use of this and (A.1) allows (A.8) to be written

$$\Psi(s) \equiv P - E \sum_i A_i(s/l_i - \eta_i) \qquad (A.10)$$

The tangent stiffness, K_T, is evaluated as follows:

$$\frac{d\Psi}{ds} = - \sum_i A_i \frac{d\sigma_i}{ds}$$

$$= - \sum_i A_i \frac{d\sigma_i}{d\varepsilon_i} \frac{d\varepsilon_i}{ds}$$

$$= - \sum_i \frac{A_i}{l_i} \frac{d\sigma_i}{d\varepsilon_i} \qquad (A.11)$$

The derivative required in (A.11) for the constitutive law of Chapter 3 is

$$\frac{d\sigma}{d\varepsilon} = \frac{KE}{K+qE\left|(\sigma-2\mu\sigma_y-\sigma_0)/2K\right|^{q-1}} \qquad (A.12)$$

The derivative for the non-linear kinematic hardening rule is

$$\frac{d\sigma}{d\varepsilon} = \frac{\Lambda}{(\Lambda/E+1/[C-\alpha_0\gamma\mu])} \qquad (A.13)$$

where

$$\Lambda = \exp[-\gamma\mu(\varepsilon-\sigma/E-\eta_0)]$$

APPENDIX B

THE NUMERICAL SOLUTION OF THE NON-LINEAR KINEMATIC HARDENING RULE IN 3-DIMENSIONS

As is usual, the constitutive equations can be expressed in the form

$$d\underline{\sigma} = D_{ep}\, d\underline{\varepsilon} \qquad (B.1)$$

where D_{ep} has the form

$$D_{ep} = D - (D\underline{a}\ \underline{a}^T D)/(h+\underline{a}^T D\ \underline{a}) \qquad (B.2)$$

D is the elasticity matrix, $\underline{a}$ is the normal to the yield surface, and h depends on the hardening rule and can be derived in the manner now described.

The flow rule for plasticity is

$$d\underline{\eta} = \lambda\underline{a} \qquad (B.3)$$

where the factor λ has the form

$$\lambda = \underline{a}^T d\sigma/h \qquad (B.4)$$

(By definition if the derivation of D_{ep} is carried out using λ obtained from (B.4), then (B.2) will be obtained.)

The consistency condition is expressed by

$$df = \frac{\partial f}{\partial \underline{\sigma}}\, d\underline{\sigma} + \frac{\partial f}{\partial \underline{\alpha}}\, d\underline{\alpha} = 0 \qquad (B.5)$$

Since $f = f(\underline{\sigma} - \underline{\alpha})$ then $\frac{\partial f}{\partial \underline{\sigma}} = -\frac{\partial f}{\partial \underline{\alpha}} = +\underline{a}$ and

$$df = \underline{a} \cdot (d\underline{\sigma} - d\underline{\alpha}) = 0 , \qquad (B.6)$$

The hardening law is

$$d\underline{\alpha} = \frac{2}{3} C \, d\underline{\eta} - \gamma \, \underline{\alpha} \, dp \qquad (B.7)$$

Substitution from (B.3) and pre-multiplication by $\underline{a}$ results in

$$\underline{a} \cdot d\underline{\alpha} = \lambda(CA^2 - \gamma A \, \underline{a} \cdot \underline{\alpha}) \qquad (B.8)$$

where $A = (2\underline{a} \cdot \underline{a}/3)^{\frac{1}{2}}$. Using consistency (B.6) and (B.4) it can be seen that

$$h = CA^2 - \gamma A \, \underline{a} \cdot \underline{\alpha} \qquad (B.9)$$

The numerical solution itself may be performed as follows. Suppose $\underline{\sigma}$, $\underline{\varepsilon}$, $\underline{\alpha}$, and $\underline{\eta}$ have initial values $\underline{\sigma}_i$, $\underline{\varepsilon}_i$, $\underline{\alpha}_i$, and $\underline{\eta}_i$ and that an increment of total strain $\Delta\underline{\varepsilon}$ is given, then at the end of the increment their values become $\underline{\sigma}_e$ $(= \underline{\sigma}_i + \Delta\underline{\sigma})$, $\underline{\varepsilon}_e$, $\underline{\alpha}_e$, and $\underline{\eta}_e$, and it is required that the following be satisfied:

$$f(\underline{\Sigma}_e) = 0 \qquad (B.10)$$

where $\underline{\Sigma} = \underline{\sigma} - \underline{\alpha}$,

$$\underline{\sigma}_e = D(\underline{\varepsilon}_e - \underline{\eta}_e) , \qquad (B.11)$$

$$\Delta \underline{\alpha} = \frac{2}{3} C \Delta \underline{\eta} - \gamma \underline{\alpha}_i \Delta p , \qquad (B.12)$$

and

$$\Delta \underline{\eta} = \lambda \underline{a}_i \qquad (B.13)$$

Using (B.13), (B.11) can be written

$$\underline{\sigma}_e = D(\underline{\varepsilon}_e - \underline{\eta}_i - \lambda \underline{a}_e) \qquad (B.14)$$

and (B.12) can be rewritten

$$\underline{\alpha}_e = \frac{2}{3} C \lambda \underline{a}_e + (1 - \lambda \gamma A) \underline{\alpha}_i \qquad (B.15)$$

where $A = (2\underline{a}_e \cdot \underline{a}_e / 3)^{\frac{1}{2}}$ (B.16)

Combining (B.15) and (B.14) it can be shown that

$$\underline{\Sigma}_e = \underline{\sigma}_e - \underline{\alpha}_e = D(\underline{\varepsilon}_e - \underline{\eta}_i - \lambda \underline{a}_e) - \frac{2}{3} C \lambda \underline{a}_e - (1 - \lambda \gamma A) \underline{\alpha}_i \qquad (B.17)$$

which may be written as:

$$\underline{F} = D(\underline{\varepsilon}_e - \underline{\eta}_i - \lambda \underline{a}_e) - \underline{\Sigma}_e - \frac{2}{3} C \lambda \underline{a}_e - (1 - \lambda \gamma A) \underline{\alpha}_i = 0 \qquad (B.18)$$

In order to solve (B.18), a Newton-Raphson procedure is employed. $\underline{F}$ is a function of $\underline{\Sigma}$ and λ, i.e. $\underline{F} \equiv \underline{F}(\underline{\Sigma}, \lambda)$. Suppose that $\underline{F}(\underline{\Sigma}, \lambda) \neq 0$ and that the solution is $\underline{F}(\underline{\Sigma} + \Delta \underline{\Sigma}, \lambda + \Delta \lambda) = 0$, then the following first order expansion may be obtained:

$$\underline{F}(\underline{\Sigma}, \lambda) + \frac{\partial \underline{F}}{\delta \lambda} \Delta \lambda + \frac{\partial \underline{F}}{\delta \underline{\Sigma}} \Delta \underline{\Sigma} = 0 \qquad (B.19)$$

$$\text{or} \quad \Delta\underline{\Sigma} = -\left(\frac{\partial \underline{F}}{\partial \underline{\Sigma}} \right)^{-1} \left[\underline{F} + \frac{\partial \underline{F}}{\partial \lambda} \Delta\lambda \right] \tag{B.20}$$

Similarly, from (B.10) it may be shown that

$$f(\underline{\Sigma}) + \frac{\partial f}{\partial \underline{\Sigma}} \cdot \Delta\underline{\Sigma} = 0 \tag{B.21}$$

Combining (B.20) and (B.21) gives

$$\Delta\lambda \frac{\partial f}{\partial \underline{\Sigma}} \left[\frac{\partial \underline{F}}{\partial \underline{\Sigma}} \right]^{-1} \frac{\partial \underline{F}}{\partial \lambda} = f(\underline{\Sigma}) - \frac{\partial f}{\partial \underline{\Sigma}} \left[\frac{\partial \underline{F}}{\partial \underline{\Sigma}} \right]^{-1} \underline{F} \tag{B.22}$$

Writing $\underline{n} = \frac{\partial f}{\partial \underline{\Sigma}}$ and $H = \frac{\partial \underline{F}}{\partial \underline{\Sigma}}$ and substituting for $\Delta\lambda$ in (B.19) from (B.22) gives:

$$\Delta\underline{\Sigma} = -H^{-1} \left[\underline{F} + \frac{\partial \underline{F}}{\partial \lambda} \left[\frac{f - \underline{n} \cdot (H^{-1}\underline{F})}{\underline{n} \cdot \left[H^{-1} \frac{\partial \underline{F}}{\partial \lambda} \right]} \right] \right] \tag{B.23}$$

The derivatives required in (B.19) are:

$$\frac{\partial \underline{F}}{\partial \lambda} = \gamma A \, \underline{\alpha}_i - (D + \frac{2}{3} C) \, \underline{a}_e \tag{B.24}$$

$$\text{and} \quad \frac{\partial \underline{F}}{\partial \underline{\Sigma}} = -\lambda(D + \frac{2}{3} C) \frac{\partial \underline{a}}{\partial \underline{\Sigma}} - I + \lambda\gamma \frac{\partial A}{\partial \underline{\Sigma}} \underline{\alpha}_i \tag{B.25}$$

$$\text{where} \quad \frac{\partial A}{\partial \underline{\Sigma}} = \frac{2}{3A} \underline{a} \cdot \frac{\partial \underline{a}}{\partial \underline{\Sigma}} \tag{B.26}$$

and I is the unit matrix.

The above procedure is valid for solving the non-linear kinematic hardening rule in all situations. However, in certain subspaces of general stress space, such as plane stress, it may be more convenient to use a modification of (B.12). The natural way to do this

is to use a similar modification to the one proposed by Ziegler (1959) for Prager's hardening rule. In this case (B.12) becomes

$$\Delta\underline{\alpha} = C\Delta p \frac{(\underline{\sigma}_i - \underline{\alpha}_i)}{\sigma_0} - \gamma \underline{\alpha}_i \Delta p \qquad (B.27)$$

The equations (B.19) to (B.23) do not depend on (B.12) and are not changed by adopting (B.27). Thus it is only necessary to alter the derivatives $\frac{\partial F}{\partial \lambda}$ and $\frac{\partial F}{\partial \underline{\underline{\Sigma}}}$. They become:

$$\frac{\partial F}{\partial \lambda} = - D\underline{a} - A(C\underline{\sigma}_i + (C+\gamma)\underline{\alpha}_i) \qquad (B.28)$$

and

$$\frac{\partial F}{\partial \underline{\underline{\Sigma}}} = -\lambda D \frac{\partial \underline{a}}{\partial \underline{\underline{\Sigma}}} - I - (C\underline{\sigma}_i + (C+\gamma)\underline{\alpha}_i)\lambda \frac{\partial A}{\partial \underline{\underline{\Sigma}}} \qquad (B.29)$$

APPENDIX C

CREEP AND THERMAL STRAINS IN A MULTIBAR STRUCTURE

C.1 Integration of Creep Strain and Creep Damage

Suppose that the value of creep strain in a particular bar is v_i, then new value of creep strain is given by

$$v_{i+1} = v_i + \Delta t_i \dot{v} \qquad (C.1)$$

where $\dot{v}$ is given by (6.2) evaluated at the current value of stress and Δt_i is given by

$$\Delta t_i = \frac{\sigma_{max}}{\dot{v}_{max} E c} \qquad (C.2)$$

where σ_{max} and $\dot{v}_{max}$ are the maximum absolute values of stress and creep rate respectively in all the bars, and c is a constant. It was found that in general a value for c of 1 was sufficient to ensure that the time to rupture did not vary substantially with the size of c although larger values were used since this did not impose an unacceptable overhead on computer processor time and made sure that the solutions were reasonably accurate. The damage was integrated by the same method using the same value of the time step that was used to integrate strains.

C.2 The Effect of a Change in Creep Strain on a Structure

In general, the change in creep strain in a particular bar is not compatible with the changes taking place

in the rest of the bars. This incompatibility must be accommodated by changing the stresses in the bars and this is done by using the following method. Suppose that the change in creep strain in bar j is Δv_j, and that the change in the external mechanical load is ΔP, then equilibrium and compatibility require that

$$\Delta P = \Sigma A_j \Delta \sigma_j \qquad (C.3)$$

where A_j is the area of the jth bar, and

$$\Delta \delta = \Delta \varepsilon_j \ell_j , \quad \text{for all } j, \qquad (C.4)$$

where $\Delta \delta$ is the change in displacement common to all of the bars, and ε_j and ℓ_j are the total strain and length respectively of the jth bar. Since the total strain change may be broken down into an elastic and a non-elastic strain change, then, using (C.4), (C.3) can be rewritten as

$$\Delta P = \Sigma A_j (\Delta \delta / \ell_j - \Delta v_j) E \qquad (C.5)$$

where it is assumed that the change in non-elastic strain is all due to the change in creep strain. Equation (C.5) can be solved for $\Delta \delta$:

$$\Delta \delta = (\Delta P + E \Sigma A_j \Delta v_j)/K \qquad (C.6)$$

where $K = E \Sigma A_j / \ell_j$. The change in total strain can then be found from this change in displacement, from which

the change in elastic strain, and hence in stress, can be calculated.

In general, however, since the stresses have changed, the constitutive laws with respect to plasticity will not now be satisifed. Hence, at this point the change in plastic strain is calculated and equilibrium satisfied in the normal way.

C.3 Thermal Strains

Suppose that the change in temperature in bar j is $\Delta\theta_j$, then, assuming that the only change in non-elastic strain is the change in thermal strain, the change in stress is given by

$$\Delta\sigma_j = (\Delta\delta/\ell_j - \alpha\Delta\theta_j)\, E \qquad (C.7)$$

where α is the coefficient of linear thermal expansion. As in the case of creep strains the effect of the change in stress on the plastic strains is calculated and equilibrium satisfied again.

APPENDIX D

THE ACCELARATED MODIFIED NEWTON-RAPHSON METHOD

The acceleration method used in the finite element program is a two-parameter secant Newton method described by Crisfield (1979, 1984). In this scheme the displacement for each iteration is modified in order to increase the rate of convergence of the modified Newton-Raphson method. The notation is the same as that used in equations (7.11), (7.12) and (7.13). The residual force vector after the addition of the kth displacement increment is $\underline{\Psi}(a_k)$ which will be shortened to $\underline{\Psi}_k$. In the modified Newton-Raphson scheme, the next displacement increment is $\underline{a}^*_{k+1}$ which is given by

$$\underline{a}^*_{k+1} = K^{-1}\underline{\Psi}_k \qquad (D.1)$$

where K is the tangential stiffness matrix calculated at the beginning of the current load step as defined in equation (7.15). Now define

$$\underline{\gamma}_k = \underline{\Psi}_k - \underline{\Psi}_{k-1} \qquad (D.2)$$

The modified displacement increment for the accelerated scheme is now given by

$$\Delta\underline{a}_{k+1} = A_{k+1}\Delta\underline{a}^*_{k+1} + B_{k+1}\Delta\underline{a}_k \qquad (D.3)$$

where A_{k+1} and B_{k+1} are scalars defined by

$$A_{k+1} = -C_{k+1}/D_{k+1}$$

$$B_{k+1} = A_{k+1}\ (1-E_{k+1}/D_{k+1}) - 1$$

where C_{k+1}, D_{k+1} and E_{k+1} are defined by

$$C_{k+1} = \Delta \underline{a}_k^T \underline{\Psi}_{k-1}$$

$$D_{k+1} = \Delta \underline{a}_k^T \underline{\gamma}_k$$

$$E_{k+1} = \left[\Delta \underline{a}^*_{k+1} \right]^T \underline{\gamma}_k$$

The iteration is started by

$$\Delta \underline{a}_1 = \Delta \underline{a}^*_1 = K^{-1} \underline{\Psi}_0 = K^{-1} \underline{\Psi}(\underline{a}_0) \qquad (D.4)$$

APPENDIX E

NUMERICAL SOLUTION OF CONSTITUTIVE EQUATIONS

The numerical solution of the constitutive equations is based on equations (3.9)-(3.10), (7.1)-(7.7) and (7.17)-(7.18) with the infinitesimal quantities replaced by finite increments and tensors replaced by vectors representing the arrays by which they are stored in a computer for use by a finite element program. For each iteration during the solution process to find equilibrium between the internal and the applied forces of a mesh, a displacement increment is calculated according to equation (7.13). From this, an increment in total strain for each element can be found:

$$\Delta \underline{\varepsilon} = B \, \Delta \underline{a} \qquad (E.1)$$

Using the constitutive laws, a corresponding stress increment can be calculated by

$$\Delta \underline{\sigma} = D_{ep} \Delta \underline{\varepsilon} \qquad (E.2)$$

The value of D_{ep} is the same as that given in equation (7.18). For an element in which the material has not yielded D_{ep} is the elastic matrix and the resulting stress increment is the one required. If the material has yielded and the increments of plastic strain and of the hardening parameter, $\underline{\alpha}$, are calculated from the stress increment: then, in general, it will be found that the consistency condition is not satisfied - i.e.

the stress point $\underline{\sigma} + \Delta\underline{\sigma}$ is not touching the yield surface. The method used to overcome this in the present program is to scale the stress increment by a scalar factor r, and to calculate the value of r, call it r_c, such that $\underline{\sigma} + r_c \Delta\underline{\sigma}$ satisfies the consistency condition once $\underline{\alpha}$ and $\underline{\eta}$ have been calculated. Finding r_c is done by expressing the yield function in terms of the factor r and then by finding the root of this function which is r_c.

The construction of the function for which the root is to be found will now be described. The elastic strain is assumed to be dependent on the stress and so the plastic part of the total strain can be written as

$$\Delta\underline{\eta} = \Delta\underline{\varepsilon} - rD^{-1}\Delta\underline{\sigma} \qquad (E.3)$$

The corresponding relationship to equation (7.4) which gives the increment in the work equivalent plastic strain is

$$\Delta\eta_e = \Delta\underline{\eta} \cdot (\underline{\sigma} - \underline{\alpha})/\sigma_y \qquad (E.4)$$

The change in the position parameter, $\underline{\alpha}$, is given by Ziegler's hardening rule:

$$\Delta\underline{\alpha} = C\Delta\eta_e(\underline{\sigma} - \underline{\alpha})/\sigma_y \qquad (E.5)$$

(Compare this with equation (7.6).) In this expression C is normally the slope of the hardening curve as it is in equation (7.6). However, this would approximate

the hardening curve that is given by the constitutive equations by a tangent. In order to overcome this, C is calculated to be the slope of the secant which connects the initial and final points on the hardening curve. The expression of C must be given in terms of η_e since these two points are usually specified in terms of η_e. Thus, C is

$$C = \frac{m K}{\Delta \eta_e} \left[\left(\frac{\eta_e + \Delta \eta_e}{m} \right)^{1/q} - \left(\frac{\eta_e}{m} \right)^{1/q} \right] \qquad (E.6)$$

In this expression, m is derived from Masing's rule and is equal to 1 on the initial loading of the element but becomes 2 for the rest of the loading sequence. Using equation (E.6), equation (E.5) can be written:

$$\Delta \underline{\alpha} = \frac{K}{\sigma_y} \left[\left(\frac{\eta_e + \Delta \eta_e}{m} \right)^{1/q} - \left(\frac{\eta_e}{m} \right)^{1/q} \right] (\underline{\sigma} - \underline{\alpha}) \qquad (E.7)$$

The new values for stress, $\underline{\sigma} + \Delta \underline{\sigma}$, and position of the centre of the yield surface, $\underline{\alpha} + \Delta \underline{\alpha}$, can now be substituted into equation (7.2) to give the new value of the yield function. In order to find the value of r at which consistency is satisfied, a Newton-Raphson method is used to find a zero in the yield function which is expressed as a function of r. The derivative of F with respect to r is given by the following expressions:

$$\frac{dF}{dr} = \frac{\partial F}{\partial \underline{\sigma}} \cdot \left[\Delta \underline{\sigma} - \frac{d\underline{a}}{dr} \right] \qquad (E.8)$$

$$\frac{d\underline{\alpha}}{dr} = - \frac{G}{\sigma_y^2 q} \left[\frac{\eta_e - \Delta \eta_e}{m} \right]^{((1-q)/q)} [(\underline{\sigma} - \underline{\alpha})^T D^{-1} \Delta \underline{\sigma}] (\underline{\sigma} - \underline{\alpha}) \qquad (E.9)$$

This is the background to the method adopted to find a stress increment in an element given the total strain increment. There are certain details of the actual procedure used that overcome the problems encountered when trying to find the zero of the yield function which will now be discussed.

It is possible that the trial stress increment given by equation (E.2) produces a stress point $\underline{\sigma} + \Delta\underline{\sigma}$ that lies inside the yield surface when yielding should be occurring. In this case, which will be called unloading, it has been found necessary to move the yield surface 'backwards' to maintain consistency. This situation and the one in which $\underline{\sigma} + \Delta\underline{\sigma}$ lies outside the yield surface ('loading') are handled by the program in much the same way. However, there are differences.

In the loading case the value of F usually varies monotonically from negative at r=0 to positive r=1. Thus, there is a single zero between r=0 and r=1. The initial value of r for then Newton-Raphson scheme is taken as 1 in this case. If it is the first time the element has yielded after a reversal of the loads applied to the structure, then this value for r is inappropriate since the derivative in (E.9) is undefined in this situation. In order to find a starting value of r on first yield, a sequence of values of r is generated and tried, one at a time, until one gives a positive value of F. The sequence is produced according to the following scheme.

$$r = 0.5$$

$$r_{i+1} = (r_i + 7)/8 \qquad \text{(E.10)}$$

The program checks before embarking on the Newton-Raphson algorithm that the conditions described above are obtained in each case. Other possible exceptions occur in practice and the program deals with these as far as possible. The most important of these exceptions is that where F remains negative for all values of r less than 1. Here a search is performed to find a value of r for which F is positive. Once such a value for r is found, an interval halving algorithm is used to get close to the root and the Newton-Raphson procedure is then used to complete the process. If the increment of work equivalent plastic strain is positive, then there will always be a value of r greater than 1 such that $F > 0$. If it is not positive, then r is taken to be 1 and the increment of $\underline{\alpha}$ is calculated so that consistency is satisfied. It is also possible that F at r=0 is positive. If the stress point still satisfies consistency then the change in α is not large enough to make a difference to the numbers stored by the computer and the program continues with r=0, i.e. no stress increment.

The unloading case is basically the same as the loading case described above with positive and negative exchanged. However, there are some differences. In order to check that a zero of the yield function exists for $r > 0$, an upper value of r needs to be tried. In the loading case this value of r was 1. In the unloading case, however, r is usually greater than 1. An upper

value of r is taken to be the value at which the increment in work equivalent plastic strain is zero. Also, it is possible there is no value of $r > 0$ for which $F < 0$. Again, in this case, r is taken to be 1, and an increment in $\underline{\alpha}$ found to satisfy consistency.

REFERENCES

ABAQUS, 1983. Theory Manual, Version 4.4, Hibbit, Karlsson and Sorenson Inc.

ABAQUS, 1984. Theory Manual, Version 4.5, Hibbit, Karlsson and Sorenson Inc.

Armstrong, P. J. and Frederick, C. O., 1966. A mathematical representation of the multiaxial Bauschinger effect. CEGB (UK) Report RD/B/N731.

Blackmon, D. R., Socie, D. F. and Leckie, F. A., 1983. Application of continuum damage concepts to creep-fatigue interactions. ASME Symposium on Thermal and Environmental Effects on Fatigue, Portland OR, June 1983, 45.

Brown, M. W. and Buckthorpe, D., 1985. A crack propagation based effective strain criterion. Presented at the 2nd International Conference on Multiaxial Fatigue, Sheffield, December, to be published.

Brown, M. W. and Miller, K. J., 1973. A theory for fatigue failure under multiaxial stress-strain conditions. Proc. Inst. Mech. Engrs., 187, 745-755.

Brown, M. W. and Miller, K. J., 1979. Initiation and growth of cracks in biaxial fatigue. Fatigue Engrg. Mater. Struct., 1, 231-246.

Chaboche, J. -L., 1978. Description thermodynamique et phenomenologique de la viscoplasticite cyclique avec endomagement. Thesis, University Paris VI. ONERA publication 1978-3.

Chaboche, J. -L., 1981. Continuous damage mechanics. A tool to describe phenomena before crack initiation.

Nucl. Engrg. Design, 64, 233-247.

Chaboche, J. -L. and Cailletaud, G., 1986. On the calculation of structures in cyclic plasticity or viscoplasticity. Comp. Struct., 23, 23-31.

Chaboche, J. -L. and Lesne, P. M., 1986. On the non-linear fatigue damage accumulation. Presented at the International Conference on Steel Structures, Budva, Yugoslavia, September.

Chaboche, J. -L. and Rousselier, G., 1983. On the plastic and viscoplastic constitutive equations - parts I and II. Trans. ASME, J. Press. Vessel Tech., 105, 153-164.

Crisfield, M. A., 1979. A faster modified Newton-Raphson iteration. Comp. Meths. Appl. Mech. Engrg., 20, 267-278.

Crisfield, M. A., 1984. Accelerating and damping the modified Newton-Raphson method. Comp. Struct., 18, 395-407.

Dyson, B. F. and McLean, D., 1977. Creep of Nimonic 80A in torsion and tension. Metal Sci., 11, 37-45.

Feltner, C. E. and Sinclair, G. M., 1963. Cyclic stress induced creep of close-packed metals. Joint Int. Conf. on Creep. Inst. Mech. Engrs., Paper 7.

Fenn, O., 1979. Behaviour of structures subjected to cyclic plastic deformation. M. Phil. Thesis, University of Leicester (UK).

Fuchs, H. O. and Stephens, R. I., 1980. Metal fatigue in engineering. Wiley, New York.

Goodall, I. W. and Ainsworth, R. A., 1977. Failure of structures by creep. 3rd Int. Conf. Pressure Vessel Technology, Tokyo, ASME, Part II, 871-885.

Hashin, Z. and Rotem, A., 1978. A cumulative damage theory of fatigue failure. Mater. Sci. Engrg., 34, 147-160.

Hayhurst, D. R., Dimmer, P. R. and Morrison, C. J., 1984a. Development of continuum damage in the creep rupture of notched bars. Phil. Trans. R. Soc. Lond., A311, 103-129.

Hayhurst, D. R., Brown, P. R. and Morrison, C. J., 1984b. The role of continuum damage in creep crack growth. Phil. Trans. R. Soc. Lond., A311, 131-158.

Hayhurst, D. R. and Krzeczkowski, A. J., 1979. Numerical solution of creep problems. Comp. Meths. Appl. Mech. Engrg., 20, 151-171.

Hayhurst, D. R., Lavender, D. A., Worley, N. G. and Salim, A., 1985. Assessment of the θ-projection method for the representation and extrapolation of creep data for a 1%Cr, 1/2%Mo, 1/4%V steel tested at 565°C. Int. J. Press. Vessels Piping, 20, 289-317.

Kachanov, L. M., 1958. Time of the fracture process under creep conditions. Izv. Akad. Nauk SSSR. Otd. Teck. Nauk 8, 26-31.

Krieg, R. D. and Krieg, D. B., 1977. Accuracies of numerical solution methods for the elastic-perfectly plastic model. Trans ASME. J. Press. Vessel Tech., 99, 510-515.

Lavender, D. A. and Hayhurst, D. R., 1986. An assessment of higher-order isoparametric elements for solving an elastic problem. Comp. Meths. Appl. Mech. Engrg., 56, 139-165.

Leckie, F. A. and Hayhurst, D. R., 1974. Creep rupture of structures. Proc. R. Soc. Lond. A340, 323-347.

Lemaitre, J., 1986. Local approach of fracture. Engrg. Fract. Mech., 25, 523-537.

Lemaitre, J. and Chaboche, J. -L., 1985. Mecanique des materiaux solides. Dunod, Paris.

Lemaitre, J. and Plumtree, A., 1979. Application of damage concepts to predict creep-fatigue failures. Trans. ASME. J. Engrg. Mater. Tech., 101, 284-292.

Majumdar, S. and Maiya, P. S., 1980. A mechanistic model for time dependent fatigue. Trans ASME, J. Engrg. Mater. Tech., 102, 159-167.

Manson, S. S., Nachtigall, A. J., Ensign, C. R. and Freche, J. C., 1965. Further investigation of a relation for cumulative fatigue damage in bending. Trans. ASME. J. Engrg. Indust. 87, 25-35.

Masing, G., 1926. Eigenspannugen und verfestigung beim messing. Proc. 2nd Int. Congress of Applied Mechanics, 332-335.

Matthies, H. and Strang, G., 1979. The solution of nonlinear finite element equations. Int. J. Num. Meths. Engrg., 14, 1613-1626.

Megahed, M. M. and Ponter, A. R. S., 1979. Creep and plastic ratchetting in a simple structure. University of Leicester (UK), Department of Engineering, Report 79-9.

Megahed, M. M., Ponter, A. R. S. and Morrison, C. J., 1980. A study of time independent material ratchetting. University of Leicester (UK), Department of Engineering, Report 80-14.

Miller, K. J., 1982. The short crack problem. Fatigue Engrg. Mater. Struct., 5, 223-232.

Miller, K. J. and Zachariah, K. P., 1977. Cumulative damage laws for fatigue crack initiation and Stage I propagation. J. Strain Anal., 12, 262-270.

Miner, M. A., 1945. Cumulative damage in fatigue. Trans. ASME, J. Appl. Mech., 67, A-159 - A-164.

Nayak, G. C. and Zienkiewicz, O. C., 1972. Note on the 'alpha'-constant stiffness method for the analysis of non-linear problems. Int. J. Num. Meths. Engrg., 4, 579-582.

Owen, D. R. J. and Hinton, E., 1980. Finite elements in plasticity: theory and practice. Pineridge Press, Swansea.

Pascoe, K. J., 1961. An introduction to the properties of engineering materials. Blackie, Glasgow.

Phillips, D. V. and Zienkiewicz, O. C., 1976. Finite element non-linear analysis of concrete structures. Proc. Inst. Civ. Engrs., Part 2, 61, 59-88.

Raynor, D. and Skelton, R. P., 1983. The effects of cracks in high strain fatigue testing. Presented at: NPL/UKAEA Symp. Techniques for High Temperature Fatigue Testing, Preston, UK, September.

Schreyer, H. L., Kulak, R. F. and Kramer, J. M., 1979. Accurate numerical solutions for elastic-plastic models. Trans. ASME, J. Press. Vessel Tech., 101, 226-234.

Shield, R. T. and Ziegler, H., 1958. On Prager's hardening rule. ZAMP, IXa, 260-276.

Socie, D. F., Kurath, P. and Koch, J., 1985. A multiaxial fatigue damage parameter. Presented at the 2nd Int. Symp. on Multiaxial Fatigue, Sheffield, UK, December.

Taylor, M. Q., 1985. Fatigue life in 316 stainless steel. University of Leicester (UK), Department of Engineering, Final Year Undergraduate Project Report.

Ziegler, H., 1959. A modification of Prager's hardening rule. Quart. Appl. Maths., 17, 55-65.

Zienkiewicz, O. C., 1977. The finite element method. 3rd ed. McGraw-Hill.

Zienkiewicz, O. C. and Cormeau, I. C., 1974. Visco-plasticity - plasticity and creep in elastic solids - a unified numerical solution approach. Int. J. Num. Meths. Engrg., 8, 821-845.

DEFORMATION AND RUPTURE OF STRUCTURES DUE TO COMBINED CYCLIC PLASTICITY AND CREEP

by David A. Lavender

ABSTRACT

The effect of creep-fatigue conditions on structural components is not completely understood, and so the prediction of the behaviour and lifetime of such components is often unreliable and inaccurate. One of the methods proposed to improve the predictions is continuum damage mechanics, which provides a general description of material behaviour under degrading conditions.

An estimate of life is usually based on the initial behaviour of a component. However, the work of previous researchers has shown that accurate predictions of the creep life of structures require that the stress redistribution due to the growth of damage is taken into account. In this thesis, this work is extended to fatigue and the effect of fatigue damage on life and deformation is studied for multibar model structures.

The non-linear kinematic hardening rule is introduced as a constitutive law for cyclic plasticity that models many aspects of the cyclic behaviour of metals. Its properties are studied and it is extended to include the effects of damage on cyclic deformation.

Creep-fatigue is studied by combining the models for fatigue and creep. Using published material data, the creep-fatigue behaviour of a two bar structure is studied and the results are compared with some experimental results.

A study is made of finite element methods for solving problems involving plasticity and an example problem is solved. A model for the multiaxial behaviour of damaged material is proposed and examined for simple cases.

The studies show that stress redistribution has a significant effect on fatigue life and the qualitative properties of the uniaxial models are very close to experimental observations. However, a lack of suitable and consistent experimental data on material behaviour means that the lifetime predictions and the multiaxial models are of uncertain accuracy.